External real time control of E.coli range expansion

Dimitrije Milunov

THÈSE DE DOCTORAT

UNIVERSITÉ PARIS CITÉ

External real time control of *E. coli* range expansion

UMR 168 - Physico-Chimie Curie, Institut Curie
UMR 7057 - Laboratoire Matière et Systèmes Complexes

Soutenue par :

Dimitrije Milunov
Le 16.02.2023

École Doctorale 474

Frontières de l'Innovation en Recherche et Éducation (FIRE)

Spécialité

Biologie moleculaire et structurale et biochimie, biophysique moleculaire
.

Rapporteurs :

Stéphanie Descroix - DR CNRS, Institut Curie, Université Pierre et Marie Curie - UPMC

Meriem El Karoui -Professor University of Edinburgh,

Examinateurs :

Olivia du Roure - DR CNRS, ESPCI, Université Paris Cité

Hans Geiselman - DR CNRS, Université Grenoble Alpes

Directeur de thèse:

Pascal Hersen - DR CNRS, PSL, Sorbonne, Institut Curie

Table of contents

1 CONTENTS

2 ACKNOWLEDGMENTS

First of all I would like to specially thank all of my coworkers and members of our team. Many thanks to Celine Cordier, a friend, college and a fellow felinophile who was the first one that introduced me to molecular biology, wet lab work and microfluidics. Thank you for your constant support, kindness, friendship, scientific insights and hard and dedicated work that enabled the lab to work smoothly, professionally and in organized manner. The lab definitely wouldn't be the same without you. Many thanks to Sylvain Pouzet, Matthias Le Bec, Simon Barral, Sara Bonavia, Thomas Wyatt, Maud Hofmann and Victoria Reichel who shared their journey with me. Thank you for your friendships during difficult times, for all the fun we had, for your constant support and your witty and unlimited sense of humor. Sylvain, Sara and Maud, many thanks to you for your constant optimism and positivity and your capability of always finding silver lining when things look black. Many thanks to Alvaro Banderas. Thank you for your friendship, advice, great scientific talks, seminars, jokes and insights and for being there for me whether for personal issues or experimental and scientific work. Many thanks to Benoit Sorre and Karine Guevorkian for your scientific inputs and feedback. I would like to give a special thank to Lydia Robert and Remy Chait for agreeing to be part of my thesis advisory committee. You were an excellent scientific support and many thanks to your discussions. If I could I wouldn't have chosen better members. And finally a huge thank to my advisor, Pascal Hersen for the support and guidance throughout my PhD and giving me the opportunity to work in his lab.

Zahvalnica ne bi bila potpuna bez posebne zahvalnosti meni dragim i bitnim ljudima. Posebno se zahvaljujem mojim roditeljima, majci Ljiljani i ocu Radovanu, na velikom strpljenju, neograničenoj ljubavi i podršci svih ovih godina, svim neprospavanim noćima, žrtvovanjima i lekcijama koje ste me naučili. Hvala vam, bez vas ne bih uspeo ni delić onoga što sam postigao. Hvala mojim prijateljima koje takođe smatram delom svoje porodice. Aleksandra Šljukić, Nemanja Đorđević, Milica Ivković, Marija Miljuš, Ljubica Cimeša, Lara Bücher, Eugenia Covernton, Chiarra Fracassi i Anđela Stojev, hvala vam na vašem prisustvu u mom životu, vašem humoru, savetima, inteligenciji i što ste tu bili tokom svih ovih godina i mojih mentalnih cepanja.

3 ABBREVIATIONS

- RNAP: RNA polymerase
- LB media: Lysogeny broth media, nutritionally rich media used for bacterial growth
- M9 media: minimal medium for *E.coli*
- PIV: particle image velocimetry. Optical technique to analyze movements from the time lapse sequence of images
- PDE: partial differential equation
- ODE: ordinary differential equation
- PI control: Proportional-Integral control algorithm. Defined and detailed explanation in chapter
- PID control: Proportional-Integral-Differential control algorithm. Defined and detailed explanation given in chapter
- MPC control: Model predictive control

4 PREFACE

Since the dawn of time, humans have been seeking to have the power to influence a system in order to achieve a certain goal - ancient Greeks for instance used flow regulators in their water clock design to enable precise measurement of time. Despite utilizing the concepts behind the what we nowadays define as control, its mathematical and theoretical foundation started developing way later, in the 18th century, with the first foundation grounded by Leibnitz. The echo of ideas that shaped his philosophy could be found in one of his quotes on free will:

> *"Omnes actiones sunt determinatae, et nunquam indifferentes quia semper datur ratio inclinans quidem non tamen necessitans ut sic potius quam aliter fiat"*
>
> *[All actions are determined and never without influence because there is always a reason which inclines us even if it is unnoticed so that we act thus and in no other way]*

Leibnitz, De liberatate, Opera, ed. Erdmann, p 669.

Leibnitz thought that all of our thoughts are made of simple fundamental concepts that have the potential to be symbolically represented. He theorized that by knowing these concepts and rules guiding them, we could put these symbolic representations in a certain order to create an engine capable of creating new thoughts and obeying and imitating human beings. With this Leibnitz essentially equated the human cognition with modern computational terms capable of being reproduced in a controllable logic device.

Three centuries later during the World War II, while working on guided missile technology, Norbert Wiener realized the importance of the feedback in both the technological devices and in living organism. In his famous book "Cybernetics Or Control and Communication in the Animal and the Machine" [1], Wiener introduced the concept of cybernetics – which he classified as "entire field of control and communication theory whether in the machine or in the animal". Life is supported by a myriad of self-regulating mechanism and like any process based on self-regulating mechanism, it wouldn't be possible without the feedback mechanisms. Any systems that has a goal needs to have an information of the current state and how distant the desired goal is from it. Based on this difference the system applies corrective measures that drive it towards the desired goal. If the feedback didn't exist, the rockets wouldn't be able to find the target as they wouldn't be capable of updating the position of the avoiding plane, human body wouldn't be able to regulate the blood sugar level etc. In addition to this, in his famous work Wiener extended the notion of homeostasis in cellular colonies and the rise of structure and organization within them, for which he thought are processes parallel with the ones that occur within the human society.

Owing to the advances in science and technology, cybernetics and control theory has since then spread to different domains, giving rise to machine learning algorithms, multifunctional human prosthetics, synthetic biology, gene expression control and many more.

"I feedback, therefore I am" [2]

This headline sums up the reasons why I am so enthusiastic about control theory. It is everywhere and it has a powerful ability to be at the same time quite mathematical but also fully capable to answer to the reality. We are surrounded by feedbacks and in a way we could say that we own our existence to them. They exists on the level of one individual but also more interestingly at the level of groups where it has the capability to coordinate cooperation and interaction. Namely similarly to multi agents systems which are much better at solving difficult problems than an individual agent, **organisms living in a community are inherently more resilient to environmental changes then the ones living a individualistic lifestyle. Thus can we and if so, to what degree we could control biological communities?** Afterall from humans to microbes, most living systems are living in some form of a community.

In this study I focused on investigating the possibility of externally controlling how dense bacterial colonies grown in a microfluidic device expand in space. The thesis roughly consists of three parts. The first two parts discuss the importance of gradients, cooperation and self-organization at a colony level and how it makes bacterial colonies more resilient to foreign insults. It includes the results of the studies I conducted on the experimental system to understand its dynamics and asses the possibility of applying external control to regulate the invasion speed of the colony. The last part of the thesis focuses on gene expression noise and in particular of gene expression noise of RNA polymerase. Similarly to cooperation, stochasticity of gene expression noise can limit the precision at which one could externally control living systems. Genes are organized into multiple interacting regulatory circuits where expression of one gene impacts the expression of the other ones, thus noise from one gene can propagate downstream throughout the genetic circuit. Increased noise levels can lead to significant phenotypic variation inside a population, again offering resistance or significant resilience of the community to imposed environmental changes. In this study one way of perturbing the colony is through direct IPTG modulation of RNA polymerase. Other methods (nutrient and antibiotic modulation) among many other molecules, also impact the RNA polymerase of the system. As RNA polymerase is involved in transcription - the first step of gene expression, it has the potential to propagate throughout the entire system. Therefore the part of this thesis is dedicated to the study of how the RNA polymerase noise depends on certain environmental conditions.

5 ABSTRACT

Advances in microfluidics, sensory technology and synthetic and molecular biology enabled the rise of a novel scientific field in which fundamentals of control theory can be applied to externally control and regulate cellular bioprocesses-cybergenetics. So far, cybergenetics was able to successfully control complex multi-stable and adaptive gene networks at the population and the single cell level, but challenges in the control of biological multiagent-like system composed of multiple interactive components have not yet been addressed. In this study, we focused on dense biofilm like colonies of *E. coli* which were grown inside a multilayered microfluidic device whose geometry enabled the growth of the colonies in one direction. Similarly to biofilms, it is widely known that dense **E.coli colonies exhibit remarkable levels of spatial organization that come as a consequence of the complex interplay between nutrient and chemical gradients and metabolic interactions between different layers of the colony**. These interactions make both dense colonies and biofilms more resistant to antimicrobial agents treatment consequently making them difficult to eradicate. **Thus can we and to what extent we could externally control this system remains an open question?** To answer this we firstly quantitively analyzed the growth patterns inside the colony to understand the dynamics of the system. We used three different strategies to perturb the colony and to see the impact on the spatial growth patterns - modulation of RNA polymerase by inducible promoter and biochemical modulation of the cellular resources by nutrient change and antibiotics. Since the cells were nonmotile, the invasion speed of the colony could be regarded as a global descriptor of the colony spatial growth dynamics. Thus having this in mind we finally used the understanding of the systems dynamics, knowledge of colonies response to various stimulus and a custom made control platform to externally control the invasion speed of the colony.

Key words: Escherichia coli, cybergenetics, microfluidics, control theory, spatial patterning, range expansion, particle image velocimetry

6 ABSTRACT DE THESE

Contrôle externe en temps réel de l'expansion des colonies d'E.coli

Les progrès de la microfluidique, de la technologie sensorielle et de la biologie synthétique et moléculaire ont permis l'émergence d'un nouveau domaine scientifique dans lequel les principes fondamentaux de la théorie du contrôle peuvent être appliqués pour contrôler et réguler de manière externe les bioprocessus cellulaires : la cybernétique. Jusqu'à présent, la cybernétique a été capable de contrôler avec succès des réseaux génétiques complexes, multi-stables et adaptatifs au niveau de la population et de la cellule unique, mais les défis du contrôle de systèmes biologiques de type multi-agent composés de multiples composants interactifs n'ont pas encore été relevés. Dans cette étude, nous nous sommes concentrés sur des colonies denses d'E. coli, semblables à des biofilms, qui ont été cultivées à l'intérieur d'un dispositif microfluidique multicouche dont la géométrie permet la croissance des colonies dans une seule direction. De même que pour les biofilms, il est largement connu que les colonies denses d'E.coli présentent des niveaux remarquables d'organisation spatiale qui sont la conséquence de l'interaction complexe entre les gradients nutritifs et chimiques et les interactions métaboliques entre les différentes couches de la colonie. Ces interactions rendent les colonies denses et les biofilms plus résistants aux traitements antimicrobiens, ce qui les rend difficiles à éradiquer. La question de savoir si et dans quelle mesure nous pouvons contrôler ce système de l'extérieur reste donc ouverte. Pour répondre à cette question, nous avons d'abord analysé quantitativement les modèles de croissance à l'intérieur de la colonie pour comprendre la dynamique du système. Nous avons utilisé trois stratégies différentes pour perturber la colonie et voir l'impact sur les modèles de croissance spatiale - la modulation de l'ARN polymérase par un promoteur inductible et la modulation biochimique des ressources cellulaires par des changements de nutriments et des antibiotiques. Comme les cellules ne sont pas mobiles, la vitesse d'invasion de la colonie peut être considérée comme un descripteur global de la dynamique de croissance spatiale de la colonie. En gardant cela à l'esprit, nous avons finalement utilisé la compréhension de la dynamique des systèmes, la connaissance de la réponse des colonies à divers stimuli et une plateforme de contrôle faite sur mesure pour contrôler de manière externe la vitesse d'invasion de la colonie.

Mots clés : Escherichia coli, cybernétique, microfluidique, théorie du contrôle, structuration spatiale, vélocimétrie par image de particules.

7 RÉSUMÉ

Contrôle externe en temps réel de l'expansion des colonies d'E.coli

Depuis l'aube des temps, les Hommes voulaient avoir le pouvoir de contrôler des différents systèmes à des fins d'atteindre les objectifs divers. Les anciens Grecs ont, par exemple, utilisé des régulateurs de débit d'eau pour obtenir une mesure précise du temps dans la conception de leurs horloges hydrauliques. Bien que les concepts du contrôle, tel qu'on le définit aujourd'hui, aient été appliqués depuis longtemps, les fondements mathématiques et théoriques n'ont commencé à se développer qu'au 18e siècle à base des travaux de Leibniz. Ces récits sur le libre arbitre font preuve des idées qui ont façonné sa philosophie:

> "Omnes actiones sunt determinatae, et nunquam indifferentes quia semper datur ratio inclinans quidem non tamen necessitans ut sic potius quam aliter fiat".
>
> [Toutes les actions sont déterminées et ne sont jamais sans influence parce qu'il y a toujours une raison qui, même inaperçue, nous incite à agir ainsi et pas autrement].

Leibniz, De liberatate, Opera, ed. Erdmann, p 669.

Leibniz disait que toutes nos pensées sont construites sur la base de concepts fondamentaux simples qui ont le potentiel d'être représentés symboliquement. Il a théorisé qu'en connaissant ces concepts et les règles qui les guident, nous pouvions placer ces représentations symboliques dans un certain ordre pour créer un moteur capable de créer de nouvelles pensées, d'obéir et imiter les êtres humains. Avec cela, Leibniz a essentiellement assimilé la cognition humaine aux termes informatiques modernes capables d'être reproduits et contrôlés dans un dispositif logique.

Trois siècles plus tard, pendant la Seconde Guerre mondiale, alors Norbert Wiener, qui travaillait sur la technologie des missiles guidés, a réalisé l'importance de la rétroaction, tant dans les dispositifs technologiques que dans les organismes vivants. Dans son célèbre ouvrage "Cybernetics Or Control and Communication in the Animal and the Machine" [1], Wiener a introduit le concept de cybernétique, qu'il a classé comme "un domaine entier de la théorie du contrôle et de la communication, que ce soit dans une machine ou un animal". Il pense que la notion de rétroaction et d'autorégulation est un concept central de la vie quotidienne. Par exemple, si nous observons la vie, elle se caractérise par une myriade de mécanismes d'autorégulation et, comme tout processus basé sur un mécanisme d'autorégulation, elle ne serait pas possible sans les mécanismes de rétroaction. Mais qu'est-ce qui fait qu'un certain

mécanisme est un mécanisme de rétroaction ? Tout système ayant un objectif doit disposer d'informations sur l'état actuel , sur l'objectif souhaité, ainsi que la distance qui les sépare Sur la base de cette différence, le système applique des mesures correctives qui le rapprochent de l'objectif souhaité. Dans le cas de Wiener, le retour d'information était indispensable, car autrement les missiles ne seraient pas en mesure de réajuster la position réelle de leur cible, l'avion qui essaye de s'échapper, le corps humain ne serait pas capable de réguler le niveau de sucre dans le sang, etc.

Grâce aux progrès de la microfluidique, de la technologie sensorielle et de la biologie synthétique et moléculaire, la cybernétique appliquée et la théorie du contrôle sont passées du domaine électrique et mécanique au domaine biologique, formant ainsi un tout nouveau domaine appelé la cybergénétique. L'objectif principal de la cybergénétique est d'appliquer les principes fondamentaux de la théorie du contrôle pour contrôler et réguler les processus cellulaires de manière externe. Jusqu'à présent, la cybergénétique a été capable de contrôler avec succès des réseaux génétiques complexes, multi-stables et adaptatifs au niveau de la population et de la cellule unique. Les défis du contrôle de systèmes biologiques de type multi-agent composés de multiples composants interactifs n'ont pas encore été relevés. Dans cette thèse, je me suis concentré sur des colonies denses d'E. coli, semblables à des biofilms, qui ont été cultivées à l'intérieur d'un dispositif microfluidique multicouche, dont la géométrie permet une croissance unidirectionnelle des colonies. Similaire aux biofilms, les colonies denses d'E.coli présentent des niveaux remarquables d'organisation spatiale. Ceci résulte d'une interaction complexe entre les gradients nutritifs et chimiques et les interactions métaboliques entre les différentes couches de la colonie. Ainsi se forment les colonies denses ou les biofilms, qui eux sont plus résistants aux traitements antimicrobiens et plus difficile d'éradiquer. La question de savoir si et dans quelle mesure nous pouvons contrôler ce système de l'extérieur reste ouverte. Pour y répondre, nous avons d'abord fait une analyse quantitative des modèles de croissance à l'intérieur d'une colonie pour comprendre la dynamique du système. J'ai utilisé trois stratégies différentes pour perturber les colonies et observer l'impact sur les tendances de leur croissance spatiale : 1) la modulation de l'ARN polymérase par un promoteur inductible, la modulation biochimique des ressources cellulaires par 2) des changements de nutriments et 3) des antibiotique. Comme les cellules d'E.Coli ne sont pas mobiles , la vitesse d'invasion de la colonie peut être considérée comme un descripteur global de la dynamique de croissance spatiale de la colonie. En gardant cela à l'esprit, nous avons finalement utilisé la compréhension de la dynamique des systèmes, la connaissance de la réponse des colonies aux stimuli divers et une plateforme de contrôle faite sur mesure pour contrôler de manière externe la vitesse d'invasion de la colonie.

Cette thèse se compose de trois parties. Les parties 1 et 2 traitent le sujet de l'importance des gradients, de la coopération et de l'auto-organisation au niveau de la colonie, ainsi que la manière dont ces facteurs rendent les colonies bactériennes plus résistantes aux agressions extérieures. Les résultats des études que j'ai menées sur le système expérimental pour comprendre sa dynamique et évaluer la possibilité d'appliquer un contrôle externe pour réguler la vitesse d'invasion de la colonie sont compris dedans.

Les deux premières parties se composent de plusieurs chapitres. Comme mentionné précédemment, le chapitre suivant ce résumé (chapitre 7) commence par l'importance des biogradients dans les microorganismes. Malgré leur petite taille, les microorganismes présentent des niveaux remarquables d'auto-organisation et de comportements complexes en raison des gradients imposés de nutriments, d'oxygène et/ou de produits chimiques. En plus des gradients imposés de l'extérieur, les colonies de micro-organismes ont également un impact et des changements sur la façon dont leur micro-environnement local est façonné par leur métabolisme, la consommation des ressources, l'excrétion de métabolites potentiellement utiles et l'excrétion de déchets, etc. Bien que les modalités de coopération des micro-organismes soient profondément imbriquées, nous pouvons clairement en distinguer trois essentielles : la protection, l'alimentation croisée et la division du travail. Lorsque les cellules s'engagent dans une alimentation croisée, différentes cellules se spécialisent dans la production de différentes ressources métaboliques vitales pour l'ensemble de la colonie et les échangent. La coopération offre une protection contre les agressions extérieures - Dans ce cas, la couche externe de la microcolonie finit par assumer le rôle de protection et devient un bouclier pour les cellules internes situées à l'intérieur de la colonie. Enfin, les cellules peuvent jouer différents rôles dans l'organisation de la colonie, par exemple une partie d'entre elles peut développer de multiples flagelles pour explorer rapidement l'espace, tandis qu'une plus petite partie des cellules peut être laissée derrière pour coloniser un nouvel espace. Après avoir couvert l'auto-organisation dans le monde microbien et présenté brièvement le même sujet dans d'autres domaines de la vie, le chapitre se termine par l'introduction de la question principale qui motive la recherche dans cette thèse. Comme les gradients chimiques et nutritifs jouent un rôle majeur dans l'établissement de l'hétérogénéité à l'intérieur de la colonie et sont une force motivante pour l'augmentation de la coopération et de l'organisation cellulaire, pouvons-nous perturber ces gradients pour obtenir une réponse désirée de la colonie dans son ensemble ? Le système modèle choisi est celui des colonies bactériennes E.coli, et en particulier leur expansion.

Le chapitre suivant est consacré à l'explication de la manière dont nous pourrions étudier ces colonies denses d'E.coli en laboratoire sur de longues périodes. La réponse réside dans l'utilisation d'un dispositif microfluidique qui, outre la possibilité d'effectuer des expériences à long terme, offre la possibilité de contrôler étroitement l'environnement. Au cours des deux dernières décennies, la technologie microfluidique est devenue un standard dans la recherche scientifique, en particulier dans le domaine de la microbiologie. Elle permet un contrôle rapide et précis des conditions expérimentales et donne la possibilité d'obtenir des informations spatio-temporelles et de paralléliser différentes expériences indépendantes à des taux qui ne pourraient

pas être atteints par des méthodes macroscopiques conventionnelles. Après avoir répondu à la question de savoir comment nous pouvons observer les cellules, le chapitre se concentre sur la manière dont les données obtenues peuvent être étudiées de manière quantitative. Pour déduire le taux de croissance et le taux d'expansion de la colonie bactérienne, un algorithme mathématique appelé vélocimétrie par image de particules a été utilisé. Cet algorithme est principalement utilisé en physique et en dynamique des fluides où il est largement exploité pour déduire la vitesse des fluides. En raison du caractère non invasif de l'algorithme, il a progressivement commencé à être utilisé dans les études biologiques pour déduire la croissance. Les aspects mathématiques de cet algorithme et la façon dont il peut être utilisé dans notre conception expérimentale sont couverts dans cette section

Le chapitre suivant est consacré à l'explication de la manière dont nous pourrions étudier ces colonies denses d'E.coli en laboratoire sur de longues périodes. La réponse réside dans l'utilisation d'un dispositif microfluidique qui, outre la possibilité d'effectuer des expériences à long terme, offre la possibilité de contrôler étroitement l'environnement. Au cours des deux dernières décennies, la technologie microfluidique est devenue un standard dans la recherche scientifique, en particulier dans le domaine de la microbiologie. Elle permet un contrôle rapide et précis des conditions expérimentales et donne la possibilité d'obtenir des informations spatio-temporelles et de paralléliser différentes expériences indépendantes à des taux qui ne pourraient pas être atteints par des méthodes macroscopiques conventionnelles. Après avoir répondu à la question de savoir comment nous pouvons observer les cellules, le chapitre se concentre sur la manière dont les données obtenues peuvent être étudiées de manière quantitative. Pour déduire le taux de croissance et le taux d'expansion de la colonie bactérienne, un algorithme mathématique appelé vélocimétrie par image de particules a été utilisé. Cet algorithme est principalement utilisé en physique et en dynamique des fluides où il est largement exploité pour déduire la vitesse des fluides. En raison du caractère non invasif de l'algorithme, il a progressivement commencé à être utilisé dans les études biologiques pour déduire la croissance. Les aspects mathématiques de cet algorithme et la façon dont il peut être utilisé dans notre conception expérimentale sont couverts dans cette section.

Le chapitre 9 couvre la notion de théorie du contrôle dans les systèmes biologiques et techniques. La rétroaction négative donne au système la capacité de contrôler de manière prévisible et précise un processus sur une gamme de conditions environnementales qui perturbent le système. Pour ce faire, on mesure/capte activement et en temps réel la sortie du contrôle et on la compare à la valeur souhaitée. Sur la base de la différence entre ce que nous voulons et ce que nous avons réellement, le contrôleur, qui permet la rétroaction négative, modifie la commande de manière appropriée afin que la sortie du système soit maintenue au niveau souhaité malgré les perturbations ou les changements imprévus de l'environnement. Outre l'examen du système technique et du système biologique, le chapitre 9 traite également de la manière dont nous pourrions fusionner les deux pour obtenir un contrôle assisté par ordinateur du système

biologique. Il s'agit également d'une introduction au contrôle assisté par ordinateur de l'expansion d'E.coli, abordé au chapitre 10. Le principal composant du contrôle assisté par ordinateur de l'expansion d'E.coli est la boucle de rétroaction conçue en externe. Son objectif principal est que la vitesse d'expansion suive un ensemble de valeurs de référence fournies par l'utilisateur. La conception se compose de trois éléments cruciaux 1) un mélangeur microfluidique qui fixe la concentration appropriée d'IPTG/nutriments/antibiotiques dans le milieu. Le mélangeur microfluidique est basé sur le mélange passif de deux fluides. La concentration d'un produit chimique spécifique peut être modulée par la fréquence à laquelle le fluide est mélangé. 2)Puce microfluidique qui permet le développement et le suivi de l'invasion des colonies d'E.coli. 3) Ordinateur qui observe et contrôle la vitesse d'invasion d'E.coli.

La dernière partie de ma thèse se concentre sur le bruit de l'expression génétique, en particulier sur celui de l'ARN polymérase. De façon similaire à la coopération, la stochastique du bruit d'expression des gènes peut limiter la précision à laquelle les systèmes vivants peuvent être contrôlés depuis l'extérieur. Les gènes sont organisés en de multiples circuits de régulation qui interagissent entre eux. L'expression d'un gène ayant l'impact sur l'expression des autres gènes, le bruit d'un gène peut donc se propager en aval dans le circuit génétique. Des niveaux de bruit accrus peuvent conduire à une variation phénotypique significative au sein d'une population, offrant à nouveau une résistance ou une résilience significative de la communauté aux changements environnementaux imposés. Dans cette étude, une façon de perturber la colonie était de moduler directement l'IPTG de l'ARN polymérase. D'autres méthodes comme changement des nutriments et utilisation des antibiotiques, parmi de nombreuses autres molécules, ont également eu un impact sur l'expression de l'ARN polymérase dans le système. Etant donné que l'ARN polymérase est une enzyme impliquée dans la transcription de gênes, la modulation de son activité a le potentiel d'impacter l'ensemble des protéines de système. Ceci étant, la 3ème partie de cette thèse est consacrée à l'étude des effets que les certaines conditions environnementales ont sur le bruit de l'ARN polymérase.

8 BIOMOLECULAR GRADIENTS – DRIVING FORCE FOR SPATIAL PATTERNING AND COOPERATIVE BEHAVIOR IN BIOLOGY

All multicellular complex lifeforms that we know today and that ever existed on Earth evolved from just simple single cell microorganisms that were able to cooperate between each other[3]. Thus, in a way, the cooperation could be thought as one of the prerequisites for the existence and emergence of the complex multicellular lifeforms [4] or as Martin A. Nowak puts it:

> *"Perhaps the most remarkable aspect of evolution is its ability to generate cooperation in a competitive world. Thus, we might add 'natural cooperation' as a third fundamental principle of evolution"* [4]

The question of what initially causes microbes to cooperate is a complex one. To begin answering it, we must first examine the environmental conditions under which the cooperative behavior takes place. One well-known example of microbial cooperation is the consumption of sucrose by the yeast cells. In order to consume sucrose, yeast cells must first break it down to fructose and glucose using an enzyme called invertase. Interestingly, it has been observed that in low-sucrose environments where sharing resources is essential for survival, yeast cell clusters were able to grow better than the single cells [5]. Further experimental evolution experiments on wild type yeast cells grown in the same low-sucrose environment [3] showed that from the initial 12 colonies, 11 developed the opportunity to form clumps. Another study involving two *P.fluorescens* strains and their subjection to ecological disturbances showed similar results [6] . In this study one of the strains had the opportunity to form a complex cooperative community, but on the expense on growing slower (wrinkly strain). Another strain on the other hand could not form the cooperative communities but could grow at maximum possible growth rate (smooth strain). These strains were mixed equally in the growth media. Although the smooth strain outcompeted the wrinkle one, at certain levels of ecological disturbance actually the wrinkled one (the one that could form higher level communities) outcompeted the smooth one.

All of these examples guide us to two conclusions. First, that the evolutionary benefit of cooperation boosts the probability of survival in hostile and changing environments and enables cell to expand, develop and colonize new areas. The second one concerns the role that the environment has in the development of cooperation. To further illustrate the importance that the environment and more specifically gradients play in the formation of gene expression landscapes and cooperation and what implications does cooperation have on a population as a whole, I will firstly focus on microorganisms. Then to highlight how the same modalities of cooperation are omnipresent in different realms of life, I will briefly show the role of cooperation and gradient sensing in development and evolution, cancer and wound healing.

8.1 IMPORTANCE OF BIOGRADIENTS IN MICROORGANISMS

Although the modalities at which microorganisms cooperate are deeply intertwined, we can clearly identify three essential ones – protection, cross-feeding and division of labor. When cells engage in cross-feeding, different cells specialize in producing different metabolic resources vital for the colony as whole and exchange them. Cooperation offers protection from external insults. The outer layers of the microcolony assume the protective role and becomes a shield for the inner cells positioned inside the colony. Lastly cells can take different roles in the colony organization, for instance one fraction of them could develop multiple flagella to quickly explore the space, while a smaller portion of cells could be left behind to colonize new space.

Despite being small, microorganisms show remarkable levels of self-organization and complex behaviors due to imposed nutrient, oxygen and/or chemical gradients. In addition to externally imposed gradients, colonies of microorganisms also impact on and change how their local microenvironment is shaped by their metabolism, consumption of the resources, excretion of potentially useful metabolites and excretion of waste material etc.

Maybe the most prominent and clinically relevant example is the example of bacterial biofilms and dense microcolonies. Aside from the oceans, the biofilm lifestyle dominates in all the other habitats, accounting for almost 80% of all bacterial and archeal surface habitats and approximately 40-80% of the entirety of habitats on Earth [7]. Biofilms are initially formed upon bacterial adhesion to the surface, following with bacterial secretion of extracellular polysaccharide matrix which encloses the growing assembly. Bacteria also form densely packed microcolonies which share multiple characteristics with the biofilms (cooperation, self-organization, resilience to treatment) but lack the extracellular matrix. Living in this kind of assemblies offers bacteria many evolutionary and environmental advantages as it triggers cells within the assembly to differ in their phenotype, leading to heterogeneous bacterial population (a consequence of them experiencing a different microenvironments). A stochastic population model [8] showed that if the bacterial response rate to environmental changes is low, the bacterial populations with a higher degree of phenotypic population variation will have a higher net growth rate compared to populations with lower variation in their phenotypes. This was experimentally shown in highly dense *E.coli* microcolonies grown in a microfluidic chip [9]. In here the authors wanted to see how the cells on the colony level respond to the nutrient switch from glucose to acetate. Before introducing the results of the study, it is worth to first mention that it is known that microcolonies of *E.coli* engage in cross-feeding[10]–[12]. As stated earlier the term cross-feeding means that different cells inside the population specialize in producing and exchanging different metabolic resources which are vital for the survival of the colony as whole.

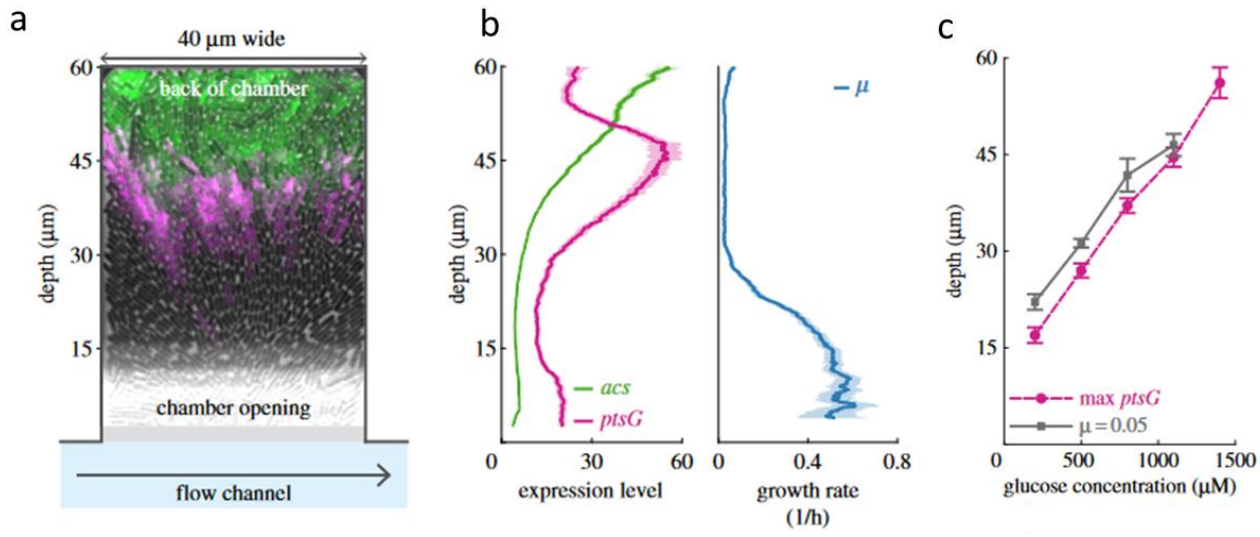

Figure 7.1. Cross-feeding in dense bacterial populations of *E. coli* grown in a microfluidic chip. (a) Microchannel consists of a main channel through which the media flows and the side channel in which bacteria are growing. As bacteria grow they drive the cell outside the chamber into the main channel where they are washed away with the flow. Bacteria near the main channel at the chamber opening have access to glucose and grow at a maximum speed. As we go deeper inside the chamber glucose becomes more and more limiting and cells start expressing high infinity glucose importers *ptsG* and start secreting acetate. In addition to *ptsG* as we go deeper inside the chamber cell take advantage of the secreted acetate by activating the *acs* genes. To illustrate acetate cross-feeding bacteria *ptsG* and *aceB* were tagged. Secreted acetate prevents the cells at the back of the chamber to die off due to lack of nutrients **(b)** Expression levels of ptsG and acs genes and the growth rate as a function of chamber depth. Growth rate is the highest at the channel opening and steadily decreases to zero due to depletion of the nutrients (mainly glucose). After glucose is completely depleted from the media the *ptsG* expression falls to basal levels. *Acs* genes which are involved in secreted acetate consumption continue having higher and higher expression as we go towards the dead end of the chamber. **(c)** Growth rate and ptsG expression depend on the glucose concentration in the media. Figure taken from [10]

What happens with *E.coli* dense assemblies is that cells on the colony edge, where glucose is abundant grow fast and are responsible for colony expansion. They consume the available glucose and partially ferment it to acetate. As we go deeper in the colony, glucose becomes growth limiting. As the glucose becomes a limiting factor, the growth rate steadily decreases and cells start expressing progressively high infinity glucose importer- *ptsG*. After a certain depth inside the colony, the *ptsG* expression drops to zero. This happens at a position where glucose levels are almost entirely zero. At this position cells start expressing genes *acs* and *aceB*, both associated with acetate consumption. It was shown that cells lacking *acs* gene, have considerably lower growth rate in the acetate consuming regions than the WT cells.

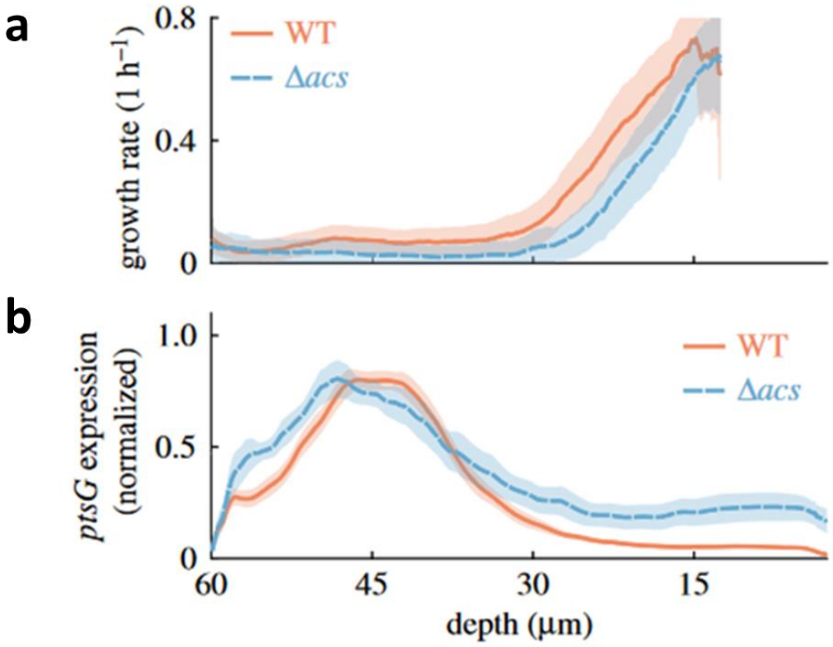

Figure 7.2. Comparison of the WT strain and strain lacking acetate consumption gene. Glucose is abundant at the channel opening. As we go deeper inside the side channel the glucose concentration decreases. As glucose becomes more and more limiting the cells start expressing high infinity glucose importer genes (ptsG genes) which are responsible for the glucose import in low glucose concentrations. Additionally cells partially ferment glucose to acetate which is to be consumed at the far back of the channel which lacks glucose. In this way cells at the front and the back engage in acetate cross-feeding which enables the growth in the region lacking glucose far back inside the side channels. **a)** Comparison of the growth profiles inside the side channel between the two strains. Strain lacking the acs genes is unable to consume acetate and thus cells at the far back of the side channel are not able to grow and engage in cross-feeding. This results in the growth profiles being shifted towards the channel opening, as cells at the back are not able to grow **b)** Limitation of glucose in both strains as seen by glucose importer genes. Glucose importer genes reach maximum expression levels just before 45μm, after which the the ptsG expression starts decreasing. This coincides with the start of acs gene expression which reaches 50% of its maximum value around 45μm (figure 7.1.b). This points to the conclusions that cells in this region start engaging in cross-feeding. Since cells that lack the acs genes are not able to grow, there is a switch in growth profiles as it was seen previously in a). Figure taken from [10]

So how do cells benefit from this? To see this let us return to the nutrient switch study. The study has shown that thanks to the spatially phenotypically structured population, a portion of the population (the acetate feeding one, situated deeper in the colony) successfully continued growing after the switch from glucose to acetate due to their acetate feeding pre-switch phenotype. Furthermore in another study [13] the same team observed spatially structured populations are more tolerant to the applied antibiotic pulse then the ones who aren't. Namely for 50μg/ml streptomycin pulse of 3h parts of the structured population were able to survive the pulse, unlike the bacteria in batch cultures.

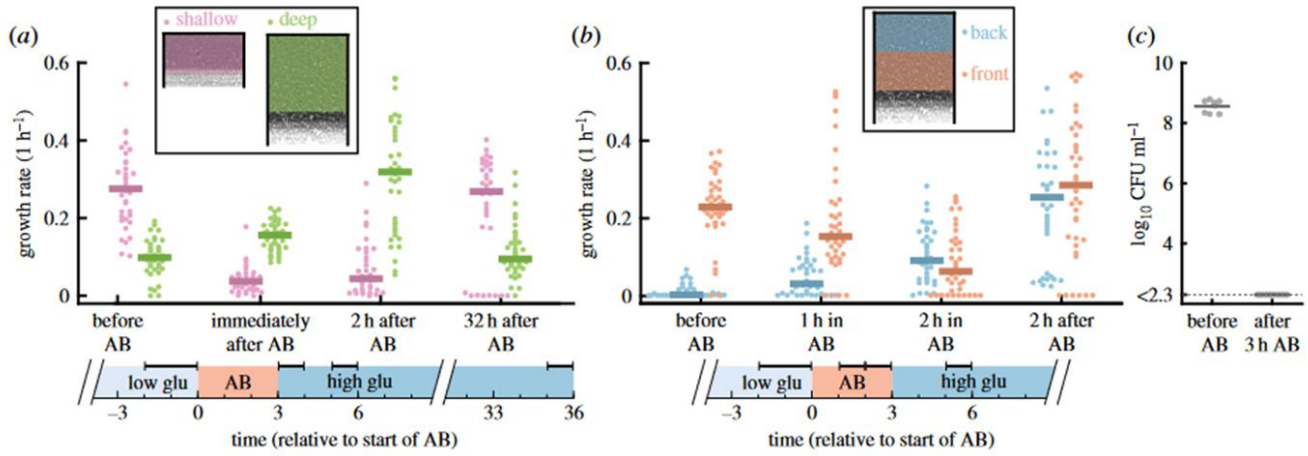

Figure 7.3. Applying 50µg/ml streptomycin pulse of 3h to structured colonies. **(a)** Comparison between shallow and deep chambers. Deeper chambers provide more protection than the shallow ones in the case of an antibiotic pulse. Cells near the channel opening provide a protection against environmental insults and protect the cells behind. **(b)** growth rate inside the side channel at different time points during the antibiotic pulse. As cells in the front lower down the growth rate due to the antibiotic treatment, more nutrients are able to penetrate deeper inside the side channels. Consequently cells at the back experience transiently higher growth rates then prior to the impulse **(c)** cells in well mixed cultures were not able to survive the antibiotic pulse, while cells both in shallow and deep chamber were. Figure taken from [13]

This goes in line with what was already known that biofilms and densely packed bacterial assemblies are more resilient to antibiotic treatments, as the outer, faster growing layer protects the slowly growing cells inside the colony.

Contrary to protection role in sheltering the interior cells, the outer cell layer can potentially starve them through nutrient consumption. Extreme starvation of the interior cells, could be detrimental for the entire colony, as the interior cells are critical for the colony survival in the case of an external environmental shock. An interesting way of preventing this can be found in gram positive bacteria, *Bacillus subtills*[14], [15].

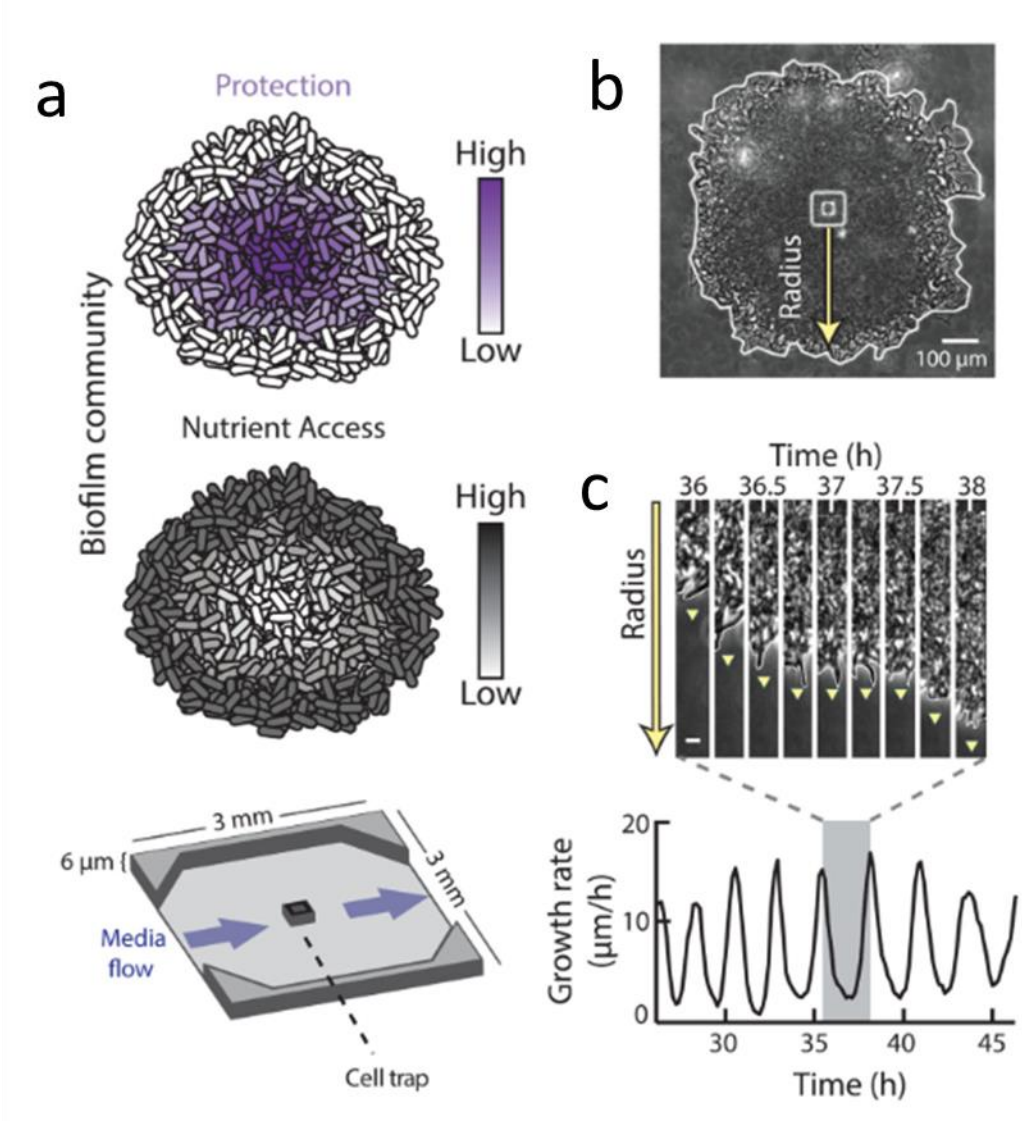

Figure 7.4. Cooperation between the outer and the inner part of the biofilm in *Bacillus subtilis*. The outer layer protects the cells inside the biofilm community, but can also potentially starve them through depletion of the nutrients. In the case of an environmental insult the inner cells are crucial for the colony survival, thus it is of high interest for the colony survival to keep these cells viable. In order to prevent this, the biofilm experiences oscillations in the growth rate. When the cells at the colony front stop growing, it enables the nutrients to penetrate to the insides of the biofilm. The cause of these oscillation was shown to be ammonia. In *B.subtillis* glutamine synthetase combines glutamate and ammonium to produce glutamine, a metabolite essential for the biomass production and growth. Ammonium limitation was found as a sole source for the growth oscillations in the peripheral cells. The outer cells depend on production of the ammonia by the inner cells, thus the periodic halting in the growth rate comes as a results of inhibiting the ammonia synthesis in the inner cells of the biofilm community as a consequence of nutrient (glutamate) deprivation due to the growth of peripheral cells (which deprives the interior of much needed nutrients). Addition of ammonia in the extracellular media stops the peripheral growth oscillation. The oscillations were continued once the extracellular ammonia was removed from the media. Figure taken from [14]

In here authors found that the growth of the periphery of the colony halts periodically, increasing thereby the nutrients for the inner part of the colony comprised of the cells critical for the survival of the entire population. The cause of this oscillations was identified to be nitrogen limitation, and more specifically ammonium. In *Bacillus subtills* (and other organisms as well) glutamine synthetase combines ammonium and glutamate to produce glutamine- an essential molecule for biomass production and growth. Cells usually consume extracellular ammonia and since ammonia itself was not present in the media, cells in the interior and periphery started engaging in metabolic cross talk. Cells in the interior took the role of ammonia producers for the cells on the outer layer of the colony. When ammonia was supplemented to the media at the concentration of 1mM the periodic halting of the growth rate stopped. As soon as the ammonia was removed, the growth halted. Furthermore it was shown that the resilience of the entire community is severely impacted when making the periphery cells produce ammonium. Production of ammonium in outer layer was made possible by making the cells express an enzyme- glutamate dehydrogenase, which starting from glutamate (component crucial for biomass growth) produces ammonium. This effectively deprived the inner layer from nutrients needed for cellular growth which led eventually to cell death

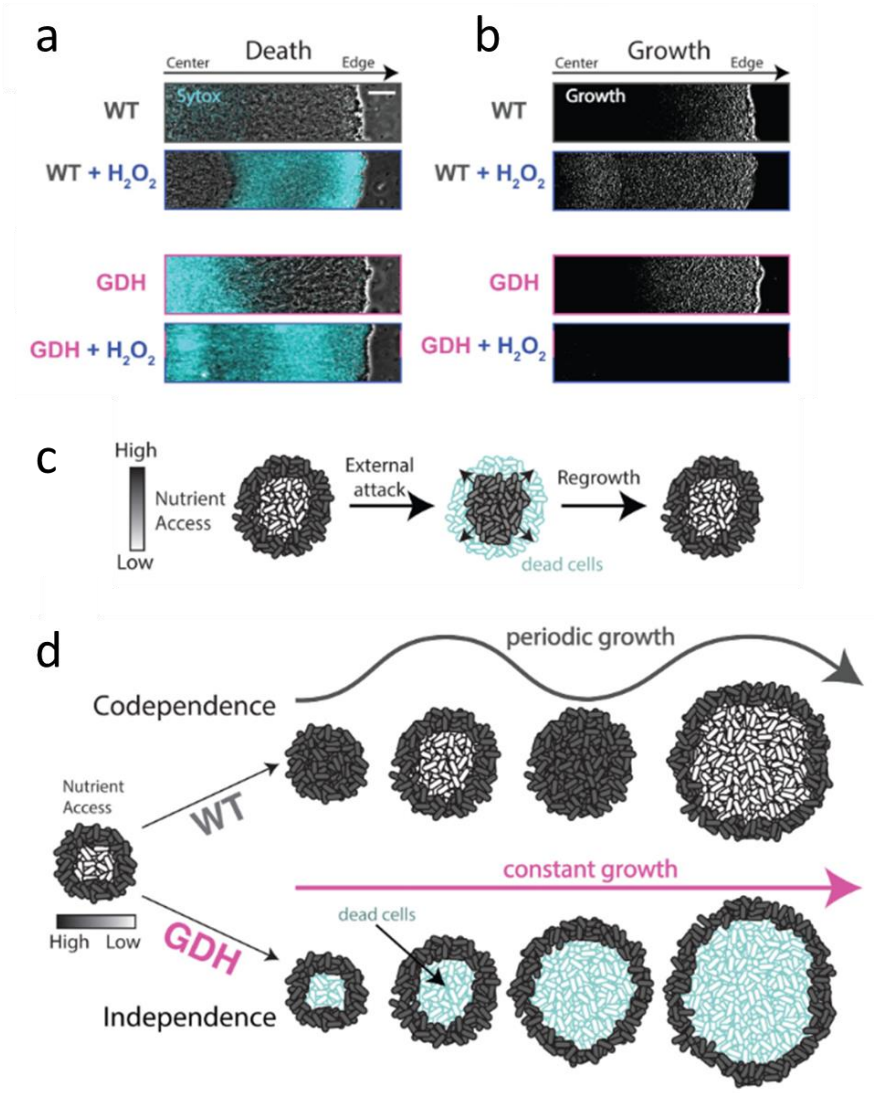

Figure 7.5. Colony survival while encountering an environmental insult. (a) Viability of the inner cells of the biofilm is crucial for cell survival when encountering environmental insults. Biofilm was stained with Sytox dye which stains dead cells. Two strains were used in this experiments- the WT whose periphery cells exhibit growth oscillations and the GDH modified where by the inner cells overproduced ammonia which resulted in lack of oscillations thus in continuous growth of the periphery cells. When cells are continuously expanding without oscillations the inner part of the biofilm becomes deprived of nutrients and eventually dies off. Adding hydrogen peroxide to the media causes cellular death in the periphery layer **(b)** Viability of inner cell is crucial for the biofilm survival. Applying hydrogen peroxide in GDH strain caused the collapse of the entire community. WT strain which experienced the same stress was able to survive the stress as inner cells were viable. **(c)** When WT cells which experience growth oscillation were subjected to external attack the outer layer of the biofilm community dies off. Inner cells which are still viable regrow and reestablish the colony. **(d)** GDH strain that experienced constant growth at the cell periphery which caused severe cell starvation and consequently the cellular death of the inner part of the biofilm community. Figure taken from [14].

Cross-feeding involving sugars was also spotted in *Pseudomonas aeruginosa*[16], a bacterial pathogen responsible for chronic pulmonary infections among patients suffering from cystic fibrosis[17] . What the authors in [16] have shown is that for the biofilms grown on pyruvate, the cells at the bottom in anoxic zone convert pyruvate into lactate which is then later used by cells in the upper part of the biofilm in the oxic zone as a carbon source. As lactate is one of the metabolites most commonly found in the lung cystic fibrosis patients [18]–[20], as authors in [16] mention, it might be plausible that this type of cross-feeding is what enables *Pseudomonas aeruginosa* to colonize and persists inside the patients lungs.

Besides carbon source cross-feeding, which seems to be a feature that has been retained across the bacterial species, in the pulmonary pathogen *P.aeruginosa* another type of cross-feeding involving electron receptors was discovered[21]. The study showed that molecules named phenazines are produced by the cells situated in the upper, oxygen richer, part of the biofilm. Phenazines are then oxidized and serve as an electron acceptor by the cells on the bottom of the film which don't have access to oxygen. They in this way support metabolic activity deep in the anoxic zone of the biofilm. It was shown both by microelectrode measurements that phenazine pool was indeed reduced deep in biofilm. Furthermore by looking at the expression of GFP based reporter used for intracellular presence of oxidized phenazines[22], the maximum was found also in oxygen depleted area. This showed that indeed cells at the bottom of the biofilm take advantage of phenazines and perform their reduction. It is noteworthy that despite its reliance on oxygen for chromophore formation, green fluorescent protein has been shown to be a reliable indicator in hypoxic regions within cells, as evidenced in [22] as well as another study focused on tumor hypoxia [23]. In order to determine whether the reason for this is to support metabolism, authors looked to visualize global metabolic activity using deuterium. Isotope incorporation technique showed two peaks of global metabolic activity- One in oxygen rich zone, and one in oxygen depleted zone, where phenazine were reduced. What further proved the hypothesis that phenazines are indeed responsible for the metabolic activity of the oxygen depleted zone is the fact that when performing the isotope incorporation technique on the cells strain which wasn't able to produce phenazines, the peak in the oxygen depleted zone was gone. Additionally the strain lacking the capability of producing phenazines was more susceptible to antibiotics and have made biofilm colonies wrinkle more in order to increase the surface so more cells have access to the oxygen[24].

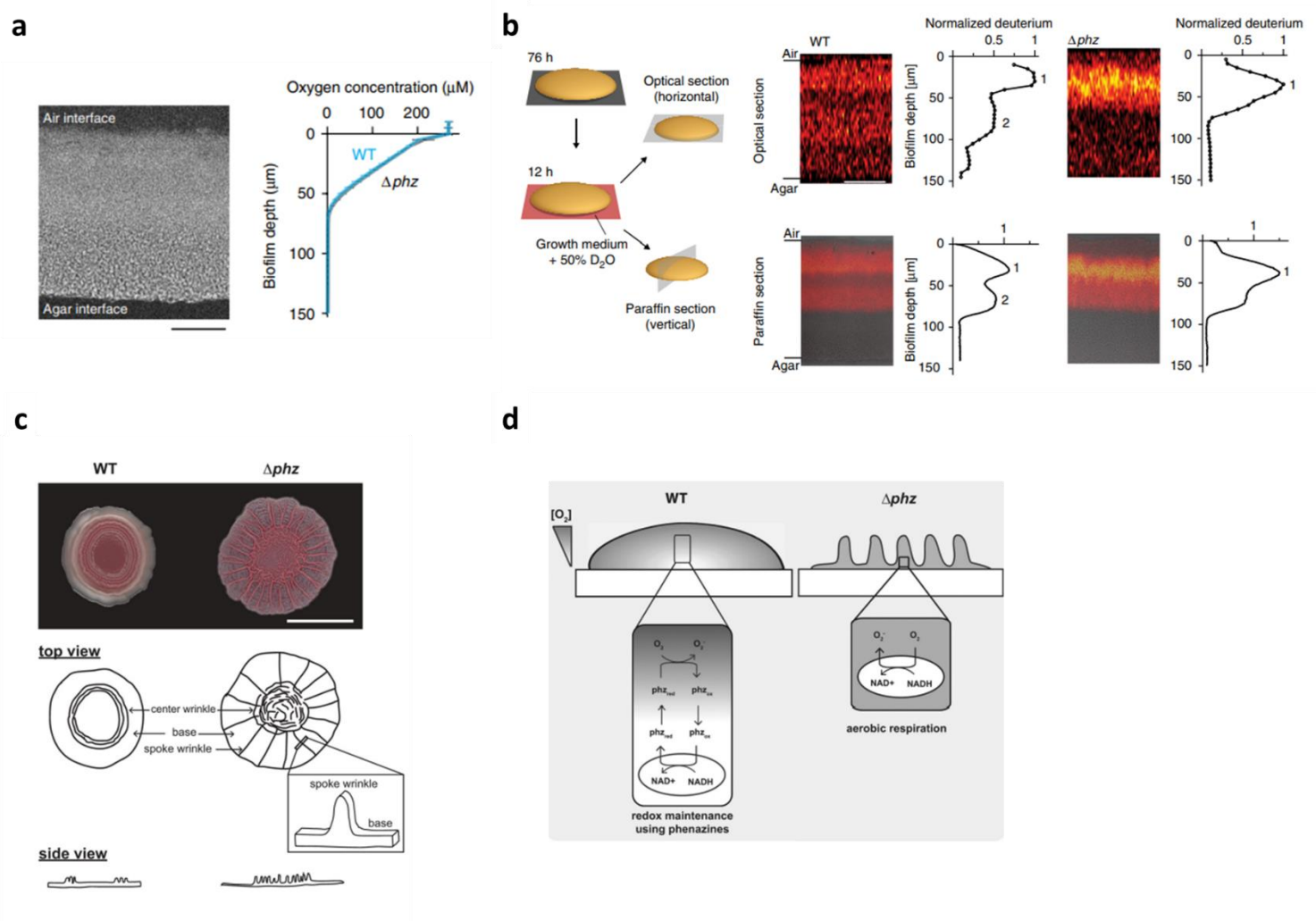

Figure 7.6. Cross-feeding involving electron receptors in biofilms of *P.aeruginosa*. (a) Biofilms of *P.aeruginosa* experience oxygen gradients. Cells at the outskirts of the biofilm near the air interface experience oxygen rich environment. As we go deeper inside the biofilm, oxygen becomes more and more depleted. To support metabolic activity, cells in the oxygen rich environment produce molecules called phenazines. Before transitioning to the anoxic zones of the biofilm, phenazines get oxidized in the oxygen rich layer. Oxidized phenazines provide a mean to support metabolic activity in oxygen depleted areas of the biofilm community. For imagining purposes phenazines were tagged with an appropriate GFP reporter **(b)** Deuterium labeling to detected the metabolic activity inside the biofilm. WT strain of *P.aeruginosa* showed two distinct peaks- one in oxygen reach area, and the other one in anoxic zone. Strain lacking phenazines Δphz was also examined with deuterium labeling to asses global metabolic activity. Unlike the WT strain, the Δphz strain lacked metabolic activity in the anoxic zone of the biofilm. Results were supported by the microelectrode measurements. **(c)(d)** Biofilms from strains lacking phenazines Δphz wrinkle more compared to the WT strain. Wrinkling increases the surface of the biofilm exposed to oxygen. Figures adapted from [24] and [21]

Cells experiencing the same microenvironment and cells involved in local cell to cell interactions also yield correlated spatial gene expression profiles. Our team has previously conducted an analysis of the spatial expression of genes involved in glucose metabolism in yeast exposed to varying glucose concentrations in the media. The analysis showed that the colony's structuration comes as a consequence of the activation of genes involved in physiological adaptation, which are all regulated by the availability of nutrients [25]. Namely here our team has used a microfluidic device that enabled the observation of a yeast monolayer over extended periods of time. It consisted of multiple side chambers (where yeast cells grew) and a main channel through which fresh media was supplied. Eventually once cells completely filled out the side chamber, a quasi-stationary steady state emerged with stable glucose gradients and stable gene expression patterns. On figure 7.8 we can see the gene expression gradient of glucose transporters expressed in low (HXT7) and high (HXT1) glucose conditions is various experimental conditions.

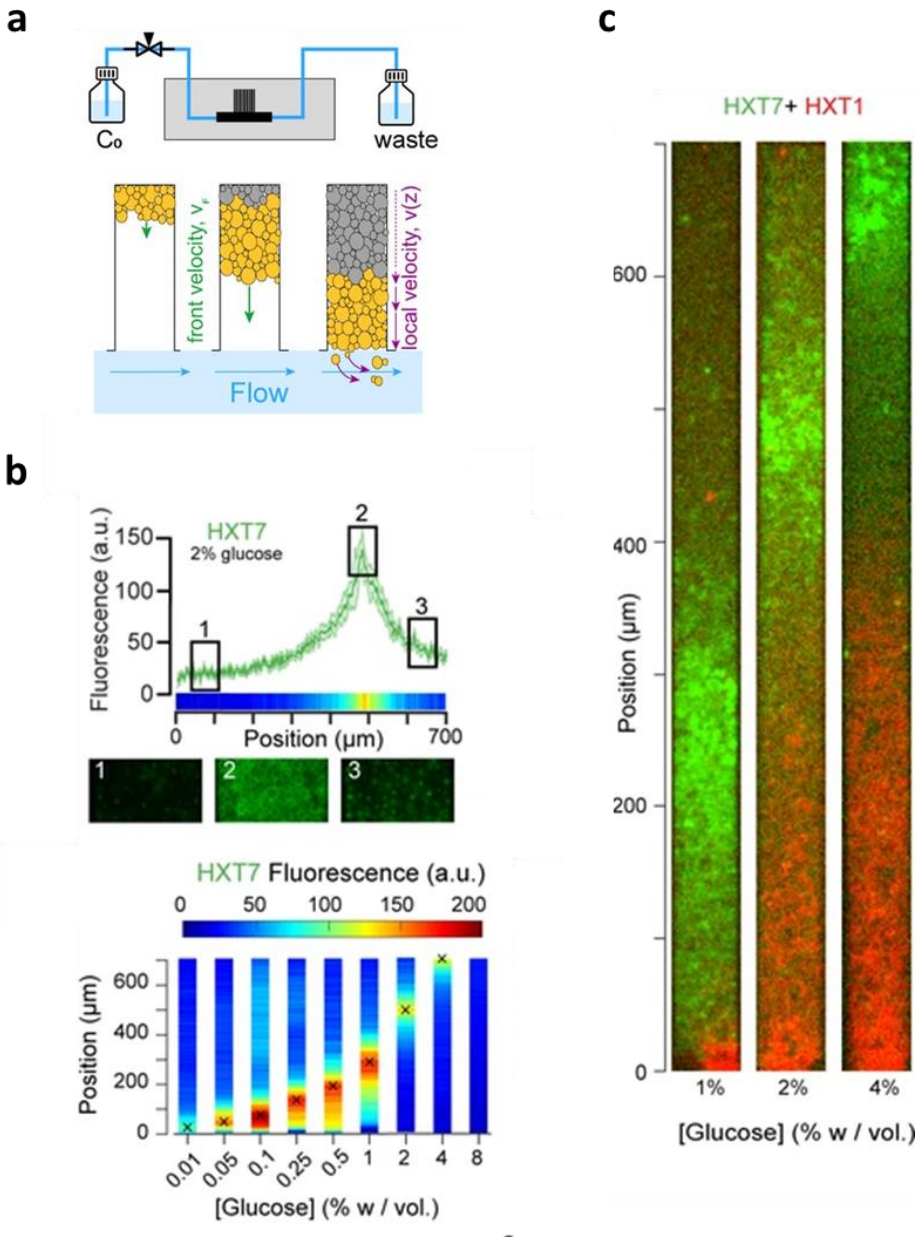

Figure 7.7. (a) microfluidic device used to observe spatial gradients of gene expression in yeast. Cells are positioned in the side chambers which are perpendicular to the main channel through which fresh media is supplied. Cells at the colony front experience environment rich in nutrients compared to the cells towards the dead end of the chamber. As cell fill out the channel quasi-stationary steady state with stable glucose gradients and spatial gene expression profiles is formed. **(b)** Upper figure represents the gene expression profile of the glucose transporter expressed in low glucose HXT7 in media supplemented with 2% glucose. Lower figure represents the same transporter but with different concentration of the glucose in the media. With increasing concentration the peak of gene expression transitions towards the dead end of the channel. **(c)** Two glucose transporters one expressed with high glucose (HXT1) and the other one in low glucose conditions (HXT7). Increasing glucose concentration in the media moves upward the boundaries of gene expression profiles so that both boundaries go deeper inside the colony due to increased amount of glucose felt in the side chambers. Figure taken from [25].

For each condition stable gene expression landscape correlated with the growth rate was reported. Furthermore high degree of spatial correlation among different groups of genes and different conditions was seen. This effectively showed that depending on the glucose concentration we could divide the colony into two distinct regimes – actively growing population and growth arrested one.

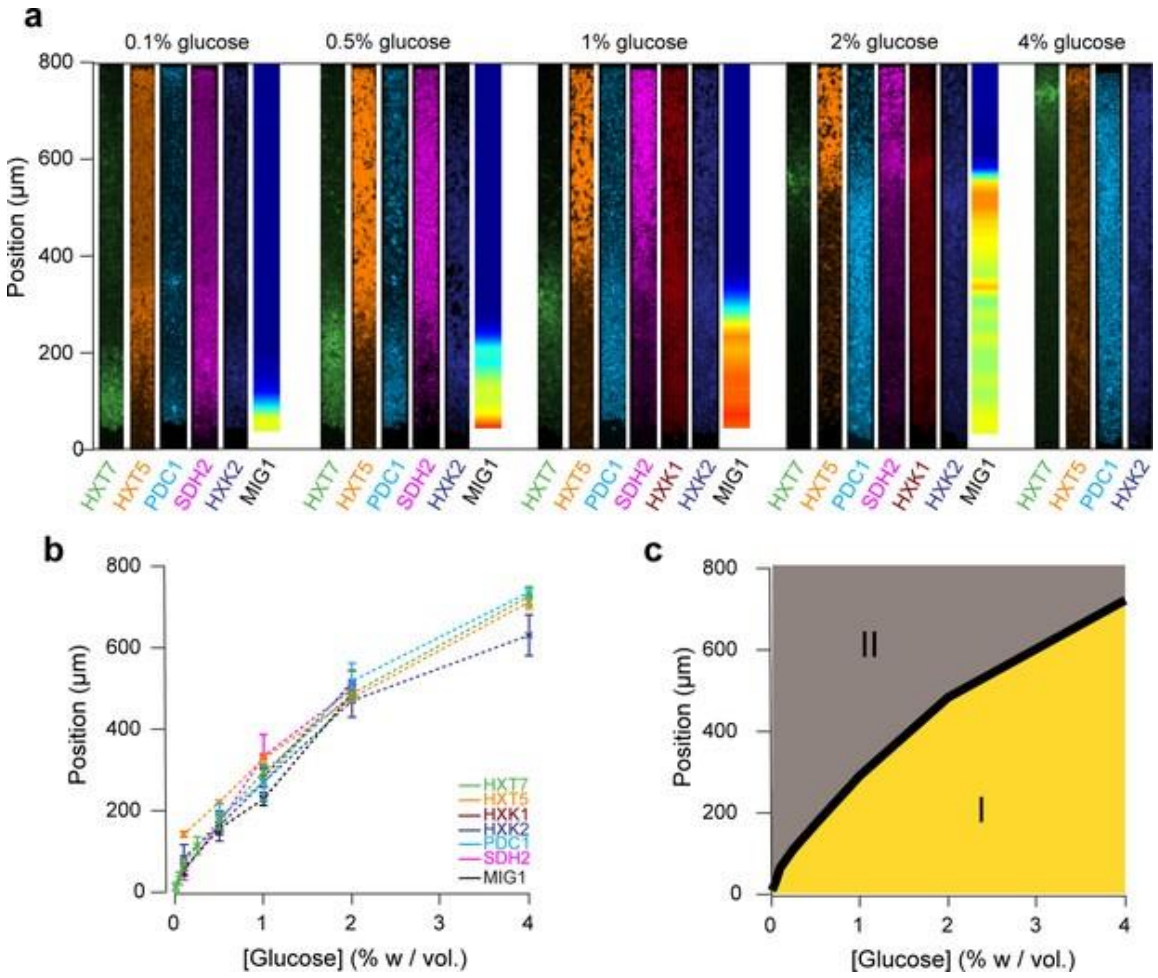

Figure 7.8. Gene expression landscapes. **(a)** Landscape of different genes in different experimental conditions involved in metabolic state responses (SDH2-involved in cellular respiration, subunit of mitochondrial respiratory chain complex; PDC1-one of the key enzymes in alcoholic fermentation), glucose transporters (HXT7;HXT5), metabolic enzymes (HXK2-expressed when yeast cells are grown on a fermentable media such as glucose. Switching to nonfermentable media, makes HXK2 repressed) produce highly spatially organized patters. **(b)** Spatial gene expression profiles are highly correlated. Data describing the evolving positions of the peak of gene expression and the evolving position of a high-low gene expression switch switching (and low-high) with the rising glucose concentration fall on the same curve across different genes. **(c)** Two distinct regime could be determined depending on the glucose concentration – regime I bellow the curve, which consists of actively growing cells which consume glucose, and regime II above the curve which consists of cells in growth arrested regime. Figure taken from [25].

So far I have mentioned some of the ways how gradients impact spatial patterns and self-organization in microbial communities, but I haven't mentioned another important example, the chemotaxis. Chemotaxis represents the ability of microorganism to adjust and direct their movement in response to chemical gradient. The chemical gradient can either direct the movement towards it (chemoattractant) or can drive the movement away from chemical gradients (chemorepellent). Chemotactic response is extremely sensitive, for instance *E.coli* chemotactically responds to as little as 10nM aspartate-concentration (which corresponds less than 10 molecules of aspartate in the volume of the *E.coli* cell!) [26]. While a lot is known of how the chemotactic behavior is regulated, the ecological role of chemotaxis is still not completely understood [27]. It is mostly accepted that the chemotaxis is used by the cells to find food [27][28]. Here the chemoattractants (chemicals whose gradient attracts the bacteria towards them) direct the cells movement alongside the gradient, towards the higher concentration of chemoattractants. Although the flagella expression machinery indeed starts being expressed at lower growth [29], not all chemoattractants are good source of metabolites and energy nor all nutrients are good chemoattractants. Some new studies point out the importance of chemotaxis for the colonization of the new territory [30] [31]. The study in [30] pinpoints one of possible ecological role of the chemotaxis- boosting bacterial range expansion by helping bacteria to colonize new territory. It was shown that adding to agar small quantities of chemoattractants such as serine or aspartate made *E.coli* bacterial populations expand twice as fast as opposed to those who weren't supplemented with it and which only expand due to random diffusion and growth. The reason of this faster expansion of the colonies supplemented with serine and aspartate lies in the fact that the cells at the edge of the colony begin to express flagellar proteins and experience chemotactic motion. As a result of them chemotactically moving, bacteria rapidly expand in space. As they expand in space, some of the bacteria divide and leave their offspring daughter cells behind. While the chemotactically activated cells undergo rapid expansion and occupy new space, they do not fully consume the available nutrients, instead, they leave behind the nutrients to be used for the daughter cells which have the role to grow and colonize the newly acquired space. Opposed to this strategy is the colony expansion by simple growth and diffusion, where cells expand as they consume resources, leaving behind a nutrient depleted area, in which cells do not grow.

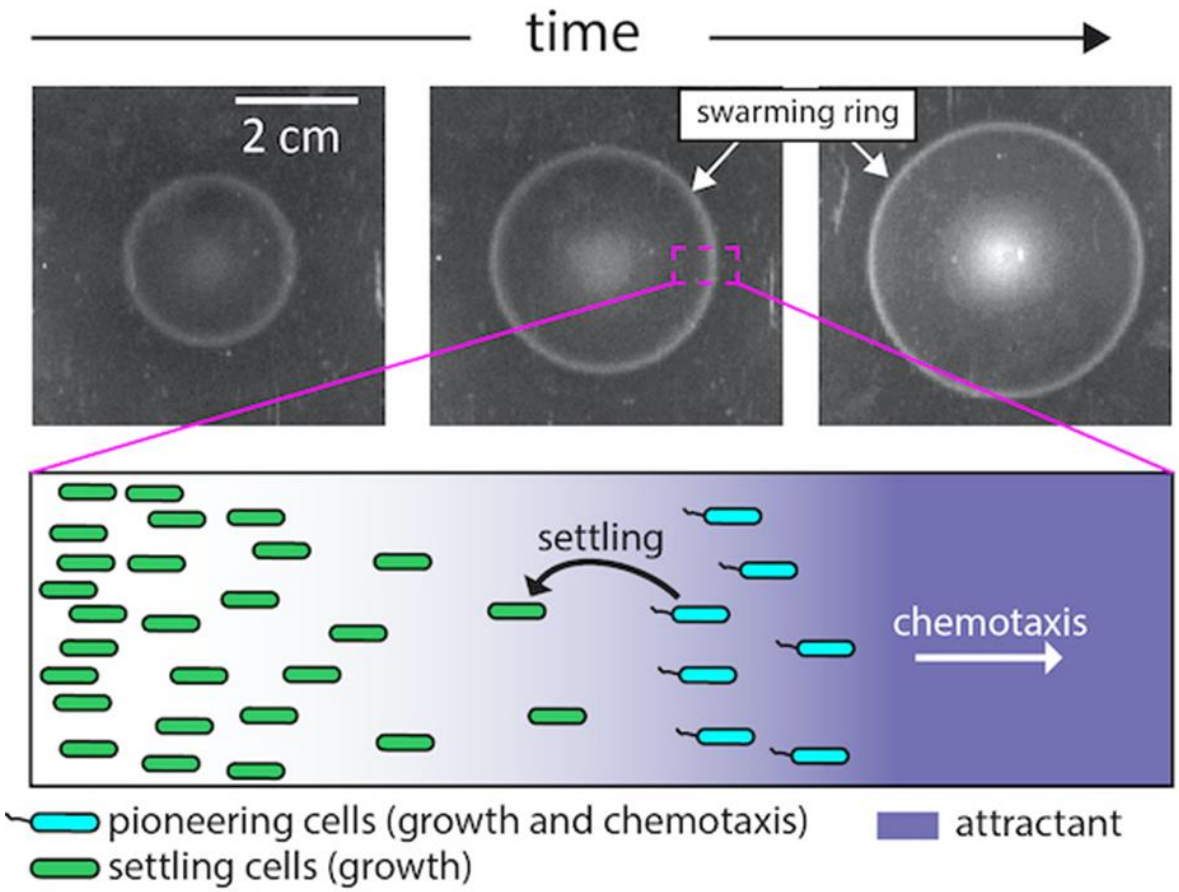

Figure 7.9. Importance of chemotaxis in colonization of the new territory. Addition of small quantities of serine or asperate to the agar medium made E.coli populations expand as twice as fast compared to those who weren't supplemented with these chemoattractants. Cells at the outskirts of the colony experiencing chemotaxis have a pioneering role. They express flagella and expand into the new space. In the process of expansion some of them divide, leaving their offspring to colonize new areas. Figure taken from [32]

It is interesting to mention another study [28] that explored chemotaxis and how cells were able to move collectively as a group by utilizing the oxygen gradient formed by the cells. In order to chemotactically move, *E.coli* needs to metabolize the chemoattractant- aspartate. To metabolize aspartate cells need to consume oxygen. What was shown was the fact that the formation of the oxygen gradient inside the traveling band helps cells in the back to experience more of the chemical attractant. The center of the travelling band has the highest population density and experiences oxygen limitation. Since the cells in the center of the band are not growing, due to oxygen limitation, they don't consume the aspartate. This helps cells in the back to experience more aspartate concentration which in turn enables them to keep up with the front and maintain their collective movement as a group.

In the same manner as *E.coli* in *Pseudomonas* the pioneers in dispersal and colony expansion are the swarming cells positioned at the colony front. In [31] the authors took wild type cells and hyperswarming cells (cells that have a mutation on the fleN gene which gives them multiple flagella, consequently resulting in 100% better dispersal compared to the wild type strain) of *Pseudomonas* and mixed them in same concentration on agar. The hyperswarming strain came from evolution experiments and its hyperswarming capability came at a cost of having a lower growth rate in well mixed conditions (approximately 10% lower compared to the wild type). Interestingly when compared to the WT cells on agar where gradients play a role, they outcompeted the wild type cells, despite the lower growth rate. In well mixed liquid cultures this was not observed. Besides finding food and colony expansion, the chemotactic behavior is also implicated in the mushroom like biofilm formation in *Pseudomonas*[33]. Here the stalk of the tree is formed by cells who have downregulated their motility and the cap of the mushroom is formed by motile cells, as they climb and aggregate on the top of the nonmotile cells, presumably because of the nutrient gradients.

8.2 COOPERATION AND SPATIOTEMPORAL GENE EXPRESSION LANDSCAPES IN OTHER SYSTEMS

In the previous section we have seen how microbial cells read and interact with various gradients (nutrient, chemical, oxygen etc.). In this chapter for completeness I would like to expand on the topic and cover other systems besides microbial ones.

As said before gradients are a powerful driver for spatial heterogeneity. Besides heterogeneity, they can also convey positional information-for instance in previous chapter depletion of nutrients at a specific depth inside the colony activates ptsG gene expression in *E.coli*. Multicellular systems have brought exploitation of gradients to a whole new level as it could be seen in the development of an embryo. In early embryo stage all the cells are essentially equivalent and have the potential to differentiate to any of the form possible[34]. As time progresses cells at a certain position further differentiate into a specific type. This identification to which cell type a certain embryonic cells needs to differentiate is done through chemical signaling factors called morphogens. Morphogens act as providers of spatial information[35] and are small diffusible molecules. They are a key regulator of the development of an embryo and form a gradient within the developing tissues. Cells encounter and sense the local concertation of the graded morphogen leading to differential gene expression of the cells which eventually leads to cell completely differentiating from each other. Large number of morphogens have been so far detected such as Bone Morphogenic Proteins (BMP), Bicoid (Bic), Sonic-Hedgehog, DPP and activin[36]. Of course additional mechanism besides morphogen might play a role such as in establishing the activation pattern of the developmental genes, for example such that in Hunchback gene [37]. Gradients might have also played as a target for evolution as seen in [38] with Bone Morphogenetic Proteins (BMPs). BMPs represent a morphogen which could be found across species, ranging from *Drosophila* to modern day humans. In this study authors focused on BMP morphogens in two species of flies– *Megaselia* and *Drosophila*. Namely dynamics of the BMP in both species are initially similar, but they start to differ in later developmental stages. In early gastrula *Megaselia's* gradient broadens compared to the one of *Drosophila*, which remains static. This is due to a genetic change in the egr-positive feedback loop which happened between the two fly species. The change of width has had a big evolutionary effect on further cell development. While both cells experiencing *Megaselia's* and *Drosophila's* BMP gradient develop into extraembryonic tissue- which has a protective role for the embryo, *Drosophila's* static BMP gradient enables the cell to differentiate into a single extraembryonic tissue-amnioserosa, while *Megaselia's* cells with their sensed gradient has retained the formation of two distinct tissues – amnion and serosa.

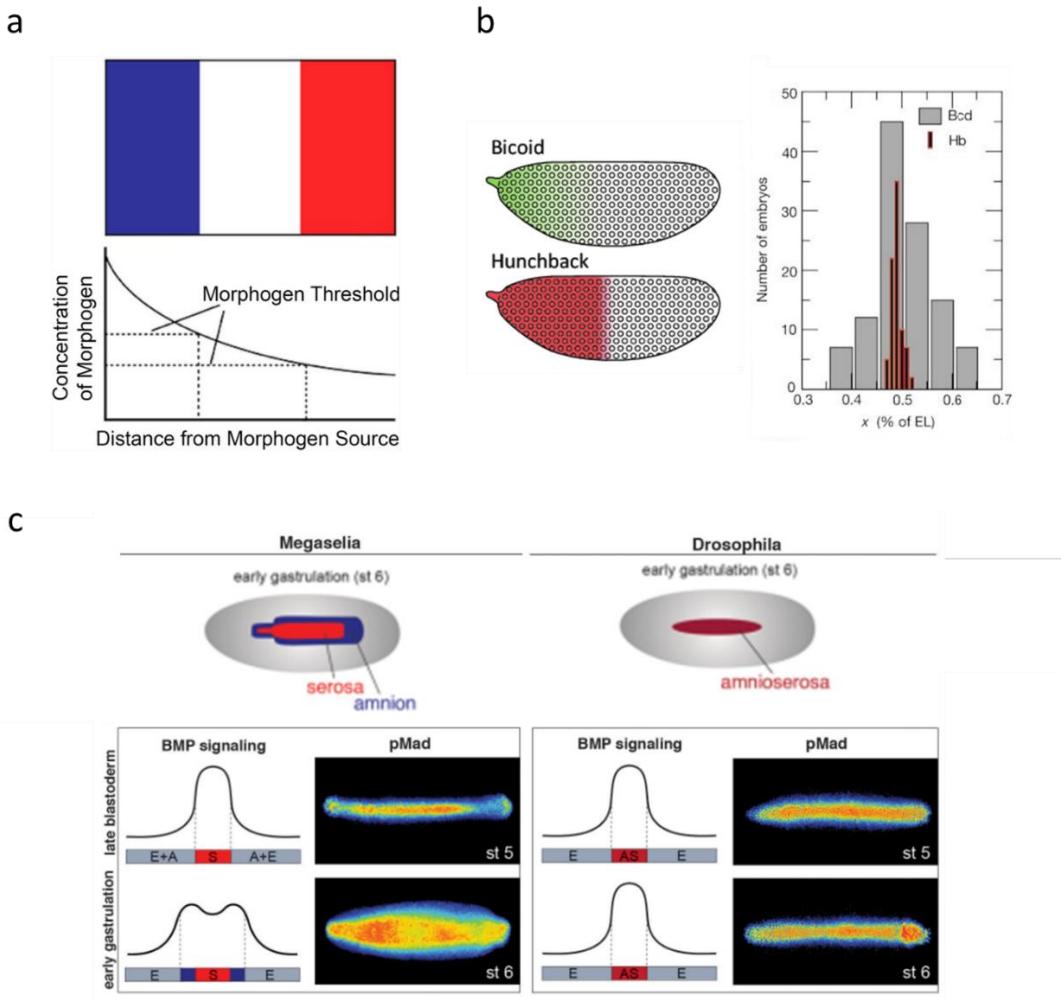

Figure 7.10. Importance of gradients in development - morphogens. **(a)** Morphogens are diffusible molecules which form a gradient in developing tissues. While cells are initially the same, as time passes cells encounter and sense the local concertation of the morphogen. This leads to differential gene expression and consequently to cellular differentiation based on the sensed concentration of the morphogen. **(b)** Example of the Hunchback gene expression activated by a Bicoid gradient. In early embryonic development of Drosophila embryo a Bicoid gradient is formed. As a response to this gradient the downstream Hunchback gene gets presumably activated in a threshold manner. Cells measure the local concertation of the Bicoid and if this concentration is higher then a specific threshold value, cells are going to activate the Hunchback gene expression. Intriguingly the hunchback gene expression pattern was astoundingly reproducible, compared to variability of the Bicoid morphogen who presumably made it. This suggests that other processes, besides morphogens might play a role in Hunchback gene expression. **(c)** Gradients can also be an evolutionary target as seen in two fly species *Megaselia* and *Drosophila* experiencing the BMP gradient. Cell experiencing BMP gradient develop into extraembryonic tissue- which has a protective role for the embryo. Initially in both fly species BMP gradients look the same, but over time the BMP gradient of *Megaselia* changes. The difference between the two species is due to the genetic change in the egr-positive feedback loop. As a consequence *Megaselia's* cells with their sensed gradient has retained the formation of two distinct tissues – amnion and serosa while *Drosophila's* static BMP gradient enables the cells to differentiate into a single extraembryonic tissue-amnioserosa. Image taken from [38]

Another common example of how gradients impact cellular organization is the example of hypoxia in the tumor microenvironment. As cancer progresses, cells rapidly proliferate, increasing the volume which tumor occupies. A Tumor (as the rest of the body) gets its oxygen through blood vessels. Since the rate of proliferation surpasses the rate of creating new blood vessels (angiogenesis), the tumor "outgrows diffusions limits of the local blood supply"[39]. This leads to hypoxia and a segregation of cells into two types:

-aerobic cancer cells (outer layer of cells, closer to the blood vessels and capillaries which have access to oxygen)

-hypoxic cells (cells situated deeper in the tumor tissue deprived of oxygen)

Both of them engage in cellular metabolic crosstalk involving lactate as described in [40]. The lactate crosstalk is of huge interest to cancer research. This is nicely depicted in [41] which elegantly summed up work from [42]–[44]

> *"…lactate is drawing the attention of the cancer research community, not as a byproduct of fermentative glycolysis, but more as a metabolic modulator at the interconnection between different cancer hallmarks including, sustained angiogenesis, evasion of immune surveillance and reprogramming of energy metabolism. "* [41]

Hypoxic cells engage in glycolysis and consume glucose to produce ATP and maintain their integrity. Compared to respiration, glycolysis is energetically inefficient (glycolysis provides 2 ATP per glucose, while on the other hand respiration provides 38 ATP per glucose). It has been shown that tumors in which cells engage in glycolysis are linked to a worse health outcome. Namely this comes as a result of glycolytic cells secreting lactate which causes a shift in the pH of the tumor microenvironment towards an acidic one. This acidic environment facilitates the evasion of the immune system by the tumor and promotes angiogenesis, which is the process of developing new blood vessels that supply the tumor with essential nutrients and oxygen[45]. Additonally lactate promotes the tumor adaptation to hypoxic conditions. Study conducted in [40] focused on lactate crosstalk inside the tumor microenvironment. As stated before as a byproduct of glycolysis hypoxic cell secrete lactate which is then transported into the aerobic cells through MCT1. In aerobic cells, which have access to oxygen, the lactate gets converted to pyruvate and undergoes oxidative phosphorylation in mitochondria. In this way more glucose penetrates deeper inside the tumor microenvironment. When MCT1 was deleted, the cells in the oxygen rich area switched to respiration since they couldn't use the lactate anymore, which lead to cell tumor necrosis in the anoxic part of the tumor microenvironment.

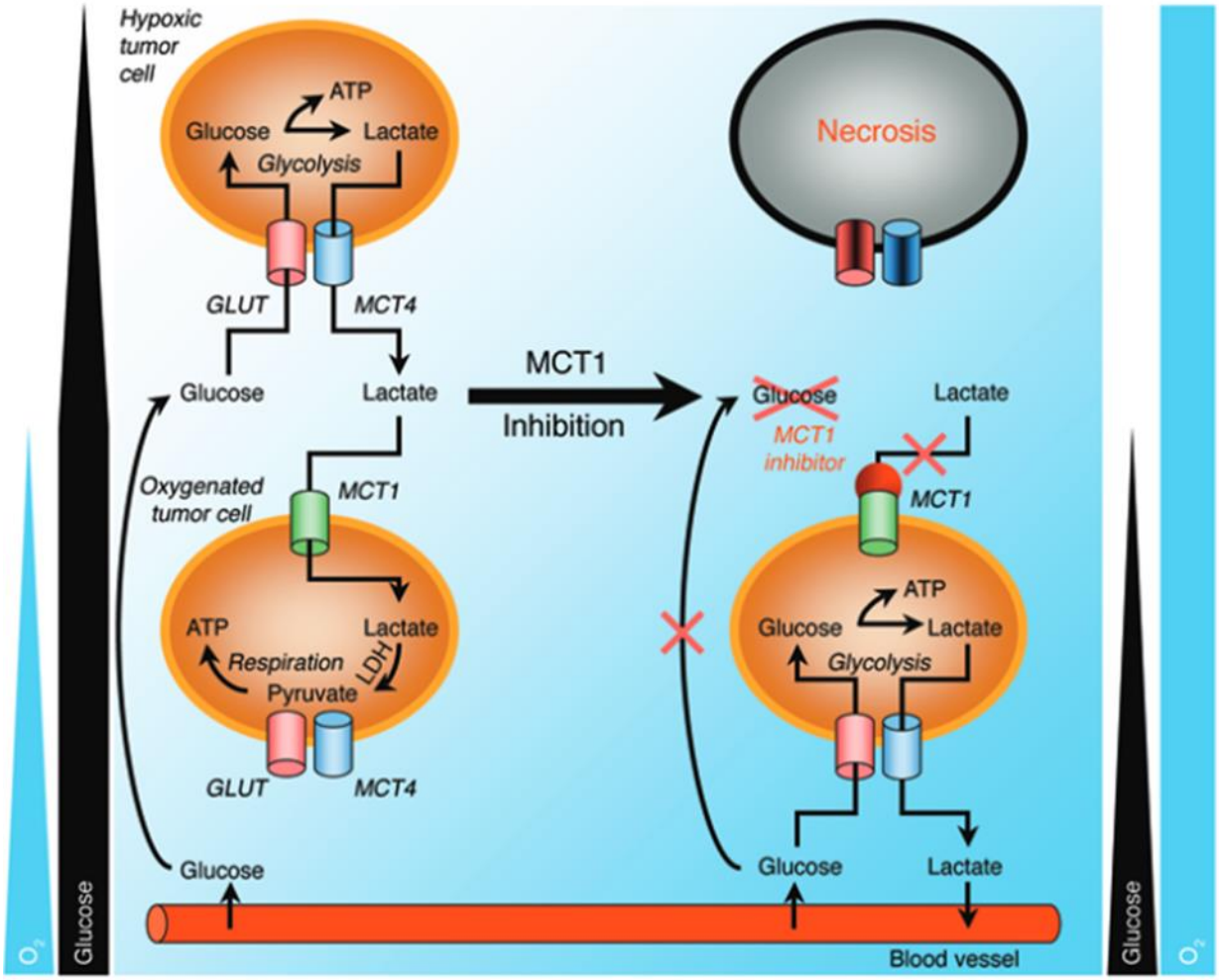

Figure 7.11. Importance of lactate cross-talk in tumor cells. Hypoxic cells in the tumor microenvironment engage in glycolysis and depend on the glucose to produce energy. As a products of glycolysis they secrete lactate which is up taken by cells in aerobic zone near the blood vessels, through MCT1. Oxygenated cells further convert lactate to pyruvate which later undergoes oxidative phosphorylation in mitochondria. In respiration cycle, lactate is more preferable carbon source then glucose. This helps glucose gradients to penetrate deeper inside of the tumor microenvironment, thus reaching hypoxic tumor cells. Deletion of the MCT1 disables the oxygenized tumor cells to consume lactate. As a consequence they switch from lactate oxidation to full glucose respiration. This switch leads to the increased consumption of most of the glucose resources by aerobic cell, which narrows down the glucose gradient, consequently leading to tumor cell death in the hypoxic zone due to starvation. Survived cells decrease their oxygen consumption, thus expanding the oxygen gradient. Figure taken from [40]

These results were further supported by the results presented in [46]. In this study, the researchers carried out a knockdown of mitochondrial ribosomal proteins (L28 and L12) and cytochrome oxidase in pancreatic tumor cells. The objective of this approach was to reduce the mitochondrial activity and, consequently, the process of respiration, which occurs within the mitochondria. This knockdown did indeed result in the decrease of respiration and the subsequent increase of glycolysis, which consequently resulted in the increase of the tumor growth in vivo. On the other hand increasing mitochondrial metabolism, and thus respiration (by expressing the UCP1 protein or by pharmacologically treating the animals with dichloroacetate-DCA) showed increased levels oxygen consumption, increased tumor hypoxia and slowed down growth.

Going further on the importance of the oxygen gradients, one of their widely known role is in normal wound healing [47]. Wound healing repair process requires increased amounts of energy, which is being provided by ATP. Higher yields of ATP are enabled by the oxidative phosphorylation in mitochondria. A key substrate for this are oxygen and it's radical derivatives-reactive oxygen species (ROS), who have been reduced with added electrons, to make them more reactive. For instance, it was reported that the gradient of H_2O_2 generated by Duox activity in epithelial cells in zebra fish is required for the quick recruitment of the leukocytes to the wound[48]. This gradient stimulated recruitment of leukocytes is based on increasing the directionality of leukocyte migrations and tissue infiltration.

With this example I will be concluding the overview of how other cells besides microbial ones interact with gradients. The idea of these two sections was to see how living systems cope and operate when exposed to various chemical or nutrient gradients. Now in the next section we will be returning back to system of interest-microbes and the questions that we wish to pose in this thesis.

8.3 CLOSING REMARKS AND RESEARCH QUESTIONS DRIVING THIS THESIS

Considering that chemical and nutrient gradients are instrumental in creating heterogeneity within a colony and are representing a driving force for the development of cooperation and cellular organization, I became interested in investigating whether manipulating these gradients can elicit a particular response from the colony at a global level as a whole? In this study I focused on examining the range expansion of the *E. coli* bacterial colony. Namely since in this work I focused on motionless strains the range expansion of the colony is nothing more then a resulting growth of all the individual cells within the colony itself, and thus represents a global descriptor of the colony growth as a whole. Having this in mind one could, by perturbing the growth patterns inside the colony, potentially achieve the desired colony expansion. But before investigating this further, I first needed to answer the question of how bacterial colonies can be observed over long periods of time and how they could be studied in quantitative manners? The answer to this question lies in the use of microfluidic devices. Using microfluidic devices enables both long term experiments and tight control over the environmental conditions, both of which we seek from our experimental design. Now once the experimental system enabling quantification is defined and set, we need somehow to perturb the growth patterns within the bacterial system itself. There are several different ways of how we can possibly control growth of a single cell in well mixed conditions (access to nutrients, antibiotics, direct modulation of some of the key components of the protein expression machinery). How these modalities can translate to the microfluidic settings and how they can be used to perturb the growth of cells within a structurally organized colony and to what extent they can be effective was an avenue that needed to be explored. Once performed this characterization of the systems dynamics gives the information how the system behaves and how it responds to an external stimuli. This provides a possible path to externally command and control systems behavior in a desired way. While big breakthroughs were made in putting a biological system under the external command, limited effort has been made with cells in multicellular communities which engage in cross talk, communicate with each other and in general impact one another. Thus can we and if so, to what extent would it be possible to manipulate how dense bacterial colonies expand spatially? A step in the right direction of answering not just the last question but all the others previously mentioned is to see first how can we quantitively study colonies of *E.coli*? The next chapter will focus on this issue. Firstly the chapter will provide a general overview of how we can investigate bacterial colonies in quantitative manner using microfluidics and what kind of information we could retrieve from these experiments. After a short introduction, the chapter will focus on what kind of strains and what kind of a microfluidic chip design was used in this study. Then lastly the chapter will focus on how can we retrieve information about the range expansion of the colony using a mathematical algorithm called particle image velocimetry.

9 MICROFLUIDIC DEVICE – A WAY TO QUANTITIVELY STUDY *E.COLI* COLONIES

9.1 STATE OF THE ART

In the last two decades microfluidic technology has became standard in the scientific research specially in the field of microbiology. It enabled scientists to precisely, locally and quickly control and change experimental conditions[49]. Additionally it gave the opportunity to obtain spatiotemporal information and parallelize different independent experiments at rates that could not be achieved by conventional macroscopic methods. In bacteriology and specifically in studies concerning *E.coli* scientist were initially focused on developing a microfluidic chip with the aim to understand better the stochastic gene expression process, antibiotic resistance, ageing and growth[50]–[54]. This required that the design of the chip enabled spatial and temporal homogeneity as the smallest change in environmental conditions could potentially lead to a cell response, which would be introducing artefacts that would be difficult to track and would consequently obscure the variable of interest[55]. This is how the mother machine came to be [51].

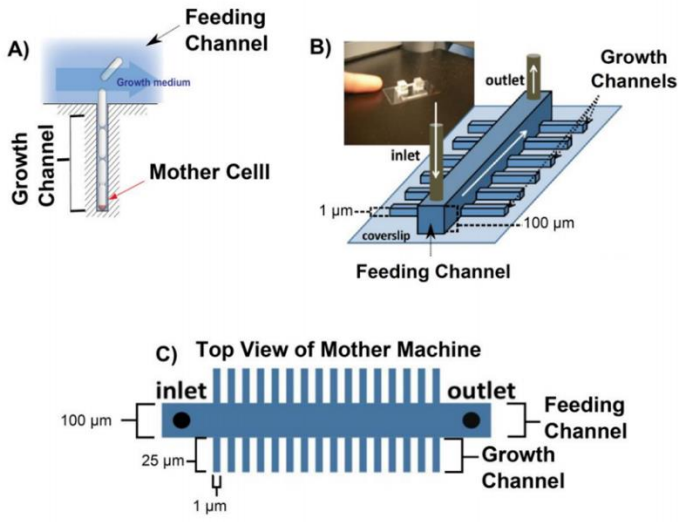

Figure 8.1. Mother machine microfluidic chip used for single cell analysis. (a) Mother machine consists of a main channel and side channels which are perpendicular to it. Fresh media is being constantly replenished through the main channel while bacteria are positioned in the side ones. The width of side channels is about the size of the width of the bacteria, and its length was chosen to be small enough so that the nutrient gradients do not develop. As cells grow they push each other. When the pushed cells reach the main channel they get washed away with the flow. This enables long term single cell experiments.**(b)** Microfluidic chip consists of an inlet which is connected to the media and the outlet which is connected to the pump. **(c)** Top view of the mother machine. Image has been taken from [56]

The chip consists of smaller side channels that are perpendicular to the main channel. Through the main channel media is constantly replenished. Media enters through to inlet, filling out the chip, and is being pulled/sucked through the outlet (usually by the action of peristaltic pump which pulls the fluid through the system). Bacteria are grown inside the side channels. The width and height of the side channels is approximately the size of one bacteria while the length is chosen to be small enough for it not to trigger the developments of gradients [51]. As they grow and divide, the offspring cell push each other alongside the channel axis eventually reaching the main channel where they get flushed by the flow. This design enabled long term high-throughput experiments at a single cell level and ensured the balanced steady state growth.

While mother machine design is crucial for the studies of stochastic processes at the single cell level and single cell analysis, if one wants to study spatial patterning and the rise of bacterial assemblies and observe their characteristics, one needs to redesign the microfluidic chip. The ideal microfluidic chip design must enable cells to continuously grow and form dense bacterial aggregates over extended period of time.

Although distinct, both in the context of the biofilms and dense layers of bacterial colonies, cells interact among themselves and with their local environment. They metabolize nutrients, release signaling molecules and waste which all together as a consequence alter the initial environment. Thus the cells themselves, through their metabolism give rise to chemical and nutrient gradients. These microenvironments help in driving the heterogeneity of the cells comprising the colony. If we want to design a chip aimed at studying spatial heterogeneity, unlike the mother machine one shouldn't look at the designs that enable a homogenous environment, but the opposite. We want cells to experience and establish gradients and non-homogeneity through their metabolic and chemical interactions. But how big should the colony be in order to achieve this heterogeneity? Previously mentioned studies have had demonstrated that nutrient and chemical heterogeneity occurs on a micrometer scale [21], [25], [57]–[60]. Having in mind this two main designs were developed and used for studying the *E.coli* bacterial aggregates. The first that can be seen on figure 8.2 and described in [57]. The chip was optimized to grow bacteria in monolayer over extended period of time and it consisted of three ports cell inlet (through which cells are loaded in the device), media inlet (through which fresh media is supplied) and waste outlet. Firstly the cells are loaded into the device through cell inlet port. One part of the cells becomes trapped in 1μm cell trap channel. Flow from the media port washes away cells that do not enter the trap towards the waste port. As trapped cells continue growing, they eventually fill out and form a bacterial colony aggregate inside trapped channel. Owing to the open connection with the main channel all the frontal cells that start to grow out of this trapped channel are washed away with the flow. In this way the design enabled scientist to study the bacterial aggregate over extended period of time. What was further showed in this study is that the growth and the expansion of this dense colony leads to transition from unorganized to organized and orientational alignment of the cells inside of the colony which is followed by a slow down of the maximum growth rate. The authors speculated that the reason for growth rate slow down could have been either the mechanical pressure generated by the colony itself (as some studies that

have shown that E.coli growth rate directly responds to mechanical pressure) or the waste that has been generated by the bacteria living in the colony, or the combination of both.

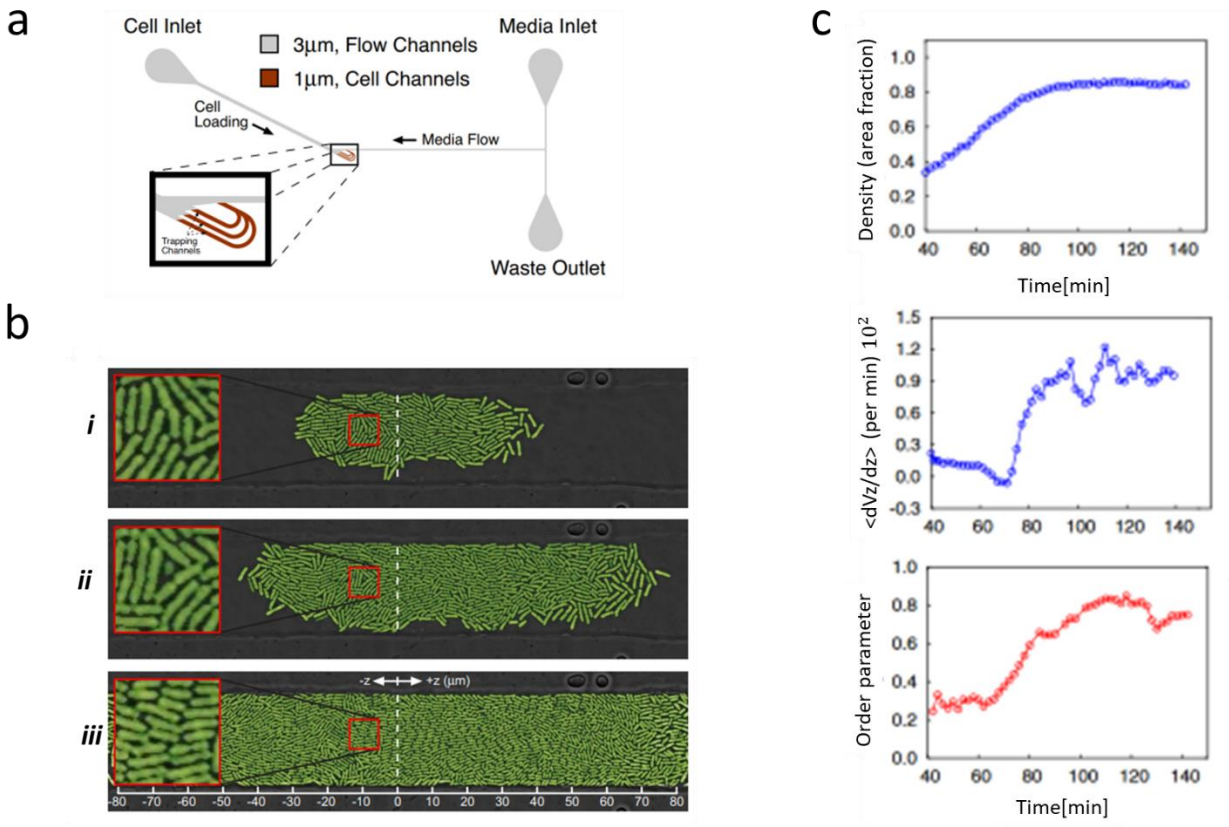

Figure 8.2. Microfluidic chip for studying high density *E.coli* bacterial colonies growing in monolayer over extended periods of time. **(a)** Design of the microfluidic chip which enables continuous growth of the cells trapped in the cell channels. Fresh media is constantly replenished through the media inlet. Cells escaping into the main channel are being washed away with the fluid flow coming from the media inlet **(b)** Cellular growth inside the trapped channels. With the cells division, *E.coli* colony expands and fills out the cell channel. With expansion of the colony, cellular orientation becomes more ordered and pointed toward single direction (horizontal axis). **(c)** quantification of the cellular density, growth rate and order parameter which quantifies colonies orientation in time. Figure from [57]

Second type of design that has become prevalent for studies in *E.coli* and in other microorganisms [9], [13], [25], [58], [61], [62] is the design that is closely related to the mother machine mentioned earlier. An example of one design is shown on figure 8.3. In general it consists of a main channel, through which media is continuously replenished and side channels where the dense population of bacteria reside. As bacteria grow they eventually fill out the entirety of the side channels. Any cells that end up in the main channel due to the growth get pushed away by the flow towards the waste outlet.

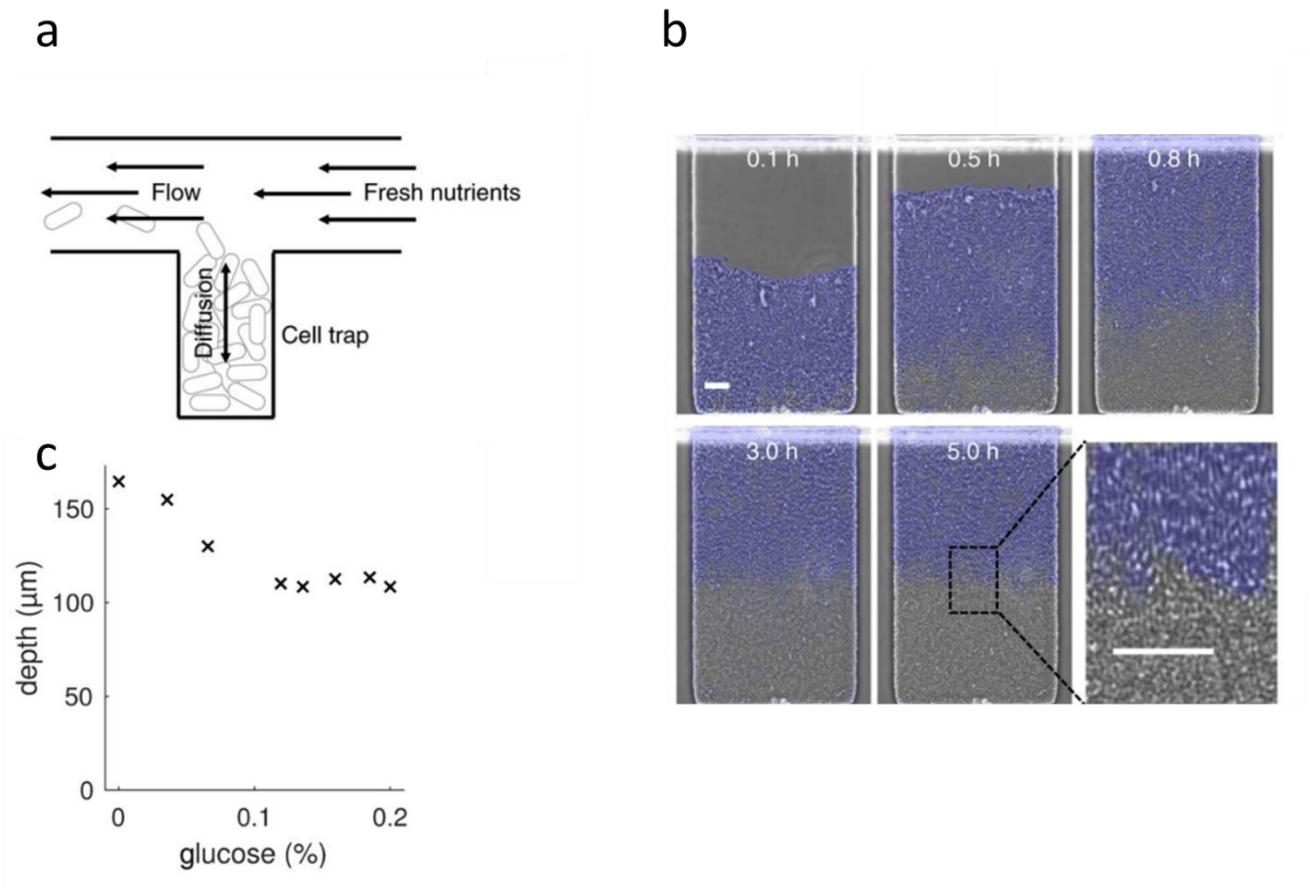

Figure 8.3. Another microfluidic chip design to study expansion of high density E.coli colonies. **(a)** Chip design is similar to the mother machine design which is used to study single cells. It consists of an inlet and an outlet. Through the input inlet the fresh media is supplied. Fresh media flows through the main channel. Perpendicular to it are the side channels (chambers) where bacteria grow. The size of the chamber is chosen so that cells inside of it experience nonhomogeneous environment. This is the biggest difference between this chip design and the design of the microfluidic chip. As cells grow they expand and fill out the side chambers. When the cells reach the main channel, they get washed away with the fluid flow towards the waste outlet. **(b)** Blue color represents the movement inside the colony in the side chambers. Since the cells have deleted flagella they are motionless, thus the movement inside the chamber stems only from the cellular growth. Due to the chip design and gradients that are formed, nutrients can only penetrate to a certain degree inside the chambers. This explains why only cells near the chamber opening are experiencing growth. **(c)** The more glucose there is in the media, the smaller the depth of the growing layer inside the side channel. Figure taken from [60]

What kind of studies can be conducted with this design? Some of the results using this type of design were mentioned before (cross-feeding, antibiotic resistance) in the previous chapter, but two of them are worth mentioning here [58], [61] as they will be important for the study conducted for my PhD.

In order to determine the growth inside the chip, authors in [58], [61] performed inter-image differences and later conducted the particle image velocimetry (which will be the topic of the next chapter). On figure 8.3.b the results of inter-image differences are shown in blue color. The bluer the color, the more movement the region experiences. As cells are nonmotile and the motility comes from the growth itself, the blue color symbolizes the region of active growth. Two authors made two important observations:

1) When investigating bacterial growth inside the side channels of various depths and geometries, if and only if the depth of the side channels was lower than the layer of active growth, the bacterial growth inside the side chambers was impacted.

2) The depth of the growing layer could be modulated by changing the concentration of the glucose in the media. Interestingly, the higher the concentration of the glucose, the smaller the layer involved in active growth is.

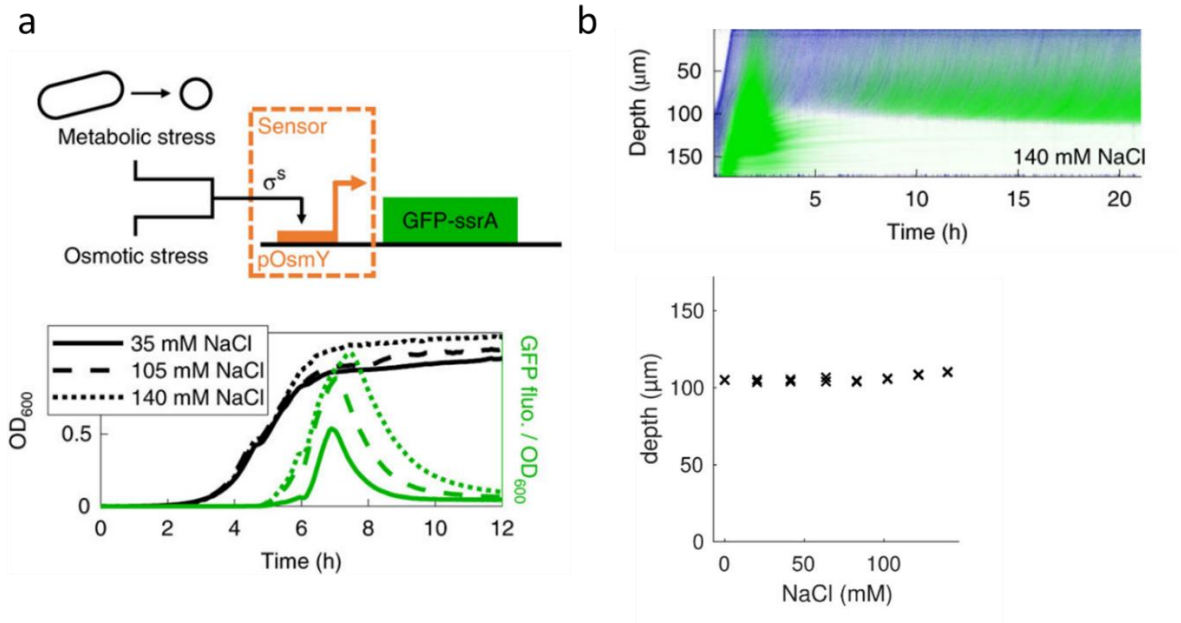

Figure 8.4. Engineering metabolic sensor to determine the growing zone inside the colony. **(a)** Expression of rpoS gene codes for alternative sigma factor. It represents a general stress response and it is triggered when cells encounter stationary like conditions, osmotic shock, oxidative stress, low temperature or acidic pH shift. Members of its regulon involve acetate metabolism genes. Since the cells in the dead end of the chamber experience stationary like condition and engage in acetate consumption the starting idea was to tag the part of the rpoS gene regulon with a fluorescent protein. The metabolic stress sensor was build by putting the GFP under σS responsive promoter pOsmY. This enabled the modulation of the signal by increasing the NaCl concentration. **(b)** Cells at the dead end of the chamber experience stationary like conditions and the lack of growth as previously shown. The growing layer of the colony corresponds to the value obtained both by PIV estimates and from cellular movement estimates. Concentration of the NaCl in the media modulates just the fluorescent signal strength obtained from the metabolic sensor, not the positional value it gives. Figure taken from [60]

Furthermore in the same study the authors created a strain that has the ability to sense metabolic stress by expressing green fluorescence protein. In here the main aim was to characterize and confirm the size of the growing layer. As mentioned before as we go deeper in the colony, nutrients become more and more scarce and at one point completely depleted. When this does happen the metabolic stress is triggered by expressing appropriate set of genes. General stress regulator in *E.coli* is controlled by expression of rpoS gene which codes for alternative sigma factor. This factor gets activated when *E.coli* transitions to the stationary phase or when the cells are subjected to osmotic shock, oxidative stress, low temperature or acidic pH shift [63]. Besides this, the rpoS gene is also activated when cells encounter stationary phase like conditions, such as carbon source limitation and thus including the members of the regulon involved in acetate metabolism such as poxB, acs and actP [64]. Studies mentioned before had already shown that at the end of the growing zone, cells engage in cross feeding by producing acetate for cells at the back. Thus the area in between the two layers-growing and nongrowing should be a position where cells activate their rpoS gene expression. To visualize this, the authors made a metabolic stress sensor which was built in the manner so its strength could be modulated by increasing the

NaCl concentration and where GFP was put under σS responsive promoter pOsmY. The visualization of the stress is shown on figure 8.4.b It can be seen that the metabolic stress signal indeed starts at the end of the growing zone.

In [57] response of dense bacterial colonies grown inside the microfluidic chip to antibiotic pulse was studied. Chips with similar design mentioned earlier in this thesis have showed that dense bacterial populations provide better protection and had better survival rates when treated with an antibiotic insult. In this study authors dynamically tracked the growth rate and the expression of the Tetracycline (Tet) resistance genes-TetR and TetA. They subjected the dense colony with the tetracycline concentration of 100μg/ml, which is lethal for well mixed liquid populations. Tetracycline is a member of antibiotic family that binds to the ribosomes and inhibits translation. In the absence of antibiotic TetR gene represses the expression of itself and of TetA, which codes for efflux pumps. When tetracycline diffuses the membrane and enters the cell, TetR binds to it, before it reaches its target-the ribosome. By binding to the antibiotic, the TetR stops the repression of itself and the efflux pumps (coded by TetA) which pump out the antibiotic.

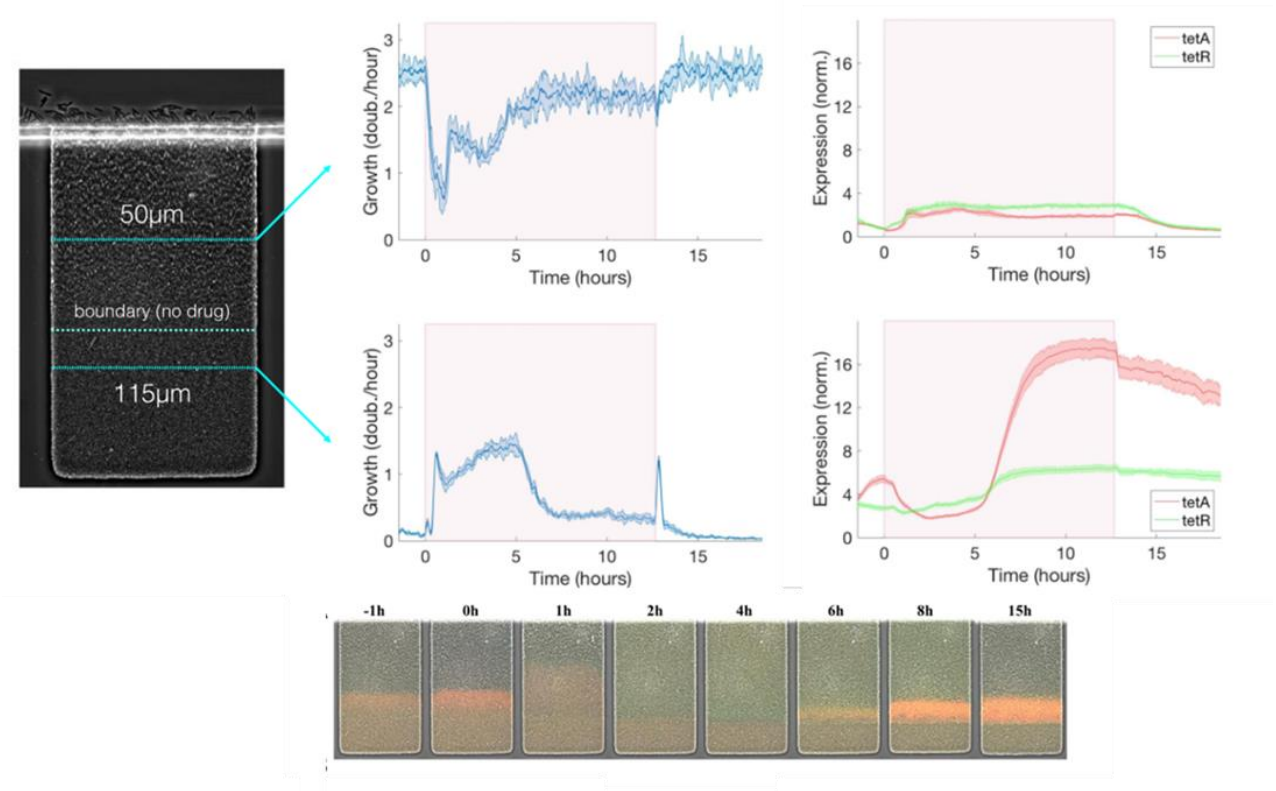

Figure 8.5. Impact of antibiotics on dense bacterial colonies inside the microfluidic chip. After the system reached quasi-stationary state the authors switched from media without antibiotics to the media containing tetracycline at a concentration of 100μg/ml. This concentration was shown to be lethal for well mixed liquid populations. Immediately after the switch to antibiotic containing media, the cells near the channel opening had a sudden decrease in the growth rate. Sudden decrease in the growth rate enabled more nutrients to flow deeper inside the chamber. This combined with the fact that they had tetracycline (Tet) resistance genes at a higher level compared to the ones in the colony front, led to a sudden increase in the growth rate deeper inside the channel. After this transient behavior, the system reestablished the new quasi-stationary steady state, with the surviving cells repopulating the entire channel. Once the cells repopulated the channel opening, the nutrients once again became depleted for the cell near the dead end of the chamber. Since these cells were once activated and were growing at a higher paste, they also had higher expressions of the resistance genes. Once they became arrested due to nutrient depletion, the dilution due to the growth stopped. The stopping of the dilution helped them to retain the accumulated levels of resistance genes, TetR and TetA at a much higher level then before. The antibiotic pulse lasted about 12h, when the media was once again switched to the one not containing the antibiotic. Figure taken from [57]

Upon antibiotic treatment, cells at the outer layer next to the channel opening have a sudden decrease in the growth rate. With the sudden decrease in the growth rate, cells at the front consume less of the available nutrients, which enables their penetration deeper within the colony. This activates the cells that weren't previously metabolically active. The transient growth of cells at the back happens for some time, after which the old boundary is reinstated. Looking at resistance genes of the cells positioned at the back of the colony, their expression increases during the exposure as a consequence of tetracycline treatment. Namely cells deep within the colony sense the presence of the drug and trigger the tetracycline resistance response. All of these transiently activated cells will once again become dormant and consequently due to the lack of dilution retain most of their acquired high levels of antibiotic resistance gene expression.

Here we have seen how we can observe formation and study dense colonies using microfluidic chips, but how can we interpret such data and retrieve information about spatial distributions of the growth rate? The answer lies in applying particle image velocimetry algorithm. The next chapter of this thesis will aim to bring closer what in fact is this algorithm is and how it could be applied in our experimental design. In addition to that information about the strain and chip design specification used in this study would be given.

9.2 SETTING UP THE PIPELINE TO OBSERVE AND ANALYZE BACTERIAL ASSEMBLY IN THE MICROFLUIDIC CHANNEL

9.2.1 Strains used

In order to study and control the formation of the growth patterns inside the microfluidic device one needs to have the control over the growth rate. Cellular growth rate is tightly coupled with the global physiological state of the cell. Every change in the growth rate is accompanied by change in cell phycological state, and vice versa. For cell to divide it needs to double it's biomass, and replicate and segregate its chromosome. The core part of this processes represents the protein expression machinery, with its main parts transcription and translation. By modulating components of transcription and translation one can have the control of the growth rate. This can be achieved in three ways

1) by upshifting/downshifting the growth media to a richer/poorer one. Although effective this completely changes the metabolic state of the cell.

2) by applying antibiotics targeting protein expression machinery. Small concentrations of antibiotics make parts of the gene expression machinery less effective. To combat this cell redirects its resources towards targeted part of the protein expression machinery to fix the issue. Since internal cellular resources are limited this comes at the expense of other processes which consequently slows down the growth rate. Problems with this method lies in the fact that higher concentrations of antibiotics might kill the cells and furthermore with prolongated antibiotic exposure mutants tolerant or resistant to antibiotic may arise.

3) genetically modifying the cell so its protein expression machinery components can be modulated externally through changing the concentration of a certain chemical in the system (inducers for instance) or by applying different light signals (optogenetics).

The first two methods are general and strain independent. On the other hand the third approach requires a specific strain and doesn't suffer from the obstacles the two previously mentioned methods do. I chose to use a specific strain (PP2 strain) that was developed and described in [65] and which had its RNA polymerase under the influence of an IPTG inducible promoter. In here I will present some of the key important aspects of the strain. In addition to PP2 I also used a WT strain with fluorescently tagged RNA polymerase that would be described afterwards (PP1).

PP2strain – IPTG inducible RNA polymerase (RNAP) strain

RNA polymerase (RNAP) is an essential part of the protein expression machinery. It represents a key regulator of cellular overall physiological state- it initiates transcription, the first step in gene expression and thus its range of influence spans everywhere from cell division and growth to basic maintenance and to stress response of the cell [66]–[70]. Unlike eukaryotes, the prokaryotes and thus the *E.coli* have only one type of RNA polymerase. The core of RNA polymerase in E.coli consists of several different subunits summarized in table 8.1. which was adapted from [71]

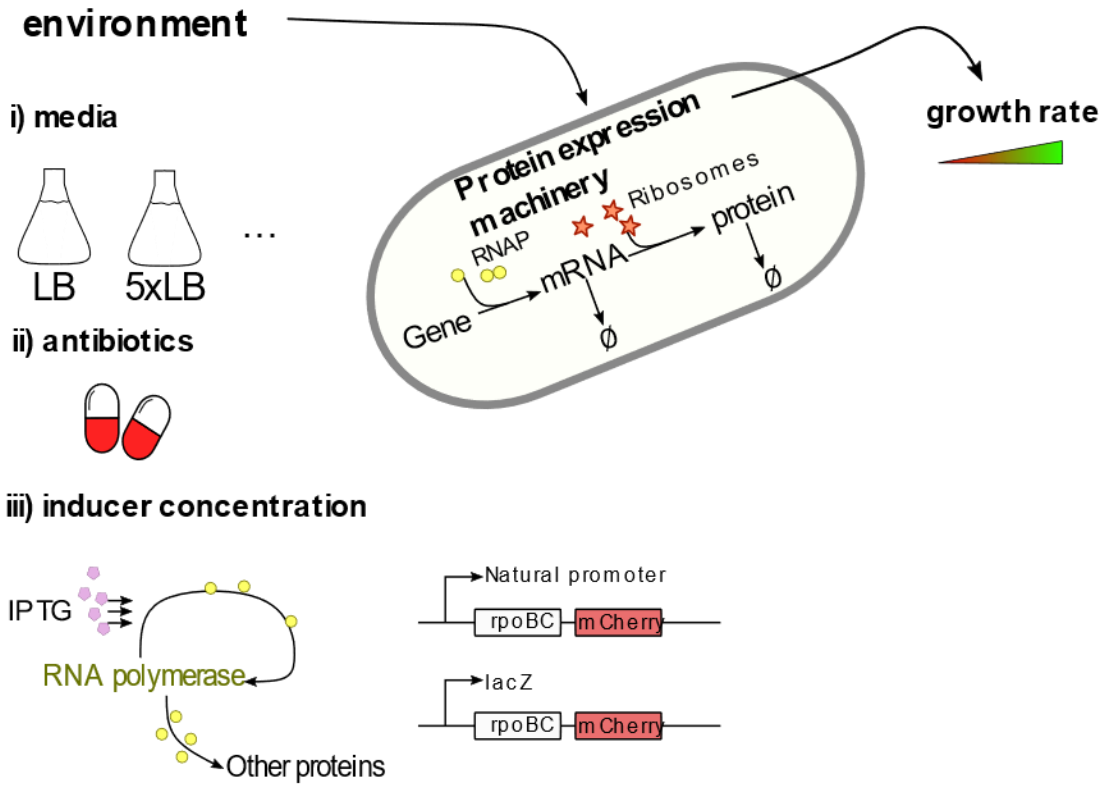

Figure 8.6. Three modalities of controlling the growth rate of E.coli. **(i)** Growth rate can be modulated through changing the growth media itself. This modality impacts the entire metabolism of the cell and leads to global rewiring of the gene expression. **(ii)** antibiotics targeting a certain component of the gene expression machinery, which again leads in global changes in the gene expression **(iii)** using construct as the one described in [65] which consists of RNA polymerase under the control of an IPTG inducible promoter. RNA polymerase consists of several subunits. One of them β' which is described by rpoBC gene was put under the control of an IPTG inducible reporter and was fused with mCherry. This modality of control impacted solely on RNA polymerase and not on the other essential components of protein expression machinery (such as ribosomes)

Subunit (gene)	*Major role*	*Quantity (n=)*
α (rpoA)	Initiation of RNAP assembly[72], interactions with DNA and transcription factors for transcriptional regulation	2
β (rpoB)	With the β' subunit it represents the biggest part of the core enzyme. ββ' subunits form a clamp which is responsible for the DNA binding. Besides this it has a role in RNA binding, RNA synthesis, σ factor binding	1
β' (rpoC)	Same as above- Responsible for DNA and RNA binding, RNA synthesis, σ factor binding, ppGpp binding site	1
ω (rpoZ)	RNAP folding, ppGpp binding site	1

Table 8.1. Subunits of RNA polymerse. Table adapted from [71]

Besides the subunits taking part in the formation of the core enzyme, in order to perform a specific transcription RNA polymerase also need a factor which directs the RNAP to perform transcription at the right target site. This factor is called σ factor.

The PP2 strain which was extensively used in this work is a strain that derived from the E.coli K-12 BW25113 strain which is nonmotile. Main genetic modification that was done in PP2 strain by authors in [65] was the one that the natural promoter of rpoBC genes was replaced with an IPTG inducible one. In order to prevent mutations that would relieve the repression the authors put two copies of lacI repressor gene. With introducing a strong transcriptional terminator and a selection cassette the authors succeeded in completely isolating the rpoBC gene from the upstream ribosomal proteins. The β and β' subunits represent the core of an enzyme and can be used as a proxy for overall concentration of RNAP in a cell[73] , thus with having rpoBC genes under the inducible IPTG promoter one can modulate the expression of RNAP in a cell. In order to quantify in vivo the expression of RNAP, the authors performed chromosomal fusion of the rpoC gene with the mCherry fluorescent reporter.

With changing the IPTG levels the engineered strain was able to modulate its RNA polymerase expression and its growth rate. Interestingly the growth rate response to different IPTG levels was bistable like, where the strain either experiences maximum growth or no growth at all, with a narrow transition in-between

PP1 strain

Unlike the previously mentioned one, this strain has retained the natural promoter of RNA polymerase. It derives as well from its parent E.coli K-12 BW25113 non motile strain and the only difference is that it has the chromosomal fusion of the rpoC gene with the mCherry fluorescent reporter which enables tracking in vivo the RNAP in the cell.

9.2.2 Growth conditions

All measurements started from a single colony picked from the LB+1000μM IPTG agar plate which was incubated overnight in LB media with 1000μM IPTG at 37°C. The overnight culture was diluted 100 fold in the morning into 5ml of fresh media or the M9 media supplemented with glucose. When the diluted culture reached mid-exponential phase cells were concentrated by spinning on 5000rpm for 7min. The supernatant was resuspended in 100μl of the fresh media and loaded inside the microfluidic channel

For all measurements, where IPTG concentration differed from 1000μM the diluted overnight culture was spun for 5min at 15000rpm. Cells were then washed with the media containing the appropriate level of IPTG. This operation was repeated 4 times. Cell were then left at least for 2 generations in the 5ml media containing the appropriate IPTG concentration, before loading them into the microfluidic device. Upon loading the cells were left to grow and fill the side chambers of the microfluidic device, eventually reaching the quasi-stationary regime.

For the antibiotic shake flasks experiments, the overnight 5ml culture was diluted 1:100 into 50ml of 5xLB growth media. OD600 was measured at specific time intervals. When the cells reached mid exponential phase the media was supplemented with antibiotic (250μg/ml doxycycline)

9.2.3 Microfluidic device and microscopy

The microfluidic chip used in this thesis was developed by previous PhD student in the lab[25]. It consists of a main channel which is 1mm wide and 25μm high through which nutrients are flown. Perpendicular to the main channel one could find long dead-end side channels which serve as chambers where cells grow and expand. Side channels have the height of 4.5μm, length of 800μm, and width of 5μm, 10μm , 25μm or 50μm. Side channels were deliberately made long enough so nutrient and chemical gradients could be developed. As cells grow they reach the main channel when they are flushed away by the flow

Microfluidic chip was made by pouring the 10:1 mix of polydimethylsiloxane (PDMS) and curing agent (Sylgard 184 kit; Dow Corning) on the master wafer. The poured mix was degassed and then cured for at least 3h at 65°C. After curing, the chip was peeled off and removed from the master wafer with its inlets and outlets were punched out. The chip and a glass coverslip (24 × 50 mm #1; Menzel-Gläser) were treated with plasma for 1min after which the two were bonded and incubated at 65°C for at least 4h

Before loading the cells inside the microfluidic chip, the chip was treated with distilled water with the addition of pluronic F-127 (Sigma) at the concentration of 5g/L and left on room temperature to rest for 30min. Pluronic was used to passivate the surfaces and was added also to the growth media as well at the same concentration. This concentration was shown that it doesn't influence the growth rate of E.coli[74].

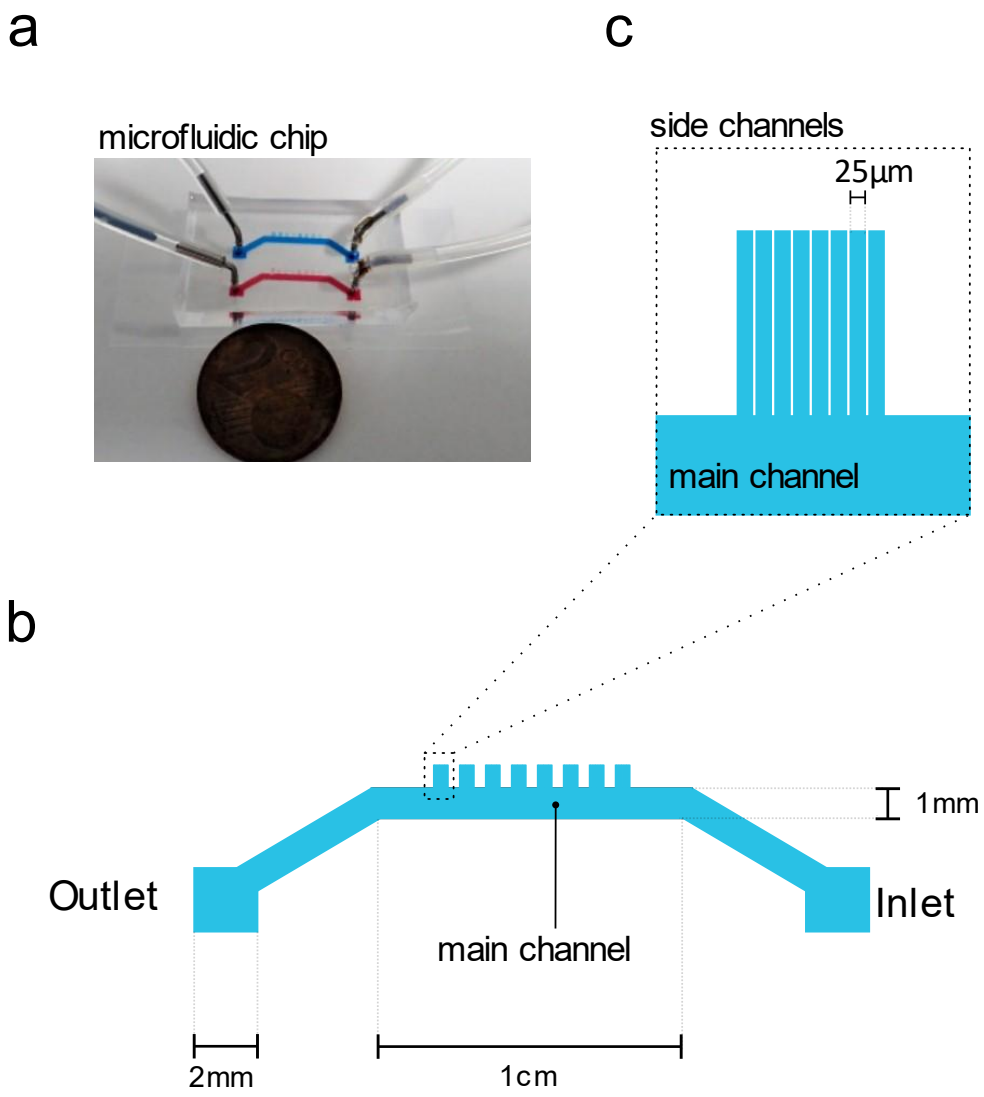

Figure 8.7. Microfluidic system used in the thesis. **(a)** Microfluidic chip enabling long term observation of colony invasion. The size of the microfluidic chip compared to a coin. Image taken from [25]. **(b)** Design of the chip. The dimensions of the main channel are shown in the image. The chip consists of an inlet which is connected to the media, main channel through which the media flows, side channels which are perpendicular to the main one and in which bacteria are growing and the outlet which is connected to the waste The height of the main channel is 25µm **(c)** Dimensions of the side channels. Side channels height is 4.5µm and their length 800µm. The width of the channels which were used in the experiments, if not stated otherwise, was 25µm. Besides 25µm, the chip consists of the side channels with the width of 5 µm, 10 µm, 50 µm.

After 30min of the pluronic incubation of the microfluidic chip, the cells were concentrated by centrifugation (7min, 6000rpm) and loaded inside the device. The chip was then placed inside the centrifuge and was span for 7min at 2500rpm to force the cells to enter the side channels. Following the loading, the inlet and the outlet of the microfluidic device were connected to the media and the trash respectively. Liquid media was first flowed rapidly for 5-10 min at the flow rate of 200µL/min to clean the main channel from excess cells, after which the flow was adjusted to 5µL/min. The cells were left to recover inside the microscope chamber at 37°C with constant media flow at least for 4h before the imaging has started. Images were acquired by using Olympus IX71 microscope with Olympus 10x objective (0.25NA), CoolSNAP HQ2 CCD Camera, PI piezo Z-stage, and Prior H117 motorized XY stage. For fluorescent images mCherry filter cube and 103 W/2 mercury short-arc lamp was used. The exposure time for fluorescent images was set to be 250ms and for the bright field the exposure time was set to be 10ms. Images were taken every 5min.

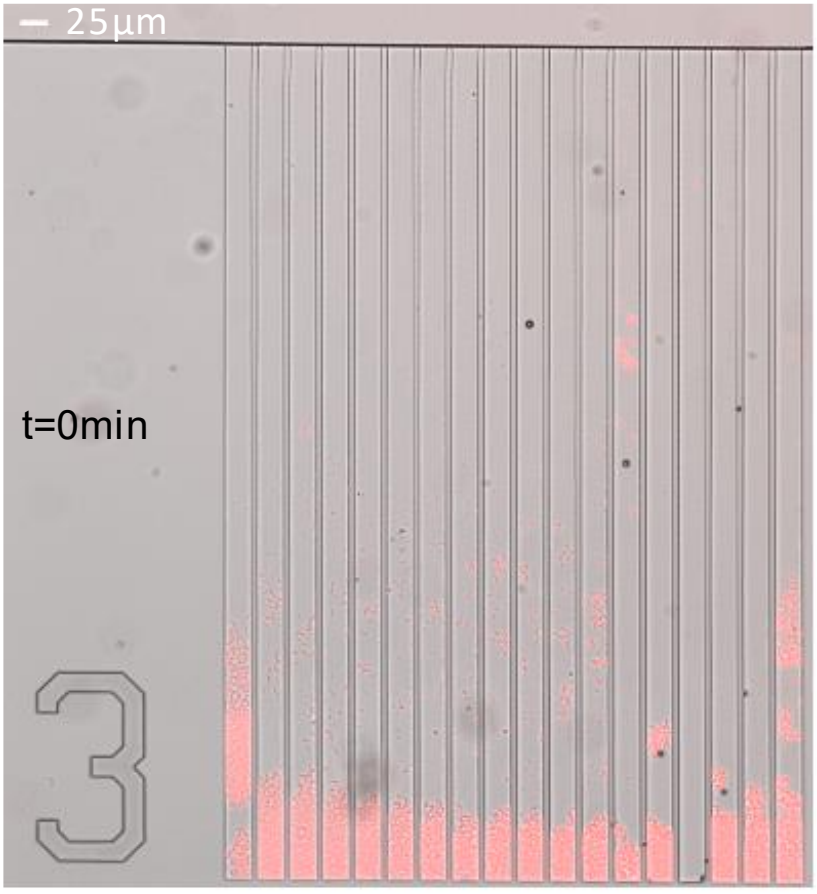

Figure 8.8. Cells inside the microfluidic device upon the loading of the chip with bacteria and connecting it to the flow. Cells were loaded inside the side chamber by spinning. Upon connecting the device to the flow cells inside the main channel were flushed away with the flow. Side channels aren't homogenously filled. Due to the centrifugal force, most cells reside initially at the dead end of the chamber but some cells might be present throughout the side channel. Since

the side channels didn't fit into the field of view, two images corresponding to two positions were stitched using the method described in [75]. The result of the stitching represents this picture.

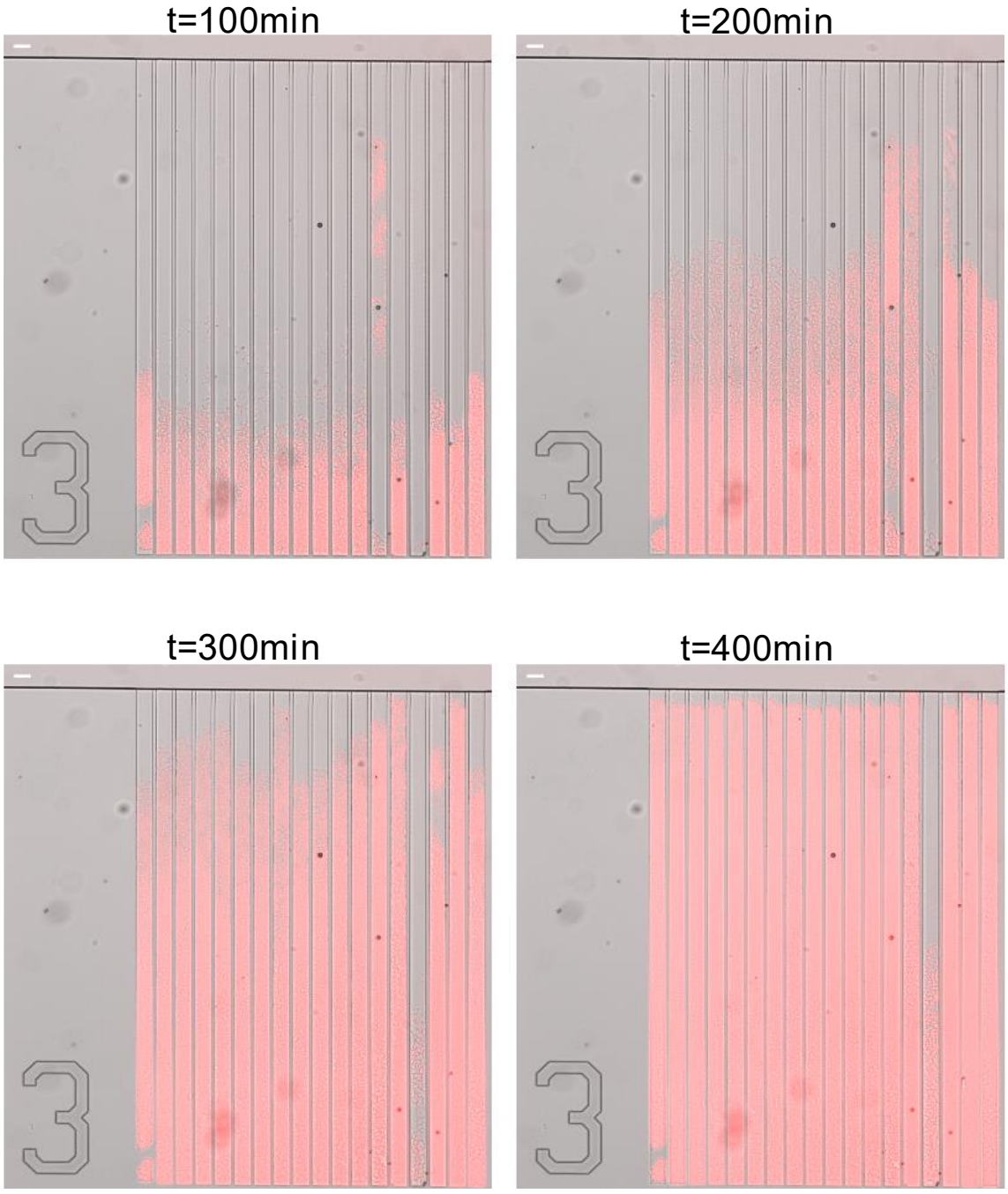

Figure 8.9. Cells inside the side channel divide and grow. As they grow cells move towards the main channel gradually filling up the entirety of the side channel. Channels with similar initial cell seeding reach the main channel in approximately the same time. Cells in the channel which had been barely seeded with the cells (4th one from the right) were the last one to reach the main channel. Upon reaching the main channel, quasi-stationary regime is achieved.

9.2.4 Controlling the environment inside the microfluidic chip with a microfluidic mixer

To set an appropriate concentration of a specific chemical such as IPTG or antibiotic inside the media or to modulate the nutrient composition of the media in real time during the experiment a rapid and controlled mixer with good time resolution was developed. The fluid mixer in my thesis is based on the principles of passive microfluidic mixing of the fluids[74], [76]. Passive fluid mixing is achieved by alternating between the two inputs at a specific rate. To alternate fast enough between the media valves from Lee Company were used. Process of delivery through the microfluidic tubing smooths out the fast oscillatory changes made by inputs alternations giving a fluid with specific ratio between the two inputs. Physically speaking this low-pass filter nature is a result of the diffusion process. Diffusion is a slow process, but by applying PWM (pulse width modulation) and sending small portions of fluid increases the contact between the fluids mixing, which consequently enhances the diffusion process.

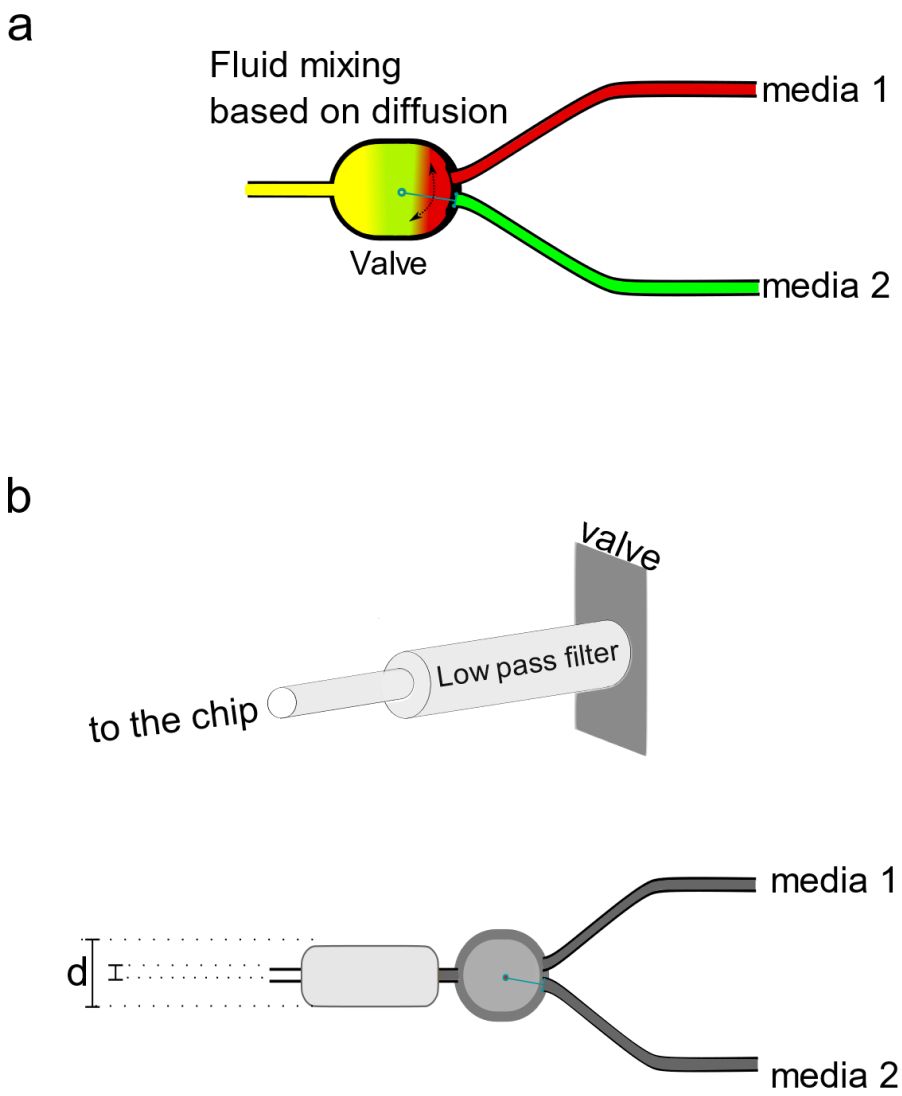

Figure 8.10. Microfluidic mixer. a) Microfluidic mixer is based on passive diffusion between the fluids. One of the media contains the chemical which perturbs the growth while the other one doesn't. Valve is switched between the two media at a specific frequency which sets the appropriate concentration of the chemical at the output. **b)** To enhance diffusion and consequently mixing low pass filter was introduced in the system. It consists of a tube of a larger diameter *d* which slows down the fluid and increases the contact surface between the media.

Arduino Uno was used to effectively control the valve. Although formally inputs/outputs of both the valve and the Arduino operate at 5V, from experience it was spotted that sometimes a voltage drop occurs on Arduino outputs. This is why a relay was applied so that the high voltage of the Arduino output is high enough to switch on the valve. Connection between the MATLAB and the Arduino is serial via the USB cable.

For all of the fluid mixer experiments, 50ml deionized water and 50ml deionized water containing 25µl of 100µM fluorescein were used. A peristaltic pump (ISMATEC REGLO Digital peristaltic pump) was used to deliver fluids to the microfluidic chip. Control of the pump and Arduino micro controller unit which operates the solenoid valve (The Lee company LHDA0531115H) was implemented using a MATLAB script. Acquired data and system control parameters were transmitted via serial communication using serial port.

Initial experiments showed oscillations of the fluorescein signal (which I used for mixing characterization). I identified two possible causes of this problem

1) the fluids didn't mix properly –portions of fluid that didn't mix at all which caused the fluorescence signal oscillation

2) peristaltic pump itself. Namely peristaltic pump are known to have strong pulses in the flow rate and cause vibrations and noise, and thus it might be possible that this caused pressure misbalance and eventually contraction of the microfluidic device itself.

Namely both of this problems stem from system not being able to average out fast oscillatory changes given by the valve. One way to deal with this problem easily is to lower down the cutoff frequency of the entire system to small enough values which will attenuate these oscillations and enable proper mixing. In acoustics similar problems are solved by using a low pass filter. Namely by adding the tube with a higher diameter the system cuts off high frequency components of the sound signal.

Similarly, in order to enhance the diffusion process, a low pass filter was implemented by incorporating a tube with a larger radius downstream of the valve and before the microfluidic chip. It lowers down the speed of the fluid thus giving the system more time to mix the fluids before it reaches the microfluidic device positioned under the objective of the microscope. Lowering down the speed solves the problem of the pressure misbalance which prevents heavy contracting of the microfluidic device. In addition to lowering down the speed, the added low pass filter increases the contact between fluids which further increases the diffusion process.

For the fluid mixer characterization experiment a flow rate of 40µl/min was used. Image acquisition was taken every 5min. PWM frequency was varied from 0% (only water) to 100% (only fluorescein) and then back again to 0%. The fluorescence which is a proxy for fluorescein concentration was tracked in the main channel over time. Image acquisition was taken every 5min with the PWM period being 1min. Exposure time was 10ms for bright field and 85ms for fluorescence field. Low pass filter of 3cm was used in the system. Low pass filter length impacted only on the time delay, not the mixing properties. For the impact of flow rate on mixing properties, quantification of mixing was operated over a sequence of flow rates.

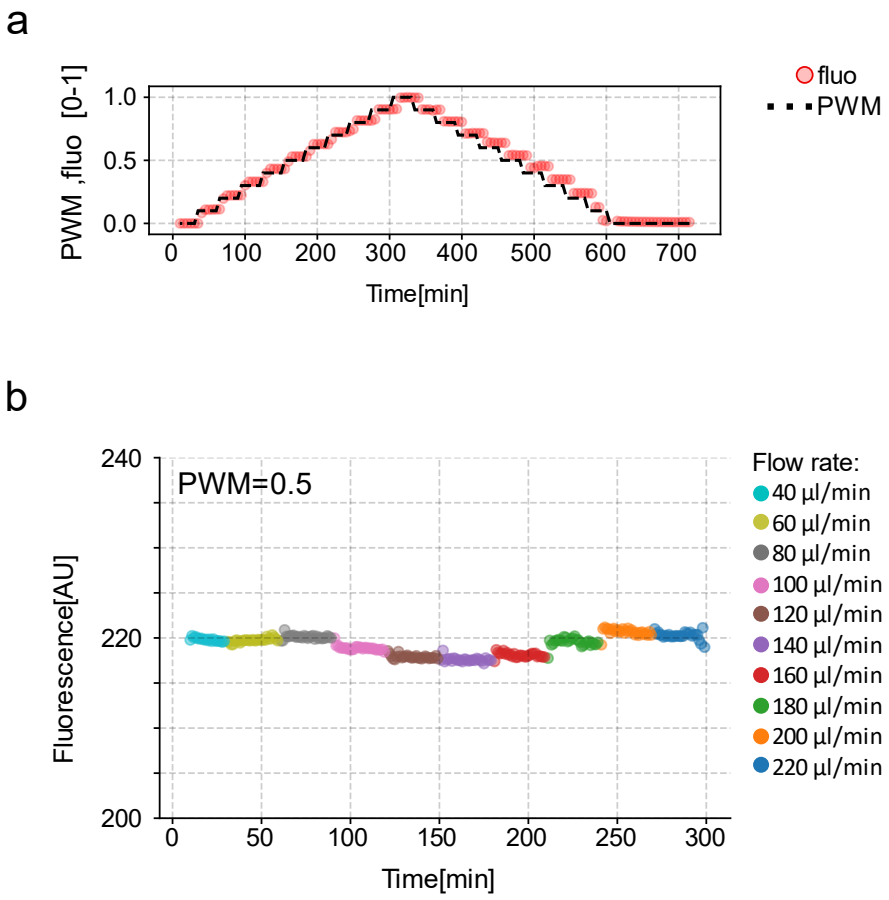

Figure 8.11. Characterization of the microfluidic mixing a) Changing the PWM signal from only water (PWM=0) to only fluorescein 1 (PWM=100%) and back to only water. The PWM signal gives the % of the period inside which valve is in the position so that fluorescein flows through the system. In the rest of the period 1-PWM valve switches back to the position where only the water flows. Fluorescence was observed inside the main channel of the mother machine and was normalized inside the range [0,1]. b) For PWM=0.5 I tested the stability of the mixing across a range of flow rates in the system. Higher flow rates can potentially impact the mixing by not providing enough time for the diffusion to take place. If this happens one should see oscillations In the fluorescence signal. Flow rates bellow 40µl/min were not tested as 40µl/min already gave satisfying results.

Mixing was stable over the wide range of flow rates. This was tested by automatically changing the pumps flow rate which was enabled by the serial communication between the main computer and the pump itself. Time of the flow rate step was chosen to be 30min. Image acquisition time was set to be 1min. Pulse width modulation time was chosen to be 0.5 (50% of time period water flow, and 50% fluorescein), with time period equal to 1min.

9.2.5 Particle Image Velocimetry – a way to infer the growth and the velocity profile of a colony

As mentioned before, in this chapter I will present the mathematical algorithm that is used to infer the growth rate and the expansion rate of the bacterial colony. The algorithm is particle image velocimetry and it is mainly utilized in physics and fluid dynamics where it is extensively exploited to infer the fluid velocity. Due to the noninvasiveness of the algorithm it gradually started being used in biological studies to infer the growth. What is this algorithm and how it can be used in our experimental design will be the topics covered with this section. I will start with the introduction of the algorithm. In here I tried to put some of the essential ideas that were settled down in beautifully written article covering the PIV method in detail [77]. Then later on I will explain it how we could apply this algorithm to biological settings and more specifically how we could apply it to our study.

Since the PIV is an optical method, the first thing one needs to do in order to determine the fluid velocity is to somehow visualize the flow. This can be done by seeding the flow with small particles. The ideal seeding consists of particles small enough not to disturb the flow. As particles move due to the fluid flow, the observed velocity of the particle should correspond to the fluid flow velocity at the same position. In order to determine the velocity of a moving particle one must measure its displacement over time. The displacement over time could be easily determined by capturing its positions in different time intervals. For simplicity let us observe the particle which moves translationally in one direction. The position of the particle at instance t_1 is x_1. Over time particle moves, so that at t_2 its position x_2. The velocity that caused then that movement can be determined as $v = \frac{x_2 - x_1}{t_2 - t_1} = \frac{\Delta x}{\Delta t}$

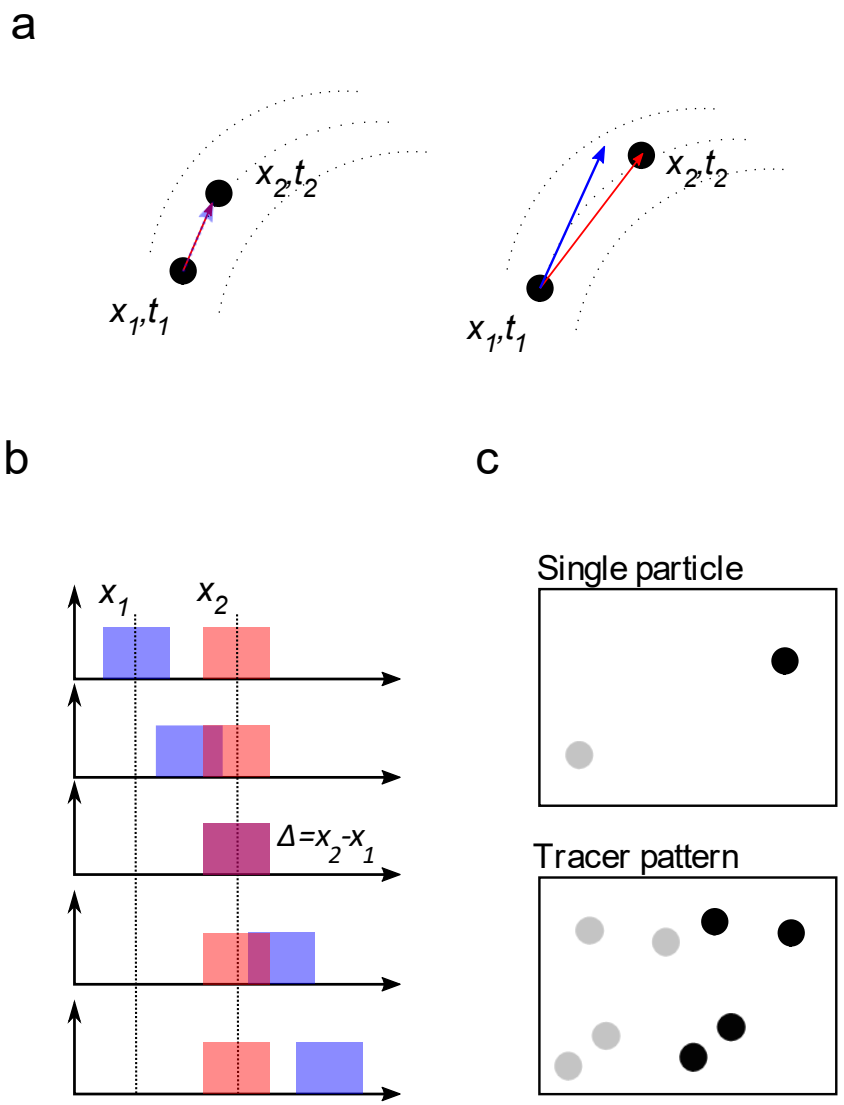

Figure 8.12. Fundamentals od the PIV algorithm. **(a)** Velocity of the particle can be estimated if we track the distance Δx that one particle took in a certain time frame Δt. When Δt⟶0 the ratio dx/dt will give an accurate estimation of instantaneous velocity at certain position. To come close to the accurate value of the instantaneous velocity one should take small enough Δt. **(b)** If at a certain time point t_1 the position of the signal was at x_1 (blue signal) and at t_2 at position x_2 (red signal), we estimate the difference between the two signals by applying cross-correlation. If we shift the blue signal in space and multiple it with a static red signal and do this for multiple shifts, the maximum result of the multiplication would be when both red and blue signal completely fit with each other. This happens when we shift the red signal at $\Delta=x_2-x_1$ compared to its initial position x_1. This represents the fundamental mathematical operation, called cross-correlation that hides behind the particle image velocimetry algorithm. **(c)** To track the velocity of fluid, fluid is usually seeded with small particles. Instead of following a single particle which is time consuming and computationally expensive, we can track the group of particles under the influence of the same flow characteristics- a tracer pattern

Of course only when Δt→0 the ratio will give an accurate instantaneous velocity at certain position. In practice this is not achievable as Δt is definite, thus we only have the approximation of the mean velocity at a interval (t_1, t_2). This estimation is good enough when the sampling frequency of obtaining the particle position is high enough (small Δt values).

Position of the particle can mathematically be represented as $\delta(x - x_{pos})$, where δ is Dirac delta signal, which is defined as:

$$\delta(x - x_{pos}) = \begin{cases} 1 & x = x_{pos} \\ 0 & x \neq x_{pos} \end{cases}$$

Thus positions at the two time instances could be mathematically described as

$$f(x) = \delta(x - x_1) \text{ , when } t = t_1$$

$$g(x) = \delta(x - x_2), \text{ when } t = t_2$$

If we perform correlation between these two functions we have

$$(f * g)(\theta) = \int_{-\infty}^{+\infty} f(x)g(x + \theta)dx$$

$$(f * g)(\theta) = \int_{-\infty}^{+\infty} \delta(x - x_1)\, \delta(x + \theta - x_2)dx$$

This correlation is zero everywhere, besides when $\theta = x_2 - x_1$ or expressed in mathematical terms

$$C(x) = \delta(x - (x_2 - x_1))$$

This example demonstrates that computing the cross-correlation between the two signals representing the position of a particle at two time instances gives the displacement itself. Extending this approach to higher dimensions would yield analogous outcomes.

An illustrative example of the cross correlation can be found on (figure 8.12b*)*. In here we have a rectangular pulse that moves along the x axis in time. Lets say that we obtained the two images and we want to determine how much the pulse moved between those two instances. Applying the correlation function between these two pulses would mean that one pulse is keep at the constant position and we let the other one freely one move alongside the x axis. At every move we would multiply the two signals and we would remember the result. One could spot that the result would be the highest when both of the pulses completely match, and this happens only when we translation of the moving pulse equals the exact displacement.

Tracking every single particle in the ensemble would be time and memory consuming. Furthermore there is the difficulty of distinguishing the movements and tracking of the particles

as their number increases. This is why instead of tracking one single particle it is more convenient to follow the tracer pattern (*figure 5.4.1c*). Let us first mark the position of all particles ($\boldsymbol{X_1}$, $\boldsymbol{X_2}$ … $\boldsymbol{X_N}$) at time instance t as a single vector $\mathbf{\Gamma}$

$$\mathbf{\Gamma(t)} = \begin{bmatrix} \boldsymbol{X_1}(t) \\ \boldsymbol{X_2}(t) \\ \vdots \\ \boldsymbol{X_N}(t) \end{bmatrix}$$

The positional vector can be expressed as a sum of Dirac delta signals, which can be denoted as $G(\mathbf{\Gamma}, t)$:

$$G(\mathbf{\Gamma}, t) = \sum_{i=1}^{N} \delta(X - \boldsymbol{X_i}(t))$$

After some finite time Δt , due to the fluid movement tracer particles take different positions which are governed by the velocity field itself - $\mathcal{U}$.

$$\frac{\mathrm{d}\mathbf{\Gamma}}{\mathrm{dt}} = \mathcal{U}(\mathbf{\Gamma}, \mathrm{t})$$

If we define $t' = t$ and $t'' = t + \Delta t$, we can mark respective positions as $G(\mathbf{\Gamma}', t')$ and $G(\mathbf{\Gamma}'', t'')$. In a similar way as before by performing the cross-correlation between the signals one could estimate the movement that happened due to the fluid movement. The cross-correlation is defined as:

$$Corr = \langle G'(\mathbf{\Gamma}'), G''(\mathbf{\Gamma}'') \rangle$$

If we consider $\varrho(\mathbf{\Gamma})$ as the probability density function of $\mathbf{\Gamma}$, one could write the correlation signal as:

$$Corr = \iint G'(\mathbf{\Gamma}'), G''(\mathbf{\Gamma}'') \varrho(\mathbf{\Gamma}''|\mathbf{\Gamma}') \varrho(\mathbf{\Gamma}') \mathrm{d}\mathbf{\Gamma}'' \mathrm{d}\mathbf{\Gamma}'$$

Where $\varrho(\mathbf{\Gamma}''|\mathbf{\Gamma}')$ represent the conditional probability density function (PDF) for $\mathbf{\Gamma}''|\mathbf{\Gamma}'$.

For a given flow field $\mathcal{U}$, $\mathbf{\Gamma}''$ is uniquely determined by $\frac{\mathrm{d}\mathbf{\Gamma}}{\mathrm{dt}} = \mathcal{U}(\mathbf{\Gamma}, \mathrm{t})$, thus

$$\varrho(\mathbf{\Gamma}''|\mathbf{\Gamma}') = \delta(\mathbf{\Gamma}'' - \mathbf{\Gamma}' - \mathbf{D}) \text{ with } \mathbf{D} = \int_{t'}^{t''} \mathcal{U}(\mathbf{\Gamma}, \mathrm{t}) dt$$

Therefore the correlation signal looks like:

$$Corr = \int G(\mathbf{\Gamma})G(\mathbf{\Gamma}+\mathbf{D})\varrho(\mathbf{\Gamma})\mathrm{d}\mathbf{\Gamma}$$

Since no particles appear or disappear from the ensemble, the PDF satisfies the following continuity equation:

$$\frac{\partial \varrho}{\partial t} + \mathcal{U}\cdot \mathrm{grad}\varrho + \varrho\ \mathrm{div}\mathcal{U} = 0$$

If we consider that the flow is incompressible (density remains constant) and that the spatial seeding of the tracer particles is homogenous

$$\frac{\partial \varrho}{\partial t} = 0\ \rightarrow \varrho = const$$

Bearing this in mind the mean of the ensemble is

$$\langle G'(\boldsymbol{X}')\rangle = \langle G''(\boldsymbol{X}'')\rangle = \int G(\mathbf{\Gamma})\varrho(\mathbf{\Gamma})\mathrm{d}\mathbf{\Gamma} = C$$

And the cross correlation is

$$\langle G'(\mathbf{X}'), G''(\mathbf{X}'')\rangle = C\delta(\mathbf{X}''-\mathbf{X}'-\mathbf{D}) + C^2$$

We can see that the cross-correlation signal has an offset of C^2. If we want to get rid of the offset, one needs to perform the cross-correlation of the signal without the mean components – or cross-covariation of the signals how it is called in signal processing. Signals defined like this consist only in one peak with zero offset which is determined by the spatial movement

$$R_{G',G''}(\boldsymbol{X}',\boldsymbol{X}'') = \langle G'(\boldsymbol{X}'), G''(\boldsymbol{X}'')\rangle - \langle G'(\boldsymbol{X}')\rangle\langle G''(\boldsymbol{X}'')\rangle$$

$$R_{G',G''}(\boldsymbol{X}',\boldsymbol{X}'') = C\delta(\mathbf{X}''-\mathbf{X}'-\mathbf{D})$$

The previous derivations are of course only true if the flow is incompressible with homogenous seeding. In other cases the location of the correlation peak is not purely determined with the flow field, but it is slightly biased. In practical experimental settings the correlation suffers from further losses either due to the imaging and processing techniques. The biggest loss in accuracy can come from the fact that we need to subsample the images, a standard procedure in PIV analysis. This is especially critical when the velocity profile is the form of gradients in the image.

9.2.6 Applying PIV method

To quantify the velocity gradients of the bacterial assembly side channels, the microfluidic chip was imaged with 10x objective in the brightfield and fluorescent field. PIV analysis was performed after the side channels were completely filled with bacteria and when the quasi stationary regime was achieved. Each time PIV algorithm was applied on a single side channel for 250 minutes in quasi stationary regime. Each channel was chosen manually by defining a region of interest (ROI) over the side channel at the beginning of the analysis. If the image contrast was poor, it was enhanced using Fiji-ImageJ brightness/contrast adjustment. PIV analysis was performed using PIV Optic flow plug in Fiji-ImageJ software. PIV method is not directly applied to the entire image, but first the ROI containing the side channel is picked and from there on divided into *nxn* smaller interrogation windows. Movement and velocity was assessed for every interrogation window inside the ROI. Inside each interrogation window movement is determined as previously described, by performing a cross-correlation between two consecutive time points. Final quasi-stationary estimation of velocity profile of the colony inside one channel was taken as median filer between in total 50 consecutive time points (250min). Median filter was chosen instead of the mean filter so that rare events such as passing of bubbles (which may block the cells movement) doesn't impact the estimation. The final velocity profile of a certain condition was taken as a mean filter of several side channels that were analyzed.

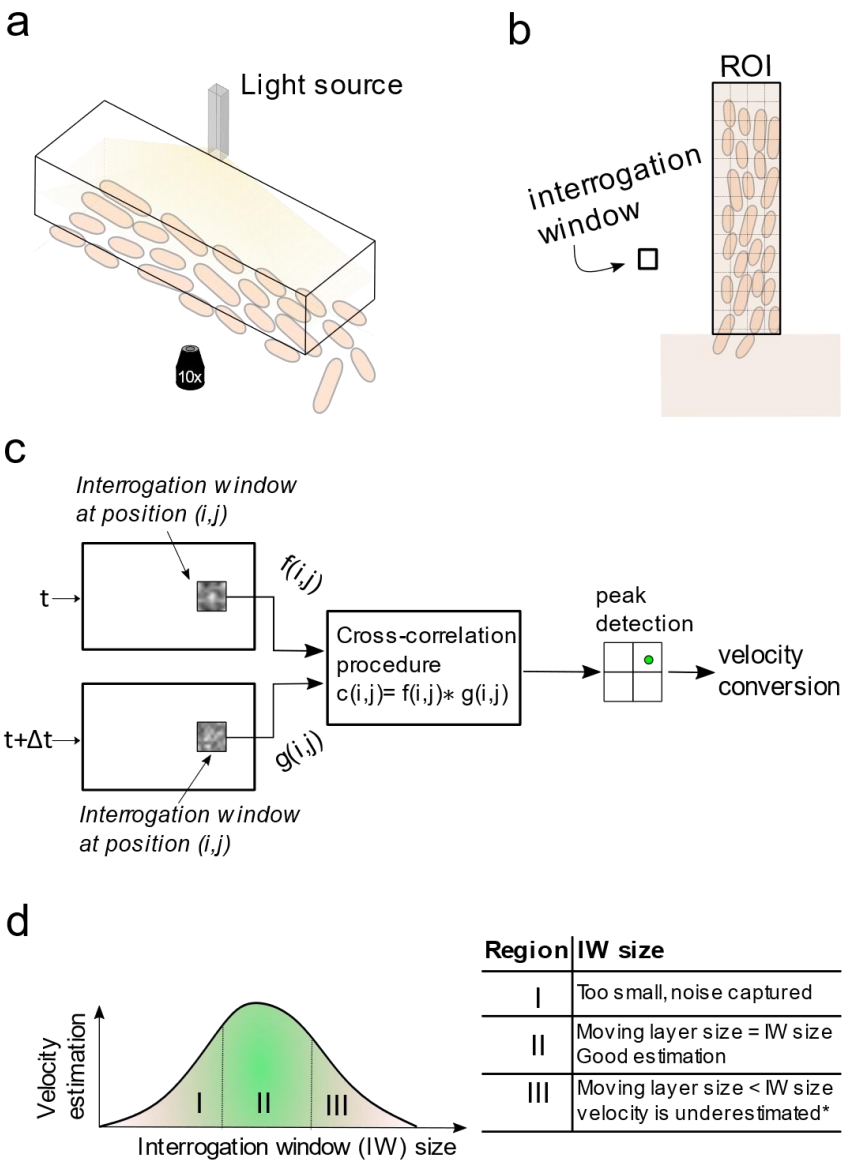

Figure 8.13. Applying the PIV method to estimate the velocity gradient formation inside the side channel of the microfluidic chip. **(a)** Side channels of the microfluidic chip were observed under the 10x objective in brightfield and fluorescent field microscopy. Instead of particles in this case we are observing the collective movement of the bacteria. **(b)** Region of interest containing the side channel was picked manually. Picked region of interest was then divided into small interrogation windows of equal size. **(c)** For each interrogation window the cross-correlation function was performed. The position of the peak in each interrogation window determines the velocity vector from which we can read the intensity and the position. In the case of the microfluidic chip it is expected that the cells are moving vertically, alongside the main axis of the side channel, with the biggest movement happening near the channel opening**. (d)** If the interrogation windows are chosen small enough the algorithm would catch only noise. When determining the velocity profile alongside the main axis we can expect that the velocity at each position would be zero, as we average out the noise. On the other hand if the interrogation windows are chosen to be bigger then they should have been, we can average out the velocity gradient, consequently underestimating the velocity at a certain position. The ideal size should be chosen after a careful inspection and it should be around the size of the moving pattern

Choosing the right size of interrogation window is critical, specially when dealing with velocity gradients in the ROI. If the size of the interrogation windows is too small, PIV algorithm will catch up mostly noise. Noise in digital image processing is white noise (independent random variables), and as such is uncorrelated. Performing PIV technique which is a cross-correlation technique under these conditions will give a velocity close to zero. On the other hand, too large interrogation window size can also underestimate the velocity. This is specially the case when dealing with velocity gradients. Underestimation of the velocity comes as a consequence of meaning up the movement inside the whole interrogation window. Thus a special attention should be given to choosing the appropriate interrogation window size. The rule of the thumb is that one should choose the size to be as the size of moving sections in the image. On figure 8.14. one could see the influence of choosing the different size of interrogation window for a side channel filled with bacteria in M9+0.4% glucose media supplemented with 1000 µM IPTG. Any other choice of interrogation window size besides the 32x32 pixel size (20.64x20.64 µm; 1 pixel=0.645 µm) gives an underestimation of the velocity profile.

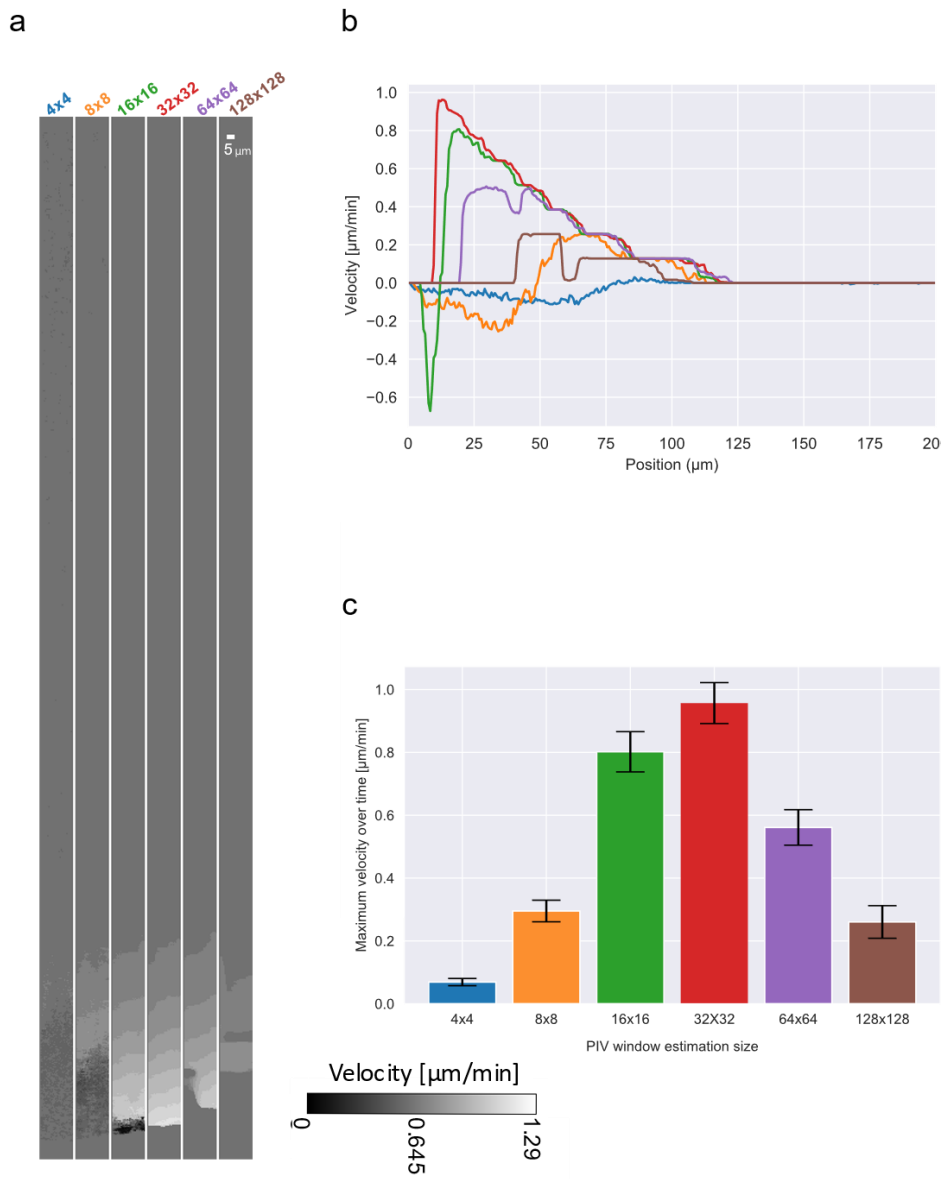

Figure 8.14. PIV estimations of the velocity profiles alongside the side channels with the different interrogation window size in M9 media. (a) Velocity profile alongside the side channel (b) Quantification of the velocity profile alongside the side channel for different interrogation windows. (c) Maximum velocity inside the side channel (velocity near the channel opening) for different interrogation windows

This interrogation window size should always be rechecked when trying out different experimental conditions. For instance in more nutritious well mixed liquid media it is known that bacterial cells cultures grow faster and are bigger in size[69], [78]–[80]. Setting aside for now the

impact of the nutrient upshift has on the establishment of the growth and velocity patterns in within the colony, let's just focus for now on the fact that the cells at the edge of the colony, near the channel opening, experience higher growth rates and thus are going to be larger in their size. Bigger cell size on the other hand infers that the size of the growing sections would as well bigger, which as a consequence would demand bigger interrogation windows to accurately estimate the velocity profile. This logic (nutrient upshift →higher growth rates→bigger cell size → bigger interrogation windows) is nicely depicted when comparing the results of the PIV analysis for two media M9+0.4%glucose supplemented with 1000 µM IPTG and more nutritious one, 5xLB supplemented with 0.2%glucose and 1000 µM IPTG.

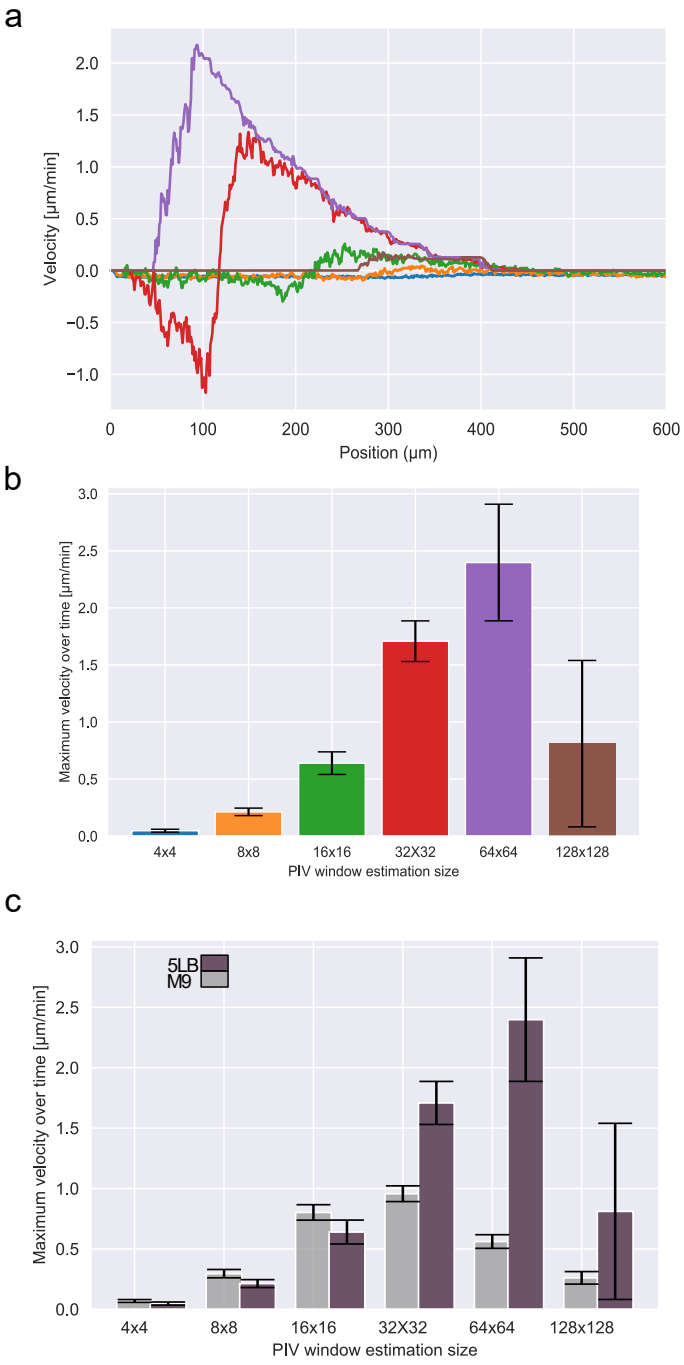

Figure 8.15. Comparison of different window sizes in two different conditions M9 media and 5xLB. (a) Velocity profile alongside the side channel for 5xLB media for different size of command windows. **(b)** Maximum velocity (velocity near the channel opening) for 5xLB media with different command windows**. (c)** Comparison of the PIV estimation of the maximum velocity for two conditions M9 and 5xLB media for different size of the command windows. There is a shift in PIV interrogation window size. One of the possible explanations for the bigger size could be that the cells growth in a richer media are bigger in their size and the bigger size of the moving pattern

From the (figure 8.15) we can see that when switching to a more nutritious media once should consider also changing the interrogation window size. So far I have talked about choosing an appropriate window to rightly estimate the velocity, but how can one be sure that the estimated velocity is actually close to the accurate one? A way how one could do that is by observing how colony front develops and populates the side channel at the initial stages of the experiment. Namely colony grows and expands inside the vertical side channel in the form of a front wave which is invading free space as seen on Figure 8.16.b.

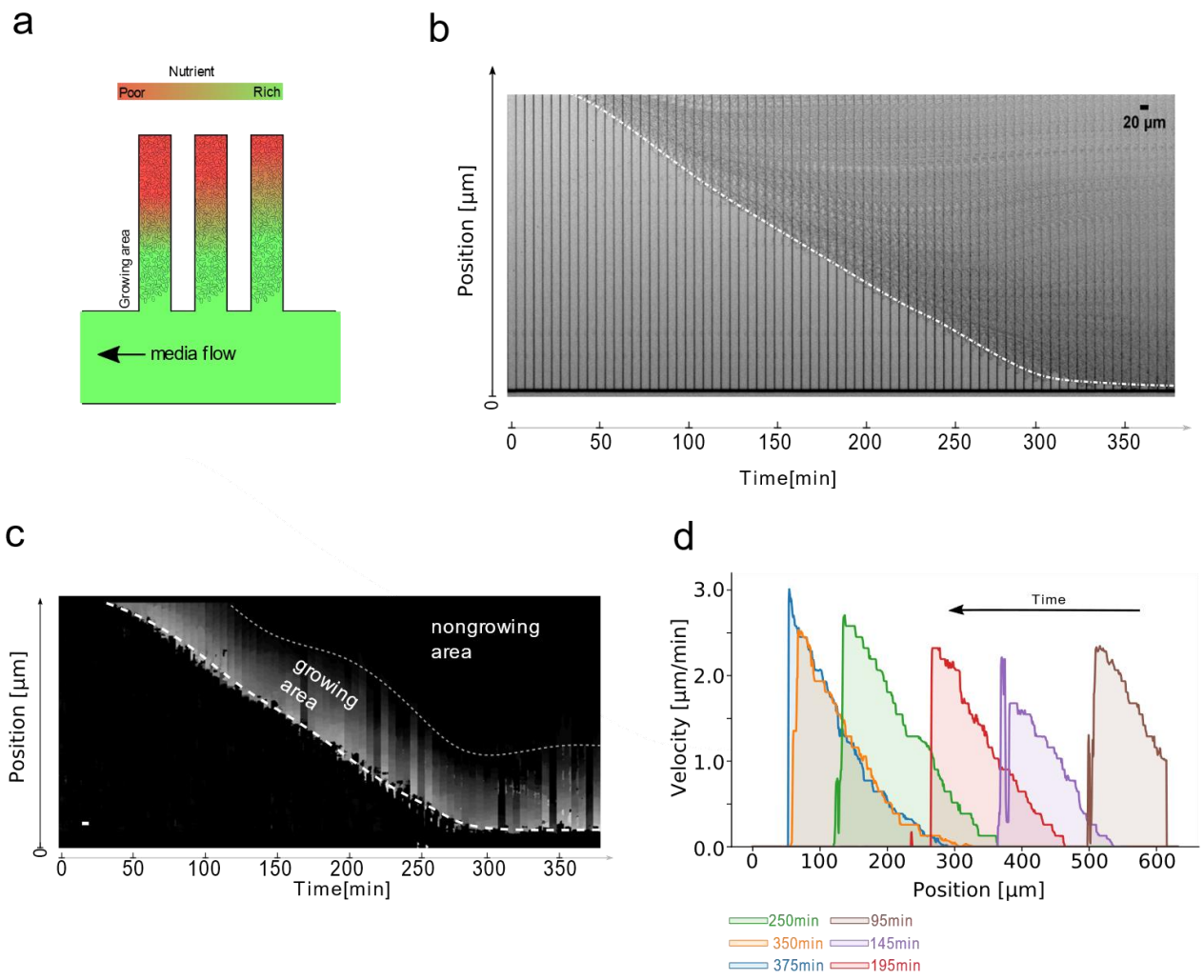

Figure 8.16. Observing the expanding colony front and evaluating the results of the PIV algorithm. (a) So far I have been focusing on quasi-stationary regime where the entire side channel is filled with bacteria and stable velocity and growth gradients have been formed. Although this regime was the focus of the study, the initial regime when the colony front expands is also of interest because we can optically test the velocity estimates obtained from the PIV algorithm. **(b)** Brightfield image of the bacterial expansion in 5xLB media containing 1000µM IPTG. At the begging of the experiment before the quasi-stationary state was formed, bacteria expand and gradually populate the side channel. Once the bacterial population reached the main channel it gets washed away towards the waste thanks to fluid passing through the main channel. **(c)** PIV estimation with 64x64 interrogation window of the cellular range expansion obtained from the brightfield image on (b). Position 0 represent the entry point of the side channel (measured from the main channel). Only frontal parts of the colony are involved in the growth and thus the range expansion, the rest of the colony is in growth arrested state. This is due to the fact that the front of the colony has access to the nutrients. As we go deeper inside the colony, towards the dead end of the chamber, nutrients become scarce and the growth stops. PIV estimation is an optical method, thus at certain instances either due to the bubble blocking the flow out of the channel or due to the low contrast PIV estimation fails to give a result (completely black sample points). White 20 µm scale is given at the lower left angle of the picture **(d)** Range expansion of the colony front. From colony expansion in the bright field and from the PIV estimations we could see that the colony front moved approximately 380µm in 155 min. If the front is moving at a constant velocity as the PIV algorithm suggests, the velocity of the expanding front should be around 2.45µm/min which is close to the actual value the PIV algorithm gave.

Initial invasion could be used to verify the results given by the PIV algorithm as we could easily optically detect how much colony has moved during a particular time frame. For instance from previous figures we could see that in the time frame of 155min the expanding colony front moved 380μm towards the channel opening. The estimated velocity corresponding to this movement is 2.45μm/min which is close enough to the actual value the PIV algorithm gave. This was repeated for various experimental conditions (LB+1000μM IPTG, 5xLB+1000μM IPTG, M9+0.4% glucose +1000μM IPTG, LB+200μM IPTG) within the range of velocities used in this study and they all corresponded closely to value estimated by the PIV algorithm, thus indicating that the algorithm performs an accurate estimation.

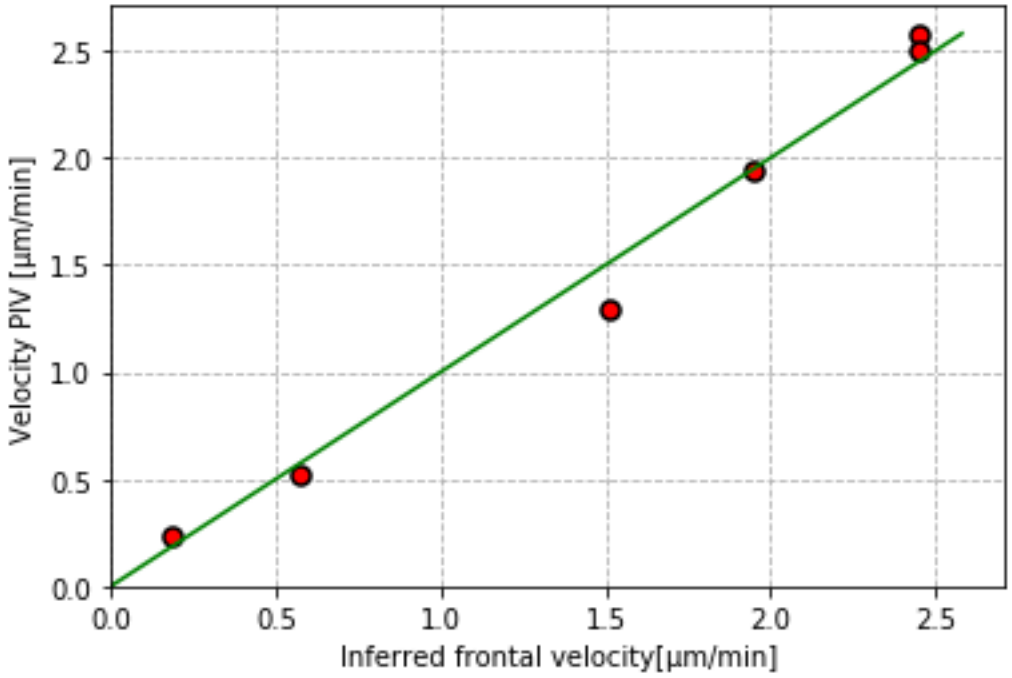

Figure 8.17. Verification of the results given by the PIV algorithm. The movement of the bacterial range expansion in a specific time frame was measured manually for several different independent experimental conditions (LB+1000μM IPTG, 5xLB+1000μM IPTG, M9+0.4% glucose +1000μM IPTG, LB+200μM IPTG). From the movement inside a specific time range, the velocity at which front is expanding was calculated. For each independent condition this velocity was compared to the velocity given by the PIV algorithm. Green line represents $y=x$ line

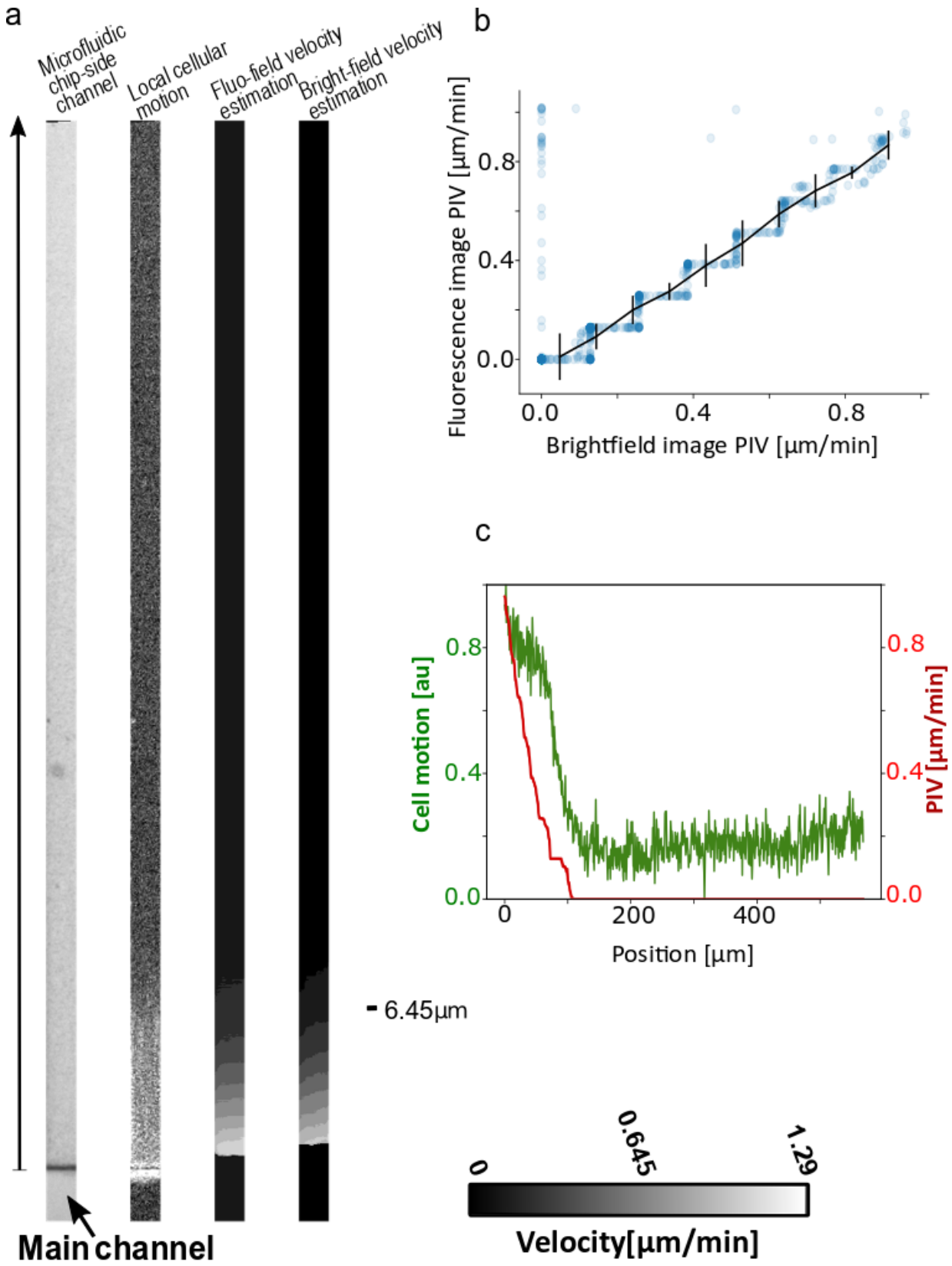
a
Microfluidic chip-side channel
Local cellular motion
Fluo-field velocity estimation
Bright-field velocity estimation
Main channel
b
Fluorescence image PIV [µm/min]
Brightfield image PIV [µm/min]
0.0
0.4
0.8
c
Cell motion [au]
PIV [µm/min]
Position [µm]
0
200
400
6.45µm
0
0.645
1.29
Velocity[µm/min]

Figure 8.18. **Validation of the PIV results – comparison with the local cellular motion and different channels (brightfield, fluorescence)**. **(a)** Side channel in brightfield with local cellular motion and velocity PIV estimation results coming from fluorescence and brightfield channels. Local cellular motion between two subsequent images was evaluated as standard deviation between the two. Since the only movement in the channel is due to growth local cellular motion determines the growing layer inside the side channel. Image shown in the figure represent the summation of all local cellular motion over 250min once the quasi-stationary regime was achieved. PIV was also applied on both brightfield (10ms exposure time) and fluorescence field (250ms exposure time) images. Images of the PIV results represent the median of the PIV results inside one channel over 250min in quasi-stationary regime. **(b)** Comparison of brightfield and fluorescent field PIV estimations. PIV method is an optical method of velocity detection that is based on image analysis. Although the results are highly impacted by the image contrast, both fluorescent and brightfield images should give approximately the same result. As one could see the results fall nicely on the x=y curve. **(c)** Results of the growing layer obtained from local cellular motion go nicely in line to those of the PIV estimation method.

In addition to this, the results of the PIV estimation can be further validated by looking at the depth of the growing area. The depth of the growing area can be determined by calculating the standard deviation of the pixels inside the side channel between two consecutive images. Cells are moving only due to the growth, thus where growth is present due to the movement standard deviation is going to be large. On the other hand areas with low standard deviation value, are areas in which pixels intensities remained approximately the same, (due to the lack of movement). Although compared to this method the PIV gives the velocity as an output we can obtain the growing area by looking at the spatial distribution of the velocities inside a side channel. Since the cells are nonmotile the movement captured by the PIV algorithm comes only due to the cellular growth. Thus growing layer represents the layer in which velocities are nonzero. Comparing growth areas obtained from these two methods gave the same result, which again indicates the accuracy of the PIV algorithm.

9.2.7 Cracks that might occur do not impact the maximum velocity

In certain conditions (specifically in LB media) cracks inside the bacterial colony occurred. It seemed that they occurred either in the nongrowing part of the colony or at the boundary between the nongrowing part and the growing part of the colony. In here I was only interested whether that cracks impact the velocity estimation or not and not what specifically causes them (even though I have thought about some ideas such as pressure disbalance caused by the oscillations of the flow rate etc.). For that reason I looked into the crack formation of three biologically independent experiments. Just one of them had cracks occurring (experiment 1). For that experiment I divided the side channels into two groups (cracks subset noted as ex1* and no cracks subset noted as ex1**), the ones with crack and the ones which lacked cracks. The other two experiments lacked cracks. For each condition and sub condition I estimated the maximum velocity of the colony (velocity near the channel opening), no statistical significance was found between them.

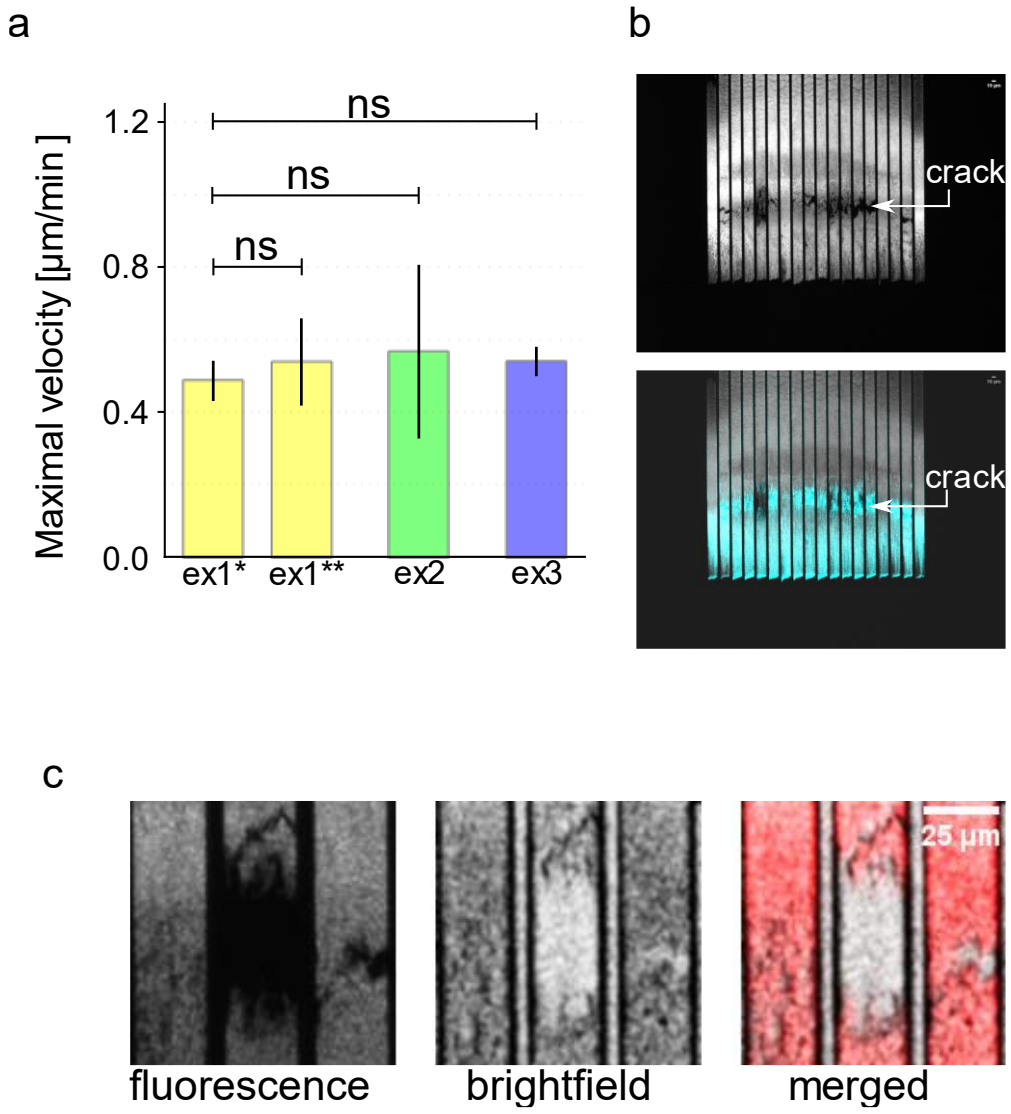

Figure 8.19. During the experiments cracks occurred in the upper nongrowing part of the colony. Cracks in the bacterial assembly do not impact the velocity estimations inside the side channels. Three independent experiments were conducted in LB media supplemented with 75µM IPTG. Two of them (ex2,ex3) lacked cracks, while in one of them in certain channels cracks occurred (ex1). For the crack occurring experiments, the side channels with the bacterial bio assembly lacking cracks were grouped inside the ex1** subset, while the channels experiencing crack occurring were grouped inside ex1*.Error bars for each independent experiment represent variation of the maximum velocity among different channels inside the microfluidic chip **(a)** Maximum velocity for each experimental set and subset. Error bars represent the variation between the maximal velocity between the side channels in the same set. No statistical significance was found between different sets and subsets. **(b)** Fluorescence channel of the crack occurring experiment. No fluorescence signal was obtained in the crack area. Local cellular motion measure was calculated over the time frame of 250ms to obtain the actively growing area. **(c)** zoom in of the crack in fluorescence, brightfield image and both of them merged together.

9.2.8 Estimation of the growth rate

Having the velocity profile validated we can proceed to estimate the establishment of the growth gradients inside the colony. Since the bacteria are non motile and the side channels are densely packed, incompressible movement only happening inside the channels due to the bacterial growth, the velocity of a colony $v(x_{pos})$ at a position x_{pos} is nothing else but the summation of all growth rates that happened prior to it. Mathematically expressed this gives

$$v(x_{pos}) = \int_0^{x_{pos}} \xi(x)dx$$

Where $\xi(x)$ represents the growth rate that is experienced by the cells comprising the colony at position x with in it. For that reason growth rate can be determined as a spatial derivative of the velocity profile

$$\xi = \frac{\partial v(x)}{\partial x}$$

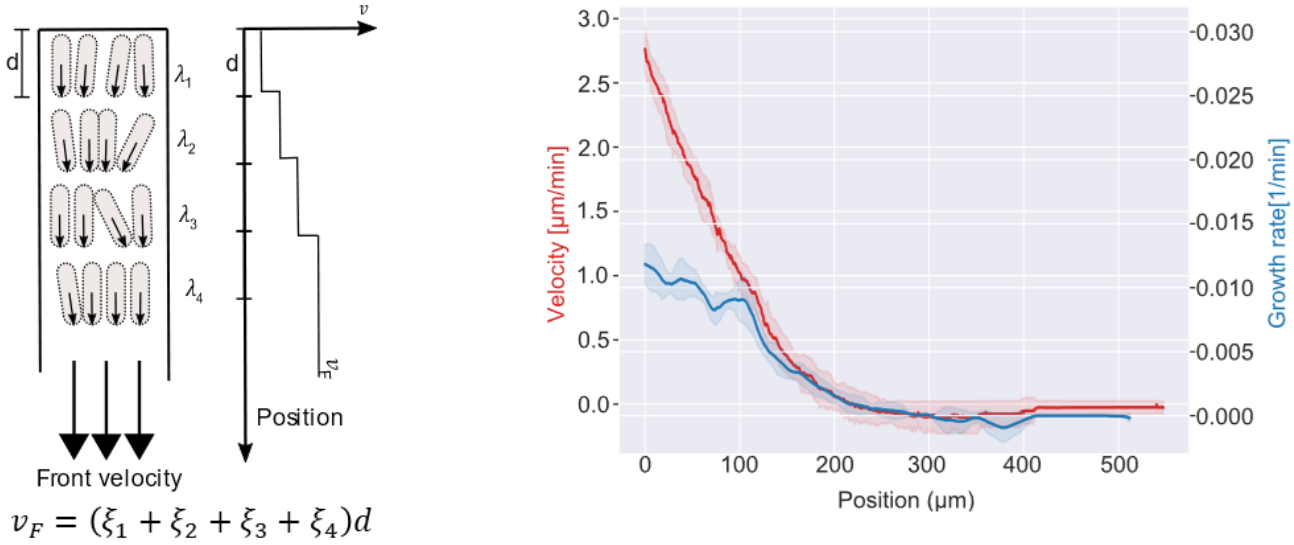

Figure 8.20. Obtaining **the growth rate information from the velocity profiles**. Since the bacterial strain lacks flagella and chemotactic capability the only reason of the movement happening inside the side channels is due to the colony growth. Thus at a certain position the velocity is nothing else but the summation of all the growth rates that happened before. Having this in mind the growth rate is nothing else but the spatial derivative of the velocity profile alongside the side channel.

Now that we have a pipeline how to study range expansion of bacterial cells and retrieve information about their growth rate and frontal velocity we must focus our attention now on how can we perturb growth inside of these colonies.

Several different strategies have been shown to be effective in well mixed liquid cultures (using IPTG inducible RNA polymerase strain, antibiotic and nutrient upshift/downshift). Since E.coli colonies grown in this microfluidic device are conceptually different then well mixed liquid culture it is questionable whether the same methods could be used in this settings. The following chapters will focus on inspecting can these modalities used to perturb and modulate growth patterns inside the colony, the ways how are they perturbing it and what changes do they trigger within the colony.

9.3 MODULATING RNA POLYMERASE LEVELS AND CELLULAR METABOLISM VIA THE IPTG CONCENTRATION AND NUTRIENT SWITCHES AFFECTS COLONY GROWTH PATTERNS INSIDE THE MICROFLUIDIC DEVICE

It was previously shown that in well mixed liquid cultures the IPTG concentration has the capability of modulating the growth rate of the PP2 *E.coli* strain by modulating the expression of RNA polymerase[65]. Unlike well mixed liquid cultures, cells in the microfluidic device experience nonhomogeneous environment with nutrient and chemical gradients being developed. Furthermore cells inside the device engage in a cellular cross talk. Thus how does the IPTG induction work and to what extent we could use it to modulate the growth structure of the colony remained an question that needed to be investigated. In order to investigate this I analyzed quasi steady state growth of the colonies inside the chambers of the microfluidic device. Velocity profiles alongside long axis of the side chambers and the colony front velocity at different IPTG concentrations are shown at figure 8.21.

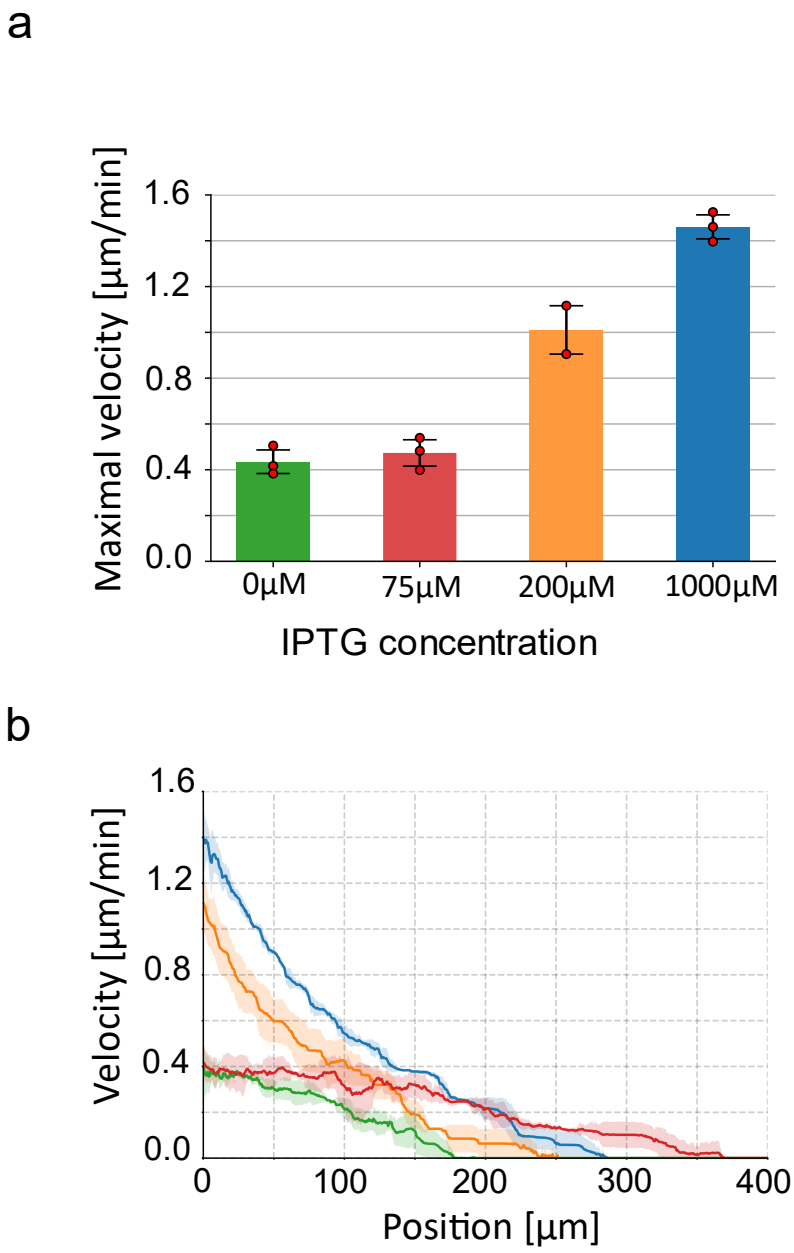

Figure 8.21 IPTG modulates the range expansion of the colony. The modulation of IPTG levels leads to changes in RNA polymerase level. Changing IPTG levels affects the cellular growth rate. As a result, the velocity profiles inside the microfluidic chip are also influenced by IPTG modulation of RNA polymerase levels and subsequent changes in growth rate**. (a)** Maximum velocity of invasion speed inside the microfluidic chip plotted as a function of IPTG concentration in the LB media. Prior to inserting the cells inside the microfluidic chip, the overnight culture of 1000µM IPTG was washed four times with LB media with an appropriate IPTG concentration and was incubated at least for an hour in such well mixed conditions. Cell loading was conducted as described in the methods section. Maximum velocities were estimated once the quasi-stationary steady state inside the channel was achieved. Red dots signify the biological replicates while the error bars are standard deviation between them. **(b)** IPTG modulation of the steady state quasi-stationary velocity profile inside the microfluidic channel. The data shown on the figure comes from one of the

biological replicates. Color code is the same as in (a). Shaded areas represent the standard deviation while the lines represent mean velocity profile observed in the period of 250min.

In well mixed liquid cultures, lower concentration of IPTG led to the decrease of the growth rate of E.coli due to the fact that with low amount of IPTG, E.coli is unable to synthesize new RNA polymerase. In a similar manner, in a microfluidic device lowering down IPTG levels in the media made colony expand (and grow) more slowly compared to the expansion and growth at higher concentrations. Again this is due to the fact that lowering down IPTG levels inside the media, lowers both down the access of IPTG which is needed for growth. This showed that indeed we could use the IPTG to modulate growth patterns within the colony, but how do these growth patterns arise and what determines them? Studies in [60] indicated that the cells positioned at the colony front play a major role for the entire community. To inspect this I investigated the relationship between the growth rate of the frontal cells and the size of actively growing cellular community within the colony in both different IPTG concentration and different media. When frontal cells in different media experienced a concentration of IPTG that was nonlimiting in growth for well mixed liquid cultures an interesting observation was seen. Namely experimental data points all fell on an inverse linear curve, meaning that increasing the growth rate at the colony front comes at the expense on decreasing the growing layer of the colony. If we look at the velocity profiles for instance, for a more concentrated media (5xLB) the velocity profile was steeper, shorter and did achieve higher growth rates then compared to the LB one. A similar result was reported in [58], [61] in similar chip design where the increase of the glucose in the media came at the expense of shorter growth areas. When media was supplemented with IPTG concentration of 1000μM, the IPTG was not limiting at colony growth level. This can be seen by comparing the velocity, the growth rate and the size of the growing layer of the PP2 strain supplemented with 1000μM IPTG with the PP1 strain (WT with RNAP tagged with mCherry) from the microfluidic device experiments (figure 8.22.), but also from experiments in well mixed liquid cultures.

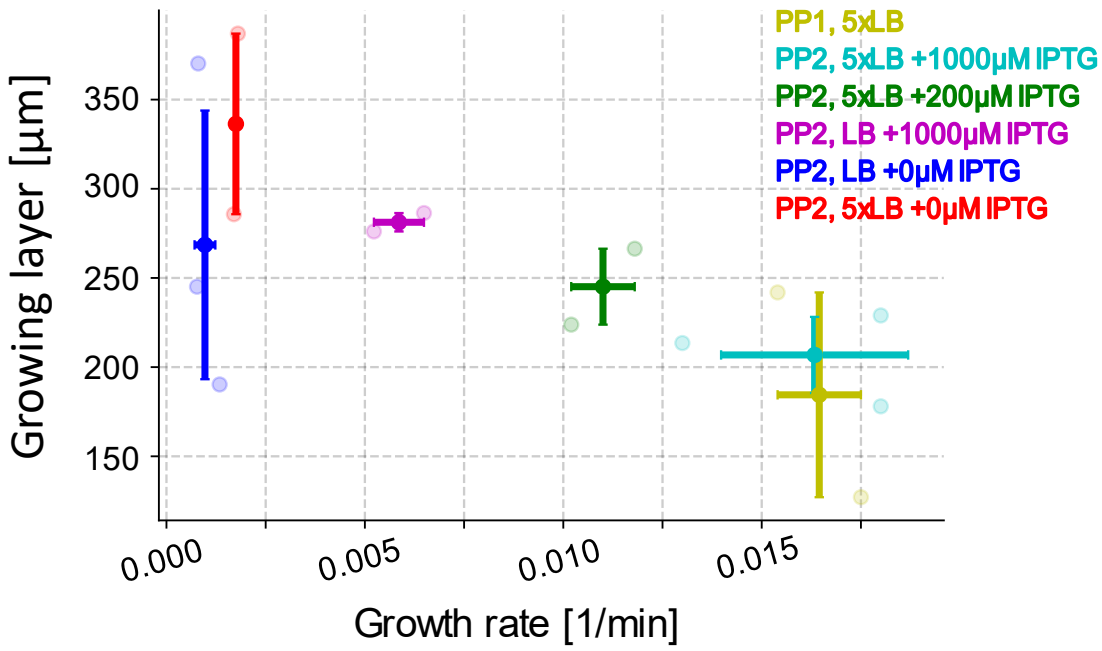

Figure 8.22. Relationship between growth rate and growing layer in different conditions and strains. Data demonstrates that as the growth rate increases, the growing layer decreases. This indicates that when cells at the forefront of the colony experience rapid growth, it comes at the expense of the growth rate in the deeper regions of the colony. When comparing the WT strain (PP1) and the IPTG inducible one (5xLB media,1000µMIPTG) there isn't significant difference, meaning that IPTG concentration at that level wasn't limiting to the colony growth. When removing the IPTG from the media cells stop dividing and only elongate with having their nutrient consumption at a low basal level. Having this in mind applying more concentrated media (5xLB vs LB media) would results in the expansion of the growing layer with little or no influence on the growth rate itself, which was experimentally observed. The error bars are standard deviations of the biological replicates.

In addition to IPTG concentrations that weren't limiting for well mixed liquid cultures, I inspected how the colony behaved when the IPTG was completely removed from the media. In that case cellular growth ceases. Substrates supplied in the media, previously used for growth, now become available (due to the fact that the slow growing cells/arrested cells stop their utilization). The cells in this case only elongate and use only basal nutrient consumption, thus applying more concentrated growth media would yield just a bigger growth zone as the nutrients would penetrate deeper inside the colony, with little or no impact on the colony growth rate itself. This indeed happened as it could be seen at (figure 8.22.).

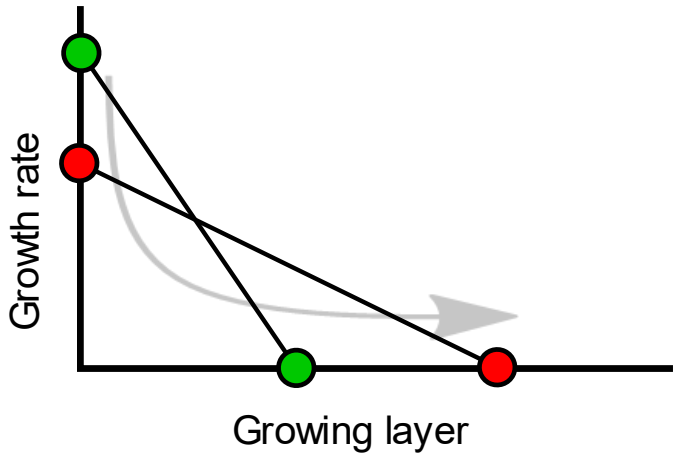

Figure 8.23. Increasing the growth rate at the colony front comes at the expense of the size of the growing layer. When cells in the colony front grow at the higher growth rates they consume more resources. This leaves cells in the back with less resources to grow, thus the growing layer consequently decreases.

Having all of this in mind we can say that the colony behavior is determined by what happens at the colony front. If cells at the colony front grow at a higher rate, less nutrients would be able to penetrate deeper inside the colony towards the dead end of the side chamber, consequently lowering making the actively growing layer of the colony smaller. An interesting way to capture how these patterns are formed would be to plot both the range expansion velocity of the colony with the growth rate associated with it. As the growth rate at a certain positional itself is a spatial derivative of a velocity profile, this value would give us information of how steep the range expansion gradient at a certain position is. Interestingly when I plotted both spatial growth rate and the velocity profile in LB media with different concentrations of IPTG or as in M9 media with different concentration of glucose all of these curves had fallen on the same respective pattern. 5xLB media supplemented with 1000µM IPTG on the other had increased the slope.

While it is not surprising that growth and velocity are interdependent, given the fact that the growth rate is derived from the velocity profile, what is interesting is the linear dependence between these variables and the consistent patterns observed across various IPTG or glucose concentrations. This pinpoints on two things:

-Firstly that the spatial velocity inside the side channels of the microfluidic chip can be represented as an exponential function of the position inside the microfluidic channel.

-That in the case of experiments with different IPTG for instance (figure 8.24.), all the experimental data basically represents the repetition of the same experiment. This would mean all the IPTG conditions that differed from the curve representing the velocity profile of LB+1000Mm IPTG would basically fall on the same if we spatially moved them.

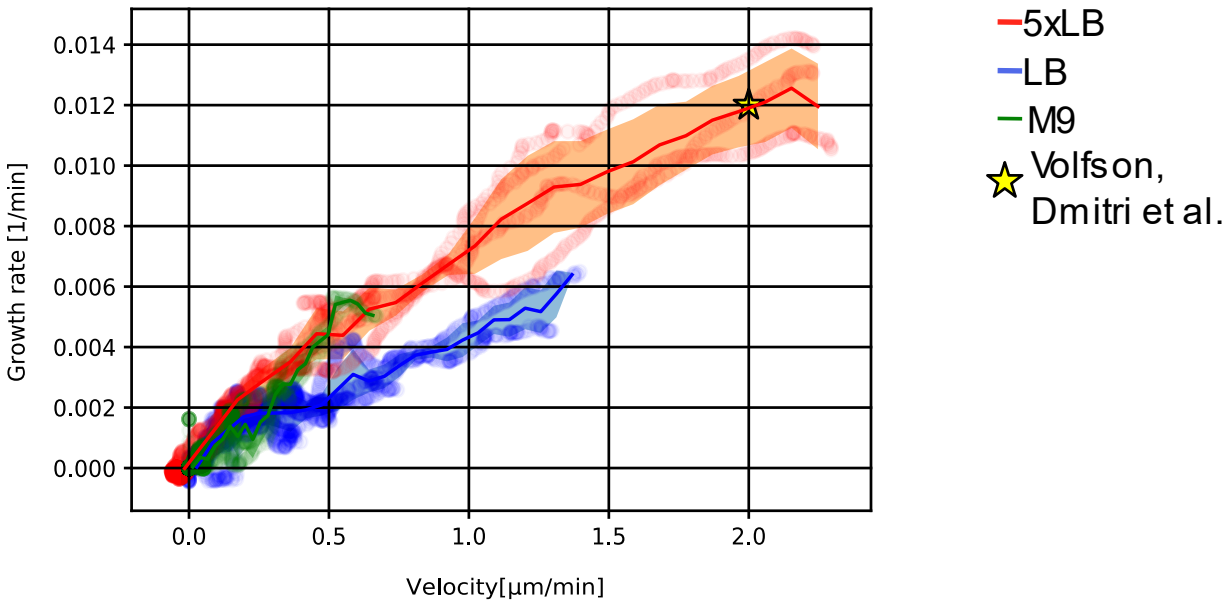

Figure 8.24. Growth rate-Velocity landscape. Although the relationship between the growth rate and velocity was expected, a linear relationship wasn't. Additionally the fact that when plotted together, velocity and growth curves with different IPTG concentrations collapse at the same one in LB media came also at surprise. Experiments with different glucose concentration also had also collapsed in the M9 media. This would mean that all the experiments were essentially replicates of the same underlying process. Reported frontal velocity and it's corresponding growth rate from a study that investigated spatial structuring of the dense E.coli colonies is also shown at the plot [57].

Bacterial growth in M9 media supplemented with 0.4% glucose and in LB media show similar growth rates in well mixed liquid cultures. In this system as well, cells at the colony front which have direct access to the main channel, in a the same manner for both LB and M9 with 0.4% glucose, share a similar growth rate. The range expansion (velocity) though is different and it is smaller for M9 media, as nutrient gradients being imposed with M9+0.4% glucose are shorter as the cells quickly get deprived from the carbon source. When looking at the growth rate of frontal cells in both M9 media with 0.4% glucose and LB media a decrease in the growth rate compared to the well mixed liquid cultures was observed. The same observation was made in [57], where authors hypothesized that either mechanical forces caused by high ordering and patterning of bacterial cells or cellular waste/ chemical signaling might, or combination of both might reduce the growth rate of cells inside highly dense E.coli colonies. All the experimental curves were obtained for quasi-stationary conditions where the IPTG concentration was kept at a constant level throughout the experiment.

Interestingly when plotting the velocity profile with the rpoBC-mCherry fluorescence an inverse relationship was found. RpoBC-mCherry fluorescence signal is a proxy for RNA polymerase concentration. On the other hand from the velocity profile one could infer the growth rate at a certain position by performing a spatial derivative (Figure 8.25). The regions of higher velocity are located closer to the channel opening and are the areas that experience more rapid growth rates. The inverse relationship between those the RpoBC-mCherry fluorescence signal and the cellular growth rate was also observed at the single cell level across various nutrient conditions (see appendix). This relationship may be explained by the fact that cells growing at a slower rate also dilute less of their cellular material. This accumulation of the proteins due to lack of dilution might explain the patterns both on a single cell level but also inside the microfluidic device. This has the potential to make colonies resilient to changes during the experiment in IPTG concentration. For instance we could imagine that even if at a certain point media was switched to the one not containing IPTG, the colony would continue to grow as nothing happened for some time since the cells positioned deeper inside the colony, towards the dead end of the chamber would still contain a big quantity of undiluted RNA polymerase. Thus I asked myself to what extent this delay could be and in general what would be the dynamical response of the colony once the IPTG is switched off during the experiment?

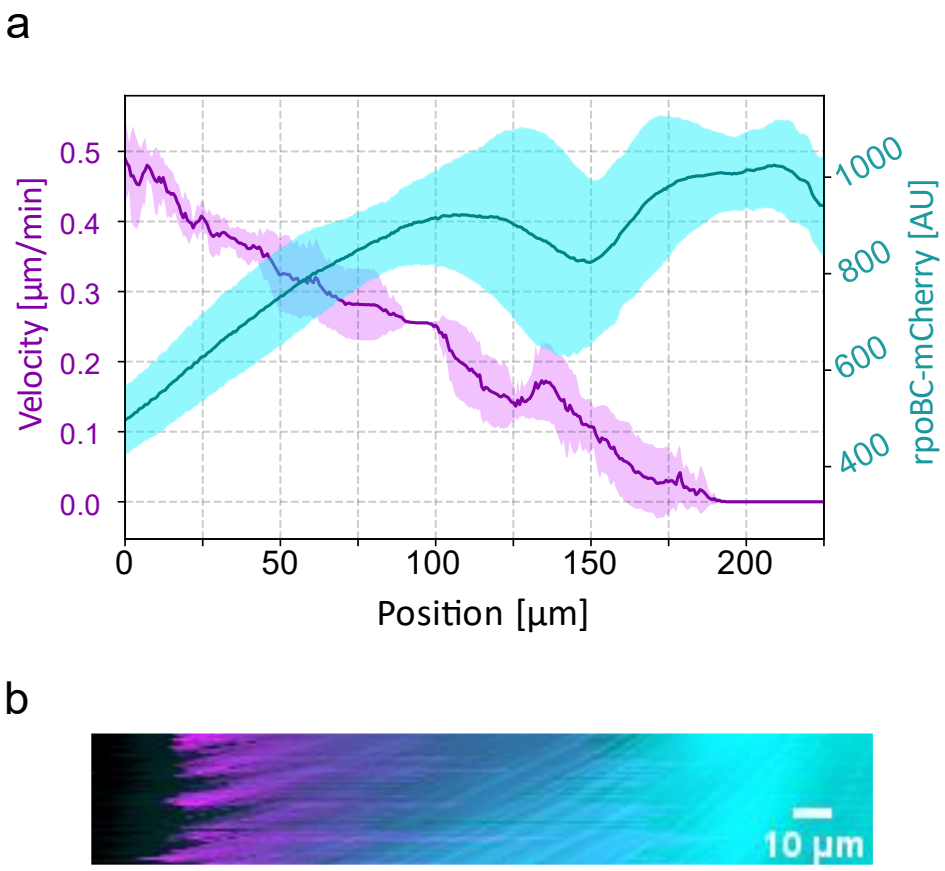

Figure 8.25. Inverse relation of the velocity profile and rpoBC-mCherry fluorescence profile in the actively growing area. Same relationship was observed in single cell experiments with different nutrient conditions (see last chapter). **(a)** Profiles of the velocity and rpoBC-mCherry alongside the side channel. High velocities are observed at the channel opening, near the main channel where the growth rates is high and the environment is rich in nutrients. As we go deeper inside the side channel the growth rate and the velocity decrease as nutrient become scarcer. **(b)** Kymograph of the rpoBC-mCherry profile and the velocity profile. Data comes from the PP2 strain in LB media supplemented with 75µM IPTG from one of the replicates. Shaded areas represent the standard deviation in 250min time frame and lines the mean value.

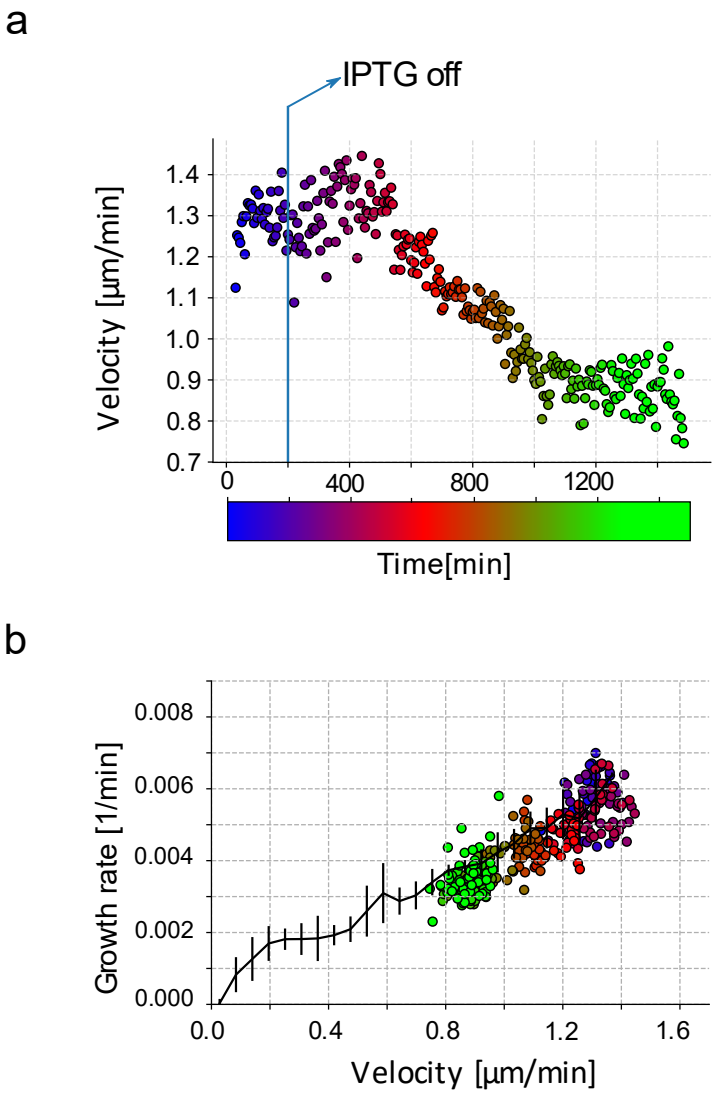

Figure 8.26. Changing the IPTG level during an online experiment. The aim of the experiment was to observe the dynamics of the system when the IPTG is removed from the media. The media used in the experiment were LB media supplemented with 1000µM IPTG and the LB media without the IPTG supplementation. The system had started from growing state with media LB+1000µM IPTG flowing through the system **(a)** Before switching to the media that didn't contain IPTG I waited until the system reached the quasi-stationary steady state. After the IPTG was removed, there was a significant time lag of approximately 5 hours before any signal changes were observed. Furthermore, over a relatively long time period of 25 hours, the reduction in velocity range was relatively small, going from 1.3 to 0.8µm/min. My hypothesis why this happens is due to the fact that cells in the back of the side channel still have large quantities of non-diluted and accumulated RNA polymerase. Initial accumulation came in the beginning stages of the colony formation where these cells were not limited by nutrients. As colony development progressed these cells fall behind. Eventually a lack of nutrients occurs which makes them lower down or ever arrest their growth rate, which in turn prevents the dilution. Once the IPTG is removed from the media frontal cells are quickly washed away, but cell in the back still have a reservoir of accumulated RNA polymerase. This explains slow dynamics that we see. **(b)** Switching off the IPTG in the media makes the colony follow previously described relationship.

Since the colony front determines the redistribution of the resources inside the colony and over all patterns that emerge I tracked how front velocity and frontal growth rate changed in real time with the changing IPTG concentration. Data from the dynamical IPTG switch is visualized at figure 8.26 from which we could see that:

- Dynamics of system is incredibly slow. After removing the IPTG from the media there is a time delay of about 4-5h before the system starts responding
- The system's response is weak, namely after 25h velocity decreased from 1.3 to 0.8µm/min.
- The systems growth rate and velocity follow previously described linear pattern

The overall dynamics of the system can be explained by its nature. As previously said one hypothesis is that the cell positioned deeper inside the chip earlier at one point in their lifetime (before the quasi-stationary steady state was formed) were exposed richer nutrient conditions and thus have had experienced higher growth rates. This had them expressing at a higher level RNA polymerase. As colony expanded and progressed, the cells at the back became deprieved of the nutrient resources. This led to either total or almost complete growth arrest. Without growth, dilution ceased and made consequently cells in the back to retain a lot of their initial RNA polymerase. Once these cells again become exposed to the nutrients (even with the lack of IPTG in the media) they have a reservoir of RNA polymerase due to accumulation of the cellular material. This makes the overall system more resiliant to changes in the IPTG concentration. To sum up, so far we have seen that the colony front plays a major role in formation of the growth patterns inside the colony. When the cells are growing at a higher pace, less nutrients seems to be avalaible for the cells in the back, consequently leading to the decrease in the actively growing layer of cells. We have seen so far that both IPTG and nutrients can be used to modulate these patterns but the nature between these two modulations remains different.While the IPTG directly targeted transcriptional machinery, the nutrient upshift/downshit impacted the entire metabolism of the cell. Because of the controlled action of IPTG it was a prime target to use it as a tool to obtain control over the range expansion of the colony. Two things regarding this metodology did stand out - the inverse relationship between the growth and the mCherry accumulation and the collapse of the velocity-growth rate data on the same curve regardgless on the concentration of IPTG level in the LB media (and actually glucose level in the M9 media and the overall linear like shape of these curves). The first one pinpoited to the fact that arrest of the cells deep within the colony (due to the lack of nutrients) prevents them to dilute their cellular products. Before these cells entered the growth arrest stage, they experienced nutrient rich environment and had high expression levels of RNA polymerase. Upon growth arrest the high concentartion of these molecules remained due to the lack of dilution, thus we could expect that the colony would be resilient to changes in the IPTG concentration, which was indeed the case when in real time the IPTG levels were switched from 1000µM to 0µM.

Before covering of the third and last modality - the impact of antibiotics on the growth patterns within the colony I wanted to dig deeper in what could be behind the linear like curves that were seen with changing IPTG concentration in LB media and glucose in M9 media. This would be the covered by the section that follows.

9.4 PHYSICAL INTERPRETATION OF THE RELATIONSHIP BETWEEN THE POSITIONAL GROWTH RATE AND THE VELOCITY.

In this section I will cover what could be behind the observed linear like relationship between the positional growth rate and spatial velocity. Since the growth rate is nothing more than a spatial derivative of the velocity profile and having in mind the experimental data, the ratio between the growth rate and the velocity can be written as:

$$\frac{\frac{\partial v}{\partial x}}{v} = \alpha$$

This ratio between a spatial derivative of a variable with the same variable is well known in physics and in material science and it represents so called attenuation coefficient. Attenuation coefficient represents how easily a material or a substance can be penetrated by the beam of light or radiation. Let us imagine that we position a source of beam particles right in front of the material (position $x = 0$). If we mark beam particle strength at the position x from the source with a $I(x)$, and the beam particle strength source at position $x = 0$ with I_0 we can write the following equation

$$I(x) = I_0 e^{-\mu x}$$

Where μ is the attenuation coefficient defined mathematically as $\frac{dI/dx}{I}$ and it is an inverse of the attenuation length. If μx is small we can use the approximation of the exponential function

$$I(x) \approx I_0(1 - \mu x)$$

From here we can see that if we chose x to take the value of the attenuation length $x = 1/\mu$ the beam strength at that position would be $I(x) \approx 0$

Following the same logic of the attenuation coefficient, we can say that the slope $\frac{\frac{\partial v}{\partial x}}{v}$ represents the nutrient attenuation coefficient of the colony. This coefficient would tell us how do the nutrient are redistributed inside the colony and at what depth they get depleted. On the following figure I plotted the inverse of the local slope $\frac{\frac{\partial v}{\partial x}}{v}$ vs the growing layer depth (position at which no movement was reported). Since the growth seemed to be described by the exponential function, it should be expected that both of these give similar results, which was indeed the case.

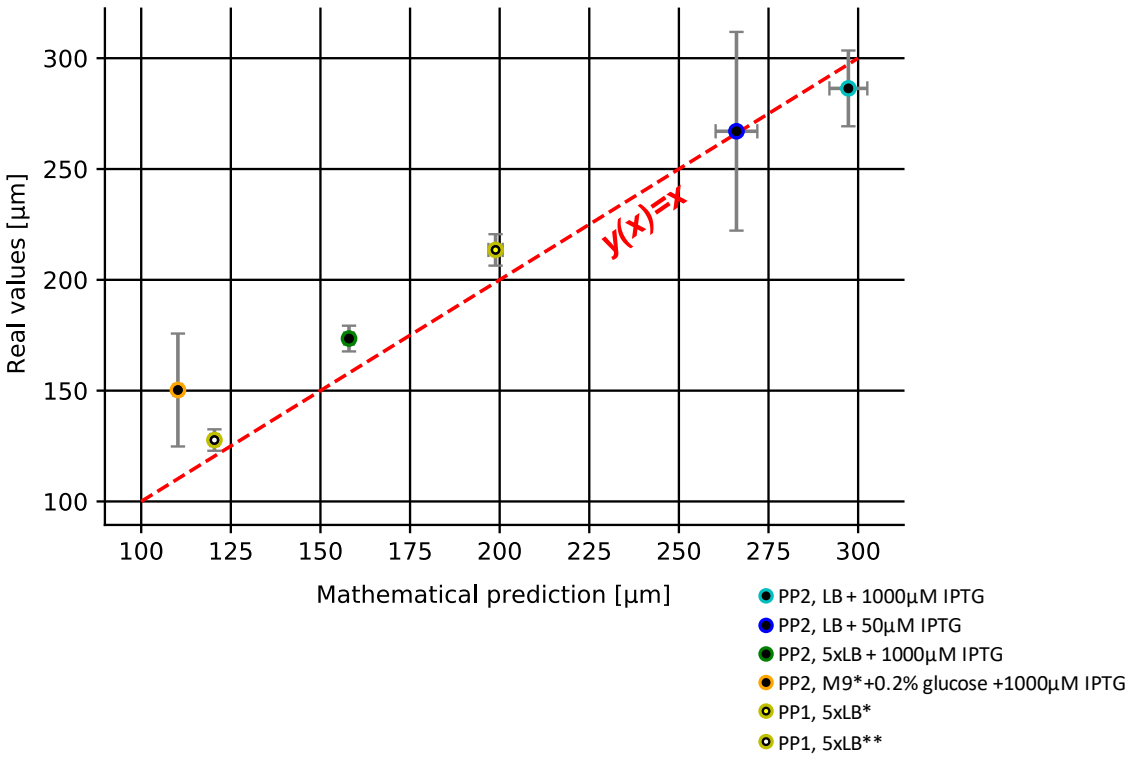

Figure 8.27. Physical interpretation of the growth rate-velocity slope. As the attenuation coefficient in material science, where the inverse of this coefficient represents the penetrative depth of a light beam/radiation, the slope of the growth rate-velocity profile at a specific position represents an nutrient attenuation coefficient. As expected, the inverse of the slop correlates perfectly with the actual growing layer of the colony.

To further elucidate the relationship, and specifically what lies behind the ratio α I used reaction diffusion equations.

Equations

Reaction diffusion equations are widely used to model formation of cellular patterns in complex multicellular like assemblies[62], [81]–[83]. They are able to describe formation of the growth patterns and to explain how bacteria move and how they collectively expand in space and time. The model consists of two partial differential equations- one describing how the nutrient profile is being developed throughout the assembly, and the other describing the bacterial growth. For the study I started from the model equations described in [81]. The model aims to describe he formation of growth and velocity patterns inside of a side channel. Since the translation is the only movement bacteria experience alongside the main axis of the side channel, equations from the [81] could be represented as:

$$\frac{\partial g}{\partial t} = D\frac{\partial^2 g}{\partial x^2} - \rho u(g, IPTG)$$

$$\frac{\partial \rho}{\partial t} = -\frac{\partial(\rho v)}{\partial x} + \varepsilon \rho u(g, IPTG)$$

Where

g – represents the nutrient profile alongside the side channel

ρ –bacterial density at a specific position within the side channel

Bacteria need energy to grow and sustain themselves. In order for this to happen bacteria need to metabolize nutrients. At the end of the side channel nutrients are being constantly replenished by the flow in the main channel. Due to the length of the side channel, nutrients diffuse throughout the side channel with a diffusion constant *D*. In addition to nutrients diffusing, the they are also consumed at the same time by bacteria. This is described by the part $\rho u(g, IPTG)$ of the first equation. Only part of the energy from the uptaken nutrients is used for the biomass production. This can be mathematically represented as $\varepsilon \rho u(g, IPTG)$, where $\rho u(g, IPTG)$ gives total nutrient uptake, and ε represents that the biomass conversion factor. At the same time cells are pushing each other causing movement. This movement, mathematically formulated as $\frac{\partial(\rho v)}{\partial x}$ causes the cell to eventually leave the side channel, thus decreasing the biomass.

In order to gain the insight into physical meaning of the experimentally obtained coefficient between growth rate and velocity I sought to analyze the equations of this system in detail. For this to happen I considered the following:

1) quasi-stationary state is achieved. Colony reaches a steady state, where nutrient concentration and growth rate form a stable gradient alongside the main channel axis.

2) Diffusion (diffusion coefficient D) is fast enough.
3) Cellular density ρ is constant alongside the channel – the whole channel is entirely populated with bacteria, differing only in the growth rate

I will considered two cases of the yield (biomass efficiency)

-constant yield

-linearly dependent yield on the growth rate.

9.4.1 Case 1: Constant yield

Having in mind the considerations (quasi-stationarity, fast diffusion, constant cellular density), the system of partial differential equations gives

$$D\frac{\partial^2 g}{\partial x^2} = \rho u(g)$$

$$\rho\frac{\partial v}{\partial x} = \varepsilon\rho u(g)$$

If we insert the expression for $\rho u(g)$ from the first equation into the second one we have:

$$\rho\frac{\partial v}{\partial x} = \varepsilon D\frac{\partial^2 g}{\partial x^2}$$

If we further integrate from the boundary of the nongrowing area (defined growing layer boundary represents the position 0) deep within in the colony inside the side chamber towards side chamber opening next to the main channel the last expression transforms into

$$\rho\int_0^x \frac{\partial v}{\partial x} = \varepsilon D\int_0^x \frac{\partial^2 g}{\partial x^2}$$

$$\rho v = \varepsilon D\frac{\partial g}{\partial x}$$

Now we have the two expressions in which we have both the growth rate $\frac{\partial v}{\partial x}$ as well as the velocity v. From experimental data we now that the ratio between the growth rate and the velocity gives a constant coefficient for a specific media. If we divide both expressions we obtain:

$$\frac{\frac{\partial v}{\partial x}}{v} = \frac{\frac{\partial^2 g}{\partial x^2}}{\frac{\partial g}{\partial x}}$$

Thus

$$\frac{\frac{\partial^2 g}{\partial x^2}}{\frac{\partial g}{\partial x}} = \alpha$$

This is an important result since it shows that under the condition of constant biomass yield, the nutrient gradient decays (at rate α) with the increasing depth of the bacterial assembly. The higher the α the faster the nutrients are depleted inside the growth channel. The exact analytical solution shows of the previous equation can be deduced by integration. By integrating from the non growing boundary deeper in the channel toward the channel opening, we can derive the exact expression for the quasi-stationary steady state nutrient field

$$g(x) = \frac{c_1\, e^{\alpha x}}{\alpha} + c_2$$

$$g(0) = 0 \rightarrow c_2 = 0$$

$$g(L) = g_{max} \rightarrow \frac{c_1 e^{\alpha L}}{\alpha} + c_2 = g_{max}$$

$$g(x) = g_{max}\frac{1 - e^{\alpha x}}{1 - e^{\alpha L}}$$

In the same manner we could derive the exact expression for velocity and growth profile using experimentally obtained relationship between the velocity.

$$\frac{\partial v}{\partial x} = \alpha v$$

From which :

$$v(x) = c_3 e^{\alpha x}$$

$$v(L) = v_{max}$$

$$v(x) = v_{max}\frac{e^{\alpha x}}{e^{\alpha L}}$$

Since $v(0)$ represents the velocity at the boundary of the nongrowing layer we can say that $v(0) = v_{max}e^{-\alpha L} \approx 0$. This assumption holds as for small αx exponential function can be approximated as $e^{-\alpha x} \approx 1 - \alpha x$. For $x = L$, we can write $e^{-\alpha L} \approx 1 - \alpha L$. Since L represents the depth of the growing layer which is an inverse of the coefficient α, we can say that $e^{-\alpha L} \approx 0$.

If we go back to the initial equations we could represent the yield as

$$\varepsilon = \rho \frac{\partial v}{\partial x} \Big/ D \frac{\partial^2 g}{\partial x^2}$$

With expressions for $v(x)$ and $g(x)$ the yield turns into:

$$\varepsilon = \frac{\rho}{D} \frac{\mu_{max}}{\alpha^2 g_{max}} (1 - e^{-\alpha L})$$

Having in mind that $e^{-\alpha L} \approx 0$ and by rearranging the equation we can write:

$$\mu_{max} = \varepsilon \frac{D}{\rho} \alpha^2 g_{max}$$

Maximum growth is a function of the maximum concentration of nutrients. Mathematically this can be formulated as $\varepsilon u(g_{max})$, where $u(g_{max})$ represents nutrient uptake for the end of the channel. From there it goes:

$$u(g_{max}) = \frac{D}{\rho} \alpha^2 g_{max}$$

Which means that in the case of having a constant yield the maximum nutrient uptake is dependent with α

9.4.2 Case 2: Growth rate linearly dependent yield

If we now expand our considerations on having a yield that is linearly depend on the growth rate, we can write:

$$\varepsilon = \varepsilon_0 \mu = \varepsilon_0 \frac{\partial v}{\partial x} = \varepsilon_0 \mu_{max} e^{\alpha(x-L)}$$

Where ε_0 is a constant.

If we mark $\varepsilon_{MAX} = \varepsilon_0 \mu_{max}$ we have:

$$\varepsilon = \varepsilon_{MAX} e^{\alpha(x-L)}$$

In here α represents the decay rate of the biomass yield inside the bacterial assembly. Interestingly when we insert the expression for ε inside one of the equations comprising the reaction diffusion system we will get:

$$\rho \frac{\partial v}{\partial x} = \varepsilon D \frac{\partial^2 g}{\partial x^2} = \varepsilon_0 \frac{\partial v}{\partial x} D \frac{\partial^2 g}{\partial x^2}$$

If we combine the last expression with the equation described nutrient profile development of the reaction diffusion system $\frac{D}{\rho}\frac{\partial^2 g}{\partial x^2} = u(g)$ we get:

$$u(g) = \frac{1}{\varepsilon_0} = const$$

This means that in the case if the yield is linearly dependent on the growth rate, the biomass uptake will remain constant. Since the growth rate itself is a exponential function, the biomass yield is this case can be described as a exponential function with the decay which is equal to α

With this I would be concluding this chapter. Now as mentioned earlier we will be continuing to the third and last modality that was shown to have potency to influence growth in well mixed cultures and transiently perturb the growth patterns inside the dense microcolonies-the use of antibiotic which can target various key components of protein expression machinery. The biggest problem with the use of antibiotics is the rise of antibiotic resistance. In the case of dense colonies, this would make them resilient to the antibiotic treatment. It was shown that dense colonies over time adapt to new circumstances in a rather quick way, thus how can we use and at which concentration we should use an antibiotic, not just to transiently modify the growth patterns but to achieve a long term modification (which could potentially enable range expansion control) are some of the question that are going in the focus of the next chapter.

9.5 DOXYCYCLINE PERTURBS GROWTH PATTERNS WITHIN THE COLONY

Previous studies [58], [61] which involved a similar chip design showed the resilience of the entire community to tetracycline antibiotic at a concentration which was lethal to well mixed liquid cultures (100μg/ml). Upon suddenly exposing the colony to the antibiotic, the growing cells induced the stress response and readjusted their gene expression. This enabled the entire colony to reach a new steady state in which cells inside the colony resumed growth at a rate 75% of that before, despite having encountered high and lethal levels of antibiotic. The reason for this comes both from the combination highly structured community and the expression of resistance genes. The dynamical range [75%-100%] can be increased if we increase the antibiotic concentration or if we switch to another class of antibiotic which triggers lower resistance levels in *E.coli* strains, like for instance doxycycline[84]. Like tetracycline, doxycycline is a bacteriostatic and a member of tetracycline class of antibiotics which binds to the 30S ribosomal subunit, preventing the association of the charged aminoacyl-tRNA with the ribosome consequently inhibiting bacterial protein synthesis [85], [86]. In [87] the authors studied the evolution of doxycycline resistance of K-12 *E.coli* strains. The study showed that highly resistant strains have significantly higher MIC of around (96 μg/ml) compared to the non resistant ones (4 μg/ml) and have decreased levels of carbon metabolism. Both of this information were crucial in determining the antibiotic concentration that would be used for control purposes and increasing the dynamic range. Cell in the back of the chip have decreased levels of carbon metabolism and consequently thus have either decreased levels of growth rate or have completely went into cell arrest regime. Additionally they have higher levels of antibiotic resistance as shown in [58], [61]. For this reason in order to assess the resilience of the community and to see to which extent it would be possible to manipulate the structure and the expansion rate of the colony assembly using antibiotics, I tested the response of the community in the presence of doxycycline. Doxycycline concertation was set at the 2.5x concentration of the previously reported MIC for highly doxycycline resistant E.coli strains grown in a microfluidic settings (250μg/ml).

To characterize to which extent the structured environments are more resilient to the antibiotic I firstly characterized the growth rate before and after the addition of the antibiotic in well mixed liquid cultures of *E.coli* in the 5xLB media supplemented with 1000 μM IPTG and 0.2% glucose.

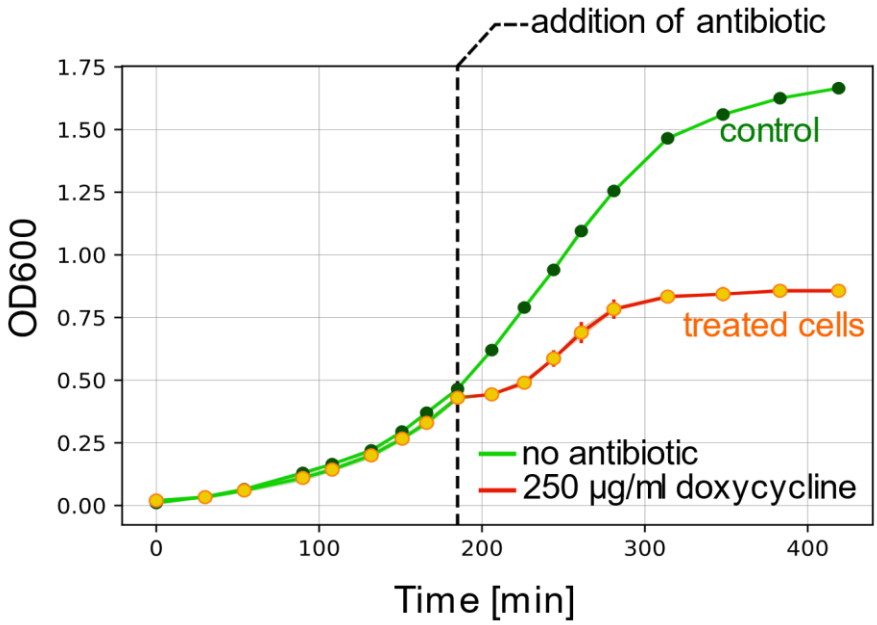

Figure 8.28. Effect of doxycycline in well mixed liquid cultures. OD600 of *E.coli* liquid cultures was tracked over time. Three biological replicates were grown overnight in 5ml 5xLB media supplemented with 1000µM IPTG. Overnight cultures were diluted 1:100 into five ($replicate_1$, $replicate_2$, $replicate_3$ & $replicate_{1\_control}$, $replicate_{2\_control}$) 50ml shake flask containing 30ml of 5xLB media was supplemented with 1000µM IPTG. Two of the replicates dilutions ($replicate_{1\_control}$, $replicate_{2\_control}$) were defined as control and were not treated with the antibiotic throughout the experiment. After the cell reached mid exponential phase 250µg/ml doxycycline was added to the media ($replicate_1$, $replicate_2$, $replicate_3$). The reported growth rate is the mean over n replicates (n=3 for treated cells, n=2 for untreated cells/control). Error bars are standard deviation among the replicates.

At high levels of antibiotic growth in the well mixed liquid cultures was arrested. To test the resilience and the impact on the structured population I used previously described microfluidic chip. The microfluidic settings enabled us to quickly change between the media and to suddenly expose the cells to the doxycycline. The impact of the doxycycline exposure on the maximum velocity of the colony front, before and after the exposure is showed on figure 8.29.

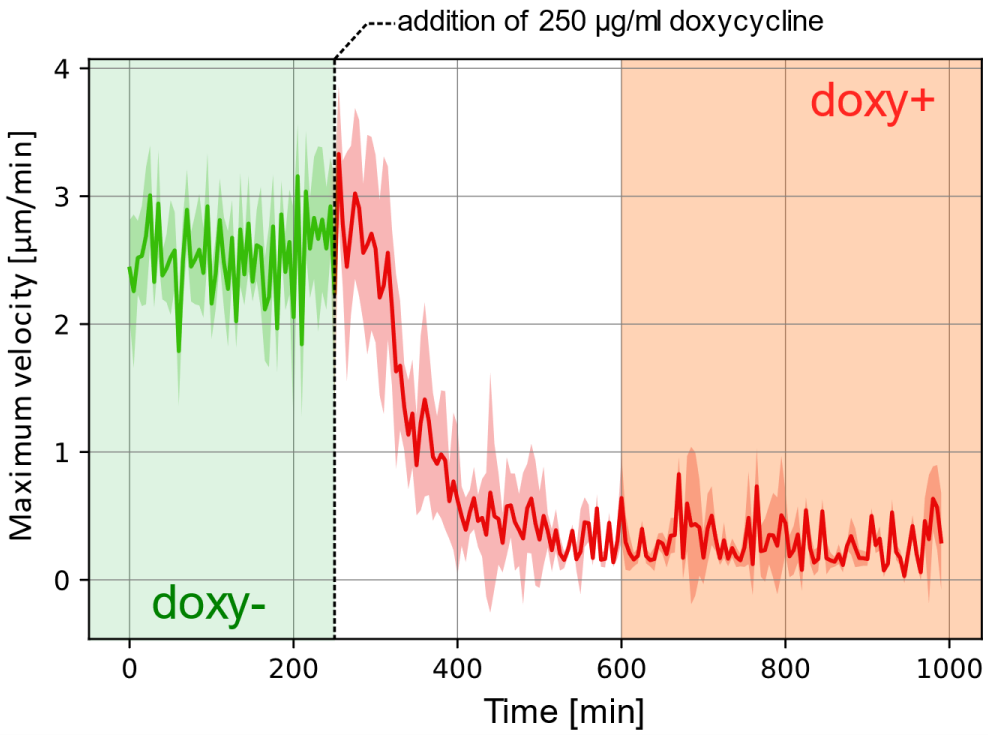

Figure 8.29. Effect of doxycycline on the colony inside the microfluidic chip. Image acquisition was started once the quasi-stationary steady state was established. Cells were grown in 5xLB media supplemented with 1000µM IPTG. Area shaded in green represent the time interval in which cells were not treated with doxycycline. After approximately 5h the media was switched to the 5xLB media supplemented with 1000µM IPTG and 250µg/ml doxycycline. After some time new quasi stationary regime was established (area shaded with red color). Shaded areas around the curve describing the maximum velocity in time represent the standard deviation between the different side channels, while the curve itself represent their mean.

After exposing cells to the antibiotic there was a short time delay before one could see the full impact of the doxycycline exposure-white shaded area of the figure 8.29. Following the reinstatement of the quasi-stationary regime with the doxycycline present (red shade area) I compared velocity profiles and estimated the maximal growth rates inside the colony for each condition.

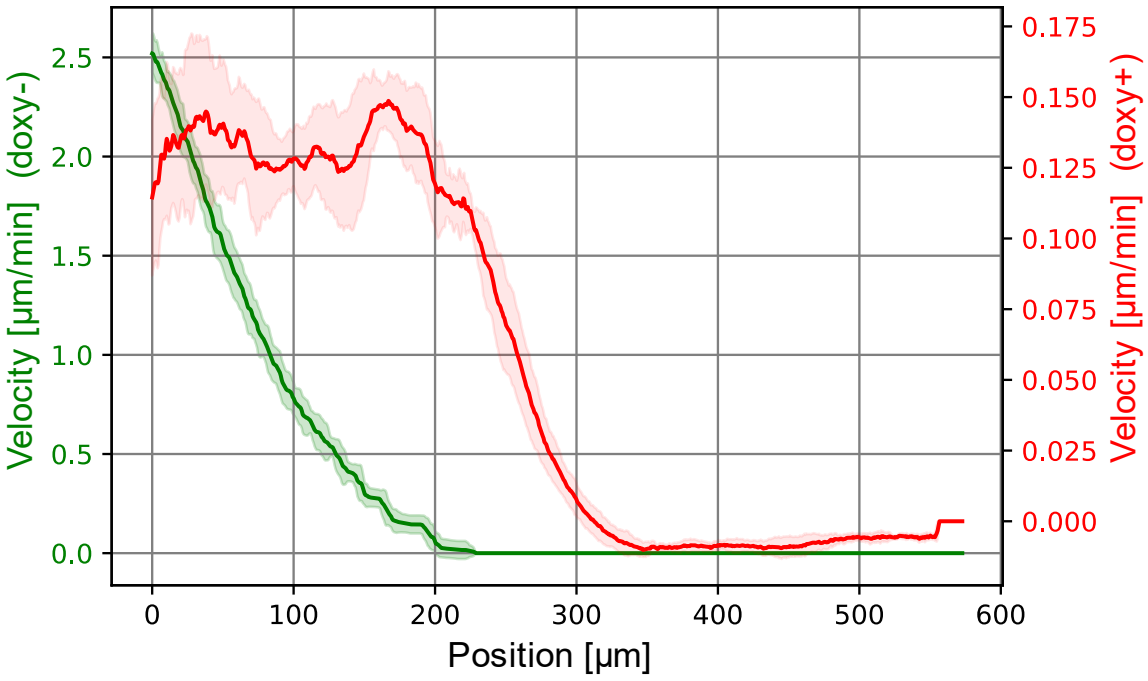

Figure 8.30. Effect of doxycycline on the colony inside the microfluidic chip – impact on the velocity profiles. Velocity profiles of the two quasi-stationary regimes defined on figure 8.29 compared on the same graph. Horizontal axis is shared and represents the position inside the side channel. Green color represents the velocity profile of system before the switching to the media containing doxycycline, while the red color represents the quasi-stationary regime following it. Upon switching to the new media, growth layer expands deeper in the colony and the maximum velocity decreases to about 6% of the one before the addition of the antibiotic.

While in well mixed liquid cultures the cells stopped growing, the bacteria living in structured populations didn't – namely there was a portion of the colony that kept growing at a much lower paste. After again switching back to the media not containing doxycycline, it was spotted that the colony started recovering. The antibiotic switch experiment and its results were in line to that what was previously shown, where the colonies exhibiting spatial structuration were resistant to the antibiotic treatment otherwise lethal to the liquid well mixed cultures.

What was also inline to the mentioned studies is the fact that antibiotics can be used to manipulate the structure and the growth profile of the bacterial assembly. Furthermore the decrease of the growth rate at channel opening is followed by the increase of the growth area. In here I saw the doxycycline concentration of 250µg/ml (2.5x the MIC concentration of the colonies highly resistant to doxycycline) was able not just to transiently modify the growth patterns in [75%-100%] range, but were able to have a long term influence. Furthermore the influence of doxycycline at this concentration increased the modification of the growth expansion range 25%.

So far I have shown how bacteria grow and how we can interpret the images to infer the range of expansion of bacterial colonies grown in a microfluidic device. I have characterized the systems behavior, analyzed the establishment of bacterial growth patterns and investigated the possibilities of perturbing the patterns by using three different modalities -IPTG, nutrients and antibiotics, all of which were shown to be capable of perturbing the system. Observing the data in velocity-growth rate space surprisingly showed linear patterns and the collapse of data regardless of IPTG concentration in LB media or glucose concentration in M9 media. The slope of these curves was defined as the nutrient attenuation coefficient with its inverse representing the size of the growing layer of the colony. Under the assumption of quasi-stationary state, fast diffusion and constant cellular density this slope was shown to represent mathematically the nutrient decay inside the side chambers of the microfluidic device.

When left on its own, system finds its quasi-stationary steady state. Once the environment has changed due to an external disturbance for instance, system senses it, adapts and moves from its previously held state towards a new one. But what if we want that the system moves at a desired trajectory and not the one it tends to move on? Also we could desire to keep a system in a specific state and make it more robust to changes, regardless of external disturbances in the environment. Both of these demands can be achieved by providing a system with the information of its current state and by making appropriate corrective measures. This is what we call a feedback and what would be the focus of the next chapter. In the next chapter firstly I will focus on how biological and technical system use feedback to their advantage followed by a short and concise explanation of the fundamentals of systems theory and control. Then I will provide an overview of the field which seeks to apply fundamentals of control to biological systems in order to predictively and accurately control them- cybergenetics.

10 CLOSED FEEDBACK LOOP SYSTEMS-REAL TIME CONTROL

Before considering what a feedback is, let us first define what is a dynamical system? Famous control theorist Astrom defines it as:

> *"… a system whose behavior changes over time, often in response to external stimulation or forcing."* [88]-page 1

Such systems are omnipresent with some of the examples being movement of sun, planets and galaxies, tumor growth, financial markets, traffic jams, weather, growth of crystals, bacterial growth, pandemics, predator-prey dynamics and so on.

Broadly speaking, we can fit all of these dynamical systems into two basic groups – feedback (closed) loop systems and open loop systems. If we have two systems which are interconnected in the manner that they impact one another, their dynamics are tightly coupled. For example lets look at the system at (*figure 9.1*). In here the output of the second system represents the input of the first one, but also the output of the first one is an input to the second one. This circular arrangement is what we call a feedback and the systems having it are called feedback systems (closed loop systems). On the contrary the system lacking this circular arrangement (interconnection) is we call an open loop system [88].

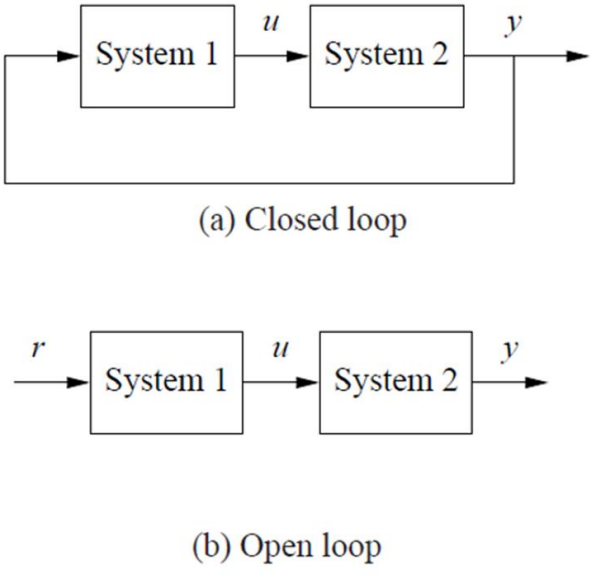

Figure 9.1. Schematic of a closed loop and an open loop system (a) Closed loop system. In here the two systems are interconnected and impact on one another. The output of the second system represents the input of the first one and the other way around. **(b)** Open loop system**.** Open loop system lack the circular arrangement described before**.** The image was taken from [88]

If engineered properly feedback systems give some remarkable characteristics that can be exploited and thus it should not come as a surprise that most of the systems that are surrounding us are feedback systems. When the feedback tends to dampen the change, system becomes more stable and has the tendency to remain in that state. This is heavily exploited by both natural and human build systems for the means of regulation. Many biological systems in order to survive and thrive require tight regulation of thermal, chemical and biological properties in face of changing external conditions. For instance glucose concentration in humans is held in an narrow range of 4-6mM [89]. The disability of the system to maintain glucose is this narrow range gives rise to a condition called diabetes. Tight regulation of blood glucose levels is achieved through interactions of diverse pancreatic hormones and particularly by insulin and glucagon. When blood glucose levels rise, the body receptors sense a change and activate secretion of insulin in pancreas by β cells. If the human body lacks energy, insulin secretion signals the liver, muscle and fat cells to use glucose. On the other hand if the sufficient energy is present, insulin triggers the signal to the liver to store the excess glucose as glycogen. When blood glucose levels fall down bellow the regulated value pancreatic α cells start releasing glucagon which signals the liver to start to break down it's glycogen storage and to release glucose. In this way the body successfully controls the glucose levels in narrow range.

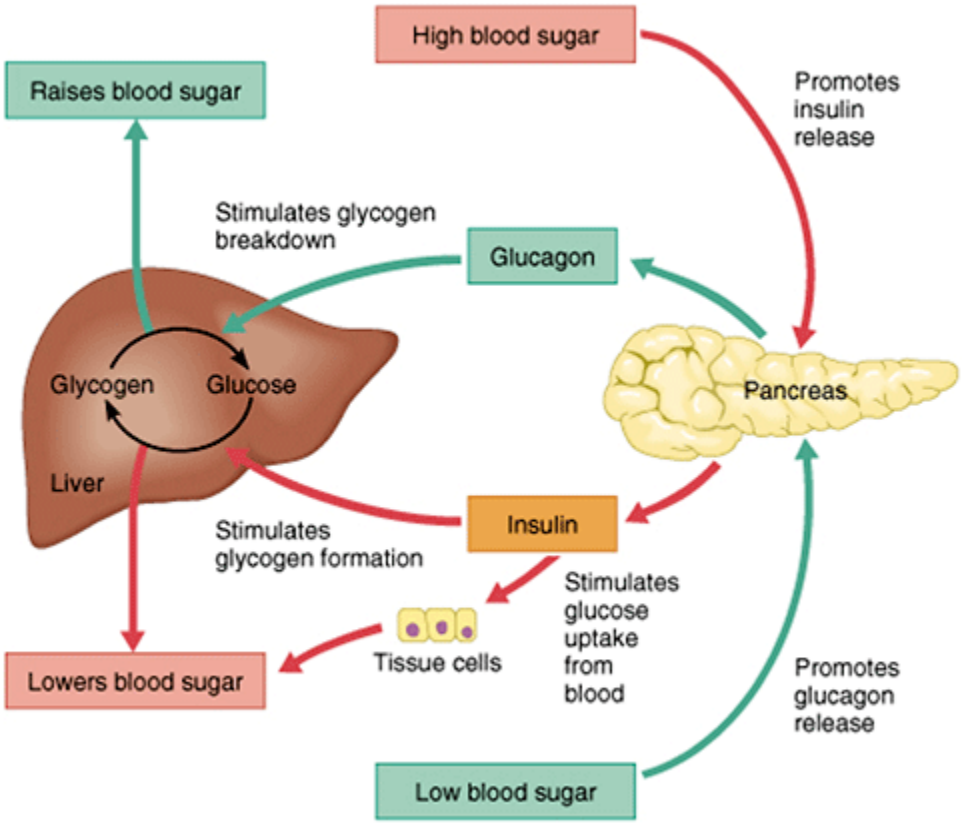

Figure 9.2. Example of a biological feedback system – Tight regulation of glucose levels in humans. Regulation of blood glucose levels is achieved through the interactions of insulin and glucagon. If the blood sugar level is high, pancreases secretes insulin which stimulates glucose uptake from the blood. If the sufficient energy is present excess glucose is stored as glycogen. On the contrary, if the sugar blood levels fall bellow a certain value, pancreas secretes glucagon which stimulates glycogen breakdown and raises the blood sugar level. Image taken from [90].

Another example of system regulation in biology is the osmoregulation in yeast. Multiple studies have been covering the perfect adaption mechanism that yeast utilize when they experience osmotic shock [91]–[94]. As a consequence of a hyperosmotic shock, the external osmotic pressure rises. This makes water molecules diffuse out of the cell which causes the turgor pressure and the cell volume to drop suddenly. This is sensed by proteins located in the membrane (Sln1). Once the sudden drop in volume in sensed, Sln1 triggers the activation of the osmoregulation Hog pathway and activates and translocates the Hog1 protein to the nucleus. Once in the nucleus, Hog1 triggers the gene expression of multiple genes among which the ones responsible for glycerol production are the most important. The rise of intracellular glycerol concentration increases the intracellular osmolarity and restores the turgor pressure. Upon restoring the turgor pressure, cell exports the Hog1 from the nucleus and stops the adaptation mechanism. Besides this in parallel cells also activate Hog1 independent mechanism. This is achieved through Fps1, a channel protein situated in the membrane which regulates the outflow of the glycerol, which upon the turgor pressure drop immediately closes. Schematic representation of the yeast osmoregulation mechanism can be seen on (*figure 9.3*)

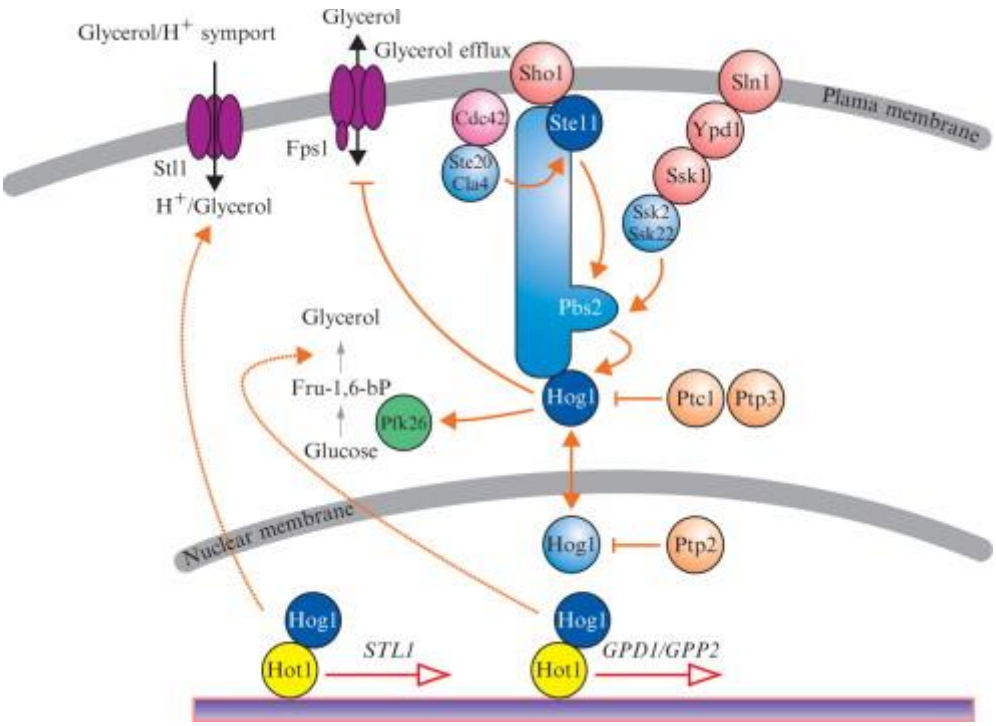

Figure 9.3. Osmoregulation in yeast, HOG pathway. Osmotic shock triggers the change in the turgor pressure which as a consequence leads to a sudden drop in volume. This is sensed by membrane localized sensor Sln1 which triggers the activation of the Hog cascade subsequently translocating the Hog1 protein inside the nucleus where it triggers gene expression of multiple genes, among which the glycerol producing ones are the most important. In addition to the activation of the Hog pathway, the osmotic shock triggers the closure of the glycerol efflux pumps Fps1. This leads to rise in intracellular glycerol concentration which reestablishes the turgor pressure. Upon restoration of the pressure the Hog1 is exported from the nucleus, the Hog pathway shuts off and the adaptation mechanism stops. Image taken from [95]

The type of the feedback which was covered by these two examples is the type of feedback that is defined as negative feedback. Besides negative feedback there is a another type of the feedback that tends to amplify the changes that occurred. This triggers the system to move away from the state that it was previously in. This eventually ends up in amplifying the change which makes the whole system more unstable. This is what we define a positive feedback loop. Although positive feedback loops are related with uncontrolled processes such as nuclear chain reactions or climate change models [96], the natural systems found a way to exploit its characteristics. For instance positive feedback loop is present during the childbirth contractions. The stretching of the walls of uterus drives contraction which in turn further stretch the uterine walls. Furthermore the benefit of having a runaway process is specially important in cellular

signaling pathways, where the positive feedback loop has a role as an amplifier and/or signal enhancer. This can be seen in the amplification and prolongation of the epidermal growth factor (EGF) receptor activity in developing *Drosohilla* egg as pointed out in [97]. The epidermal growth factor (EGF) activity is crucial for specification of dorsal follicle cells. Signal is driven by EGF receptors in follicle cells as a response to Gurken, which is produced by the oocyte. Between the oocyte and follicle cells there is a physical barrier called vitelline membrane. This membrane presents an obstacle for the Gurken signaling. *Drosophila* managed to solve this problem by developing a positive feedback loop. Namely the EGF receptors when activated, drive the expression of Rhomboid-1, which in turn activates Sptiz which prolongates and amplifies the initial trigger – the Gurken expression.

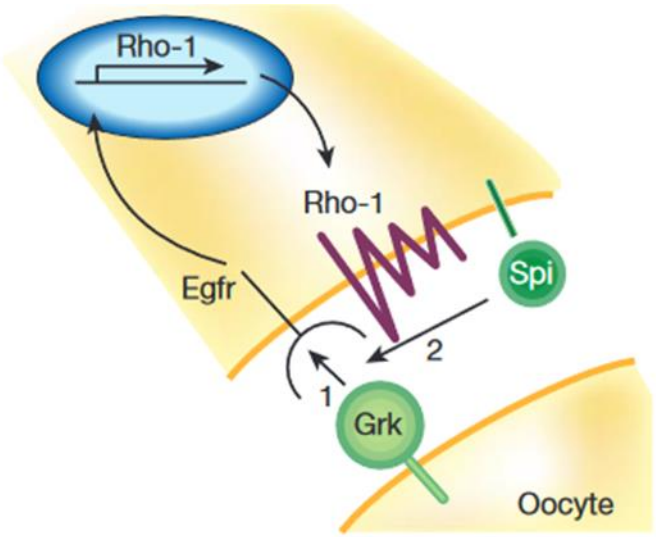

Figure 9.4. Example of a positive feedback loop involved in cell signaling in *Drosophila*.. As a response to gurken (Grk) in oocyte an EGF signal in follicle cells is triggered. This signal is crucial for specification of dorsal folical cells and it is driven by EGF receptors (Egfr). Oocyte and follicle cells are separated by a membrane which represents an obstacle for the signaling molecules. To overcome this physical barrier activation of the Egfr triggers Rhomboid-1 expression (Rho-1) in follicle cells. Once activated the Rho-1 activates Spitz (Spi) which amplifies and prolongates the expression of the initial trigger – Grk expression. Image taken from [97]

Positive feedback loops have also a role in establishing a bistable behavior in a system. System is defined as bistable, when it has only two stable states and when it has the ability to switch between them when given the appropriate input. Living systems exploit bistability as the mean to stably maintain one of the two possible, distinct gene expressions [98]. For instance the bacteria *E.coli* utilizes this concept in its expression of lactose utilization genes [99]. The basic structure of the lac operon of E.coli consist of three genes (lacZ, lacY and lacA) and two regulators (lacI, CRP)

LacZ- encodes for β galactosidase, which helps the cell to convert the lactose into allolactose and further intermediates

LacY- encodes a membrane transported lactose permease, which facilitates the uptake of glucose and similar nonmetabolizable lactose analogs such as thiomethylgalactoside (TMG) or isopropyl-beta-D-thiogalactopyranoside (IPTG) through cellular membrane.

LacA – encodes acetyltransferase which has a role in sugar metabolism

LacI- repressor of the operon. Inducers (allolactose, TMG, IPTG) bind to it and relieve the repression activity of the repressor

CRP (cyclic regulator protein)- an activator of the operon. Its activation depends on the concentration of the molecule named cyclic AMP protein (cAMP) which respond to the nutrients it the media (when glucose concentration is high cAMP levels are low). When it is present in the cell, it binds to the CRP and enables the molecule to trigger the expression of the lac operon. The cAMP levels are not affected by nonmetabolizable lactose analogs.

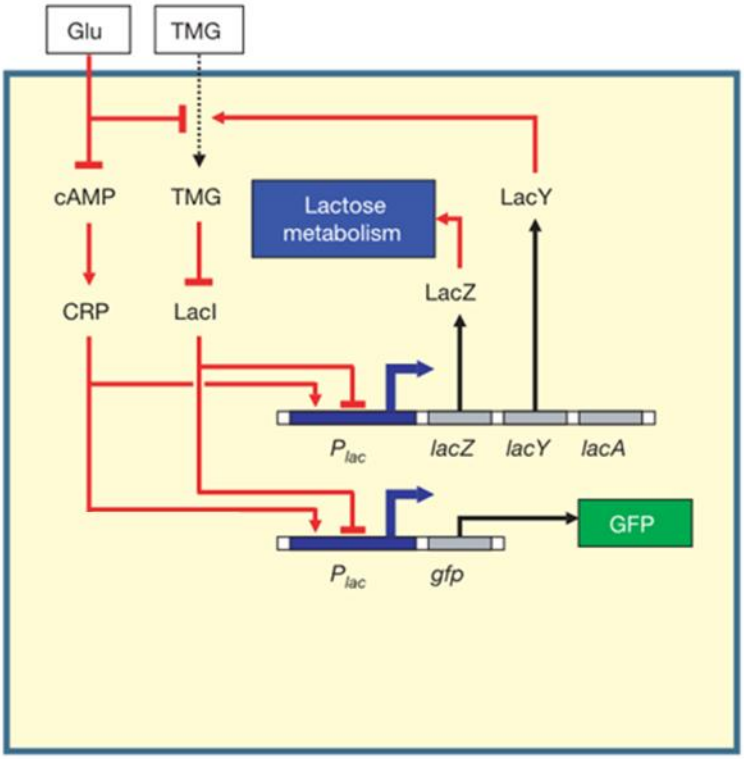

Figure 9.5. Example of a positive feedback loop and bistable behavior-lactose operon switch. The CRP (cyclic regulator protein), whose activation depends on cAMP level, is the activator of the lac operon. When external glucose levels are high the cAMP levels are low, and the other way round – when glucose levels are low, cAMP level are high. When operon is activated TMG can modulate its activation. TMG binds to the lacI which is the repressor of the operon. The important component of the lac operon which is principle component of the positive feedback loop is lacY gene. lacY gene encodes a membrane transported lactose permease. Lactose permease facilitates the uptake of glucose and similar nonmetabolizable analogs such as TMG and IPTG through cellular membrane. To track the modulation of the lac operon the authors in [99] incorporated also a GFP under the influence lac promoter. This helped them to observe the activation of the lac operon. Figure was taken and adapted from [99].

With varying the concentrations of and TMG and glucose supplemented in the media one could regulate the activity of the operon. TMG binds to lacI, relieves the repression and triggers further TMG uptake through synthesis of lacY. Thus by varying levels of glucose or TMG/IPTG concentration in the media, one can modulate the activation of the lac promoter. This positive feedback loop leads to bistability as [99] as nicely illustrated by this incorporating the green fluorescent protein (GFP) in the *E.coli* chromosome under the control of lac promoter.

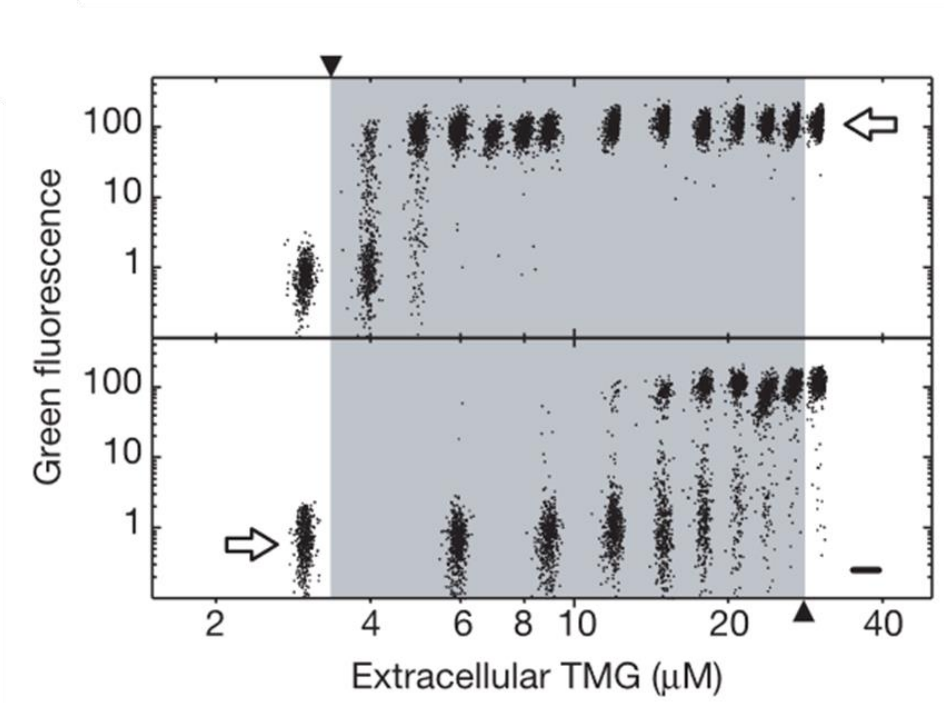

Figure 9.6. Example of a positive feedback loop and bistable behavior-Lactose operon switch modulation with TMG. Behavior of cell populations is shown. Each dot corresponds to one cell. The arrows in the figure represent the starting positions. Bistability and hysteresis in the system behavior were spotted. In the lower graph the cells were initially uninduced. When starting from the uninduced state, the TMG must increase above 30mM until full induction and activation of the lac operon. In the graph above, the cells were initially fully induced with TMG. In order to turn off initially induced cells the TMG levels need to fall bellow 3mM. Figure was taken from [99].

As examples show the benefits of having a feedback inside the system are immense. In most of the engineering problems we seek to stabilize and control the system in a predictable manner, thus most of inventions have integrated a closed negative feedback in them. One of the first devices made by humans that took advantage of the feedback loop was Ctesibius flow regulator. With the grasping of concept of time in the ancient world, there was a need of measuring it precisely. Ancient Greeks viewed time as a continuum, using the flow of a river as a metaphor of passing time. As one ancient Greek proverb says:

" πάντα ῥεῖ " [Everything flows]

It shouldn't come as a surprise that for measuring the time ancient Greeks invented the water clock. The idea was to have a big tank filled with water, with small opening at the bottom. The passed time would be a measure of how much water flew through the small opening. There was a problem though since the flow rate of the water through the opening was depending on the amount of water that was present in the tank. For it to accurately measure the time, the flow rate needed to be constant. This meant that the water level in the tank should be kept constant at a certain position. This is the problem Ctesibius solved by introducing additional tank and a

float. The additional tank represents the reservoir of water, while the amount of water (and thus the flow rate) is regulated in the second tank. When the water level exceeded a certain level, the float blocks the water from entering the second tank. When the water level decreases, the opening slowly opens, and thus the water level is again reinstated.

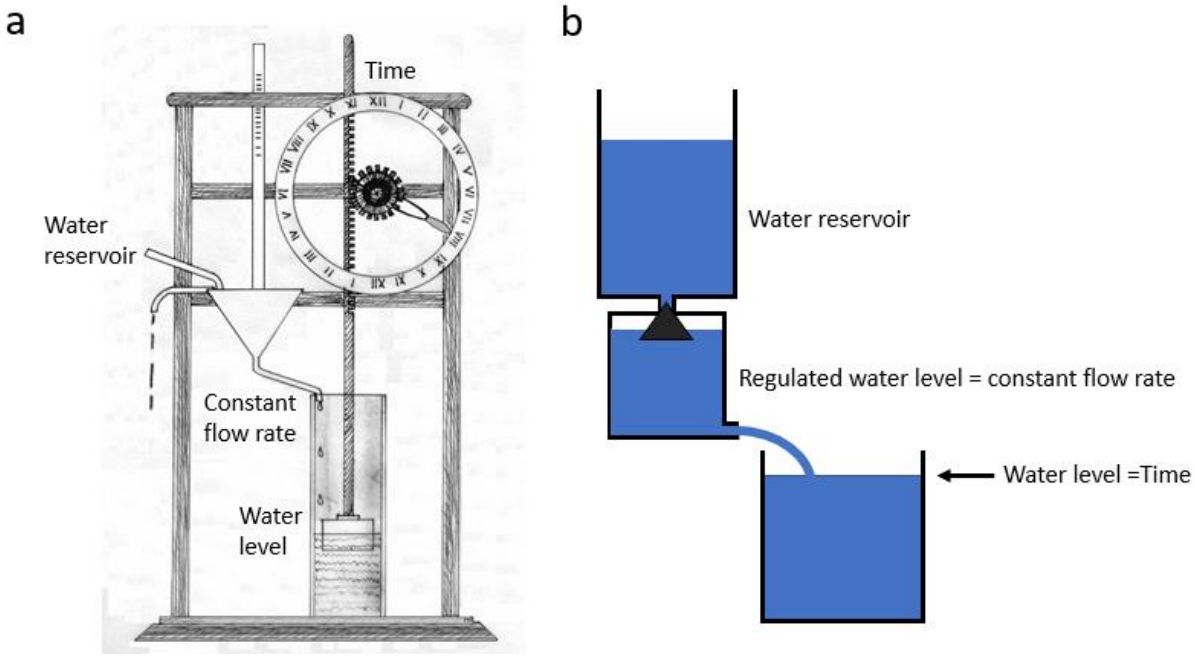

Figure 9.7. One of the first implementations of a feedback loop- Ctesibius flow regulator. (a) Water clock with Ctesibius flow regulator (b) Regulation scheme and the working principle. The main idea of the water clock is that the water level can be used as a proxy for passed time. For this estimation to be accurate the flow rate needs to be constant in time which can be achieved if a water level is kept at a constant level. This is the main idea behind the Ctesibius flow regulator. The regulator of the flow rate consists of two tanks –tank reservoir and a regulating tank where water level is kept at a constant level. Water flows from the water tank towards the regulating tank through the opening on its bottom. Regulating tanks consists also of a float. When the level of water inside the regulating tank passes a certain threshold, the float blocks the channel opening through which water enters from the tank reservoir, thus blocking the inflow of water. When the water level drops due to the flow out of the regulating reservoir, float moves and opens up the channel which enables more water to enter the system from the reservoir tank. Image adapted from [100]

With the industrial revolution in the 18th century came the Watt regulator and the rotating steam engine. The rotating steam engine performs mechanical work using steam (figure 9.8). The intention of Watt regulator was to control the speed of a running steam engine at a constant desired value. The regulator consisted of two balls which rotate along vertical axis due to the centrifugal force. The balls are linked to the aperture of the valve through which the steam is supplied to the system. This link makes the position of the aperture of the valve solely determined by the position of the rotating balls. The rotation speed of the balls is proportional to the speed of the steam engine. When the speed is increasing, balls move outwards due to the

centrifugal force. The outward position closes the aperture of the valve, which decreases the amount of steam put into the system. When the rotation speed of the balls is decreasing, the balls move down towards the vertical position, which opens up the valve and thus letting the steam back into the system.

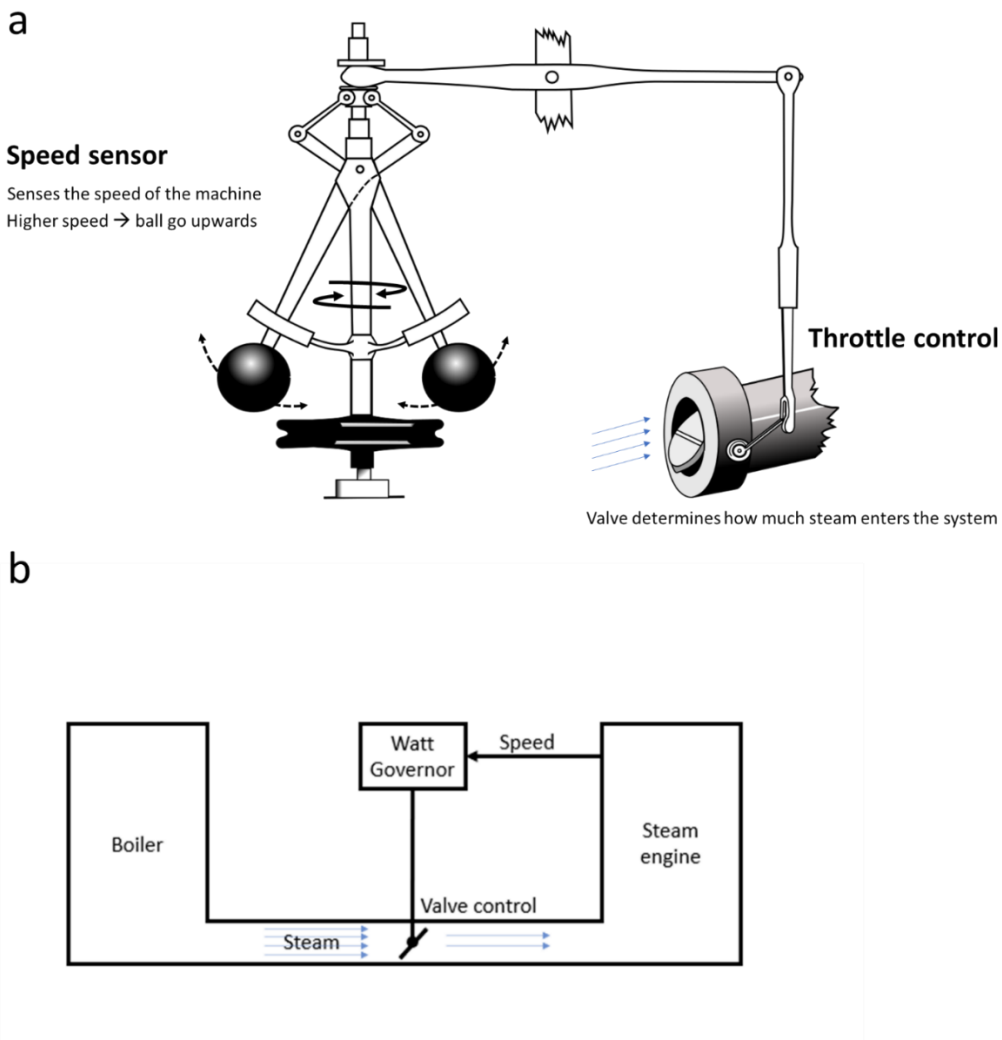

Figure 9.8. Example of a feedback system – the Watt Governor and rotating steam engine. (a) Working principle of the Watt Governor. The rotating steam engine performs mechanical work by using the power of water steam. The main objective of a feedback loop was to run the rotating steam engine at a constant speed. Speed sensor consists of two balls which rotate around vertical axis. The position of the balls is determined by the speed at which the system operates. The more steam is supplied to the system, the faster the system is running and the more the balls move outwards due to the centrifugal force **(b)** Regulation scheme. In order to keep speed of the system at a certain level, the position of the balls is linked to aperture which controls the openness of the valve. When the system is running faster less vapor needs to be let inside the steam engine (and the other way around). When the speed is increasing, balls move outwards due to the centrifugal force. The outward position closes the aperture of the valve, which decreases the amount of steam put into the system. When the rotation speed of the balls is decreasing, the balls move down towards the vertical position, which opens up the valve and thus letting the steam back into the system. Part of the image adapted from [101]

The 19th and 20th century saw further development of the mathematical tools and rise of electronics. This cleared up the path for Harold Stephen Black to invent the first real negative electronic feedback and to show its advantages in his revolutionary work [102].

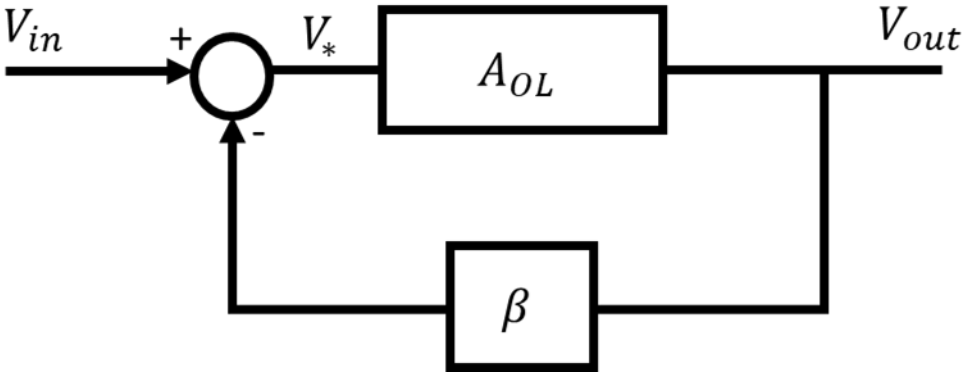

Figure 9.9. First electrical negative feedback loop – linearization of the electronic amplifier. The patent is deemed as one of the most important findings in the 20th century as it made it possible to linearize and standardize highly nonlinear electrical components. The amplifier amplifies the signal from its input to its output by the factor of A_{OL} . This amplification is highly nonlinear and different from one device to another due to manufacturing, quality of the components etc. Closing the feedback effectively makes the amplification between the input and output voltage independent of A_{OL} and proportional to the inverse of the strength of the feedback loop, $1/\beta$

The patent consisted of applying negative feedback on the electronic amplifier. The amplifier amplifies the input signal with amplification of A_{OL} . As with any electronic device, this amplification is highly nonlinear and different from one electronic device to another (due to manufacturing, quality of the components etc.). Blacks idea to overcome this consisted in the introduction of the negative feedback. Negative feedback loop senses the output and then feeds the information to the input (β). Measured sensed value and the value on the input are then subtracted and feeded to the amplifier, which then amplifies the signal.

$V_{out} = A_{OL}V_* = A_{OL}(V_{in} - \beta V_{out})$

If we define the closed loop gain as a ratio between the output voltage and the input voltage

$$A_{CL} = \frac{V_{out}}{V_{in}}$$

We have:

$$A_{CL} = \frac{A_{OL}}{1 + \beta A_{OL}}$$

When $A_{OL} \gg 1$, this means that effectively the closed loop amplification of the system would be only determined by the strength of the feedback loop β. This revolutionized electronics and is regarded as the most important invention of the 20th century, as it made possible to linearize and standardize highly nonlinear electrical components.

What can be further seen on this simple example is the fact that one needs to carefully choose the strength of the feedback loop β as it might impact the stability of the closed loop system as a whole. For instance if we chose $\beta = -\frac{1}{A_{OL}}$, the gain becomes infinite and the system unstable.

Typical modern (closed feedback) control loops follow the same logic. The core of the loop present the controller which has two inputs:

-the set point (reference level) which represents the output profile we want our process to achieve

-the output (current value) which is measured by the sensor and fed back to the controller

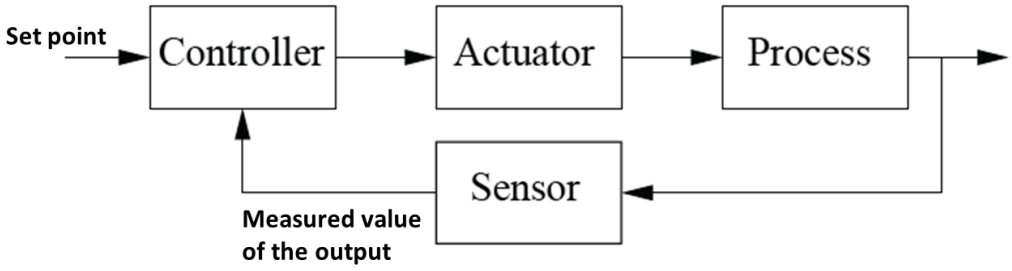

Figure 9.10. Modern control loop design. The design consists of a controller that based on the desired value and the measured value obtained from the sensor determines and send appropriate control signal to the actuator, a machine component responsible for controlling the mechanism of a dynamic system. The idea is to move the system towards the desired set point value. Image adapted from [103]

The controller calculates the difference between the two signals and uses this information to select the appropriate control action that will guide the process towards the desired value defined by the user by adjusting the control signal appropriately. The appropriate control is a result of a specific control algorithm. Based on the algorithm, we can differ different controller types. In here I will present three basic types of control algorithms (on-off control, P/PI/PID controller and model predictive control), which are commonly used. I won't further dig into the

issue of stability and how the parameter of the controllers are chosen to give a stable response. For now it is just worth mentioning that one must take special care of them when designing the controller. Besides this it is worth mentioning that not all systems are controllable.

On-off control

This type of controller is the simplest and the oldest control algorithm that existed. The algorithm of the ideal on-off control could be summed up mathematically as:

$$u = \begin{cases} u_{max}, e < 0 \\ u_{min}, e > 0 \end{cases}$$

Where e represent the current tracking error (difference between the wanted output and the actual output). The control signal in here solely depends on the sign of the error. Besides simplicity this controller is relatively easy to build, it does not have any parameters to adjust, and it quickly responds to the change due to the control signal applying minimal or maximum control effort (depending on the situation). Main disadvantage is the existence of persistent oscillations of the tracked signal present (due to the nature of the control signal which only takes two values u_{max} and u_{min}). In practical applications in order to minimize the persistent oscillation, small adaptations of the ideal on-off controllers can be made, namely the addition of the dead band or hysteresis (*figure 6.11*)

In many applications where fast response and no tight control is needed this controller is suitable. In everyday life this type of controller is used in temperature regulators, valve control etc.

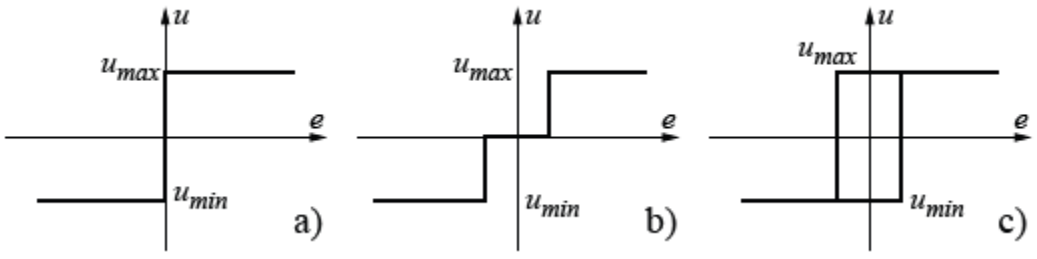

Figure 9.11. On-off control. Horizontal axis represents the error signal (difference between the reference and the measured value) while the vertical axis represents the control signal **(a)** ideal on-off control **(b)** dead band on-off control **(c)** hysteresis on-off control Taken from [88]

PID family of controllers

PID (***P**roportional-**I**ntegral-**D**erivative*) represents a remarkable family of controllers named after the three actions they perform. Sometimes, some actions can be omitted and then we can differ between P (**P**roportional), PI (**P**roportional-**I**ntegral) controllers. PID family of controller (from whom PI controllers are mostly used) account for more then 95% of engineered control loops [104].

The proportional part of the controller gives a control action which is proportional to the current error

$$u_P(t) = K_p e(t)$$

Compared to the on-off control this type of control action has the advantage of not providing the maximum effort on the control signal as a response to an error but scales it accordingly. In sensitive industrial processes this is of great importance since applying the maximum control effort on the process long term could lead to the damage of the system. Like with on-off controller the biggest advantage of this control effort is the fact that it immediately responds to the error signal.

Of course having just proportional part of the control is not enough for most of the systems. We need an integral control effort. This can be elegantly explained on the example of controlling the speed of rotation of a motor[105]. The problem of controlling the speed of rotation with only P controller stems from the fact that once the error has been eliminated the proportional action would apply zero control effort to the system. Applying zero control effort onto the motor, leads to the motor completely stopping and consequently again yielding the maximum error in the system. In order to effectively operate these systems, it is necessary to develop a controller that can store the history of previous actions. One method of achieving this is to monitor the accumulated energy in the form of the error signal over time. Essentially, the control system here would be monitoring the total error signal accumulated until the current time. This design would enable the system to continue functioning even when the current error drops to zero. Since the accumulator is mathematically an integration, we define this control as an integral control. The biggest advantage of this type of control effort is that it helps system to achieve zero error tracking.

$$u_i = K_i \int_0^t e(\tau) d\tau$$

Previous two control efforts made their decisions on their control choice based on the present and what happened in the past, but none of them is paying attention to the fact whether the system is moving in the right direction. Ideally it would be nice to have another control which depending on how close we are approaching the desired reference, lowers down the error signal,

so that the system doesn't overshoot and stops exactly at the desired reference. This prediction can be achieved with looking at the differential of an error:

$$e(t + \Delta T) = e(t) + \frac{de}{dt}\Delta T$$

Having this in mind we can define derivative action as

$$u_d = K_d \frac{de}{dt}$$

Although in theory the action of this controller is beneficial due to the fact that with it the system can anticipate what happens in the future, in practice this control effort is rarely used. This is mainly due to the fact that the signals are noisy and deriving the noisy signal usually adds up even more noise, making this control effect ineffective and even dangerous for stability of the system as whole.

Summation of these three control efforts is how we definite the PID control

$$u_{PID} = u_p + u_i + u_d$$

In here we have three parameters that we need to adjust so the systems tracks the reference right and that the system is stable. Even though I mentioned previously that I won't go into the stability analysis there is one trade off that is worth mentioning- the trade off between the speed and stability/tracking. If we want the tracking to be almost perfect and the system stable the control efforts should be low in value, so the system doesn't overshoot. This gives the sluggish response. We can make this response faster, but this comes at a price of making the system more reactive, which introduces the overshoot and makes system less stable.

Model predictive control (MPC)

The last type of control that I will shortly cover in this section is model predictive control (MPC). The essence of how this controller operates is closely related to our own human way of thinking, as said in [106]:

> *" Philosophically MPC reflects human behavior whereby we select control actions which we think will lead to the best predicted outcome (or output) over some limited horizon. To make this selection we use an internal model of the process in question. We constantly update our decisions as new observations become available "* [106] -page 1

Model predictive control (MPC) explicitly predicts what will happen in the future based on a model of the process and the input we provide. Based on the predicted future over some time horizon and the operational constraints MPC decides which control decision is optimal in order to achieve a certain control objective (tracking the reference). Since the MPC computes the optimal control it must also contain an optimization method incorporated, with a proper cost function which incorporates tracking and control constraints. If the cost function is chosen correctly, stability and tuning won't be an issue since the cost will be small for good tracking [107]. Another thing which one should think about when constructing an MPC control is the length of the time horizon – how much of a prediction in the future impacts the control effort. The time horizon should be chosen long enough, so it captures all of the dynamics of the signal being control. Failure to do so, leads to instability or poor dynamics.

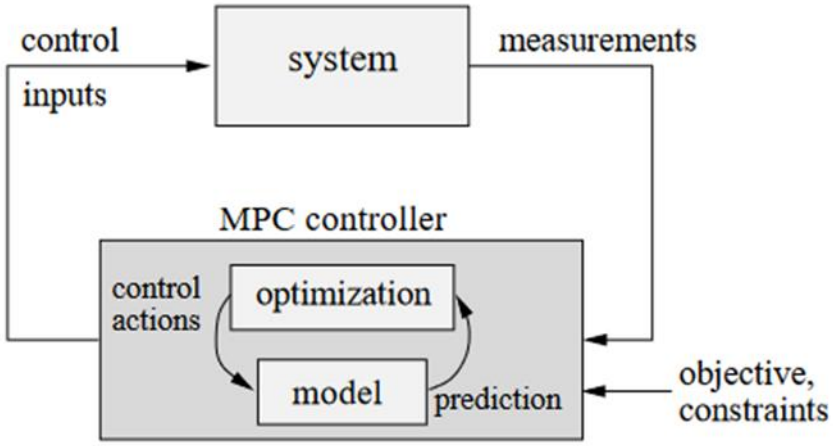

Figure 9.12. Model predictive control. MPC uses a model to predict future changes in the behavior of the system over some short time horizon. Based on the predicted changes and control constraints it calculates the optimal control needed so the measured variable follows the reference value. Taken from [107]

Cybergenetics

In the past decade the fields of system control and genetics have gradually intertwined making the novel field called cybergenetics. This broadest definition of this new field is that it aims to robustly and predictably control cellular processes. There are three different layers of cybergenetics as defined in [108]:

-**external control of cellular processes**. *In here cells are genetically modified so they respond to certain stimuli from the environment (chemical or light signal). In order to track a level of expression of a certain gene, fluorescent tags are also incorporated in the cells genome. We can either control the system on a population level, and then we have a population control, or on the level of a single cell (single cell control). Cells are growing in a microfluidic system and are observed under the microscope and a computer has a direct control over the system-it controls the microscope and the environment inside microfluidic system. Based on the output of the measured variable the computer changes the environment so that a target variable (gene expression) reaches a reference level given by the user.*

-**internal (embedded) control of cellular processes.** *It's similar to the external control, but instead of having a computer, the control in here is happening inside the cell. This requires building a synthetic circuit that will be able to sense a specific molecule inside the cell, compare it to a desired value and trigger a gene expression that will lead to the correction of the tracking error.*

-multicellular control. *In here the control happens on the scale of two species.*

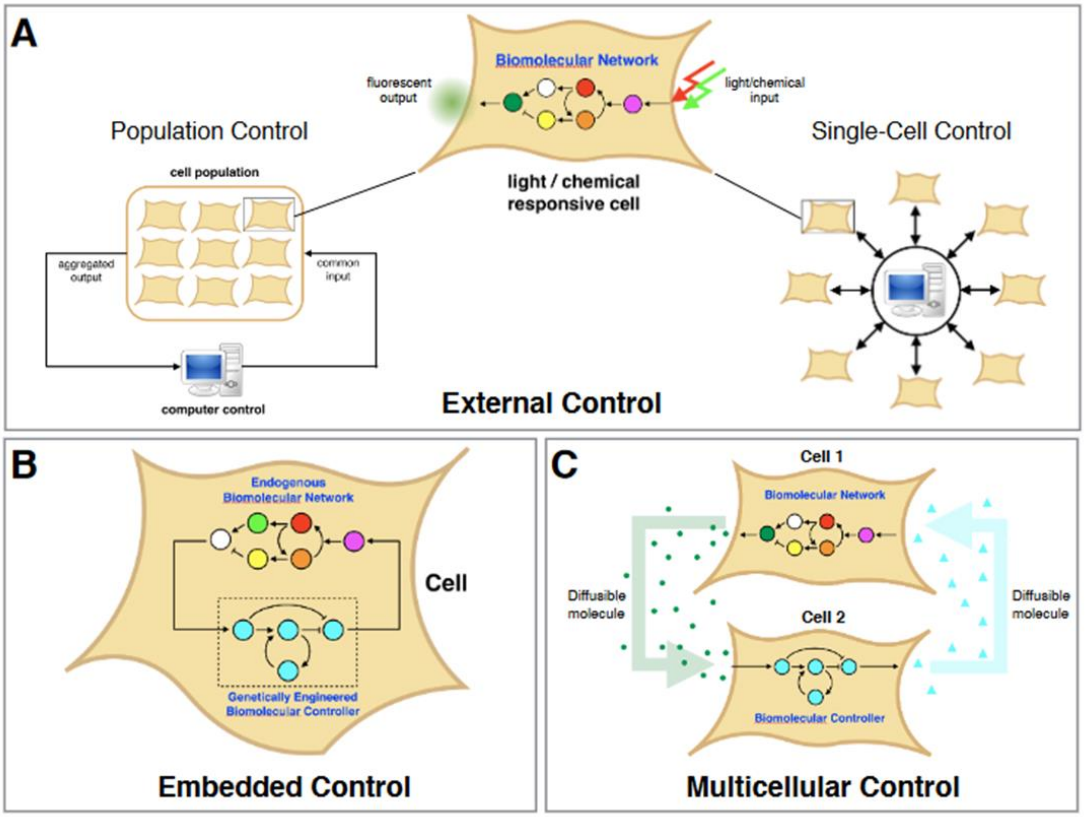

Figure 9.13. Cybergenetics and three different layers of control. (a) External control. In here the cells are genetically modified so they respond to certain cues from the environments such as chemical inducers or light. The computer tracks the changes that are happening and based on the difference between the measured gene expression and the desired one sets an appropriate control (concentration of the inducer, light intensity etc.) to drive the system towards the desired set point. Depending on whether we are controlling a single cells or population as a whole we can differ between the single cell control or population one. **(b) Embedded control.** Instead performing the control externally using the computer one could implement the control inside the cell. This requires that the cell is genetically rewired so that it can sense the control variable, compare it to the desired value and perform the appropriate action so the control variable reaches the desired reference value. **(c) Multiceelllular control**. In here the control happens between the cells. Figure taken from [108]

Here I will focus on the first level – the external control. The first breakthrough with applying external control with living systems came with [109]. In here the authors aimed at controlling the osmoregulation pathway in yeast. As mentioned previously the osmotic shock triggers the activation of Hog1. Activated Hog1 translocates to the nucleus where it activates a myriad of genes involved in glycerol production. These changes are only transient due to the adaptation mechanism. Once the osmotic balance is restored, Hog1 gets disactivated and glycerol production seizes. The extent of which the internal feedback loops can be bypassed was the topic of research in the mentioned publication where the authors explored whether it was possible to externally control the pathway (thus effectively bypassing the existing internal native feedback loops within the cell).

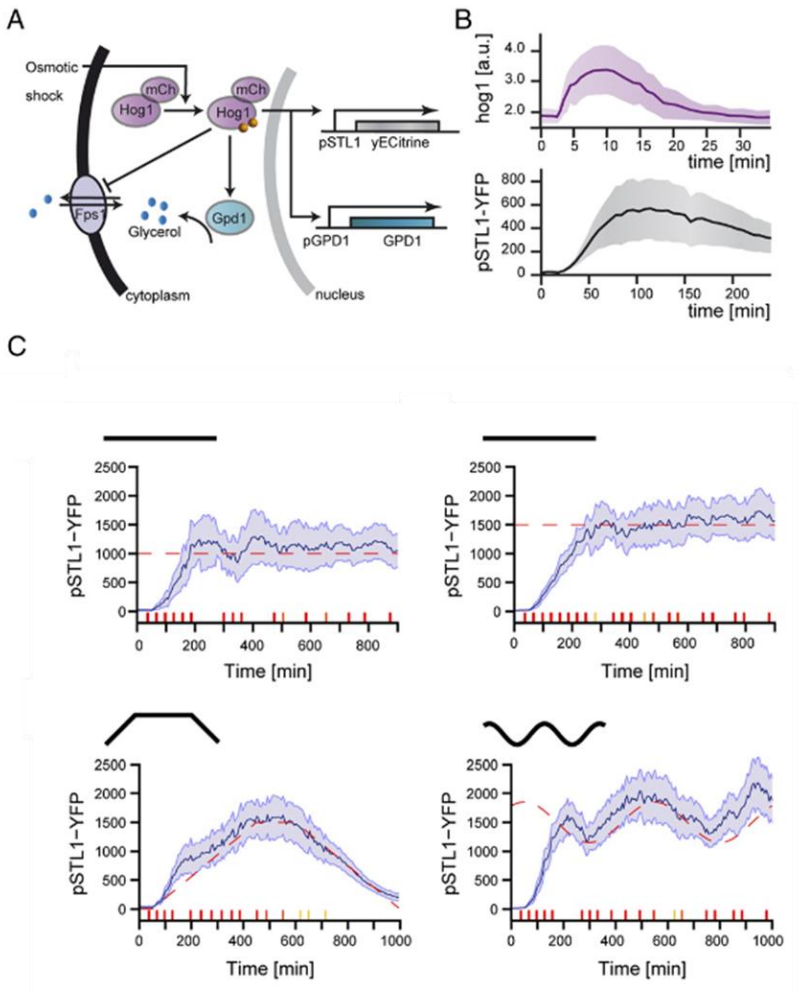

Figure 9.14. Real time control of the Hog pathway in yeast. **(a)** As described previously the Hog pathway is complex biological dynamical system which provides an ideal adaptation mechanism to osmotic stress. When cells encounter osmotic shock, proteins situated in the membrane sense the sudden drop in the turgor pressure and the drop in the cellular volume and trigger the activation of the Hog pathway. Additionally they activate the process of shutting down the Fps channels which prevents the glycerol molecules to go outside of the cell. Once the Hog pathway gets activated the Hog1 gets translocated inside the nucleus where it triggers the expression of myriad of genes with ones involved in glycerol production being the most important. With the rising glycerol concentration the cells eventually reestablish the turgor pressure and shut down the Hog pathway. As a proxy for the activation of the Hog pathway the authors put a fluorescent tag yECitrine under the control of the native promoter of the stL1 gene. The stL1 gene is activated by the Hog1. **(b)** Perfect adaptation mechanism of the Hog pathway. As cells encounter the hyperosmotic shock, Hog pathway gets activated (Hog1 gene expression). Once the turgor pressure is reestablished the Hog1 returns to the cytoplasm and the activation stops. Graph bellow represents the measured stL1 gene expression which is activated by the Hog1. Because of the perfect adaptation mechanism, instead of modulating the amplitude of the osmotic shock a better mechanism for control would be to modulate the frequency of an osmotic shock pulse signal. **(c)** control of the Hog pathway activation via frequency modulation of the osmotic pulse signal (the pulses on the horizontal axis). The color

code of the pulses represents the duration of the pulses and could be found on the next figure. Reference is shown in dashed colors. The closed feedback loop enabled the system to experience prolongated levels of Hog activation which were not obtainable in the open loop system. Figure taken from [109]

One of the genes that Hog1 activates is the sTL1 gene. This gene can be used a proxy for measuring the activation of the Hog pathway. In order to track and control the Hog1 activation, the authors put a fluorescent reporter *yECitrine* under the native promoter of sTL1 gene. By having this fluorescent tag, they had a direct readout of the activation and could use this information to control it in real time. The cells were grown inside the microfluidic chambers and the direct readout of the cells fluorescence was sent to the MPC controller. In order to achieve a desired level of activation the controller sent pulses of specific length, which activated transiently the Hog pathway to a certain level. In this way the adaptation was avoided and regulation of the Hog pathway was achieved.

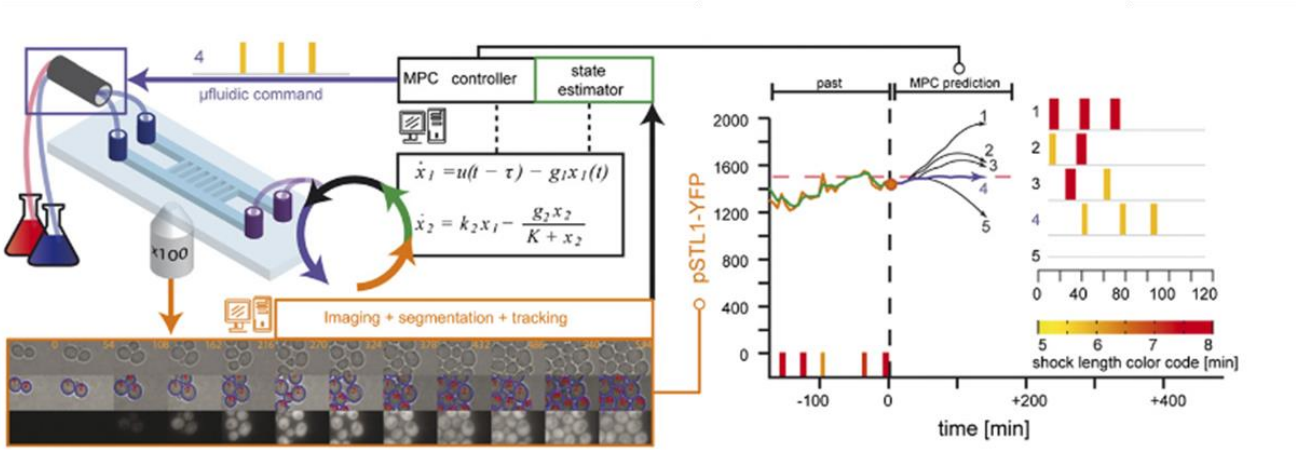

Figure 9.15. Model Predictive Control (MPC) of the Hog activation. The MPC control consists of the model which estimates the future. Based on the current value and the predicted value of the pSTL1 gene expression, the MPC controller determines the length of the osmotic pulse that needs to be applied so that the measured activation of the Hog pathway obtained from the pSTL1 gene expression follows the desired reference value. Figure taken from [109]

The previous study [109] showed that we can indeed control externally complex cellular processes and use it to drive and maintain the system in states that are normally not attainable. Following that, the next study [74] showed that it is possible to maintain the genetic toggle switch in *E.coli* in its nonstable, undecided state for long periods of time. Genetic toggle switch represents a bistable system, and as previously mentioned a system is exhibiting a bistable behavior if depending on the input, it has the capability to go to one of the two stable states. In addition to the two stable states, there exists a third one - the unstable state, through which the system only transiently passes. In [74] the authors incorporated the synthetic gene toggle switch circuit in *E.coli*. Genetic toggle switch in [74] was realized as a circuit of two gene branches which

are mutually repressing each other (GFP and RFP branch). Each branch is activated through the activity of a specific inducer (IPTG and aTC). In the stable state the system will either express GFP or RFP. Nonstable state of a genetic toggle switch would represent the case where both branches are equally activated and equally repressed. This was the main aim of the control loop-keep the system in an undecided nonstable state, where both gene expression (RFP and GFP) branches are activated at the same level. The control loop was set to follow the expression profile of the cells and to drive them to equal levels (GFP/RFP=1) by changing the concentration of the inducer molecules (aTC, IPTG) with a PI controller.

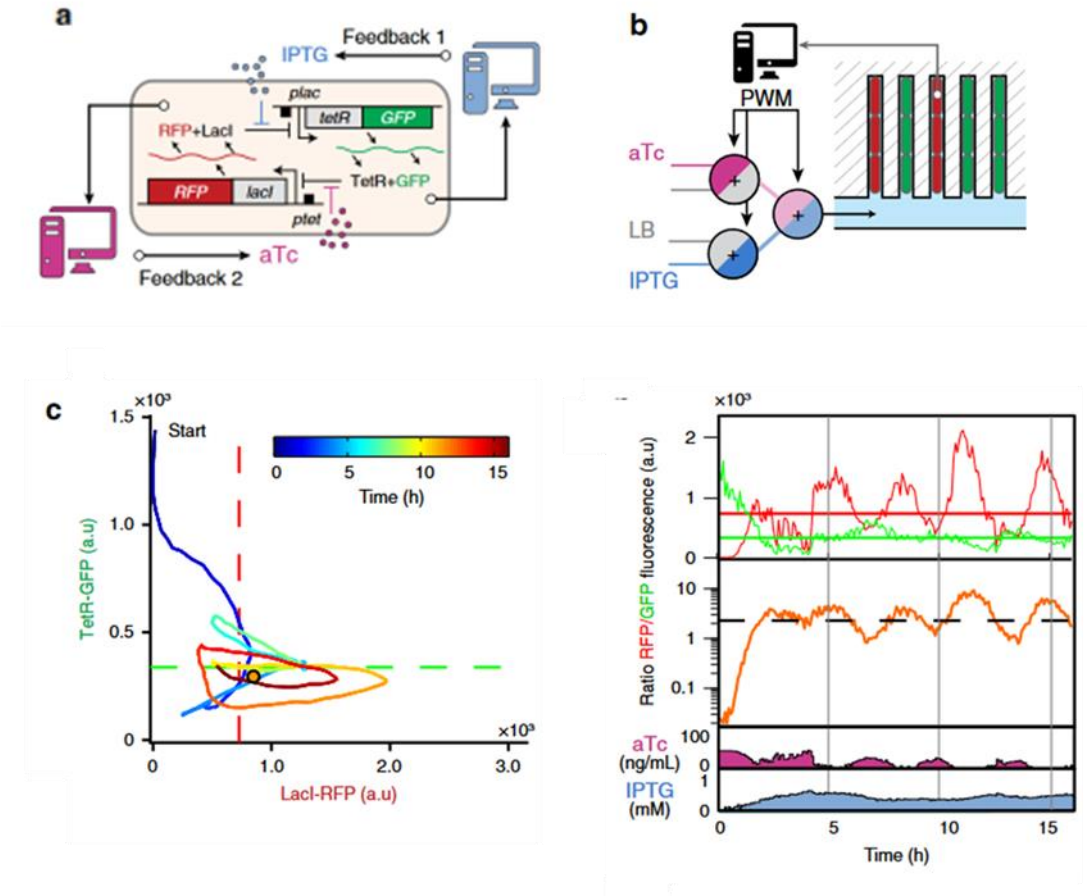

Figure 9.15. Real time control of genetic toggle switch in *E.coli*. (a) Genetic toggle switch consists of two branches that are mutually repressing each other -the GFP branch which is driven by IPTG induction and the RFP branch which is driven by aTc induction. Genetic toggle switch has two stable states, one when the cell express RFP and the other one when the cell express GFP. Besides the two stable states, the system also has a third unstable state where both RFP and GFP are produced equally. In natural systems this state is transient and cells never have the capability to maintain themselves inside of it. The goal of the external feedback loop was to maintain the cells in this transient, "undecided state" over long periods of time. This can be achieved by tracking and controlling both RFP and GFP gene expressions in time **(b)** Control strategy consists in controlling the appropriate concentration of inducers aTc and IPTG inside the media. The concentration valve consists of three valves. Appropriate mixture of the aTc and IPTG comes as a result of switching between the valves which is determined by the PWM frequency. Mixing was characterized before the control loop experiments using fluorescent dyes. **(c)** real time control of the system. System starts from GFP expression and gradually moves to the desired state. Ratio of the GFP and the RFP is maintained. Real time concentration of the IPTG and aTC are given bellow. Taken from [74]

Three valves used in pulse-width-modulation (PWM) allow the modulation of the concentrations of aTc and IPTG in real-time. Surprisingly besides control in a closed loop, sending pulses of inducer chemicals also gave satisfying results in keeping the system around its nonstable state. This indicates that other levels of control such as on/off controller might also be applicable in controlling biological systems as physically and controllably complex as bistable ones.

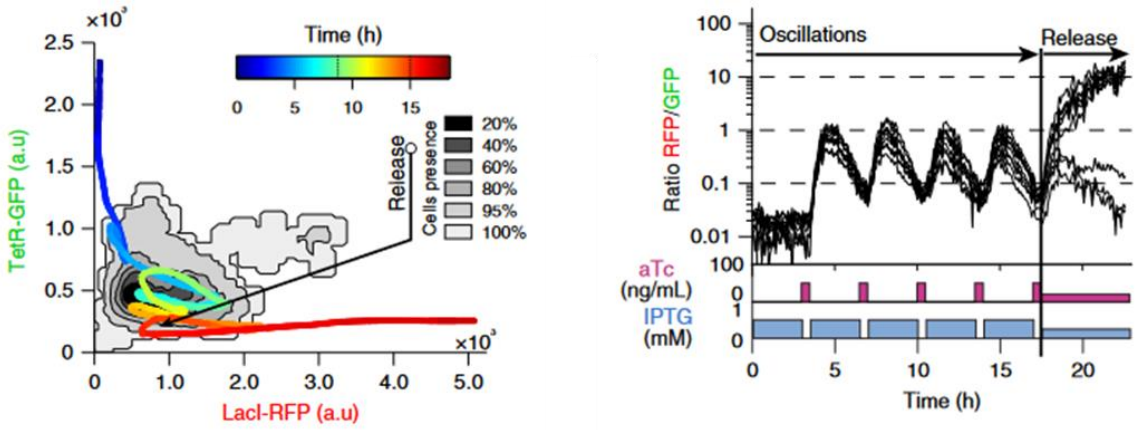

Figure 9.16. Pulsatile control of the genetic toggle switch. Besides PI control, sending aTc and IPTG at a specific frequency also enabled the maintaining of the system in the undecided, unstable state. After the pulsatile control ceased the system returned back to one of its stable states. Taken from [74]

System control covered in [74] was the first study that showed not just that it is possible to solve a complex control problem. It also has showed that it is possible to maintain the bistable system in its undecided and unstable state. Bistable system is omnipresent in biology. It occurs in signaling pathways[99] , development[110] and has been even implicated in how disease progresses[111]. Having this in mind, putting this kind of system under the predictable and robust control was a breakthrough.

Besides answering fundamental questions in science external feedback loops offer great possibilities in biotechnology. Feedback loops offer a great opportunity the maximize cellular yield of desired metabolite through controlling their cellular cell cycle status. The first step in this direction was made by [112] where it was successfully shown that we could externally control the synchronization of the cell cycle in yeast. In addition to biotechnology, having the capability to externally control biological process, especially the ones implicated in human health and disease offer unimaginable opportunities for understanding the onset and development of the disease and offers new insights into developing potentially a novel treatment. For instance the authors in [113] used the control loop to link the concentration of a of α-synuclein protein with its aggregation inside the cell, which is linked to the onset of many dieses [114]–[117]. That was

achieved by externally controlling the concentration of this α -synuclein protein in a yeast model of Alzheimer disease. The α -synuclein protein was put under the control of a galactose inducible promoter and fused with GFP. In this way by adding a certain concentration of the galactose to the system it was possible to express α -synuclein protein at a certain level. In order to minimize the error between the reference value and what was measured, the controller sets an appropriate duration of the galactose pulse by using MPC control algorithm. By using the control platform the authors have shown that the aggregation of the protein is solely a concentration dependent phenomena. Furthermore they used the same platform different treatments to probe different treatment to the dissolve the aggregates.

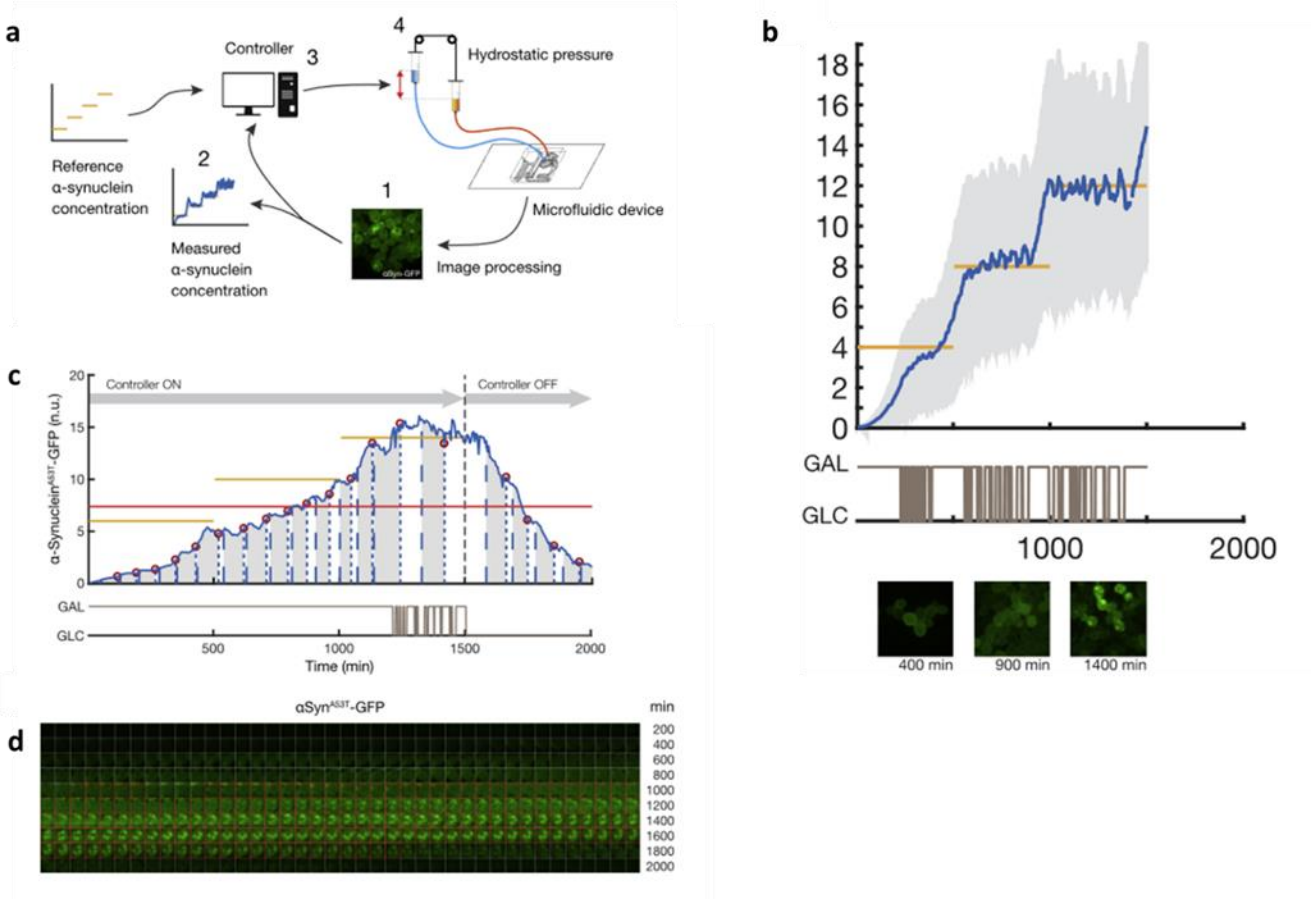

Figure 9.17. Real time control of the concentration of the α -synuclein protein in yeast model of Alzheimer disease. **(a)** Control scheme. The α -synuclein protein was put under the control of a galactose inducible promoter and tagged with GFP. The frequency of switching between the media containing glucose and galactose sets the concentration of the galactose needed for inducing the gene expression of α -synuclein protein. Based on the difference between the reference value (yellow line) and the measured GFP output (blue line), the control algorithm determined the appropriate switching frequency between the media **(b)(c)(d)** Tracking results. Real time controlling the concentration of the α -synuclein protein enabled the researchers to link its concentration with its aggregation. When the α -synuclein protein goes beyond a certain threshold (red curve, c) it starts to aggregate. Aggregation is reversible as shown when the concentration lowers down. Figure adapted from [113]

Besides bacteria and yeast, the advances were made also in the field of external control of mammalian cells [118]. As pointed out in the study, compared to bacteria and yeast, mammalian cells are much harder to handle specially in the context of feedback experiments. Culturing conditions are much more stringent for mammalian cell. In addition to that the temperature and other variables such as CO_2 levels and pH should be observed and tightly regulated throughout the experiment. Compared to bacteria and yeast, mammalian cells are bigger and highly sensitive to shear stress. Shear stress caused by the flow rate (or any mechanical force cells are subject to) can negatively impact cells viability, causing cell death [119]–[121]. Another layer of difficulty when dealing with mammalian cells is their doubling time as mammalian doubling times usually fall in 24h to 48h range [122]–[126], which means that the feedback experiments should be run over the period of a week if not weeks, compared to 2-3 days needed for microbes. Nevertheless the authors in [118] were able to externally control in real time the fluorescent protein (d2EYFP) from inducible Tetracycline promoter over extended period of time in Chinese Hamster Ovary (CHO) cells.

Closing remarks

In the previous chapters I introduced the notion of control, its origins and its applicability in controlling the living systems. When talking about the notion of controlling a system we can differ between systems with higher or lower complexity which is context dependent. For instance in biological systems we can spot different degrees of complexity. As above mentioned, when dealing with higher organism such as mammalian cells it becomes increasingly difficult to genetically engineer them and perform long term experiments thus even controlling a simple feedback loop with a fluorescent reporter becomes challenging. If we stick with organism such as *E.coli* or yeast higher complexity can be achieved if the control aim are complex physical systems such as bistable switch or controlling components that are already involved in certain pathways such as the Hog pathway.

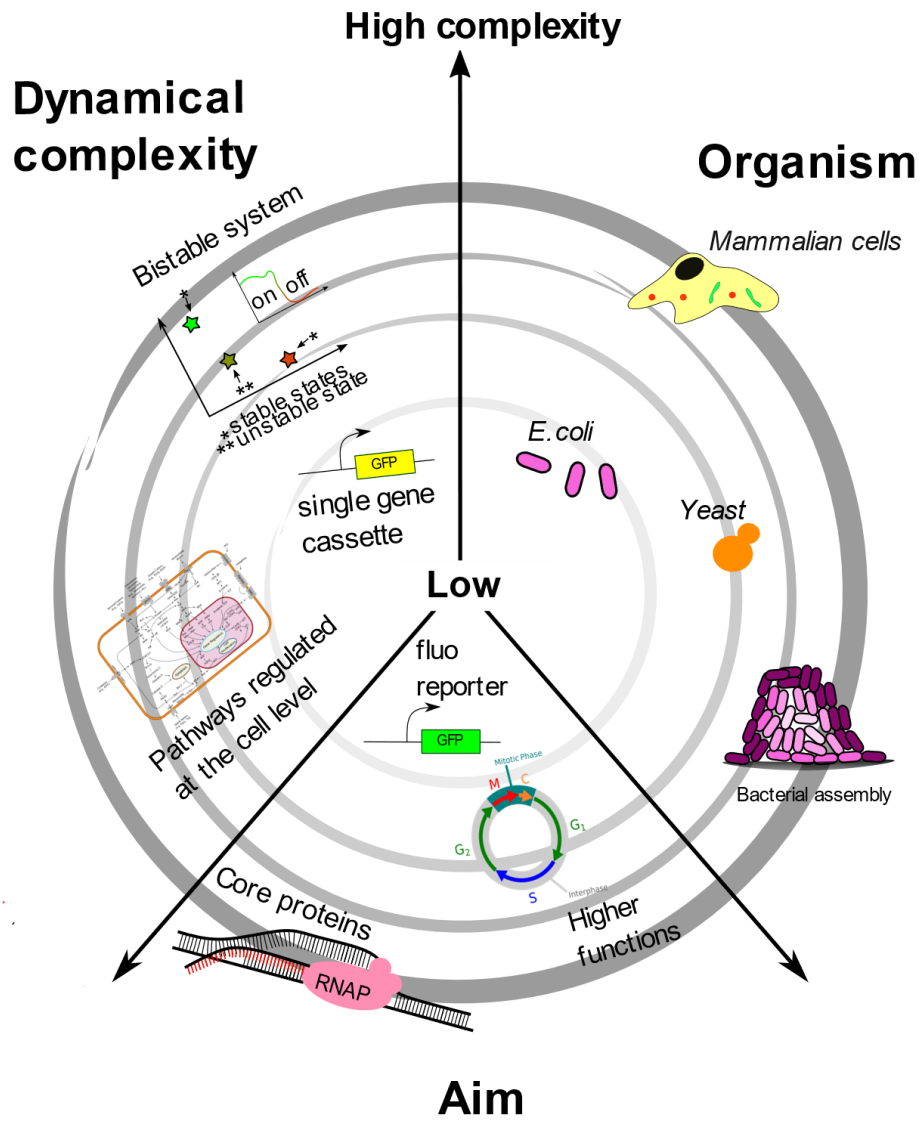

Figure 9.18. Different levels of complexity in biological system control. The more outward we go, the more complex the controlling of the system becomes. Complexity of the biological control can stem from the complexity of the dynamical system itself such (Hog pathway, bistable system), the importance of the molecule/function that we want to put under the external control (cell cycle, RNA polymerase), or the complexity of the organism or the community that we want to control (mammalian cells). For instance controlling GFP expression in real time in yeast or bacteria can be considered as a control problem with low complexity. On the other hand if we want to control the GFP expression in mammalian cell that could be considered as a complex problem due to the difficulties maintaining experimental conditions needed for mammalian cells (temperature, CO2, pH, flow rates as cells are highly sensitive to shear stress etc.), genetic manipulations that need to be conducted and low growth rates (doubling time in the range of 24-48h) that result in long term experiments. Parts of the images were taken from [127]–[129]

The main aim of this project was to examine the capability of externally controlling the range expansion of E.coli. This could be classified as a control problem of high complexity as the system is made of multiple cells which interact with each other, engage in cross talk, communicate and in general impact one another. Beyond this system is robust and resilient to environmental perturbances. An important step done previously was to thoroughly examine whether various ways of growth modulation in well mixed liquid cultures have the capability to work on highly dense colonies grown inside the microfluidic system. This was an important test which all three methods -IPTG, nutrient change and antibiotics passed. With this in mind, we can ask ourselves can we, in a similar manner to what has been done before, control the range expansion of dense bacterial colonies? The first part of the chapter covers the buildup of a control platform with it's main components – controller, the online PIV estimator and the valve which acts as an actuator which changes the environment thus consequently triggering the appropriate perturbations to the growth patters so that the range expansion follows the desired trajectory. The rest of the chapter focuses on control experiments. In order to validate the effectiveness of the control platform, the first experiments concerning control of fluorescein concentration were made before focusing on the biological control. In biological control experiments primary modality used to control the range expansion was IPTG induction of RNA polymerase due to its direct impact on protein expression machinery. This is followed by nutrient change modality and then lastly by applying antibiotics. Lastly comparison of three levels of biological control was made.

11 CLOSED FEEDBACK LOOP – MATERIALS & METHODS

11.1 DESIGN OF THE FEEDBACK LOOP AND LEVELS OF CONTROL

The main component of the computer aided control of the expansion of *E.coli* is the externally designed feedback loop. Its main goal is that the expansion velocity follows a set of reference values that is provided by the user. For this to happen the feedback loop must repetitively:

-measure the variable of interest for control purposes

-determine the appropriate level of control. In the context of the biological systems this means change in environmental conditions such as concentration of chemicals, nutrient change or a light pulse of a specific wavelength in the case of an optogenetics system etc.

-sending the control to the actuator which reads the control signal and directly impacts the environmental conditions (valve in the case of the chemical/nutrient modality or LEDs in the case of the optogenetics system).

In the case of controlling the expansion of the bacterial assembly one of the two variables can be chosen – maximal velocity or the maximum growth rate of *E.coli* colony expansion. Velocity can be inferred from the PIV algorithm. As only the cellular growth contributes to the movement the growth rate can be estimated as a positional derivative of the spatial velocity profile. This analysis, compared to the analysis done before, needs to be done online in a limited time frame between sampling two images. Having in mind that the estimated velocity profile is noisy, I opted to control the maximal velocity inside the side channels of the microfluidic chip. Since the velocity is nothing more than an integral of all the growth rates one could control the velocity by perturbing the growth of the colony. As mentioned previously growth modulation in well mixed liquid cultures of E.coli could be imposed by:

1) manipulating IPTG levels that cell experience – RNA polymerase is IPTG inducible in the PP2 strain. Changing the IPTG levels changes the RNA polymerase levels, which consequently changes the growth rate,
2) nutrient composition of the media as it's known that cells synchronize their growth rate with the availability of the nutrients in the environment, thus by changing the nutrient composition in the media one could manipulate the growth. Unlike the previous way of control this influences the entire metabolism of the cell.
3) targeting specific gene expression machinery with antibiotics. Small concentration of antibiotics make the protein expression machinery inefficient. To combat this cell employs limited cellular resources to the protein expression machinery, which comes at a price of having a lower growth rate.

All three modalities have been shown to work also on perturbing the growth patterns within a bacterial colony grown inside a microfluidic device. Although different in the way how they perturb the growth, all three modalities of growth perturbation require a proper concentration of IPTG/nutrient/antibiotic to be set. This can be achieved by passive mixing of the two media with different concentrations of IPTG/nutrient/antibiotic. The level of mixing is set by the control algorithm and the desired reference point of maximum velocity. Before activating the control algorithm and determining the appropriate control, the computer also needs to perform live PIV (particle image velocimetry) analysis. An overview of the control platform design could be seen on *(figure 7.1).* Details of the same (mixing, microscopy, media etc.) will be given further in the text.

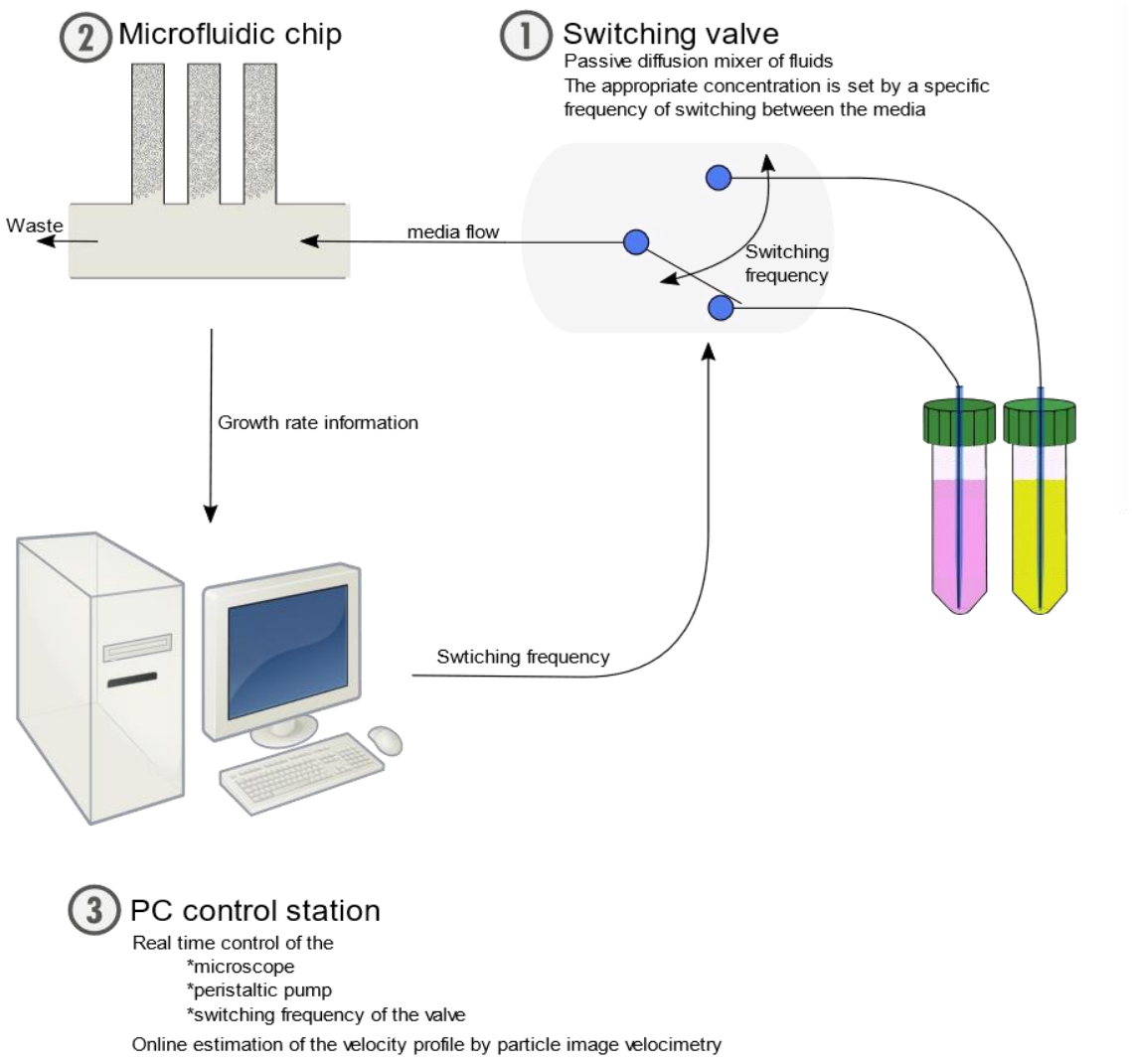

Figure 10.1. Closed feedback loop design. The design consists of three crucial components **1)<u>microfluidic mixer</u>** which sets the appropriate concentration of IPTG/nutrients/antibiotic inside the media. The fluid mixer is based on passive mixing of two fluids. The concentration of a specific chemical can be modulated by the frequency at which the fluid is mixed. **2)<u>microfluidic chip</u>** which enables development and tracking of *E.coli* colony invasion. **3)<u>Computer</u>**

which observes and controls the invasion speed of *E.coli*. For biological experiments the control algorithm was taken to be a bang-bang one. Part of the images taken from [130], [131]

11.2 MICROSCOPY AND ONLINE PIV (PARTICLE IMAGE VELOCIMETRY ANALYSIS)

Images were acquired using an Olympus IX71microscope using 10x objective, CoolSNAP HQ2 CCD Camera, PI piezo Z-stage, and Prior H117 motorized XY stage. HBO 103 W/2 mercury short-arc lamp and mCherry filter cubes were used for bright field and fluorescence field imaging. The microscope chamber was kept under 37°C throughout the experiments. In time lapse acquisition, the microscope, CCD camera, piezo, XY stage, filter cubes and lamps were all controlled by µManager [132]. Fluid mixer, µManager and the peristaltic pump were under the control of MATLAB. Besides controlling the components of the loop the MATLAB script controlled custom made autofocusing technique based on analysis of the Z stack[74], the order of operations, PIV analysis and the control algorithm.

Before the acquisition starts, the user defines the ROI where the PIV algorithm would perform its analysis and if needed defines the rotation of the image (channels should be perpendicular to the main axis of the main channel). The user defines also a desired set point, which represents the desired objective of the control algorithm. By comparing the current value of tracked variable with the reference value, the control algorithm calculates an appropriate control. Control in here is the information send to the valve regarding the switching frequency. This information is send to the Arduino via serial communication protocol.

A crucial part of the feedback loop is the velocity profile estimation. Unlike before when the estimation was done offline, this estimation needs to be performed online and in the limited time frame following the image acquisition and before determining the appropriate control signal. First choice of software was once again FIJI Image J provided plugin -the PIVanalyzer software[133], which was proven to be useful in biological studies and whose accuracy was validated earlier in this thesis. The software is part of the FIJI Image J and for it to be used online, it needs to be called and operated from MATLAB itself. This can be provided by MIJ software which represent the link between MATLAB and ImageJ[134]. Calling ImageJ and performing the PIV analysis worked accurately when the system was offline, but there was a problem when trying the same online, during the control experiment. Namely once the online acquisition has started any call of the PIVanalyzer from inside the MATLAB has lead to the micromanager abruptly terminating the session. Multiple tries to fix the solution have failed so I looked for a different one.

One solution to the problem was OpenPIV software[135]. It is free, open source, easy to operate and above all its earlier MATLAB versions offer complete execution of the program inside the command line with no GUI needed. I compared the results of the two software (OpenPIV and

PIVanalyzer), and although the two yielded similar results, in the case of 5xLB media where steep velocity gradient is observed the OpenPIV software wasn't able to capture the accurate dynamics at the beginning of the channel (figure 10.2.)

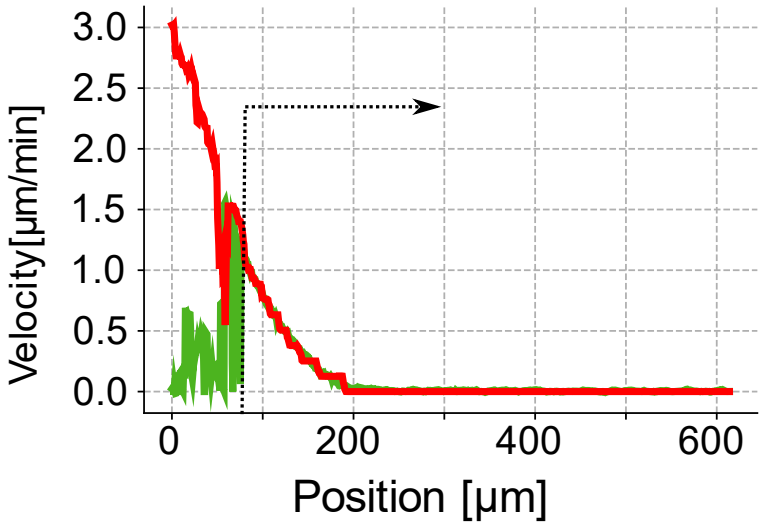

Figure 10.2. Comparison of two PIV algorithms for 5xLB media. Two velocity profiles were obtained by the two software-OpenPIV (FFT based cross-correlation) and PIVanalyzer (direct cross-correlation). Unlike the OpenPIV, software based on direct cross-correlation was able to capture the frontal velocity. Deeper in the channel both software gave similar results.

Some of the reasons behind this could be:

1) How algorithms calculate the cross-correlation signal. Both OpenPIV and PIVanalyzer perform image cross-correlation but unlike the PIVanalyzer which performs direct cross-correlation, OpenPIV performs the FFT (fast-Fourier transform) based cross correlation. FFT based correlation is computationally less expansive thus making it heavily exploited by various software, but despite that there some aspects of using the FFT based cross-correlation algorithms are overseen and neglected which impact the spatial resolution [136].
2) OpenPIV software has in it incorporated post-processing of the velocity signals with the major two being – removing the outlawyers and median filtering.
3) Online estimation of the velocity is performed directly on the images obtained in real time. Since the whole analysis needs to be done in a limited time frame, no image pre-processing such as for example enhancing the contrast could be made (unlike for offline analysis).

To determine the exact cause of the problem I removed the post-processing of the signals and there was a slight improvement, but still the OpenPIV had issues in determining the accurate velocity at the beginning on the channel in the case of 5xLB media, thus probably the first issue

alongside the third one played a role. Most of the software tools online (including the OpenPIV) performed the FFT which was the main cause of the problem. Developing the entire program using the direct cross-correlation method was considered as a potential solution but was ultimately not pursued due to the time constraints and the need for extensive code rewriting. In the end, given the available option and constraints the OpenPIV was deemed the most feasible solution and it was selected for the online estimation PIV tool despite its limitations (mainly in detecting the steepest part of the velocity profile in 5xLB media). Namely although at certain occasions the algorithm wasn't able to accurately estimate the frontal velocity it always gave good estimations of the velocity deeper inside the side channels, thus enabling the positional velocity control.

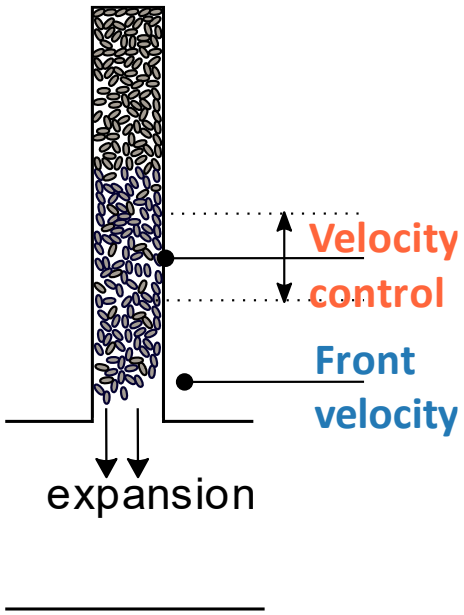

Figure 10.3. Controlling the positional velocity. FFT based software was incorporated into the MATLAB script to perform the PIV analysis. At certain instances the algorithm was not able to capture the dynamics in the frontal area. Velocity deeper in the colony on the other hand was accurately determined. Applying the control in this situation effectively gives velocity control inside the colony (positional velocity control)

The technical details involving the design and functionality of the feedback loop were given in this section. Of course in practice the feedback loop should enable tracking and control of a desired variable, but does the previously described platform do this in reality? In order to test this I externally controlled the fluorescein concentration inside the channel. The results of the test are going to be given in the next chapter.

11.3 TESTING THE FEEDBACK LOOP ON FLUORESCEIN SIGNAL INSIDE THE CHANNEL.

The effectiveness of the external feedback loop was verified on fluorescein control experiments. Fluorescein was observed and its concentrations was tracked in the main channel of the microfluidic chip in real time. For the purpose of regulating fluorescein concentration control, deionized water and deionized water containing 25µl of 100µM fluorescein were used. Similarly as in characterization experiments fluorescence was taken as a proxy for concentration of fluorescein inside the channel. At each time step the set point indicating the desired concentration value was given to the computer. Based on the current level of fluorescence inside the channel and the desired value the algorithm calculated the frequency of switching between the deionized water and deionized water with fluorescein. The switching information is given as PWM value. For instance the PWM value of 0.2 means that 20% of the one minute period valve will switch to the position which contains water and fluorescein. The rest of the period valve will switch back to the position where only water flows in the system. Due to the fast system response times and overall dynamics PI control was chosen. As stated before PI control is given as

$$u(t) = K_p e(t) + K_i \int_0^t e(\tau) d\tau$$

Flow rate of 5µl/min was used. Image acquisition and control algorithm were activated every 5min. Results of the tracking are given on figure 10.4.

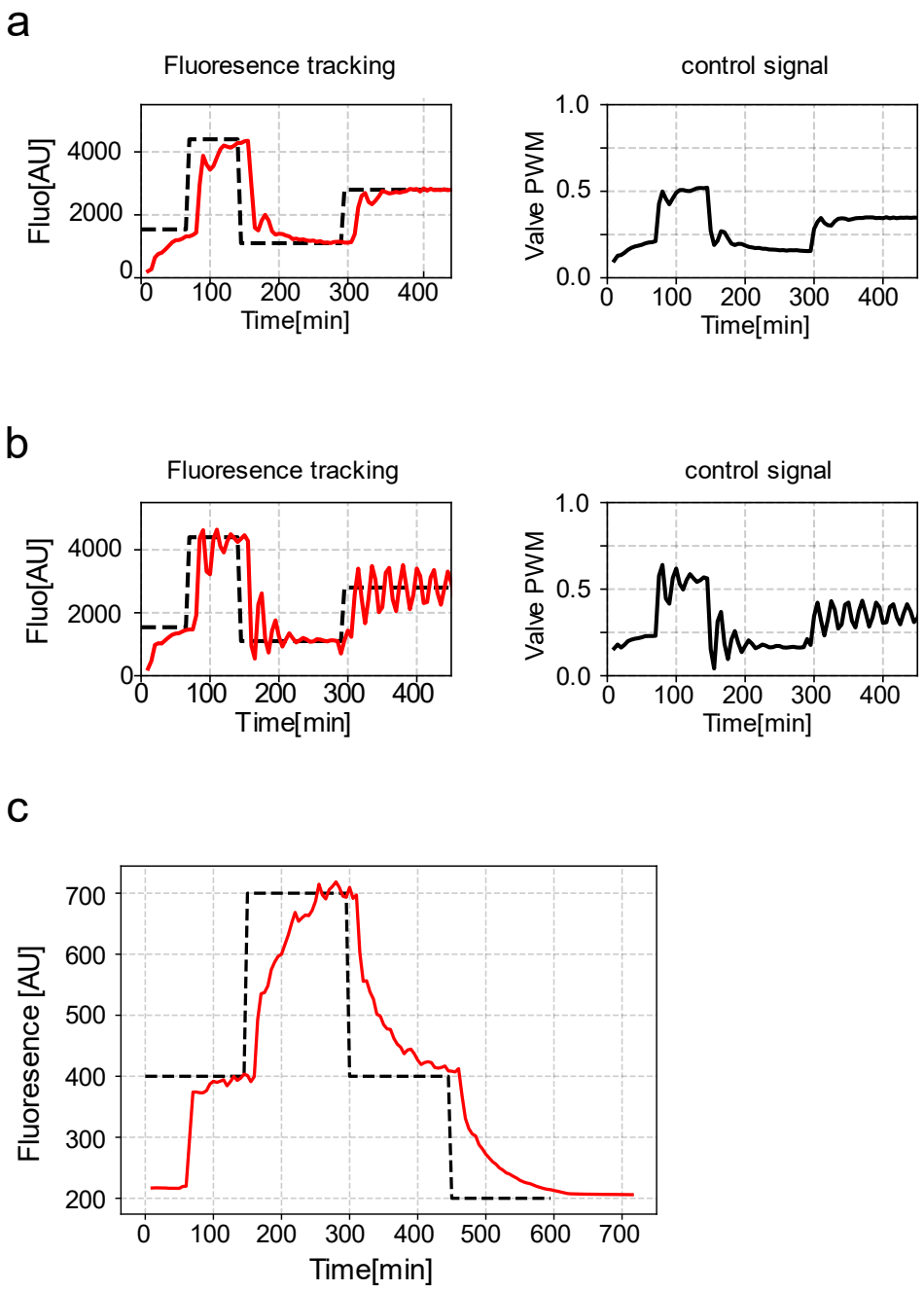

Figure 10.4. Closed loop control of fluorescein concentration inside the main channel. To test the effectiveness of the external feedback loop, the fluorescein concentration inside the main channel of the microfluidic chip was controlled in real time over extended period of time. Due to the systems fast time response and its overall fast dynamics PI control was suitable (Kp=0.00005,Ki=Kp/2). **(a)** On the left side the controlled signal (red) and the reference value (black) was given. On the right side control signal is given. **(b)** Same reference as in the previous case with increased proportional value. Increasing proportional control enables the system to have a quickly react to the reference changes but at the expense of the stability of the system (oscillations in the controlled variable) **(c)** Tracking with Kp and Ki as in (a) with a different reference signal

The quality of tracking was different for different parameters of the PI control. Increasing proportional or integral control value as expected have impacted the closed loop characteristics by increasing the speed but at a cost stability, but nonetheless in all conditions the control platform successfully drove concentration of fluorescein along the desired trajectory. Next chapters will be focused on applying this platform to our system of bacterial colonies growing in the microfluidic chamber to investigate the possibility of controlling their range expansion. At the beginning of the chapter I will focus on investigation whether using IPTG can lead to the control of range expansion? IPTG was shown to perturb the growth patterns earlier, but could this be used and could it be modulated controllably and robustly using the control platform remained an open question. IPTG was considered as primary way of modulating the growth pattern within the colony as it offered targeted modulation of the cellular protein expression machinery without the major influence on the metabolism of the cell. After IPTG results with other two modalities – nutrient upshift/downshift and antibiotics modulation will be shown

11.4 USING IPTG TO CONTROL THE FRONT VELOCITY

From system characterization experiments done before it was shown that the IPTG had the capability to perturb the growth patterns inside the colony. It is worth mentioning again here the systems responsiveness to the IPTG variations exhibited slow dynamics, limited dynamical range, big time delay and in general resilience to the IPTG level perturbation. Because of this I opted for the bang-bang control of a range expansion inside a user defined region of interest (ROI). Bang-bang control consists of a simple control law which applies the maximum control effort at the system. Bang-bang control often comes as an optimal control solution to the problem of minimizing the time needed to reach a specific set point in linear systems[137]–[140]. Because of the applied maximum control effort the system has the capability to reach its desired trajectory quicker then compared to the other controllers (but of course this comes at a price of stability). In the case of the frontal velocity controlled by varying the IPTG concentration, the bang-bang control law consisted in checking whether or not the measured value is bigger or smaller then the desired reference level. If the measured value was larger then the reference value the valve switched to the position enabling the flow of the LB media not containing the IPTG. On the other hand if the measured value was smaller then the reference level, the valve switched to the position enabling the flow of the LB+1000 μM IPTG media. To investigate the potential of using IPTG to control range expansion three different type of references were chosen

-constant references with different values

-step up reference level

-tracking of the complex reference

The only time when system was able to successfully track the reference to the fullest was the time when the initial range expansion started originally from low values and when the reference was higher then the current value of the range expansion (figure 10.6). In all the other combinations the system was unable to track accurately the desired trajectory (whether it was constant or complex) and was quite resilient to changes in the IPTG levels as it was seen in open loop characterization.

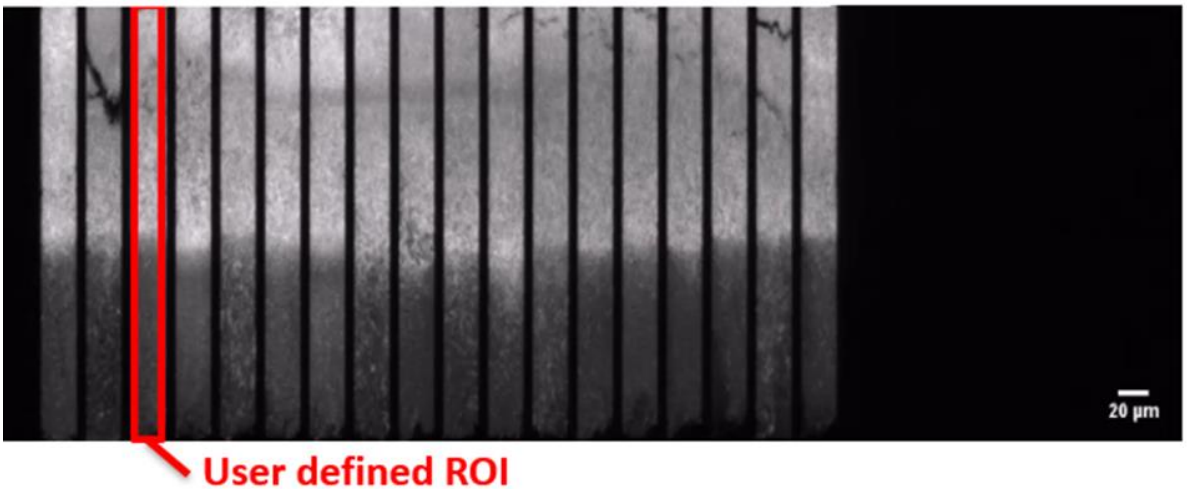

Figure 10.5. Front velocity control over a single channel. The image represents a fluorescent image obtained with 10x objective. Before the image acquisition user defines a specific region of interest (ROI) in which the frontal velocity (maximal velocity inside the side chamber) would be maintained around a specific reference point. Data from this experiment is shown on the figures down bellow.

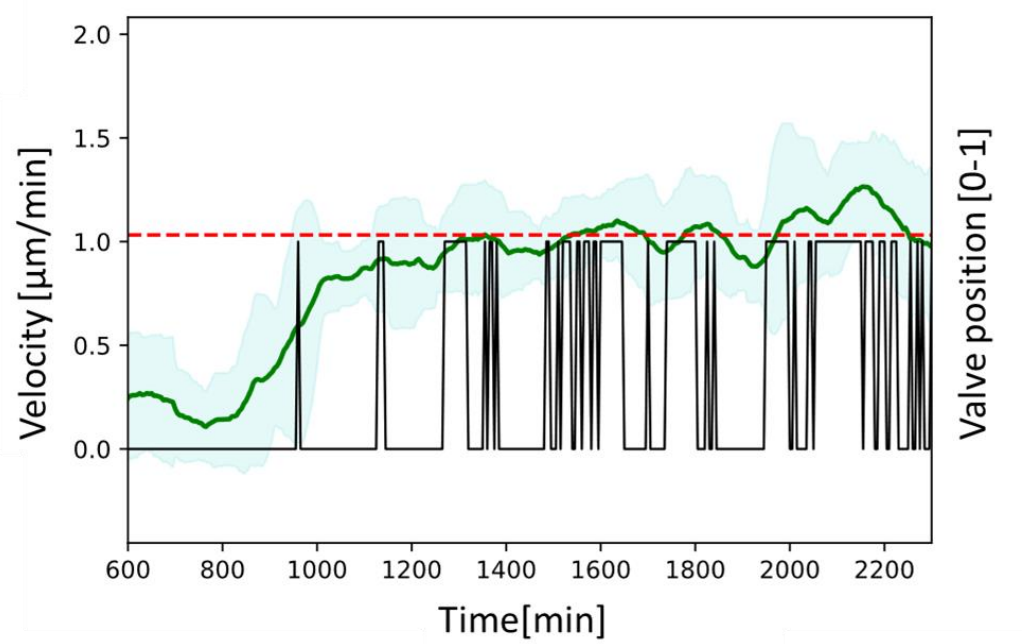

Figure 10.6. Maintaining of the frontal velocity inside one side chamber. Frontal velocity of one side chamber was followed and maintained around a desired reference level of about 1 µm/min through the time course of the experiment. At one point during the first 600min a bubble has blocked the access to the channel, limiting both IPTG and nutrient levels, and mechanically preventing the cells to get easily pushed and washed away. This resulted in limited growth and small velocities inside the side chamber. Data represented here represents the experimental data obtained after the removal of the bubble from the system. Upon the removal of the bubble system needed around 300min to dynamically start reacting and additional 300 min to reach a new steady state. On the same graph valve openness is shown. When the valve was placed in position labeled by digital value 1, the valve was enabling the flow of the LB media with 0µM IPTG. On the other hand when the valve was in position 0 the valve enabled the flow of the LB media containing 1000µM IPTG. Due to the slow dynamics and time delay the applied control law was simple bang-bang control which exhibited a maximal control effort on the system. When the measured front velocity is bellow a set point bang-bang control applies maximum control and switches to the valve position enabling the flow of the LB media containing 1000µM IPTG (position 0). On the other hand when the value is above a set point, valve switches to the position enabling the flow of the LB media without the inducer (position 1).

Interestingly at the instance when controlled was fully achieved the growth patterns of the system in a closed loop and in an open loop configuration differed. Unlike the open loop configuration where cells weren't experiencing dynamically changing environment cells in the closed loop configuration did experience it. The difference in the growth patterns could be seen from the growth rate-velocity state space where the system in the closed loop configuration was described by a steeper slope, indicating a decrease in the growing layer of the colony and a rearrangement of the growth patterns. This was validated by observing the distribution of the growth patterns of a closed loop system and an inferred open loop system with the same velocity. The inference of the growth pattern from the open loop system came from the fact that all the experiments with different IPTG concentrations had fallen on the same curve, thus a theoretical IPTG concentration which would give the same frontal velocity as the regulated one in the open loop would do the same.

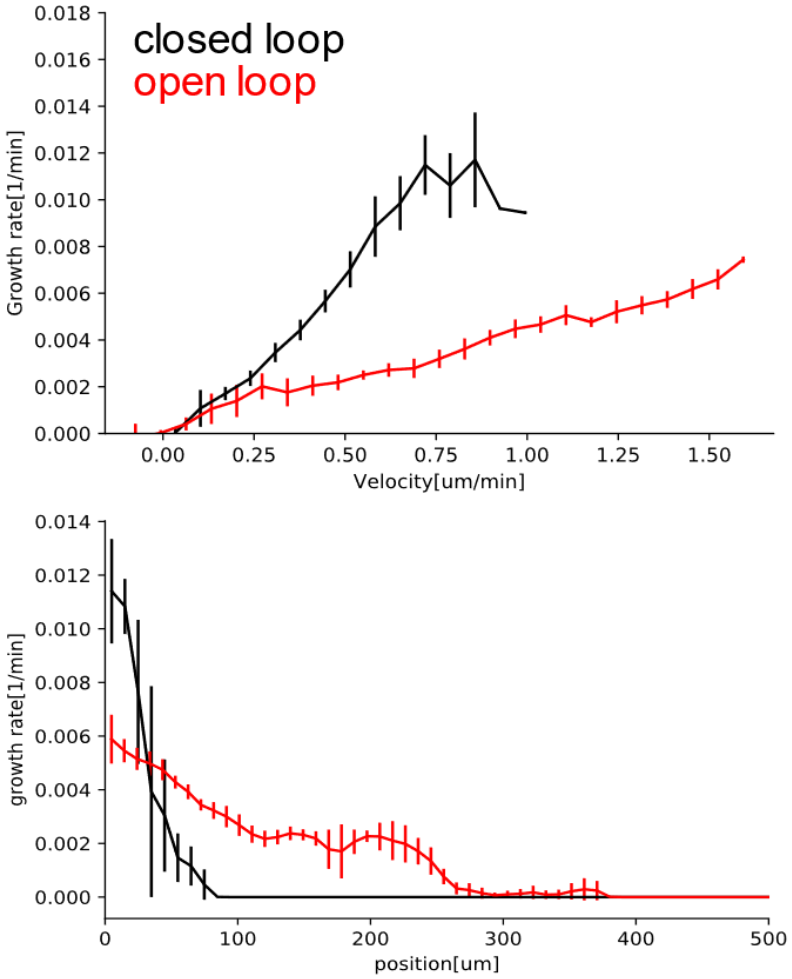

Figure 10.7. Changes in growth patterns in closed loop configuration compared to the open one. While in an open loop configuration cells experience a static environment, cells in the closed configuration experience a constantly changing environment. This dynamics translates on the emerging growth patterns inside the colony. Change in the growth patterns could be seen on the graph describing growth rate-velocity state space. Namely here, the closed loop configuration gives a curve of a much steeper slope, which indicates that in a constantly changing environment the growing layer is much smaller then the case of condition when cell experience a static one. When we compare the growth patterns of a closed loop and that one of the open loop corresponding the velocity which was regulated, the change in redistribution of growth is evident.

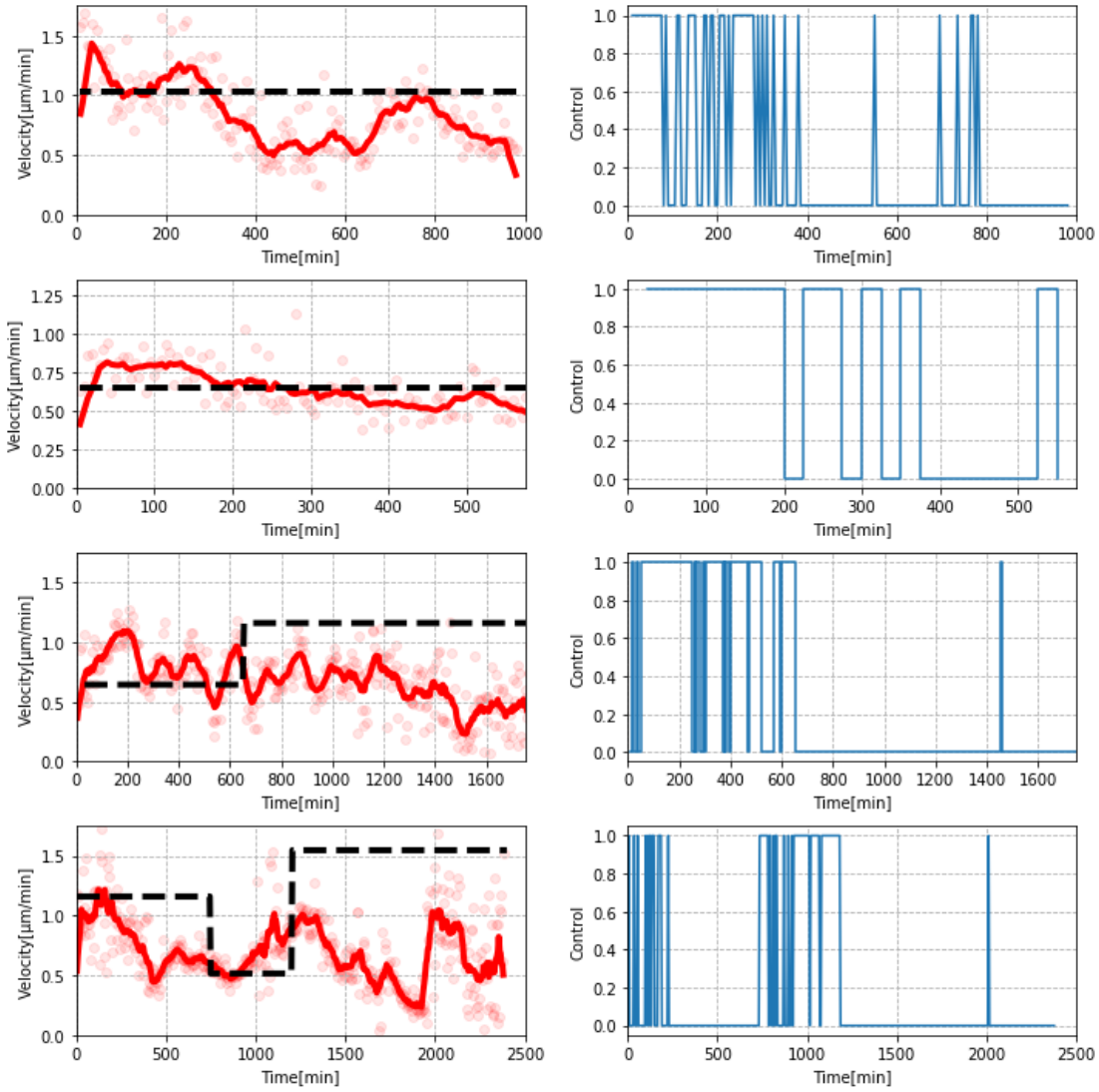

Figure 10.8. Different closed loop experiments with different reference values. On the left side the reference value and the tracking results are shown, while on the right the corresponding control signal is shown. In the first case from above the system was to a degree to better follow the given trajectory (compared to the other cases). Lowering down control sampling time also didn't help with the performances as the system wasn't able to reach the desired reference value (second figure from above) and had a continuous trend downwards. The other two cases represent a complex reference which had nonexistent control performances.

Since the range expansion velocities mostly weren't able to accurately track the desired trajectory in my last attempt to achieve some level of control I tried to see whether it would be possible to control the maximal velocity over several different channels. I repeated the previous experimental settings but now with a ROI containing the three side channels. Online and offline analysis of the controlled channels alongside the offline analysis is given on figure 10.9.

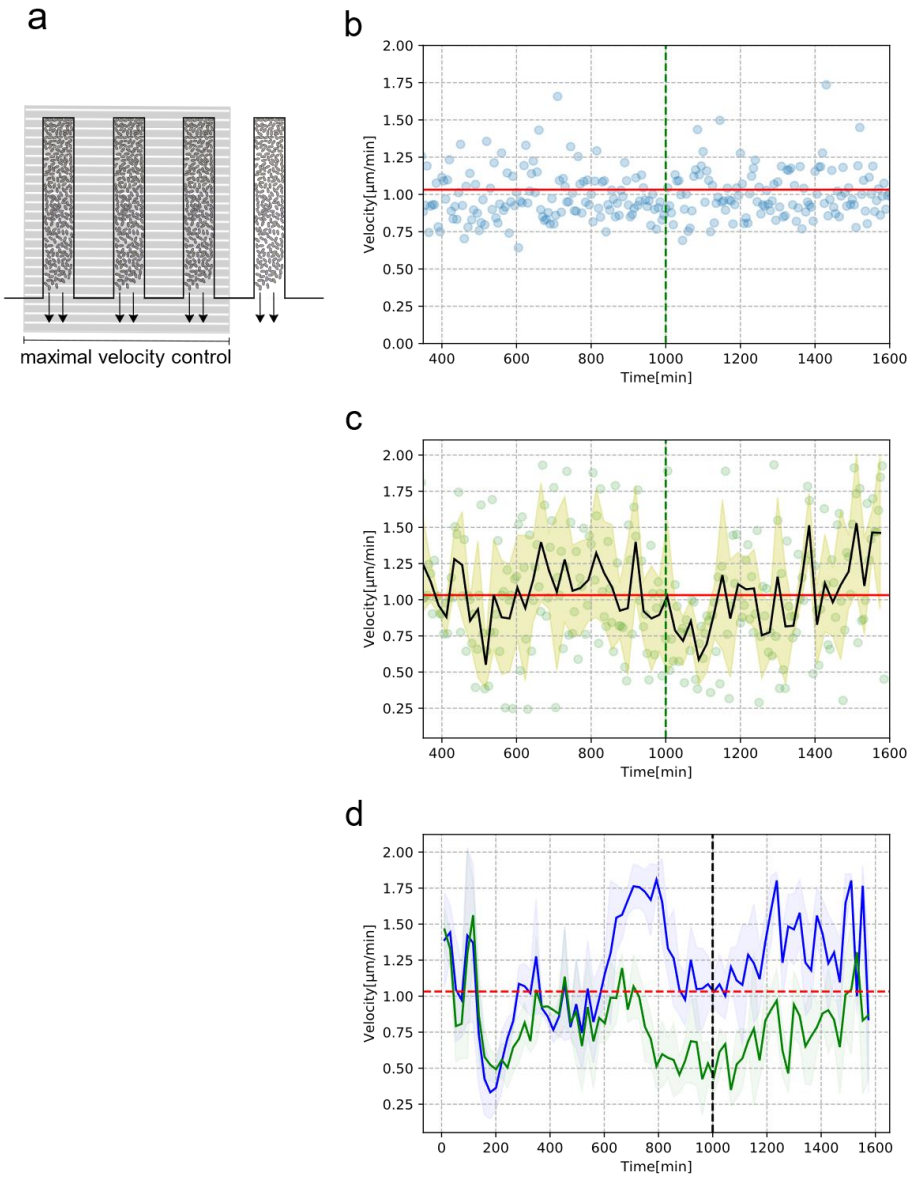

Figure 10.9. Maintaining of the frontal velocity over three side chambers with a constant reference level. a) ROI was applied over the three side channels. Reference level was picked to be around 1 µm/min which corresponded to the maximum frontal velocity over the three side channels inside the ROI. The defined closed loop control problem consisted in maintain their maximum frontal velocity over this period. Closed loop configuration lasted until 1000th min after which the system was switched to the open loop configuration. **b)** Online (during the experiment analysis **c)** offline (after the experiment) analysis . System slow dynamics and reactivity on IPTG change are clearly seen from both the open loop reaction on the IPTG change in the media and from the closed loop control experiments. **d)** Uncontrolled channels: Two uncontrolled channels compared to the reference level throughout the previous experiment. Compared to the controlled channels uncontrolled channels had a much richer dynamics during the varying IPTG concentration in an closed loop configuration.

This control problem (controlling maximal range expansion over multiple colonies) did offer some levels of control compared to range expansion colony control, but since this wasn't what I was aiming for I continued my investigation by focusing on other modalities that are capable of growth perturbation such as nutrient upshift/downshift and antibiotics. But before that I asked myself why IPTG wasn't able to do the job? From open loop characterization experiments I did see slow dynamics, time delays and general resistance of the colony to the IPTG perturbations. I hypothesized that these unsatisfying characteristics probably stem from the fact that cells in the back of the side channel still have large quantities of non-diluted and accumulated RNA polymerase. At the beginning of the experiment cells are positioned at the dead end of the side chamber. At the early colony developmental stage these cells experience high levels of nutrients, and consequently have their RNA polymerase expressed at a high level. As colony expands, these cells are left behind and start experiencing nutrient deprivation. Due to the nutrient deprivation these cells arrest their growth, preventing dilution of the molecules and thus maintain a reservoir of RNA polymerase. Once the IPTG is removed from the media frontal cells are quickly washed away, but cell in the back still have a reservoir of accumulated RNA polymerase and which they could quickly start using when nutrients become available. With this hypothesis I will be concluding this chapter and the story regarding the IPTG control. The direct and targeted influence that the IPTG had on driving primarily the RNA polymerase expression, which initially seemed to be an advantage of the IPTG control, actually became an obstacle for the colony range expansion control. Thus different modalities with a much wider range of influence on cells metabolism, such as nutrient and antibiotic control should be explored in this experimental settings. This was indeed done and the results will be presented in the following chapters.

11.5 USING NUTRIENTS TO CONTROL THE FRONT VELOCITY

IPTG modulation of the front velocity both in a closed loop configuration and in an open loop configuration had proven to be a difficult task. Huge time delay, slow dynamics and small dynamical range were just some of the problems encountered while trying to perturb the growth patterns inside the colony by modulating RNA polymerase levels with different IPTG concentrations. As mentioned previously I hypothesized that this came as a results of accumulation of RNA polymerase in the cells positioned in the non-growing layer. Once these cells got access to nutrients they resumed their growth due to the accumulated RNA polymerase. A potentially more potent way of controlling the velocities and thus the growth rate could be by modulating the levels of nutrients inside the media.

This method strongly affects the entire metabolism of *E.coli*. Like all living organisms *E.coli* as well needs nutrients to grow and sustain itself. Based on the avalaible nutrients *E.coli* coordinates its cellular physiology [141]. Limited nutrients limit the amount of precursor metabolites needed for sustaining the chemical reactions, strongly affecting cellular metabolism, flux distributions and enzymes, consequently resulting in the cells lowering down their growth rate [142]. Having this in mind we can say that the chemical composition of the cell strongly differs at the different growth rates imposed by nutrient limitation[66]. Global readjustment of the gene expression and the impact on the overall cellular metabolism could be further exemplified through the inspection of the cell size. The corresponding cell size is equivalent to the amount of products produced throughout the biosynthesis process [78]. Thus the cell size can be considered a proxy for overall cellular metabolism. Nutrient poor media offers very limited metabolic precursors pool which results in smaller growth rates and cells of comparatively small size compared to the ones grown in nutrient richer media, and the other way around. Thus we can say that the cell size is linearly correlated with the growth rate when exposing the cells to different nutrient limitation. This linear correlation is described as "nutrient growth law" [69], [79]. Previous experiments showed that the nutrient composition had the capability to modulate growth patterns and thus the range expansion within the dense growing colonies of E.coli inside the microfluidic chip. Having this in mind can we by modulating nutrient concentration in the media actually control range of expansion so that it follows a specific desired trajectory? To answer this question we utilized the same principle as before. In a similar fashion as prior IPTG control in the nutrient focused control the valve switched between two media - one with nutrient composition supporting fast range expansion inside the side chambers, and the other one supporting the slower one. M9 media with 0.4% glucose and 1000µM IPTG was chosen as the media supporting lower rates of expansion and on the other hand as nutrient rich media 5xLB supplemented with 1000µM IPTG was chosen. The main reason for this choice was based on the fact that the front velocities obtained from the multiple experiments between these two media gave the biggest possible control range. For comparison between different modalities of control the same bang-bang control law and the same sampling and control period of 5min were applied. Depending on

the distance from the reference value the valve switched between the media. If the front velocity was higher then the desired set point, the valve switched to the media supporting lower growth, and the other way around- if the front velocity was lower then the desired set point valve switched towards the media supporting higher growth rates.

Previous studies investigated the response of *E.coli* when subjected to the fast repetitive switching between the two liquid well mixed media, one supporting high growth rates and the other one triggering starvation [143]. The study had showed that over several generations cells were able to adapt to the dynamic repetitive environment. With excess substrate the cells responded promptly with increasing the uptake rates and increasing the fluxes inside the cell. Moreover in feast condition, *E.coli* stored excessive carbon in the form of metabolic intermediates which were used during the famine phase. The finding goes in line with another study [144] that had shown that 50% of this storage is aimed to be catabolized during the famine phase. For these reasons I expected that the system in my case will exhibit two different settling dynamics depending whether the system is upregulated or downregulated.

Three different types of control problems in this section were analyzed

-a step down reference

-maintaining a constant reference over a certain period after which the closed loop system configuration was turned off

-complex dynamically changing reference.

In all of the control problems the system controlled with the nutrients was more dynamically reactive when compared with the IPTG modulation.

In the first control case the system was exposed to a higher reference value. After some time the reference was switched to a lower one. The system response in this case at first didn't follow the reference and was actually moving away from the desired reference level. With time this internal disturbance which made the system to move away from the target set point was removed and the system was able to track the reference value accordingly.

The second control problem was involving following a constant reference. After a certain time the regulation stopped and the valve switched to the position enabling the entire system to experience more nutritious media. As a consequence cells drifted away from the regulated level they previously had.

Finally the third and last control problem tackled with nutrient level modulation was the problem of tracking a dynamical reference. The system response gave poor tracking results and experienced both time delay and low-pass filtering.

Compared to the IPTG control performances, control of range expansion mediated by nutrient upshift/downshift was much more versatile and offered much more capabilities. My hypothesis is that as the bacteria respond globally to changes of nutrient concentration, by rewiring their

metabolism and carbon fluxes, the response would be much stronger then just a direct interference with RNA polymerase expression done with IPTG. All in all the system was able to track simple references but did had much poorer results, with a clear low pass filtering influence, on tracking a complex one.

11.5.1 Step down reference signal response

In this study, I used a simple step-down reference signal to investigate the dynamics and response of a closed-loop system. The experiment involved applying a set point of high reference value, followed by a low one. Initially, the system's response deviated from the reference and moved away from the desired set point, resulting in an undershoot. This undershoot could have been caused by internal or external disturbances or even attributed to the non-minimum phase dynamics of the system itself (in dynamical system theory the non-minimum phase systems are classified as stable and causal ones which have unstable inverses, leading to the delays in the system output, often manifesting as an undershoot). However, in all cases after some time regardless of the cause of the undershoot, the system should be able to track the reference accurately, which indeed happened.

It's worth mentioning that online analysis and tracking were conducted on one of the side channels. While the other side channels were under the influence of the control signal, they were not in the closed-loop configuration. The tracking results of several side channels front velocity and velocity deeper inside the channel are also presented separately in the offline analysis section. As mentioned earlier these side channels were not under closed-loop control, but they were still under the same control signal's influence. Based on their previously held steady state and the environmental changes, they can follow the same trajectory, but it's not guaranteed (as again these channels are not in a closed loop configuration). The system may end up in a different stable state beyond the desired reference set point due to the cells biological stochasticity, adaptation, and slightly different response to their nutrient surroundings. As previously mentioned the online algorithm to estimate the range expansion wasn’t always able to calculate the frontal velocity, but was able only to catch the velocity positioned deeper inside the side channels, therefore enabling the positional velocity control.

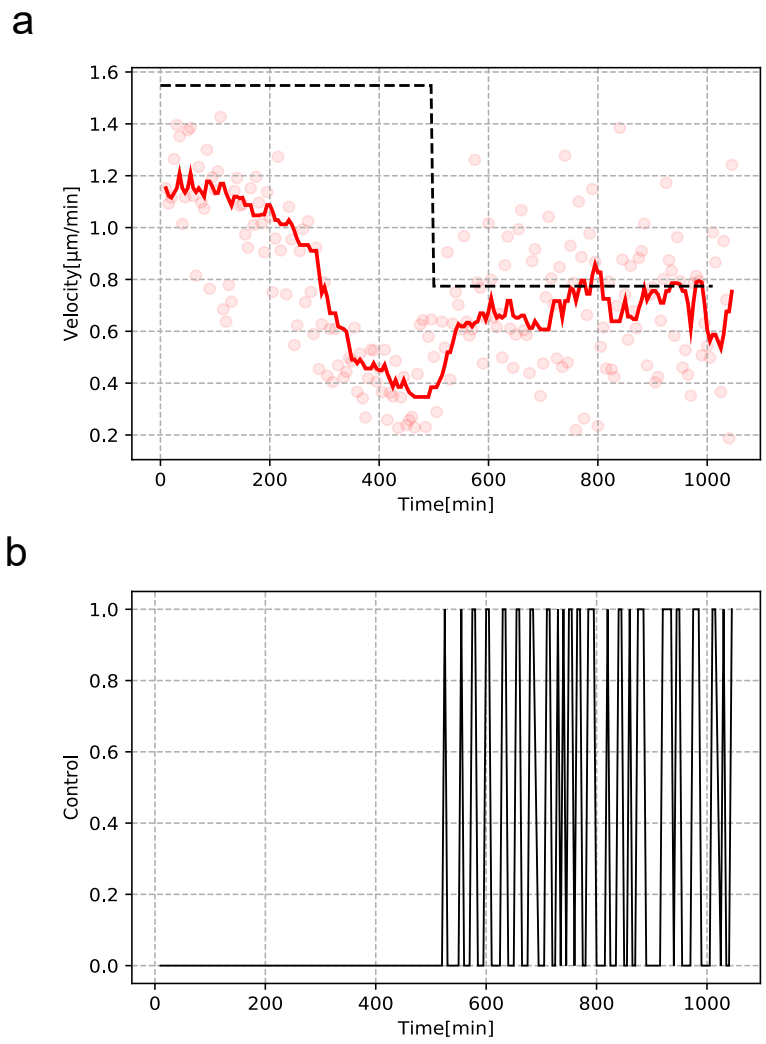

Figure 10.10. a) Results of the online velocity tracking during a step down reference signal response. The online PIV algorithm which performed the PIV estimation detected velocity deeper inside the channel thus effectively giving positional velocity control. Step down signal (black dashed lines) was given as a desired reference value to the system in the closed loop configuration. The system response is given in the red. During the first 400min the system seemed not to be able to track the desired reference and actually went towards completely different direction. After 400min the internal disturbance of the system stopped and the system started recovering and was thus able to follow the second part of the reference. b)C**ontrol signal of the online velocity tracking during a step down reference signal response**. Control value corresponding to zero represents the position of the valve enabling 5xLB media to flow through the system, while control value which corresponds to the logical 1 represents the position which enables the flow of the M9+0.4% glucose media. Control sample time was set to be 5min. Depending on the difference between the desired value and the measured value, the valve switched between the two media. If the reference value was bellow the measured one the valve switched towards the M9+0.4% glucose media. If the reference value was above the measured one the valve switched to the 5xLB media. In the first 400min while the system was experiencing internal disturbance and moved away from the reference position. During the disturbance time the control effort (according to the applied control law) switched the valve to the position enabling the flow of the 5xLB media (control signal=0) thought the system. After the stabilization and recovery the system was able to follow the second part of the reference, by modulation between the two media 5xLB (control signal=0) and M9+0.4% glucose (control signal=1)

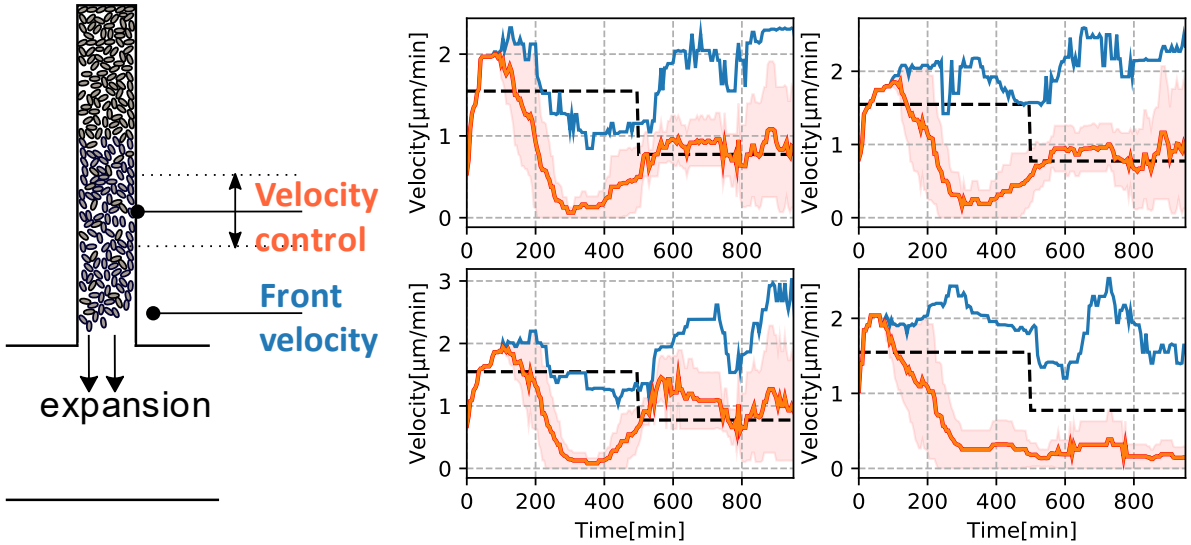

Figure 10.11. Post experimental (offline) analysis of the tracking response. Due to differences between online and offline PIV algorithms, the online algorithm (algorithm used during the closed loop experiments) wasn't able to capture the entirety of the velocity profile inside the side chambers. The algorithm was only able to detect the right velocity profile up from a certain point inside the side channel. This effectively meant that the system controlled a range positional velocity. In here blue color represents the front velocity (maximum velocity near the chamber opening) and the red color with its shaded area represents the velocity in a range where the online algorithm operated during the accurate tracking of the system (500min onwards) [161.25-354]µm from the channel opening. Four different channels are represented here.

11.5.2 Constant control loop level in the [0, 375] min time frame

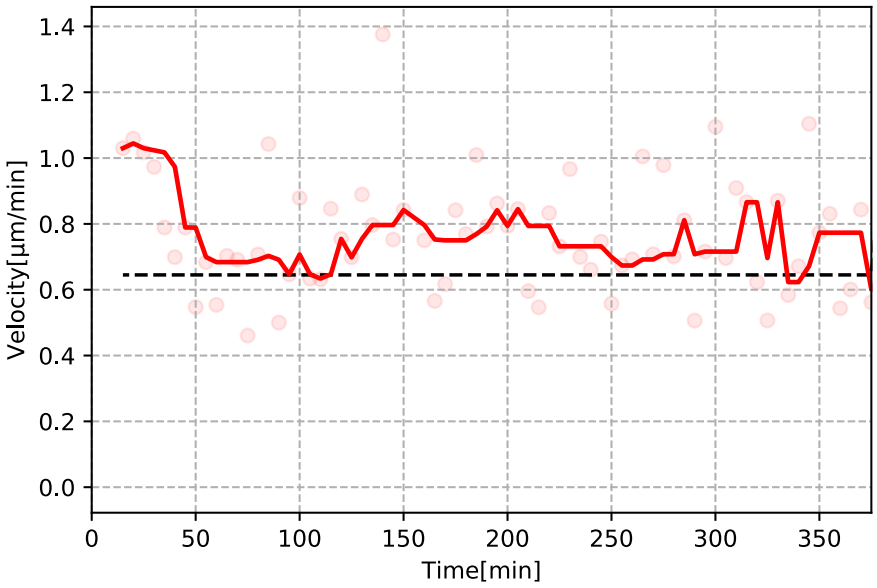

Figure 10.12. Online constant reference control of the system. The system was controlled for 375min in an closed loop configuration until the control loop was switched off. Unlike the previous case the online PIV algorithm didn't encounter problems.

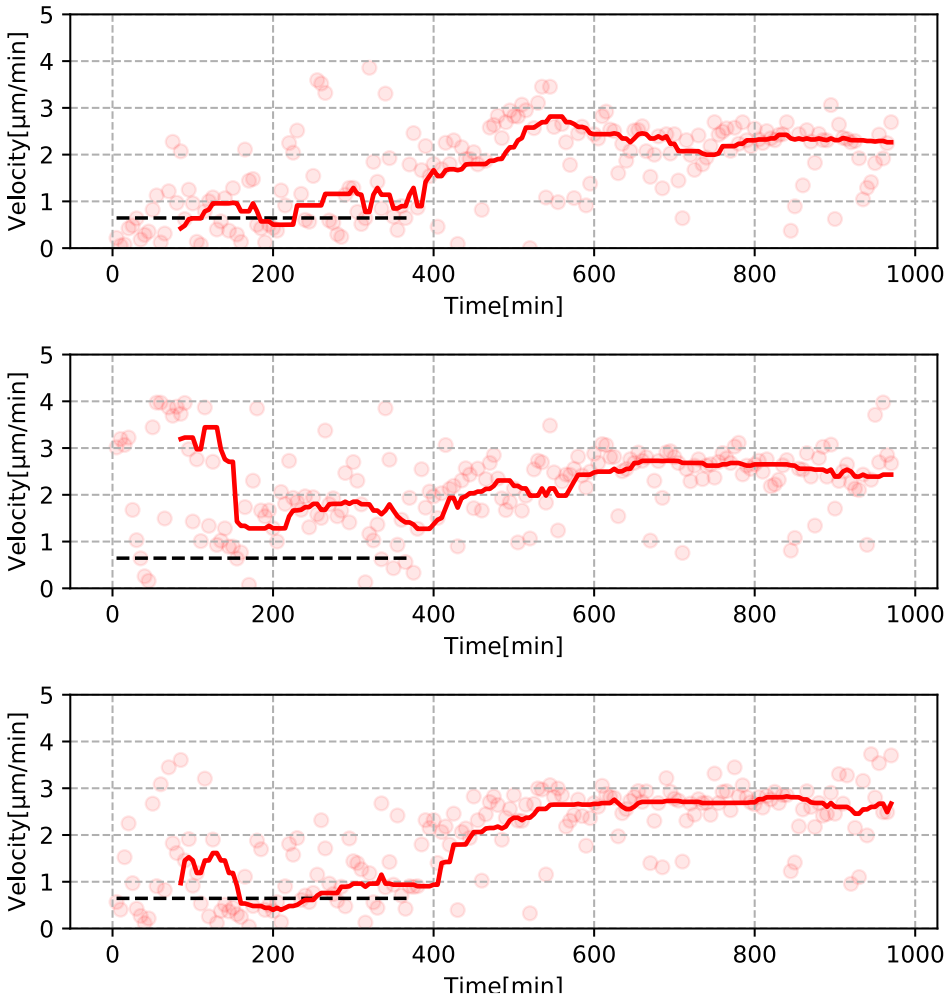

Figure 10.13. Post experimental (offline) analysis of the tracking response of three side chambers. During the first 375min in closed loop configuration all three channels settled and maintained a certain steady state. The first channel represents the controlled channel, while the other two represent the uncontrolled channels. Controlled channel successfully maintained its front velocity around the desired reference point. The other two channels also maintained their front velocities at a certain steady state. Upon deactivating the control loop configuration the valve switched to 5xLB media. Since the media provided more nutrients, all channels responded to this change by increasing their growth rates and thus velocities.

11.5.3 Complex reference set point

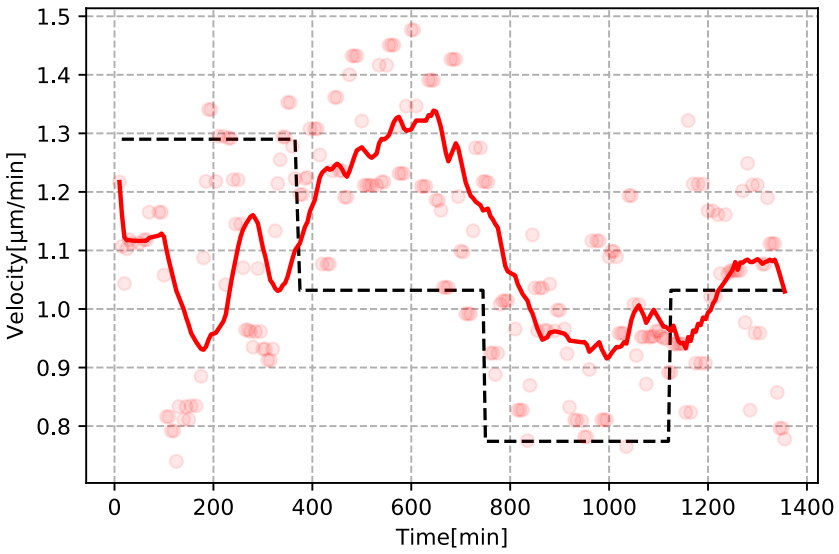

Figure 10.14. Closed loop configuration of the system with complex time changing reference. Complex time changing reference with step down and step up was given to the system in closed loop configuration. The system response is given in red. Even though the tracking performances were poor, the system did respond to the changes. A noticeable time delay can be identified. The step changes in the references apparently were too quick enough for the system to completely adapt and it appears that the system behaved like a low pass filter.

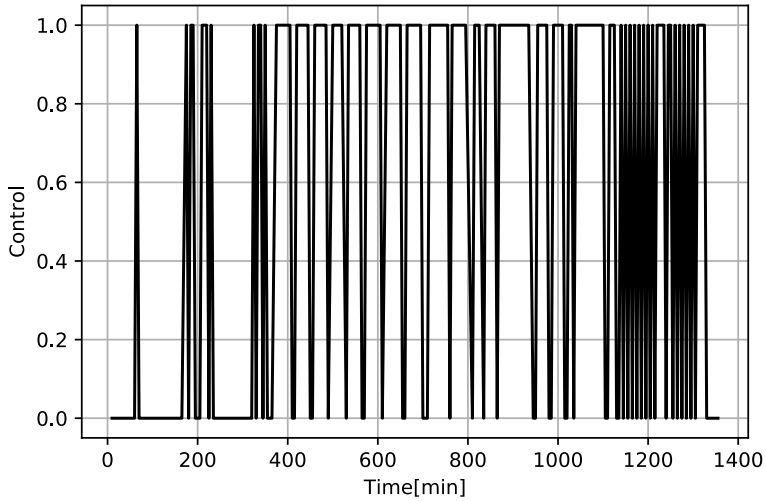

Figure 10.15. Control signal of front velocity tracking during a closed loop configuration of the system with complex time changing reference. Fast oscillation between the two media can be seen. When the control signal is at the level 0, valve is switched at a position which enables 5xLB media to flow through the system. When the control signal is at level 1, M9+0.4% glucose media flows through the system.

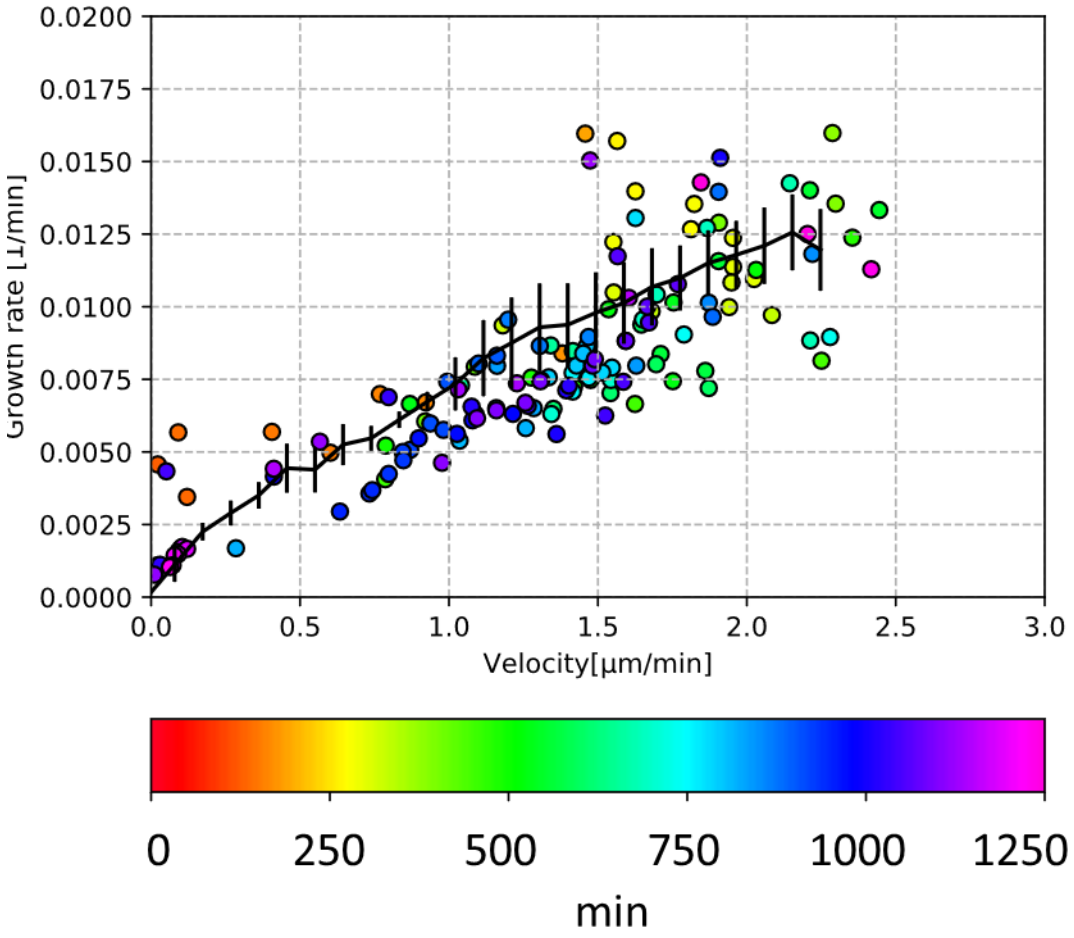

Figure 10.16. Comparison of the growth rate-velocity state space relationship in an uncontrolled system and in system experiencing control through switching between nutrients. The 5xLB characteristic obtained from open loop experiments is shown in black. The growth and velocity patterns in cells under the M9 media also followed the same pattern. Results of velocity-growth rate tracking of the colony front throughout the experiment is represented by circles and the time points are given with the rainbow color bar down bellow. Even though the closed loop system experienced oscillatory changes in nutrient media and didn't reach a steady state all of data had followed the same curves obtained in open loop experiment in growth rate-velocity state space.

Previously it was mentioned that tracking frontal velocity and the frontal growth rate of the colony over time offers a way to see how the growth patterns develop throughout the experiment. In here even though the reference was complex, velocity-growth rate data remained on the same pattern as it was in the open loop system characterization between the LB and M9 media. This is completely opposite that what was seen with the IPTG modality where the slope actually increased. One of the hypothesis I could be that based on the fact that in the case of

IPTG we are indirectly influencing the nutrient gradients, compared to the direct influence of the nutrient upshift/downshift. Oscillating between highly nutritious media and nutrient poorer media as a results leaves the colony front overall with less available nutrient compared to the static state of passing highly nutritious media through the system. In that conditions both the growing layer and the frontal velocity/growth rate decrease. On the other hand the time varying IPTG levels in the system will activate only portion of the cells that within the colony, because a lower amount of IPTG at the colony front means that cells deeper within the colony won't have access to the IPTG and will go to growth arrest. This consequently shortens down the growing layer of the colony thus leaving more nutrients for cells in front, helping them achieve a higher growth rate (as for them even with the time varying levels of IPTG, the overall IPTG concentration is not limiting and enables high growth rates). Thus from observing how the expansion and the growth rate of the colony front develops over time, we could infer how the colony replies to a given modality and what happens with the growth patterns. All in all due to its global influence on the cellular and the colony dynamics as a whole, nutrient modulation proved to be a way more effective tool to control in real time the bacterial range expansion. Simple references could be followed. For the more complex ones, the control performances were degraded.

In a similar manner to nutrients, the antibiotics influence the cellular dynamics on multiple dimensions. Thus in the next chapter, the third and the last modality, using antibiotics to investigate the potential of range expansion control is going to be covered. To compare it with the previous two modalities of control, the same control law (bang-bang) was applied.

11.6 BANG-BANG CONTROL IS NOT A GOOD CHOICE FOR THE CONTROL LAW WHEN USING ANTIBIOTICS TO MANIPULATE THE FRONT VELOCITY

Following the nutrient and IPTG based control in this chapter I will examine the possibilities of applying the same type of bang-bang control using antibiotics. The previously obtained open loop system response to 250µg/ml doxycycline in 5xLB media supplemented with 1000µM IPTG had satisfying dynamical characteristics. Its fast dynamics and settling time were promising for the purpose of closed loop control. The closed loop control was tested in 5xLB media containing 1000µM IPTG. In order to compare the antibiotic control strategy with the IPTG and nutrient one, the same control law and its parameters were chosen (bang-bang control and 5min control period). One of the media contained 250µg/ml doxycycline, while the other one was antibiotic free. The image acquisition started from an open loop condition without antibiotic in the system and from an already established quasi-stationary regime. Closed loop was activated around 250min after the acquisition started, and it lasted up until 1000min, after which closed loop was deactivated and the system was once again in the open loop regime. The second open loop regime was once again without antibiotics in the media. The system was left to settle down. Due to previously described differences between the PIV algorithms while using the 5xLB media during online control and offline control, the velocity detected and controlled inside the loop control (online) was a velocity at deeper within the colony.

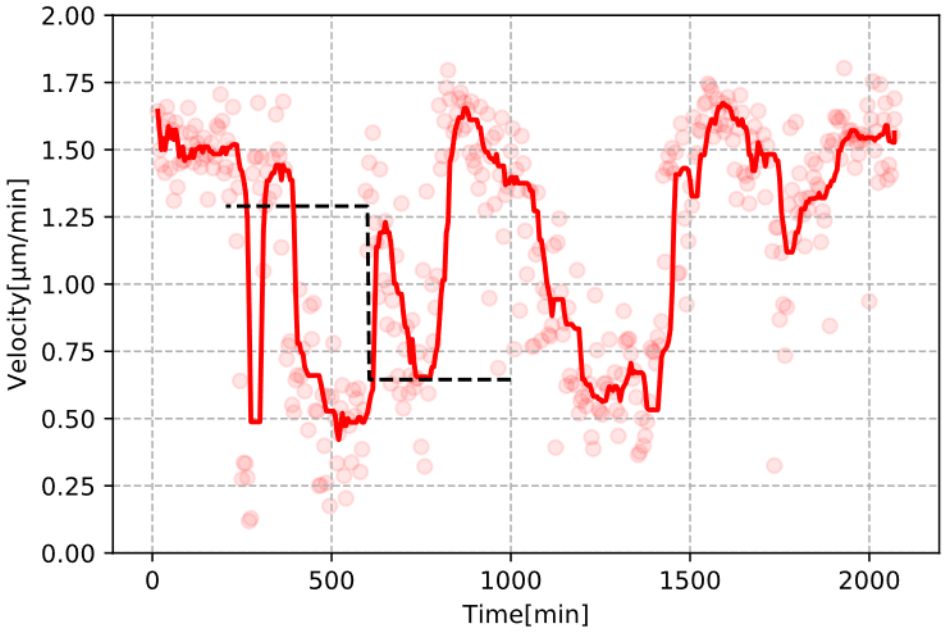

Figure 10.17. Unsatisfying tracking response of bang-bang control of expansion velocity at within the colony with modulating levels of doxycycline in 5xLB media supplemented with 1000µM IPTG. The system started from an open loop regime without the antibiotics in the media. Image acquisition started once the quasi-stationary state was established. After around 250min the closed loop control was activated. As previously mentioned the bang-bang control law switches between the two media, based on the sign of the error. One of the media was containing 250µg/ml

doxycycline while the other one was antibiotic free. When the measured value was above the reference, the control law switched to the media containing doxycycline and the other way around- when the measured value had fallen bellow the desired reference value, control algorithm switched the media not containing the antibiotic. Desired reference levels, and thus the period in which closed loop control was active is shown in black dashed lines. The bang-bang control wasn't able to track the desired reference value. Having in mind relatively fast system response and settling time, the large deviations from the set point were probably a consequence of the maximum control levels applied to the system. This pinpoints to the fact that in the case of using antibiotics other types of control which don't immediately apply the maximum control effort (such as PI control) are more applicable. After 1000th minute the closed loop regime was over, and the system was once again in an open loop configuration with the flow consisting of the media not containing antibiotics.

During the closed loop control the system wasn't able to stabilize around the desired set-point. The system had poor (or better to say non-existent) closed loop performance as the measured value deviated excessively from its target value. The deviations were caused by excessive control imposed by the bang-bang control. The fast response and settling time to 250µg/ml doxycycline, alongside the deviations and the inability of the control law to follow the set point indicate that another type of control would be more suitable in the case of modulating the speed with doxycycline.

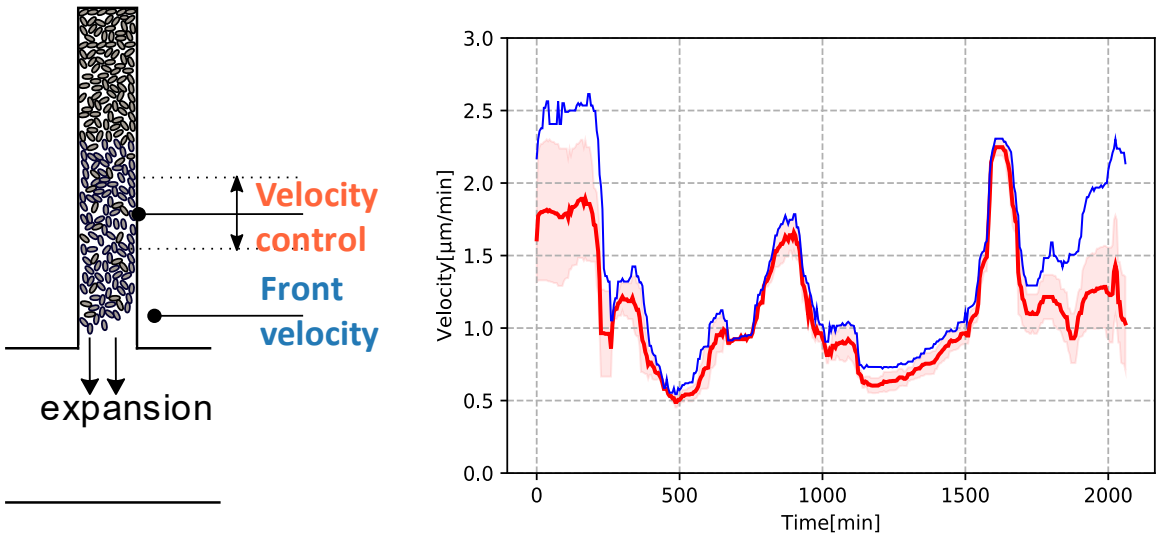

Figure 10.18. Post-experimental (offline) analysis of the tracking response. Blue color represents the front velocity (maximum velocity near the chamber opening) and the red color with its shaded area represents the velocity in range [64.5;96.75]µm from the channel opening. Upper and lower limits of the red shaded area represent the positional velocity at a corresponding upper and lower range in time. Positional range corresponds to the positional range in which the experimental data obtained for the closed loop response (online analysis) was operating during the online experiment

From previous studies with dense bacterial assemblies and from the open loop experiments with doxycycline it is known that one of the effects of adding antibiotics to the media was the growth activation of the cells positioned deeper inside the colony in the non growing layer. As mentioned previously the outer layer of the bio community has a protective role for the entire community . Upon adding antibiotics to the media, these cells cease the growth, which enables nutrients to penetrate deeper inside the colony, where the antibiotic influence isn't felt. (*Figure 8.4.3)* shows the velocity at a position in the colony where no growth was detected before the addition of the antibiotic. Activation of the closed loop (red shaded area) meant that the cells were to a degree under the influence of doxycycline. Once the closed loop stopped the transient state occurred where the entire colony was reorganizing to previously held open loop quasi-stationary state.

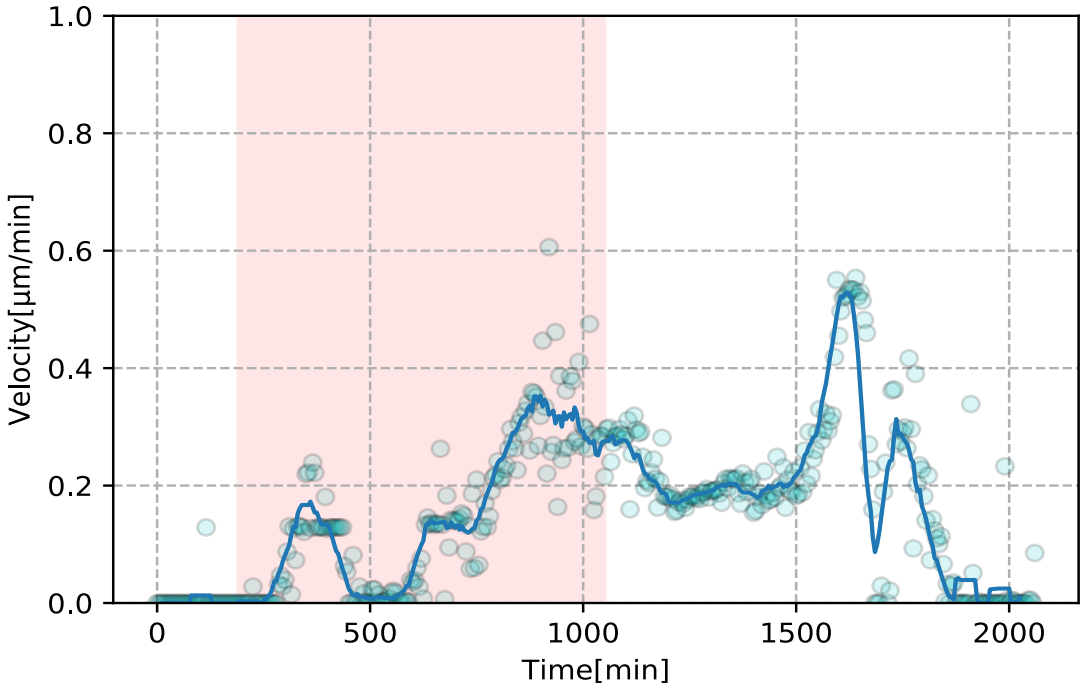

Figure 10.19. Antibiotic treatment during the closed loop configuration activates the growth of the cells positioned deep in the nongrowing layer of the colony at 258µm. Velocity profile of the cells at xx um inside the chamber. Red shaded area signifies the begging and the end of the closed loop configuration. Before the closed loop configuration and thus the antibiotic treatment the cells at this position were growth arrested. Once the configuration was switched to the closed loop one and the antibiotic was introduced into the system cell positioned at this layer were activated. Activation comes as a consequence of the growth inhibition of the colony front near the channel opening. As cells at the colony front become growth arrested, more nutrients become available for the cells in the back of the colony where the influence of the antibiotic isn't felt. After the system was switched back to the open loop configuration there is a transient regime before the quasi-stationary pre-antibiotic state was achieved.

Dynamical transition during both open loop and closed loop configurations could be seen on growth rate-velocity profile plot. The dynamical state of a system at time *t* is described by its corresponding frontal velocity and frontal growth rate. As said previously this plot sums up the information about the spatial organization of the growth rates inside the channel and provides information about the size of the growing layer and how it evolved during time. Time evolution of frontal growth rate- frontal velocity state is described by rainbow color bar. Initial and final state were plotted differently compared to the other time points (stars vs circles) to distinguish them from the other temporal points. On the same figure in black the growth rate-velocity characteristic was plotted for 5xLB media. Activation of the previously growth arrested cells deeper inside the side channel can also be read from the figure as the slope was lowered down. Furthermore after the closed loop was switched off and the transient regime has passed the system recovered and has returned to it previously held quasi-stationary regime, which can be seen from the positions of the initial and final states.

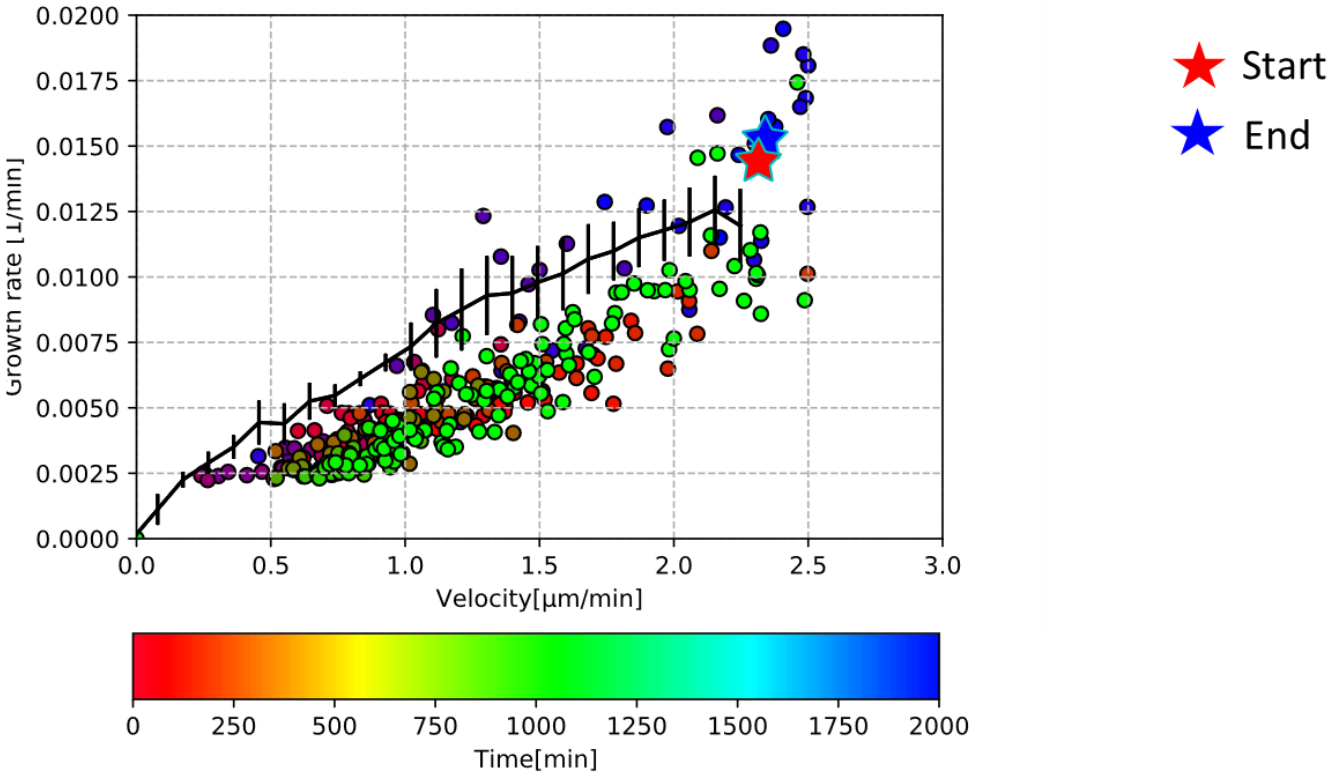

Figure 10.20. Comparison of growth rate-velocity state space relationship in a system without the antibiotic treatment throughout the experiment and in system perturbed by doxycycline treatment as described previously in this section. The black curve represents the growth-rate velocity state space relationship obtained in open loop experiments in 5xLB media supplemented with 1000μM IPTG which throughout the experiment didn't influence the antibiotic treatment. On the other hand the perturbed system at one point has had experienced doxycycline treatment. Perturbed system started in antibiotic free state. After around 250min, closed loop configuration was turned on. The closed loop configuration and thus the antibiotic perturbation lasted up until 1000th min, when the system was again switched to an open loop configuration with no antibiotic present in the media. During the perturbation period and in recovery phase the growth-rate velocity trend decreased compared to the unperturbed system. This decrease in slope signifies the increase in the growth zone inside the colony. Upon sudden treatment of the antibiotic, frontal cells decrease or completely arrest their growth rate, thus enabling nutrients to penetrate deeper inside the colony where the antibiotic influence is not felt. After recovery phase the "old" quasi-stationary regime was once again reestablished which can be seen from initial and final states almost completely aligning in the growth rate-velocity state space graph.

From all of the modalities covered in this thesis the antibiotic modality seemed to yield the strongest response and the biggest opportunities for real time control. Since of its fast dynamical response, relatively short time delay, and relatively huge dynamical range, bang-bang control was inadequate control law choice for this modality. Sadly I didn't have the time to investigate this further, specifically the application of other control laws such as the PI control that could be a potential solution of this problem. Bang-bang control applies maximal control effort on the system and in the case of doxycycline that would mean that the colony is exposed to the high concentration of antibiotic that was shown to have a drastic influence on the range expansion speed of the colony. Depending on the choice of parameters the PI control could give less triggering control efforts to the system, which would enable a more controllable response. Going in line with the available literature, applying antibiotics (in open loop and in closed loop experiments) expanded the growth deep within the nongrowing layer of colony. This comes as a consequence of growth arrest of the cells positioned at the front. As cells get growth arrested, more nutrients are being able to penetrate deeper within the colony, thus enabling growth inside the layers which experience smaller concentration of antibiotic. This spatial reorganization of the growth patterns is also seen when observing the temporal decrease of the slope on the velocity-growth rate diagram of the frontal cells. Upon removing antibiotic from the media the colony recovers and reinstates its previous quasi-stationary regime. The reinstatement of the quasi-stationary regime and the consequent reinstatement of the old growing zone could be read as well from the frontal velocity-growth rate graphs as a gradual increase in the slope.

With this I would be concluding the range expansion control part. At the beginning of my PhD we initially envisioned to use the IPTG to control the growth rate of E.coli grown in a mother machine microfluidic device. During this time in parallel I focused on two things – developing an appropriate single cell growth rate control platform and conducting gene expression noise studies. But why at the first place should one study noise in gene expression? Gene expression noise can limit the precision of genetic circuits and furthermore gene expression noise is the cause of the variability among the cells. Having huge noise means having huge variability among the cell which makes control efforts difficult. I deemed noise studies in the context of using this particular IPTG inducible RNA polymerase strain particularly important, since most of the noise originates at a transcriptional level and propagates throughout the gene expression machinery..

While developing a control platform I realized that the strain used in the study could not be easily loaded into the side channels of the mother machine. Various designs were tried but sadly non of them worked. From this era two results still do remain -the control platform described previously (which was readapted to control range expansion of the colony) and the so called noise study which will be presented in the next and last chapter of this thesis. Before going to the noise chapter it is worth mentioning that noise can also be extremely important in the context of controlling the range expansion. For instance high noise in gene expression could potentially mean that a subpopulation of bacteria might emerge that would make the entire colony more resilient to the changes of the environment.

12 ADDITIONAL RESEARCH – CLUSTERING AND NOISE IN RNA POLYMERASE EXPRESSION IN PP2 *E.COLI* STRAIN

12.1 INTRODUCTION

Initially one of the ideas of my PhD was to control *E.coli* growth rate of PP2 strain using IPTG at a single cell level using the mother machine device. The biggest hurdle with this strain was its difficulty to enter inside the microfluidic side chambers. The difficulty of getting the strain to enter the microfluidic side channels of the mother machine could have been caused by several different factors. One possibility is that the strain was too large compared to other strains that can easily enter the microfluidic channels. Technical issues with the microfluidic device itself could also have played a role. Additionally, the difference in surface properties between the microfluidic channels and the strain could have made it difficult for the strain to adhere and enter. Despite trying for several months and using different chip designs, I was unable to load the cells. Ultimately this was the reason why we abandoned this idea and moved on to explore other options. In parallel, while I was trying different microfluidic designs, I studied the noise in gene expression of RNA polymerase of PP2 strain in different experimental conditions. I considered it important for the control design as the system noise has the potency to generate undesirable control actions [145] which can be potentially limiting and could lead to poor control performances.

Gene expression can greatly vary between the cells, despite them experiencing the same conditions and being genetically identical [146]. The origins of this variability lie in the fact that many of the cellular components involved in biochemical reactions are present in very low molecule numbers[147]. These molecules experience Brownian motion and infrequent interactions which generate stochastic fluctuations [148]. Besides being informative for control design, cell to cell variability measurements also contain wealth of information regarding the regulatory phenomena and dynamic interplay of gene expression networks that can be obscured by the population based analysis [149]–[151]. Based on the origins of the fluctuation in gene expression, the total gene expression noise can be decoupled into two categories- the intrinsic and extrinsic noise [152]. The origin of extrinsic noise lies in the cell to cell differences in concentrations of transcription and translation machinery. Extrinsic noise generates correlated fluctuations in independent promoters inside the cell. On the other hand intrinsic noise originates from the stochasticity of biomolecular reactions and generates uncorrelated fluctuations and it is suppressed with increasing concentrations of the molecular species involved.

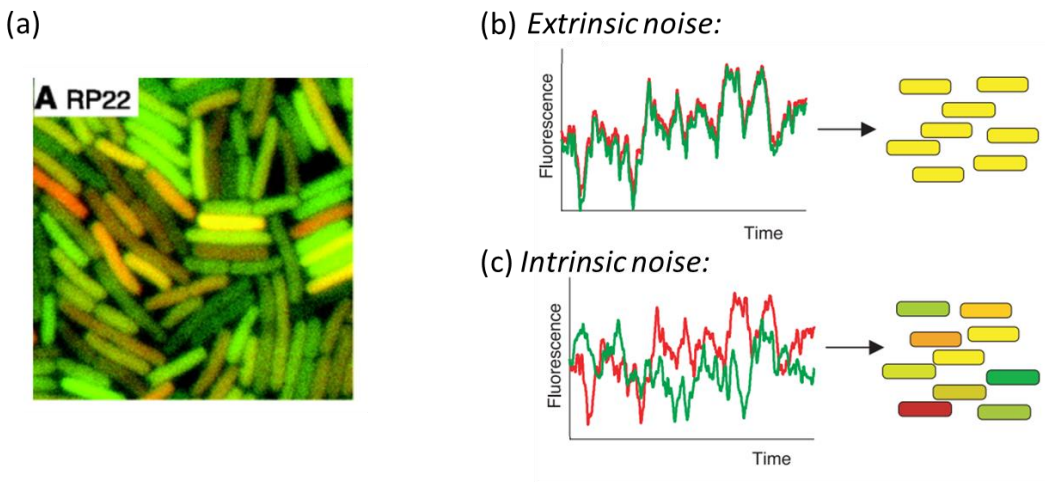

Figure 11.1. Gene expression noise. **(a)** Even though *E.coli* cells experience the same environmental conditions and had the two reporter genes controlled by identical promoter there is a significant difference between the reporter protein expression among the cells. The amount of reporter proteins expression varied from cell to cell. If both reporter proteins were expressed at the same amount of each protein appear yellow. **(b)** Even if both reporter proteins were expressed at the same level, we would still see fluctuation of fluorescence over time in a single cell. In the entire population each cell will have the same amount of the two reporter proteins, but the quantity of the both will differ from one cell to another. The origins of extrinsic noise lies in low numbers of transcription and translational machinery. **(c)** Two reporter genes might become uncorrelated in individual cells due to stochasticity of biomolecular reactions. This generates uncorrelated fluctuations in a single cell, consequently giving rise to a population of cells expressing one protein more then the other one. Figure adapted from [153]

It is known that the gene expression is dominated by mRNA numbers[152]. This makes the gene expression from the RNA polymerase itself crucial since it propagates throughout the entire transcriptional network. In [154] the authors developed an isolated system to measure noise in RNA polymerase expression in E.coli. The system was based on inducible T7 RNA polymerase expression fused with yellow fluorescent protein and specific target reporter genes, mCherry and cyan-fluorescent reporter which were put under the control of T7promoter. T7 RNA polymerase was expressed from a tetracycline promoter which made it possible to vary T7 RNA polymerase levels modulated by varying anhydrotetracycline (aTc) levels. In this isolated system the RNA polymerase wasn't coupled to growth nor size. The results were not surprising as they showed that the more RNAP concentration, the less the protein noise there is. Or, more precisely, the propagation of RNAP abundance variation to expressed protein noise is inversely proportional to the concentration of RNAP.

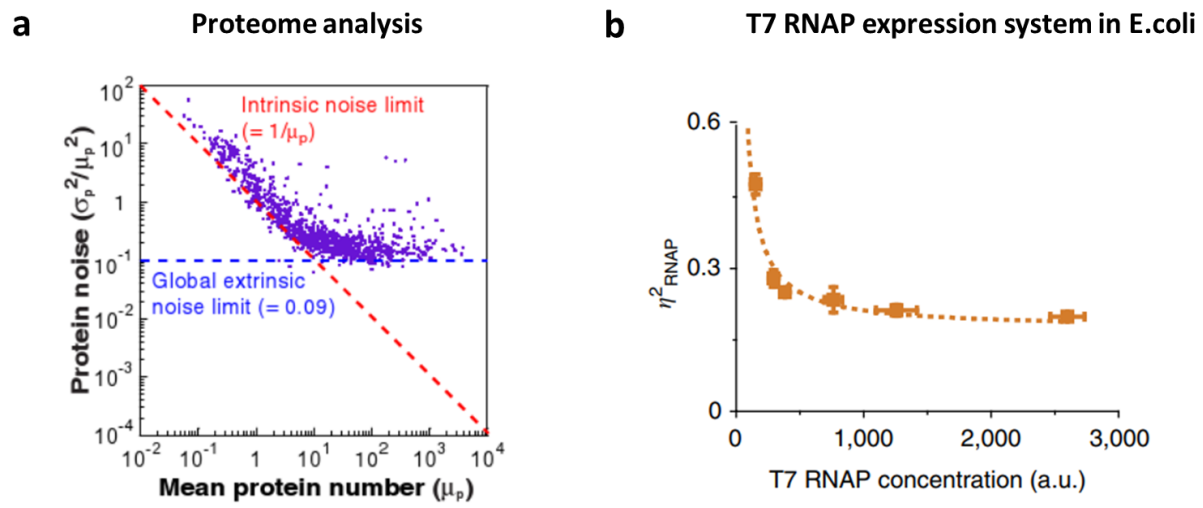

Figure 11.2. Protein gene expression is inversely proportional to the protein abundance with a lower noise limit. Above certain protein abundance level, the protein expression noise becomes independent on protein abundance levels and reaches a plateau. The plateau is determined solely by extrinsic factors such as the limited numbers of transcription and translation machinery. In the regime where the noise is inversely proportional, the noise is dominated by the intrinsic factors such as inherent biochemical reactions stochasticity. **(a)** *E.coli* proteome analysis of gene expression noise. Proteins were fused translationally with YFP in its native chromosomal position **(b)** Inducible T7 RNA polymerase expression fused with yellow fluorescent protein in *E.coli*. Levels of T7 RNAP system were modulated by varying anhydrotetracycline (aTc) levels. T7 RNAP system is not native to *E.coli* thus compared to the native RNAP polymerase it is not autoregulated, coupled to growth and size, liquid to liquid phase separated and partitioned among different cellular machinery. Figure adapted from [154] and [155]

In reality nonetheless RNA polymerase is autoregulated, partitioned between bound and free pool of RNA polymerase and liquid to liquid phase separated from cytoplasm in fast growth conditions[67], [68], [156]–[159]. As mentioned before it has been long known that *E.coli* grown in nutrient rich media reach maximal growth rate and increase their size[69], [79]. With higher growth rates, the number of RNA polymerases in the cell also increase, reducing gene expression noise of RNA polymerase to levels near its physical limit[67], [68], [154]. Both the increase in cell size and the fact that the gene expression noise levels on average decrease with the growth rate were confirmed further by global gene expression studies[160]. Large cell size has been proposed as an evolutionary adaptation that counteracts noise increased caused by high growth rate [80], [161], [162].

Property	High carbon influx conditions	Low carbon influx conditions	References
Growth rate	high	low	[69]
Cell size at division	large	small	[69]
Noise in general gene expression	low	variable	[80], [160]
Noise in RNAP expression	low	high	[154]
RNA polymerase clustering	yes	no	[156]–[159], [163]
RNA polymerase numbers	high	small	[67]–[69]
Fermentation	yes	no	[164]

Table 11.1. Properties of the *E.coli* grown in high carbon influx conditions and low carbon influx conditions.

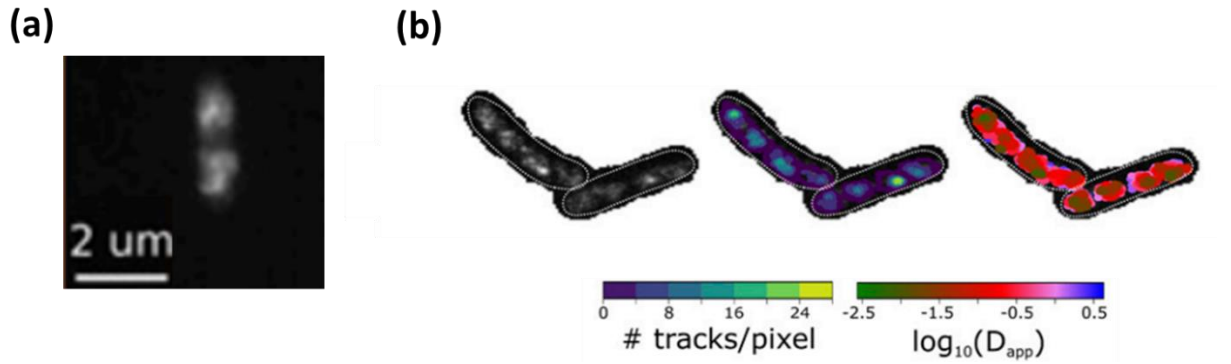

Figure 11.3. RNA polymerase clustering in *E.coli*. (a) Fluorescence microscopy image of rpoC-mCherry construct of *E.coli* which enables tracking of RNA polymerase. Cells were grown in LB media at 37°C and fixed prior to the imaging. **(b)** Live single molecule tracking of RNA polymerase (rpoC-Maple3 construct) with PALM microscopy in LB media at 37°C. Similar clusters of RNA polymerase to the ones in fluorescence microscopy was noticed. The clusters were dynamical with areas of higher density moving more slowly compared to the areas of less density. Image adapted from [156]

Although I experimentally observed that the total fluorescence signal of rpoC-mCherry (used to quantify the amount of RNA polymerase) did follow the previously established relationship (more nutrients-more RNA polymerase), the mean fluorescence per cell which is used as a proxy for concentration followed the opposite. Specifically, I hypothesized that the demands of high growth rate and increased cell size may reduce the global RNA polymerase concentration, leading to a high noise state. However, as mentioned earlier, under these growth conditions, cells also concentrate their transcriptional machinery in micro-organelle-like clusters of RNA polymerase. This suggests a potential mechanism for noise reduction, which could be explored further.

12.2 METHODS

12.2.1 Strains, media and cell preparation for noise measurements

Previously described PP1 and PP2 strains were analyzed. For both PP1 and PP2 strain, RNA polymerase was modulated through changing the carbon source in the media. Fluorescence signal of rpoC-mCherry was used as a readout of RNA polymerase in the system. Following carbon sources were used: LB, M9+0.2% glucose, M9+0.2% maltose, M9+0.2%galactose, M9+0.2% sucrose and M9+0.2% acetate. For the IPTG inducible strain (PP2 strain), media was supplemented with 1000µM IPTG. The culturing conditions were found to be used throughout the literature and were chosen so cell exhibit growth nonlimiting conditions. The following carbon source gave a wide range of growth rates (figure 11.4). It is known that the bacteria grown in different media that support the same growth rate, display the same macromolecular composition regardless of the carbon source present[69], thus the results obtained through wide range of growth rates exhibited by these different carbon sources can be extrapolated for any other nutrient source giving the same growth rate.

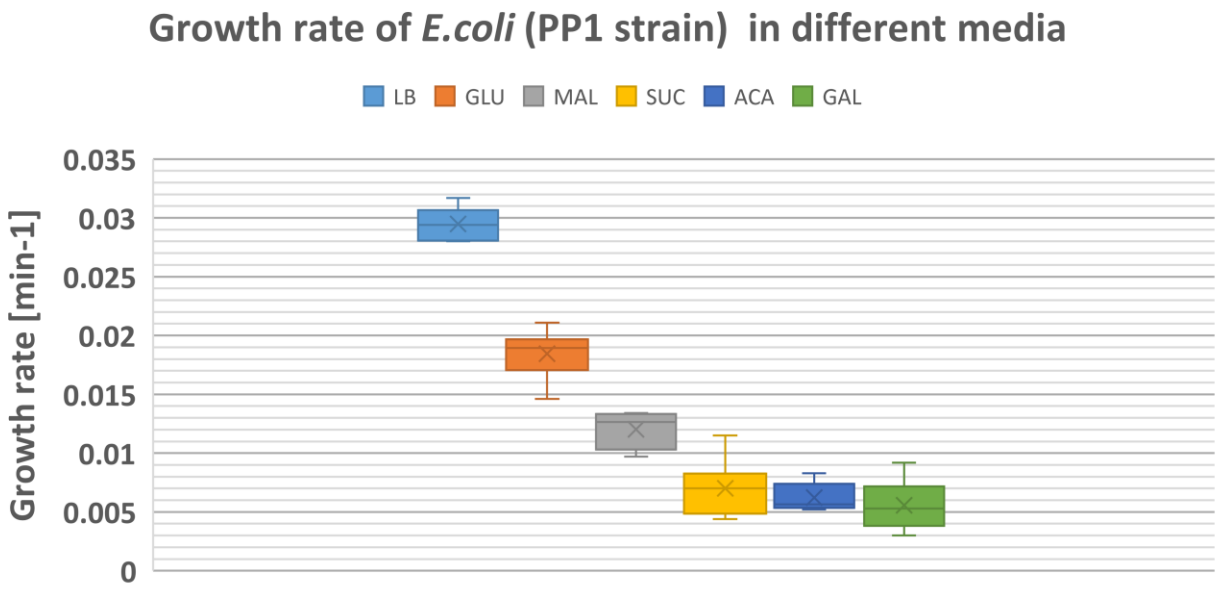

Figure 11.4 Growth rates of PP1 (WT) strain in various growth conditions. The growth rate of PP1 strain was modulated by changing the nutrient composition of the media. The fastest growth was in LB, while the two lowest ones were in acetate and galactose (both PP1 and PP2 strains aren't able to consume galactose). Error bars represent standard deviations between three independent biological replicates. Cells were first grown as an LB overnight culture and then diluted 1:1000 in corresponding media. Growth rate was determined as the steepest slope of the growth curves obtained in the plate reader experiments.

Before imaging with 100x objective the cells were fixed using the following protocol

1. *E.coli* was grown in an overnight LB culture (supplemented with 1000uM IPTG if the strain is PP2)

2. Fresh M9 media supplemented with desired carbon sources was made (supplemented with 1000uM IPTG if the strain is PP2). Overnight culture was diluted in 1:100 ratio in fresh media.

3. Media with cells was then put in 37℃ shaker. When the OD reached early exponential phase (OD=0.2-0.4) cells 5ml cultures were span for 5min at 4000rpm.

4. Following spinning the cells were resuspended in 4%PFA and were left incubated at a room temperature for 30min

5. Following the PFA incubation period the cells were washed twice with 1xPBS

4. After the washing step was done, cells were ready to be loaded to the 2% M9 agar pad and imaged.

5.Ilastik[165] was used to identify the cells and quantify their mean fluorescent intensities. Calculate the noise between the segmented cells as $\frac{\sigma_p^2}{\mu_p^2}$.

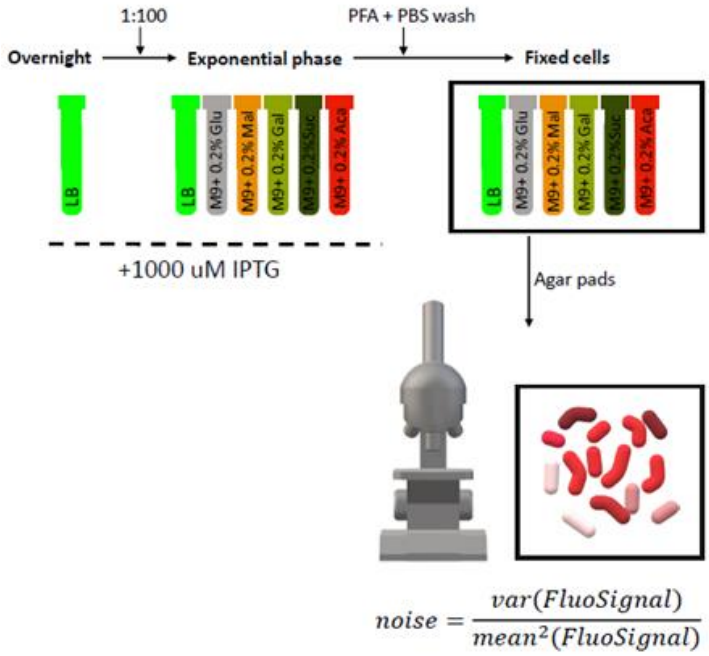

Figure 11.5. Protocol for the noise measurements. Overnight LB culture was diluted 1:100 in the corresponding media. After the cells reached the mid-exponential phase cells were fixed and washed with PFA and PBS according to the protocol above. After the fixation cells were placed on 2% M9 agar pads and were imaged under the 100x objective.

For the noise measurements only data coming from single cell microscopy analysis is presented here. Standard deviation and mean fluorescence of the entire bacterial population were used to determine the variability in gene expression in a condition. Cell size is highly depended on the nutrient used in the media, thus to compare different experimental conditions one must take this into consideration. To do so I observed variability of the protein concentration instead of number of proteins was used. Mean fluorescence per cell was used as a proxy for protein concentration. Standard flow cytometry measures the total fluorescence per cell. For obtaining the mean fluorescence per cell one must have the information of cell size. Signal used for estimation of cell size is forward scatter (FSC). Using standard flow cytometry is problematic since usual flow cytometry sensitivity measures for forward scatter (FSC) used for size estimation is around the size of bacteria itself and has limited capacity to identify the particles less than 1 micron in size [166]. Furthermore FCS is not a linearly dependent on the cell size. Since poorer nutrient sources will give of cells of comparatively smaller size then those ones grown in LB media, another more sensitive signal must be used to estimate the size. One option that can be used in this regard is the side scatter signal (SSC), which is used for inferring the cellular complexity. From [166] and from experiments it was indeed seen that the SSC is far more sensitive to detect smaller particles/bacteria, but the problem of nonlinear dependence of this signal on cellular size still stands. In the appendix I will show images that I obtained from a nonstandard flow cytometer that had 60x objective incorporated in itself. This permitted to

image the passage of every single event. Due to the time left and the need to focus on the first part of the project I was suggested to drop the project at this stage. Nonetheless the results from this nonstandard flow cytometer were promising as it shows that this tool could be used further to inspect the noise in PP1 and PP2 strains.

12.2.2 Analysis of the microscopy images and noise estimation

Microscopy images obtained with 100x objective were analyzed. Single cells were segmented in Ilastik. Prior to noise estimation, histograms of mean fluorescence data per specific condition were obtained. This was done to compare the independent biological replicates and to discard datasets that were problematic as for instance those on (figure 11.6) and (figure 11.7). Data on (figure 11.6) represents the data from three replicates of cells grown in M9+0.2% acetate. First replica for instance shows completely unrelated patterns to the other two, thus it was disregarded in noise analysis.

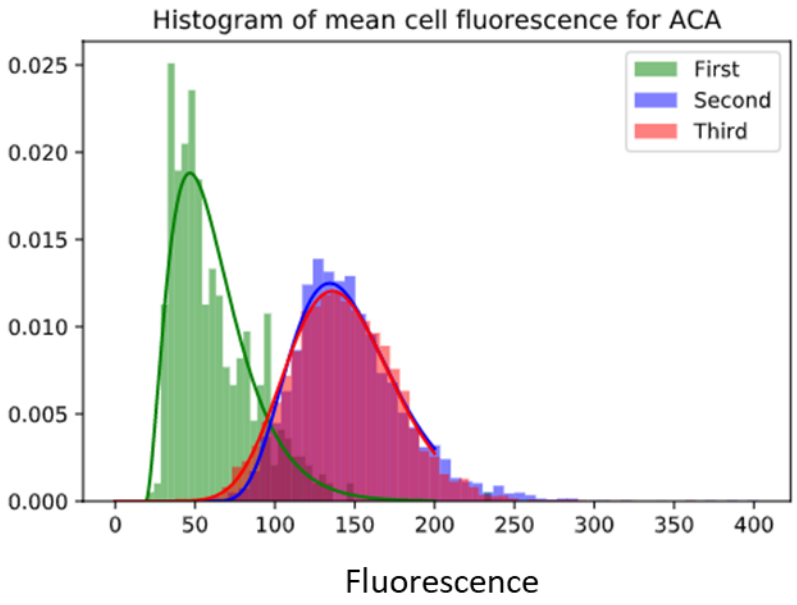

Figure 11.6. Histogram of the segmented cells grown in M9+0.2% acetate. Three independent biological replicas were analyzed. One of them showed completely unrelated characteristics (first one) and was discarded for further noise analysis.

Figure 11.7 represents the cells grown in M9+0.2% sucrose. The first replica was discarded even though its mean was quite close to the other two replicas. From closer inspection the histogram of the first replica exhibited bistable behavior with two distinct peaks that could possibly mean two distinct subpopulations.

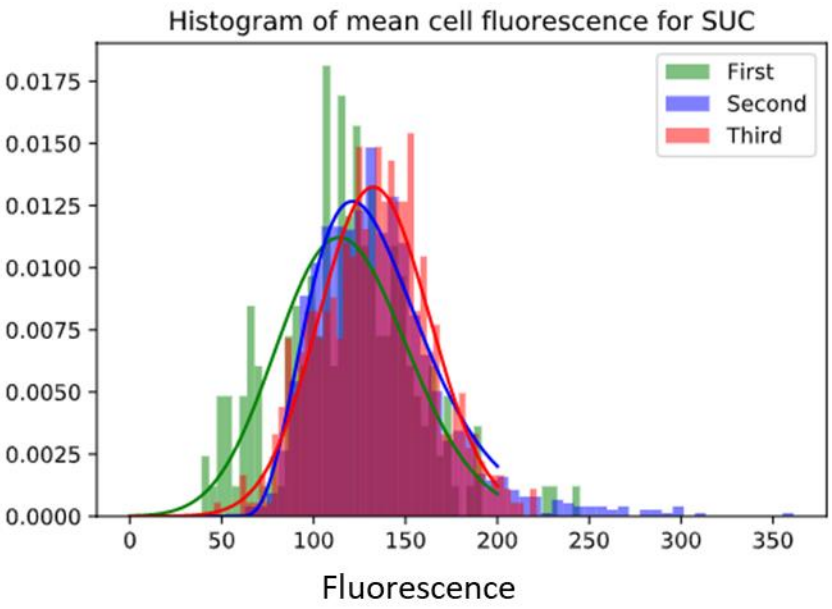

Figure 11.7. Histogram of the segmented cells grown in M9+0.2% sucrose. Three independent biological replicas were analyzed. First replica was discarded even though its mean statistics was close to the other two replicas. This was done as the cells in the first replica exhibited two distinct subpopulations

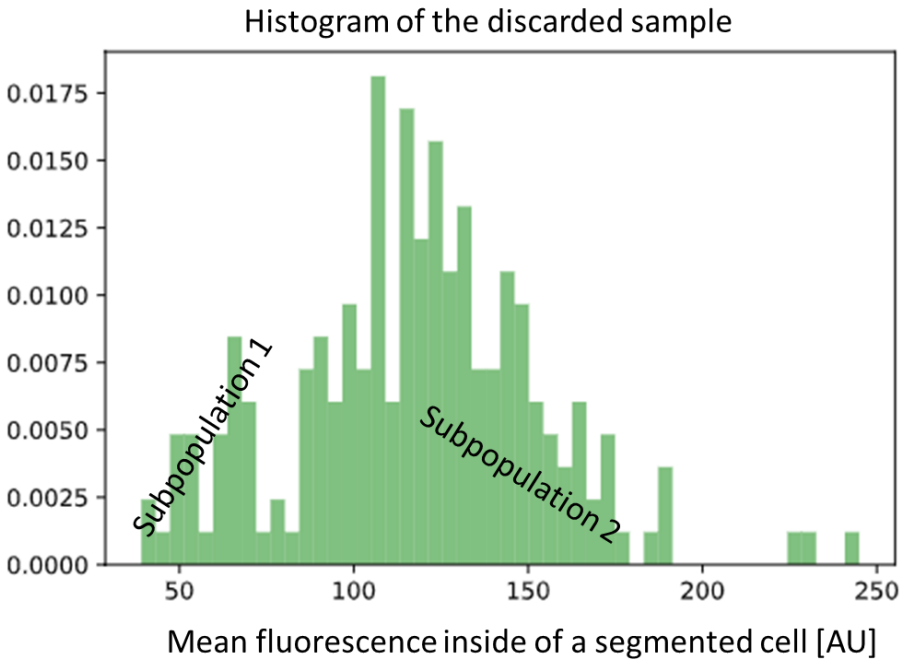

Figure 11.8. Histogram of the first replica in M9+0.2% sucrose which was discarded for further analysis. Two subpopulations were spotted- the main reason I discarded this dataset.

For the datasets that were not discarded noise was determined as:

$$noise = \frac{\sigma_p^2}{\mu_p^2}$$

Where:

σ_p – standard deviation of mean fluorescence of rpoC-mCherry inside a specific dataset

μ_P –average of the mean fluorescence rpoC-mCherry inside a specific dataset

12.2.3 Clustering analysis

As mentioned before RNA polymerase in E.coli was shown to exhibit clustering behavior due to liquid-liquid phase separation[156]. In the same study the authors adapted the method to quantify chromosome condensation[167] and nucleolar morphology[168] for the purpose of quantifying clustering of RNA polymerase inside E.coli. The E.coli strain had mCherry fused to the rpoC gene, which enabled the quantification of RNA polymerase inside the cells. On segmented images, for each cell the fluorescence intensity per pixel was normalized by the minimum and maximum value inside of the segmented cell area.

$$I_{norm} = \frac{I - I_{min}}{I_{max} - I_{min}}$$

The percentage of the pixels corresponding to the background increases with the protein clustering. This was used to quantify to what degree RNA polymerase clusters inside of the segmented area. Pixels bellow the 0.5 in the normalized threshold were classified as the background area pixels, while everything above that value signifies the RNA polymerase clusters.

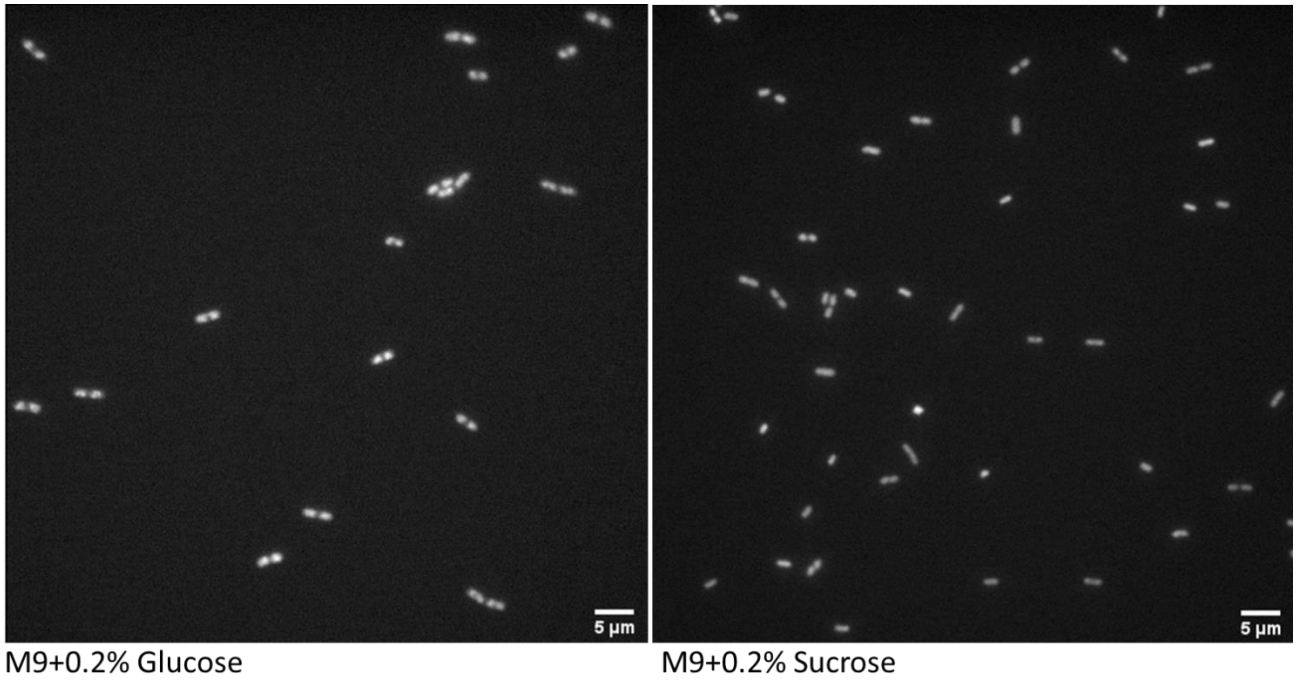

Figure 11.9. Fluorescence images of *E.coli* PP1 strain grown in two different carbon sources. Before imaging cells were fixed and placed on M9 agar according to the previously described protocol. Cells grown in glucose exhibit two bright clusters of RNA polymerase at the poles as previously described by the literature. These clusters were shown to be do to liquid to liquid phase separation and only occur in the media that enables the fast growth. Close up image of the two cells from each media with similar size is shown on figure 9.2.7.

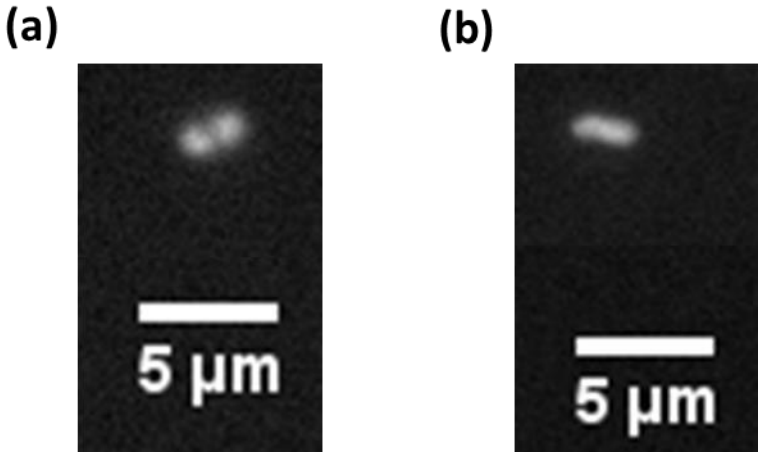

Figure 11.10. Close-up image of two cells, approximately the same size of grown in two media with two different carbon sources -glucose and sucrose. **(a)** Cell grown in M9+0.2% glucose. Cells grown in glucose media exhibit fast growth and the form clusters of RNA polymerase. **(b)** Cell grown in M9+0.2% sucrose. Sucrose as a carbon source doesn't support fast growth. The cells in poorer carbon source media also lack the formation of clusters of RNA polymerase

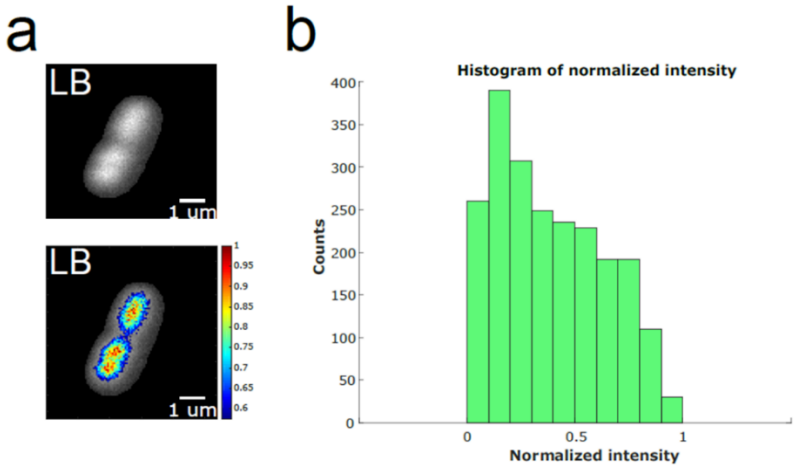

Figure 11.11. Quantification of the clustering inside the segmented *E.coli* grown in LB media. Fluorescence pixels inside the segmented area were normalized between [0,1]. The percentage of pixel which falls bellow the threshold 0.5 represents the background of the segmented area. The higher the value, the more clustering of RNA polymerase there is. (a) Pixel above the threshold 0.5 on the fluorescent image. (b) Normalized histograms of the segmented area.

12.3 RESULTS

Cells were grown overnight in LB media. In the morning cultures were diluted 1:100 and were grown in media with different carbon sources (LB, M9+0.2% glucose, M9+0.2% maltose, M9+0.2%galactose, M9+0.2% sucrose and M9+0.2% acetate). Upon reaching mid-exponential growing phase cells were fixed with PFA. Following fixation cells were washed two times with PBS and were loaded on 2% M9 agar. Fixation protocol given by the [156] demonstrated that the fixation process did not affect the localization. Cells were imaged under 100x objective and segmented with Ilastik. Features extracted from the segmented images were mean fluorescence per cell, total fluorescence per cell and cell size. As previously said it is known that cells growing in richer carbon source are bigger in size and have more total number of RNA polymerases in the cell. Features from the segmented cells coming from various conditions were plotted all together on figures 11.12 and 11.13. I found that the mean mCherry fluorescence of the cell, a proxy for RNA polymerase concentration, is inversely proportional to the cell size. Furthermore the mean fluorescence of the cell was inversely proportional total fluorescence inside the segmented cell. Since total fluorescence signal per cells is proxy of RNA polymerase numbers this suggests that with the increasing size, cell increases the total number of RNA polymerases but it decreases its concentration.

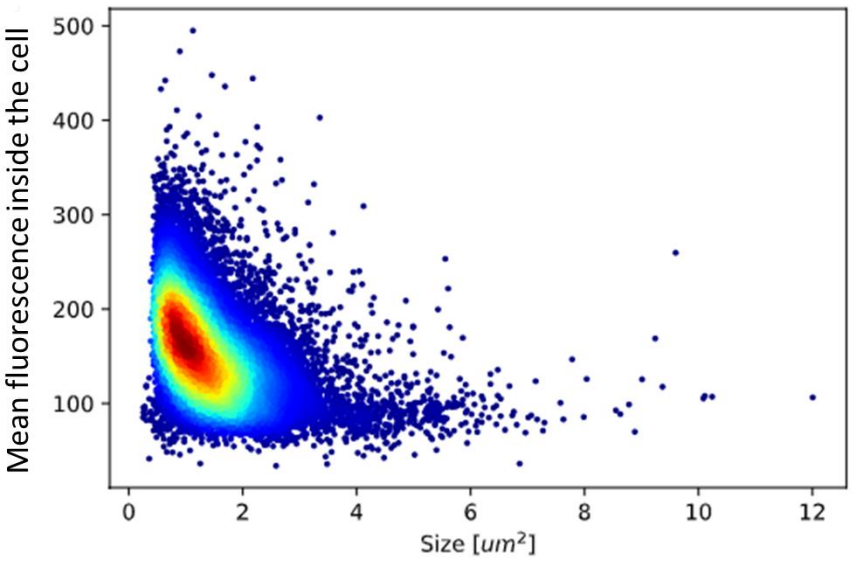

Figure 11.12. Cell size and mean fluorescence signal of mCherry. For each segmented cell across different conditions its size and the mean fluorescence signal inside of it were plotted on the same graph. Mean fluorescence signal of mCherry is a proxy measurement for RNA polymerase concentration. The mCherry fluorescence is inversely proportional to the size. This means that the bigger the cell is, the smaller the concentration of RNA polymerase. Since the bigger cells are associated with a higher growth rate and a more nutritious carbon source this was a strange result since it is known that the number of RNA polymerases increases with growth rate.

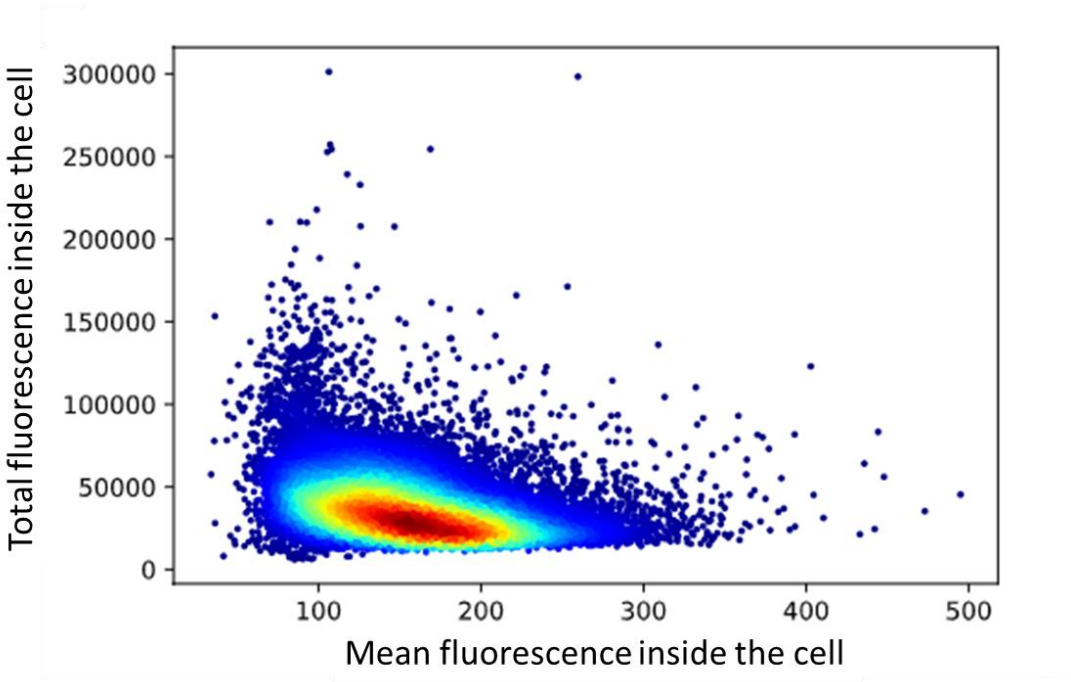

Figure 11.13. Total and mean fluorescence signal of mCherry. Similar to the previous figure for each segmented cell across different conditions its total and the mean fluorescence signal were plotted on the same graph. Compared to the mean fluorescence which is used as a proxy for RNA polymerase concentration, the total fluorescence inside a cell is a proxy for total number of RNA polymerases inside a cell. An inverse relationship between the concentration and total numbers was found. The inverse relationship means bigger cells have more RNA polymerases inside the cell which goes in line with the previous studies.

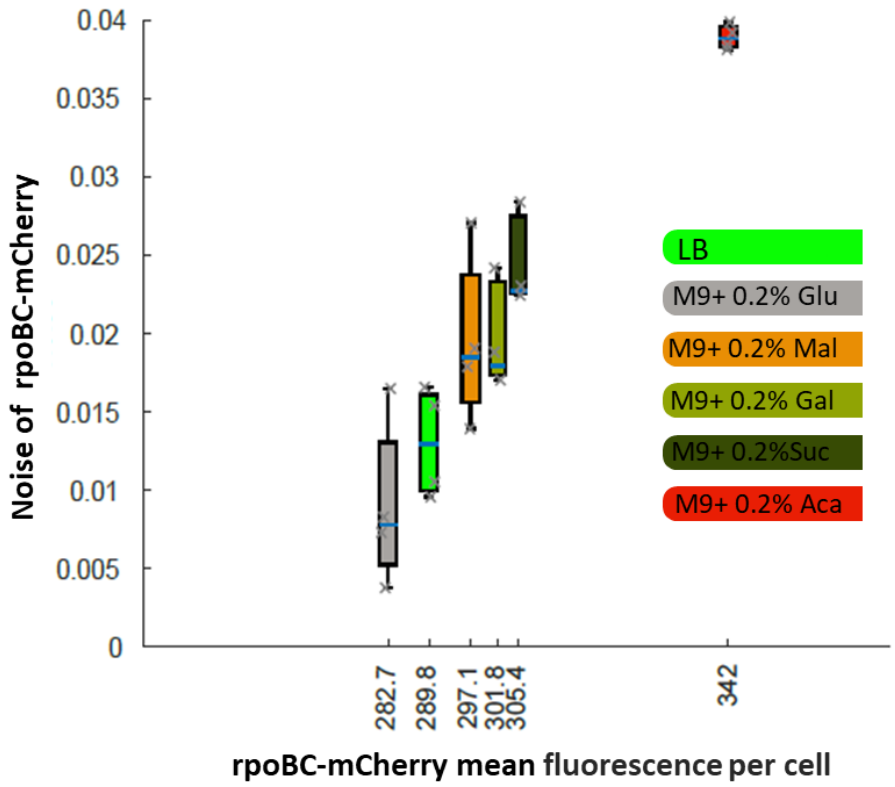

Figure 11.14. Noise of rpoBC-mCherry per different experimental conditions in the function of the mean fluorescence per cell. Biological replicates, mean and standard errors are shown on the graph.

While the increase in total number of RNA polymerases was expected for a carbon richer source, the decrease in its concentration wasn't. With richer carbon source, bacterial RNA polymerase is known to from clusters due to liquid-liquid phase separation. In order to inspect this and to see its relationship with the concentration of RNA polymerase I followed already established protocol to quantify RNA polymerase clustering of *E.coli* in fluorescent images. Clustering data from cells across different conditions were plotted against the corresponding mean fluorescence of mCherry which was used to tag RNA polymerase. To quantify the relationship between noise and clustering, the cells corresponding to a particular level were subsampled. For each subsample the noise was calculated as a ratio between the variance and the mean squared of the subpopulation.

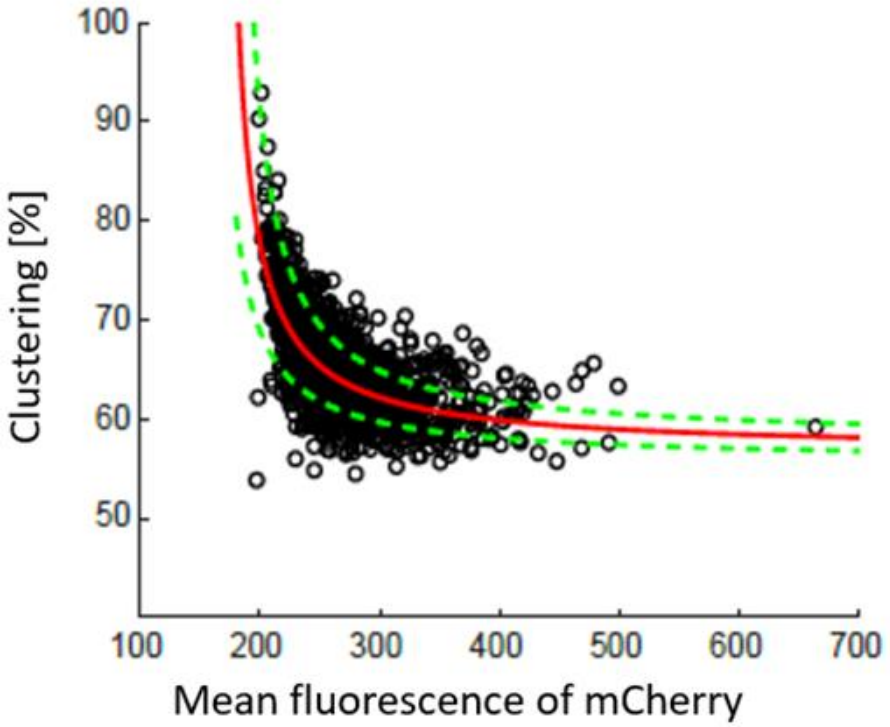

Figure 11.15. Clustering vs. mean fluorescence of mCherry inside the segmented cells. For each segmented cell across different conditions clustering and mean fluorescence of mCherry were plotted on the same graph. Red curve is a nonlinear fit the green curves are 95% confidence intervals. The inverse relationship between the mean fluorescence of mCherry, a proxy for RNA polymerase concentration and its clustering was detected.

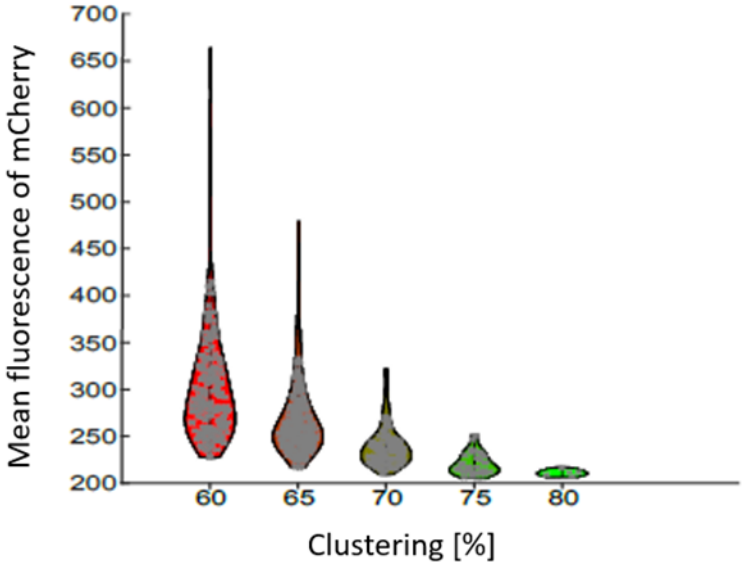

Figure 11.16. Clustering and the distributions of mean fluorescence signals across the segmented cells. For each clustering level of 60%, 65%, 70%, 75%, 80% , mean fluorescence of mCherry were subsampled. For instance for clustering level of 80%, all the segmented cells that were inside the range $80 \pm 0.25\%$ from the figure 11.15 were subsampled and their mean fluorescence distribution was plotted here. This was done in order to connect the clustering with the noise.

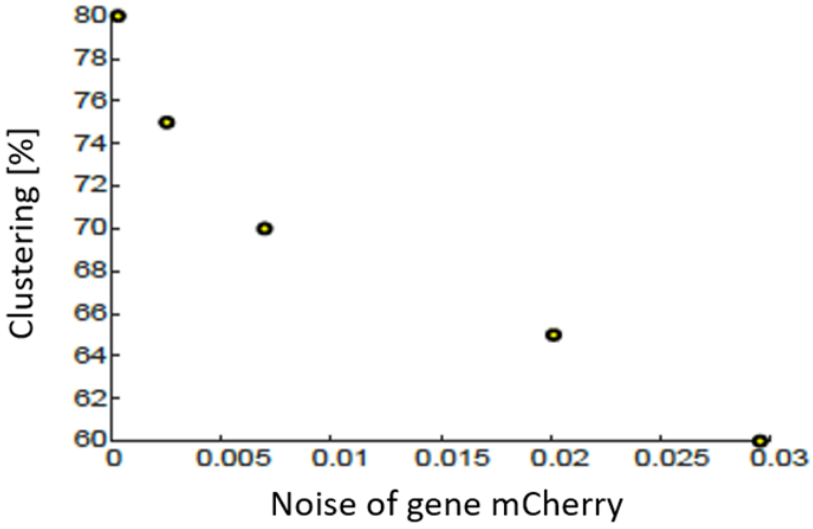

Figure 11.17. Clustering and noise of mean fluorescence signal of mCherry across the segmented cells. If from the previous figure of distributions of mean fluorescence signals across different clustering levels we calculate the noise as variance over mean squared and plot it with an appropriate clustering level we obtain this figure. Clustering increases with the decrease in noise of mCherry.

In conclusion for each segmented cell plotting its mCherry (a proxy for RNA polymerase) concentration and localization revealed a nonlinear inverse relationship. By subsampling the cells at different clustering levels I was able to connect the localization of the mCherry with the noise itself. It was found that with the increase of mCherry localization, the noise in mCherry decreases, providing some support for the theory that the clustering of the RNA polymerase indicated by mCherry readout might have a role its noise reduction.

13 DISCUSSION & PERSPECTIVES

In this thesis I focused on studying the collective growth and the collective dynamics of *E.coli* grown in a microfluidic device and investigating the possibilities to put some of the collective features such as the range expansion under the direct external real time control. Driven by nutrient and chemical gradients the microfluidic device enables the formation of spatially extended biofilm like bacterial community. Although the system lacked some of the phenotypic traits that the cells inside the biofilms have, such as the extracellular matrix production, it did share some of the collective behaviors regarding nutrient consumption, cross-feeding and resilience to environmental insults.

Upon loading the cells inside the chip, bacteria expanded and colonized free space inside the side chambers of the microfluidic chip. Once the whole colony was formed, I observed the formation of quasi-stationary regime and stable velocity profiles alongside the side channel main axis. In established colony we could differ between the nongrowing cells and cells actively engaged in growth. The boundary between the growing cells and the nongrowing layer is determined by available nutrients. Both wild type and IPTG inducible strain used in these studies had same growth and velocity profiles in IPTG nonlimited conditions. Cells actively engaged in growth established a growth gradient with the cells at the front, near the main channel experiencing higher growth rates then the ones deeper within the colony. Since the cells were motionless the only movement inside the side chambers was due to the growth rate. Namely as cells grow they push each other towards the channel opening. Having this in mind, growth rate across the channel could be estimated by differentiation of the velocity profile alongside the main axis of the side chamber. While examining the quasi-stationary response of the system to different media and different IPTG concentrations it was found that the growth rate of the front of the colony near the main channel determines the growing layer of the entire colony. Namely increasing the growth rate of the colony front came at the expense of lowering down the actively growing layer of the colony, or to put it differently the growing area of the colony is inversely proportional to the growth rate. I hypothesize that this happens due to the fact that the fast growing cells behave “selfishly” and take advantage of the supplied nutrients, increasing their growth and consequently leaving less nutrients available for the cells positioned deeper inside the colony. As earlier mentioned this went in line with the study conducted in Jeff Hasty’s team which showed that the growing layer of the colony was inversely proportional with the glucose concentration in the media. Additionally I analyzed the response of the growing layer in 5xLB and LB when depriving the RNA polymerase inducible strain from IPTG. Depriving the IPTG inducible strain of IPTG leads to growth arrest due to it’s inability to synthesize new RNA polymerase. As these cells do not actively divide they utilize the nutrients solely for their basal metabolism. As a consequence this preserves most of the nutrients compared to the cells that aren’t deprived of IPTG. Having this in mind I was expecting that applying more concentrated media would now

lead to the expansion of the growing layer. When examining the growth pattern of IPTG deprived cells in 5xLB and LB media this indeed happened.

Interestingly collective behavior and the dynamical organization of the colony can be determined if we plot the growth rate inferred from the velocity profile at a certain position and its corresponding velocity (figure 12.1). Figure 12.1 shows three velocity profiles which have the same frontal velocity but different spatial organization. Since the growth rate is nothing more then the spatial derivative of the velocity profile, decreasing slope of curve in growth rate-velocity state space indicates decrease in the growth rate of cells near the main channel at the side chamber opening

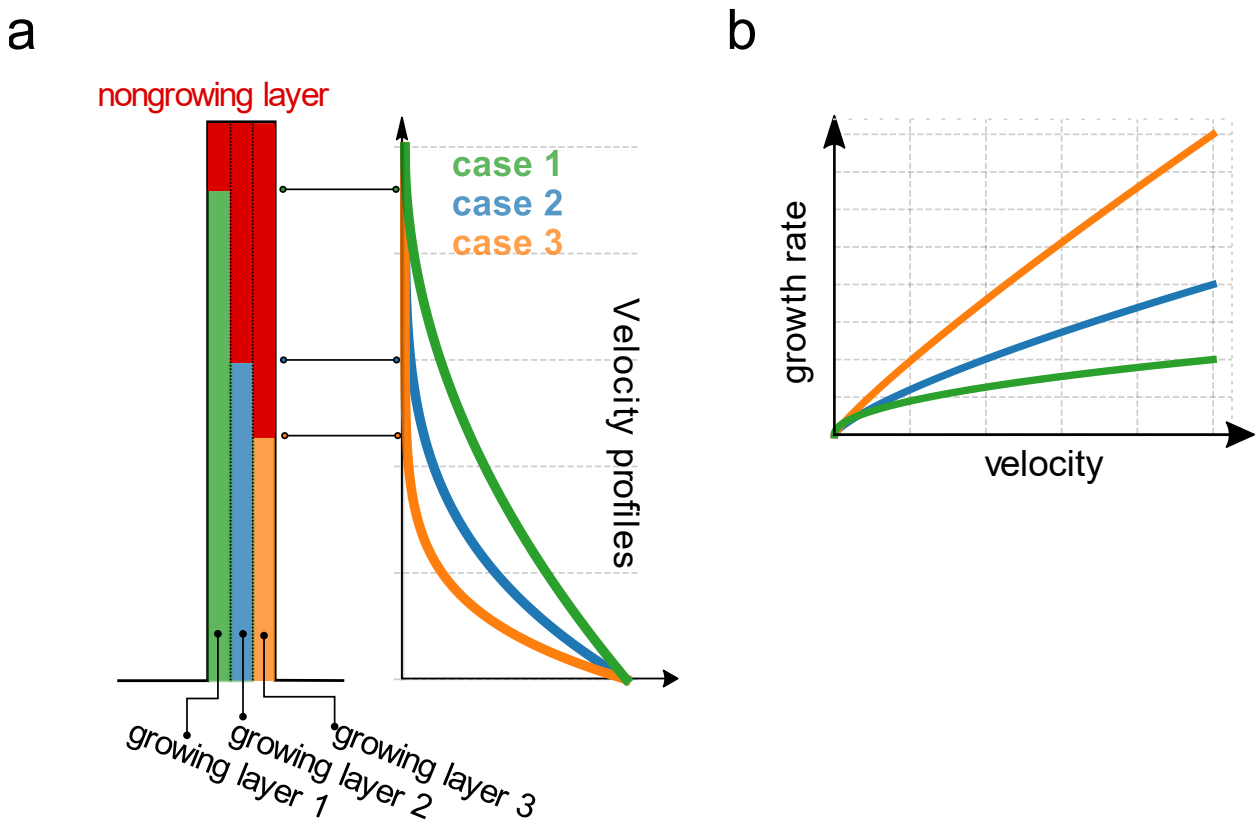

Figure 12.1. Observing the frontal velocity-growth rate space tells us about the spatial patterns of growth within the colony. Increasing slope in growth rate velocity translates to a steeper growth and velocity pattern within the colony.

Changing the IPTG levels in LB media impacted the internal organization and spatial organization of the velocities inside the side chambers, but interestingly when growth rate-velocity profiles were plotted all data collapsed on the same curve. I came to one of the hypothesis why this happens by looking at the open loop experiments where the IPTG was switched during the course of experiment from 1000µM to 0µM. The first change in frontal velocity came almost 4-5h after the change. Furthermore the dynamical range between the maximal speed prior to the switch and the post-change speed was relatively small and it took 24h to reach the new steady state. I

hypothesized that the reason for this time delay and slow dynamics could be found in the nature of system itself. Namely at the time just after the cells were loaded inside the microfluidic device and before the colony was fully formed and the quasi-stationary regime established initial bacterial invasion of the side chambers was ongoing. Cells started from the dead end of the chamber and as they grew and divided the colony front moved towards the main channel. As front moved forward, cells left behind experienced nutrient limitations and eventually complete depletion of nutrients. The growth arrest stopped the dilution and consequently left cells with the high levels of RNA polymerase and other protein expression machinery, obtained from the time when they experienced abundance of nutrients. When the IPTG was removed from the media, cells at the front stopped eventually expressing RNA polymerase and start slowly decreasing their growth, consequently enabling more nutrients to penetrate deeper inside the colony reactivating the growth of the cells which were previously arrested or that were growing more slowly. Once activated they are moving towards the front, pushing away quickly the growth arrested cells. As the IPTG isn't present in the media, the newly activated cells aren't producing new RNA polymerase, but are using their build up reservoir from the slowly growing or growth arrested phase. As no new RNA polymerase is synthesized, the RNA polymerase stock eventually becomes depleted and the growth ceases. This again redistributes the nutrient resources and starts the new iteration of reactivation of the growth arrested cells. Due to relatively slow dynamical processes the colony had the time to readapt and quickly reestablish the new steady sate. This effectively made the colony more resilient to the changes imposed by IPTG switch with the growing layer not experiencing drastic changes throughout the switch. Similar reasoning was used to describe the increase in antibiotic resistance and resilience of the colony after the exposure to the antibiotics of *E.coli* grown in a similar microfluidic device. In here similarly the growth arrest caused by the antibiotics of the front of the colony lead to the redistribution of the resources. Once the resources were redistributed the transient regime passed in which colony reestablished its previous spatial organization. In order to test the resilience of the colony and the potency of using antibiotic for control purposes and I tested the response of the colony on higher concentration of antibiotics. Upon the switch, during the time course of antibiotic the system wasn't able to reestablish its previous state. It was just after the antibiotic was switched off that the colony started to recover. In the same manner as the cells during the antibiotic treatment in the mentioned study, the growth arrest of the cells in the colony front enabled the cells in the back of the colony to reactivated the growth due to the nutrient redistribution. Unlike the reported study my cells remained in that regime during the course of antibiotic treatments. This is due to the much larger concentrations of antibiotics used in my experiments. As mentioned previously the larger concentration were used to probe the potency of using antibiotics for control purposes. The results obtained were promising as the colony readapted to a different state then the initial one compared to the perfect adaption experienced with lower level of antibiotic reported in the study.

Going back to the growth rate-velocity state space relationship the 5xLB media as predicted had a steeper slope compared to the one in LB. Same collapsing pattern happened

while looking at the data coming from multiple experiment with changing glucose concentration in the media, while keeping the IPTG level constant.

For the control part I developed an external feedback loop which tracked the front velocity inside the side channel and which made appropriate changes to the environment to drive system towards a desired state. Front velocity represents the velocity at the chamber opening, near the main channel and it is nothing more then the integration of all the growth rates inside the growing layer. The external feedback loop consisted of a microscope and its components, peristaltic pump, valve and Arduino, all put under the control of a computer and the scrip wrote in MATLAB. The control loop was initially tested on tracking the fluorescein signal inside the main channel. In order to inspect to what extent it could be possible to externally control the invasion speed of *E.coli* I used three different ways to perturb the growth rate along the side channel

- IPTG modulation of the RNA polymerase
- Nutrient perturbation
- Antibiotic induced changes

The first control imposed to the system was the IPTG one. Due to the previously mentioned resilience of the colony to IPTG modulation, slow dynamics and the time delay I opted for bang-bang control, which regularly arises in minimum-time problems due to the maximal control effort applied. For the same reasons that gave rise to the slow dynamics and resilience in an open loop system where IPTG was switched from 1000μM to 0 μM, using the IPTG to dynamically control the invasion speed of the colony was proven to be a difficult task. Once the regulated level was achieved, any other switch of reference the system didn't respond in the time course of an experiment. Interestingly though, for the level at which the system retained its velocity, the growth gradients and thus growth rate-velocity state space showed a totally different pattern then the one in the open loop system. Namely the varying levels of IPTG caused the system to increase the growth rate at the colony front consequently decreasing the growing layer of the colony. Compared to the open loop where cells are experiencing a constant environment in a closed loop environment is constantly perturbed between maximum IPTG concentration and no IPTG at all. Although in a closed loop the velocity was regulated, this regulated quasi-steady state was externally imposed by the user. I hypothesized that one of the reasons why in a constantly perturbed system we do see a change at the level of the growth profiles is due to the fact that the system experiences constantly changing environments. Namely the cells at the colony front don't completely arrest their growth as they do experience the IPTG levels required for sustaining the expression of RNA polymerase, which prevents nutrients to penetrate deeper inside the colony. Cell deeper in the colony sense decreased levels of IPTG therefore decreasing the expression of RNA polymerase and lowering down their growth rate. Unused resources are then picked up by the frontal cells which increase their growth rates. Of course this would only last during the external control, because as soon as the external control and thus environment perturbation would stop, the system would move away from the currently

regulated level and spatial organization towards the ones described previously in the steady state.

As perturbing the growth inside the side channels by modulation of the RNA polymerase level through changing concentration of IPTG in the media has proven to be difficult task I looked for other control modalities. Perturbation of nutrients and modulation of antibiotic level in the media seemed as a logical choice. Unlike the IPTG which directly and in a targeted way impacted the RNA polymerase, both of the proposed modalities impacted on the entire metabolism of the cells. The global rewiring of the cellular biomachinery could potentially perturb enough the system to enable a more dynamical control then the one with IPTG. The same type of bang-bang control was used for comparative reasons.

Nutrient control modality consisted in switching between two nutritiously different media. This control method proved to be more successful then the IPTG one, but it did had some limitations to it. Namely it could only follow slowly changing step references. Furthermore it was much easier to control the system when the reference was above the current measured value of the front velocity then in the case where the reference was bellow. One possible explanation for this behavior could be found if we look at the glycogen storage that happens in E.coli. It is know that when experiencing conditions richer in nutrients, *E.coli* stores excessive energy in the form of glycogen, which is used when the cells experience conditions not favorable for growth.

Similarly to the prior two modalities, the antibiotic modality as well consisted in switching between the two media, one containing the antibiotic and the one without it. Open loop showed excellent dynamical characteristics. The system response was quick and the dynamical range was substantial. Despite this the bang-bang control law exhibited extremely low control performances. Quick response times lead to the abrupt changes in the controlled value and influenced its inability to sustain itself near the reference levels. This indicated that actually due to its fast response time and dynamical range, the bang-bang control isn't a suitable control law when using antibiotic to perturb growth. Other control laws such as PI control law with low values of proportional and integral control could be a potential avenue to explore. What was interesting to see is that during the application of the control effort, when the cells were exposed to the antibiotic we saw an increase in the growing layer. Upon ceasing the control effort and the removal of antibiotic in the media, the growth pattern reestablished to the same ones the culture had prior to the antibiotic treatments. This was observed by examining the velocity at a nongrowing depth and by plotting the frontal velocity and frontal growth in growth-rate velocity state-space. Since the behavior of the colony and the growing layer were determined by the frontal cells, the behavior of the frontal cells describe the evolution of spatial patterns over time. The slope of the curve is seen to decrease upon beginning of the treatment, indicating expansion of the growth layer deeper inside the colony. Increase in the slope was spotted when the antibiotic was removed from the media and while the cells were recovering. This indicates recovery phase which is followed by increase in growth of the frontal cells, redistribution of the nutrients inside the media and lowering down of size the growing layer.

Interestingly inside the growing layer of the microfluidic chip the fluorescence signal coming from the rpoC-mCherry fusion which was used to quantify the of RNA polymerase inside the cells was found to be inversely proportional with the growth rate. The same surprising pattern was found in single cell microscopy measurements where I measured mean fluorescence levels per segmented cell across conditions varying in carbon source. We confirmed that the cells were indeed bigger and had higher total fluorescence indicative of RNA polymerase number at the higher growth rate. We also confirmed that cells growing in a richer carbon source also experienced clustering at higher growth rates. Additionally for each segmented cell I measured mean fluorescence per cell across different conditions and compared it to the corresponding degree of clustering. It was shown before that the clusters are due to liquid to liquid phase separation and that the clusters are dynamic. I suspected a role for RNA polymerase clusters in ensuring low noise levels despite the reduced concentration of RNA polymerase.

The work conducted here shows the power and potential of using microfluidics to study the emergent properties of bacterial collective behavior. It shed a light on how bacterial colonies distribute the resources among themselves and how they organize growth patterns. It also shows the difficulties of manipulating and dynamically controlling the system externally due to its inherent resilience to environmental insults and environmental change. Results obtained here opened many new pathways that I wish I had the time to explore. For instance if we focus on the cybergenetics, we could apply different control laws using antibiotics to manipulate the expansion speed of the colony. Applying antibiotics to the system showed the greatest dynamical range and the fastest system response, making the bang-bang control unsuitable for the control purposes. Furthermore a potential pathway to explore would be to gain a more comprehensive picture of how patterns are developed inside the side channel and to track the pattern establishment by observing the growth rate-velocity state space. Different nutrient limitations such as amino-acid or nitrogen limitation could be imposed to the system. In addition to observing the growth rate and velocity we could tag metabolic proteins with different fluorescent reporters to gain more insight what drives a specific rearrangement of the patterns inside the microfluidic chip. Exploring static environments would be of great interest to gain more insight into how the entire colony responds to a dynamically changing one. Having the comprehensive knowledge of the how the patterns form in real time could open the door to externally modulate the entire formation of the colony growth patterns. As the colony front is major driving force for determining the patterns inside the colony, controlling both the velocity and the growth rate of the colony front could guide the colony through the growth rate-velocity space, having thus the complete control over pattern formation inside.

Regarding the single cell studies and clustering, the work could be further continued by using the nonstandard FACS machine coupled with an 60x objective to image every passing event. The initial images obtained from this machine were promising and are shown in the appendix. To furthermore inspect the relationship between the RNA polymerase clusters and their implication in lowering down the concentration noise one could dissolve the clusters by applying 1,6

hexandiol noise and concentration. As a control, the behavior of the strain with inducible T7 RNA polymerase can be studied as T7 RNA polymerase is not native to E.coli and thus is decoupled from E.coli's metabolism. Since clustering seems to be dependent on the concentration of the RNA polymerase, to further inspect the relationship, a microfluidics device and the external control could be used regulate the RNA polymerase concentration inside the single cells and to observe the development of clusters.

14 APPENDIX

14.1 STRAIN

The strain used in this study were used in [70] to control expression of RNA polymerase inside *E.coli.* Unlike in the eukaryotes, prokaryotes and thus E.coli has only one type of RNA polymerase that is shared limited resource for all of the gene expression machinery in E.coli. As it was stated in xx, it is already established by previous studies that the quantity of $\beta\beta'$ subunits of RNA polymerase sets the global concentration of RNA polymerase inside *E.coli* xxx. The $\beta\beta'$ subunits are a product of rpoBC genes. In order to have the control over the expression of RNA polymerase, the authors have put the rpoBC genes under the control of an IPTG inducible promoter. The provide maximal repression and the minimize the impact of potential mutations the IPTG promoter contained two lacO genes. Furthermore a spectinomycin resistance cassette was positioned upstream. The whole construct was isolated from the influence of the upstream ribosomal proteins rplKAJL by a strong transcriptional terminator placed just after the spectinomycin resistance cassette.

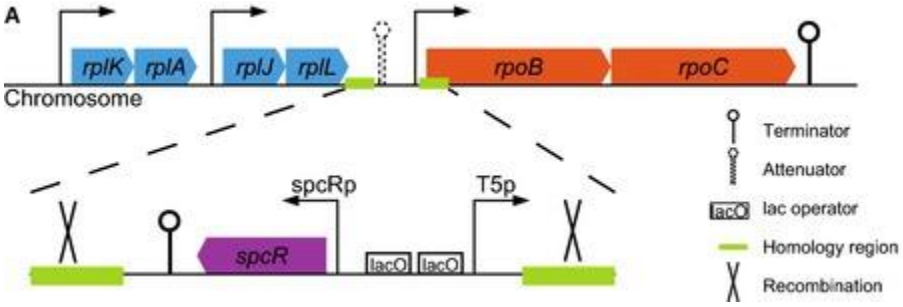

Figure 13.1 Replacement of the rpoBC promoter with an lac one, enabling the IPTG inducible control of RNA polymerase. Figure taken from [70]

In order to quantify the amount of β' subunits rpoC gene was transcriptionally fused the previously mentioned construct with mCherry via the amino acid linked CTAGAATA. This enabled observation of matured mCherry. The IPTG inducible strain was termed PP2 strain while the strain with a native promoter (WT strain with mCherry construct) was termed PP1 stain.

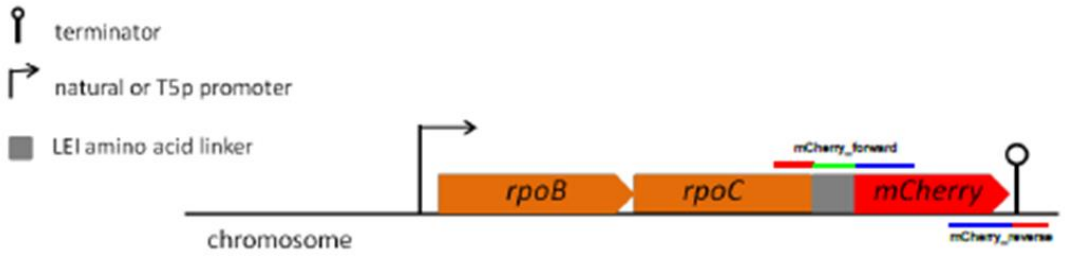

Figure 13.2. rpoBC fused with mCherry. Figure taken from [70]

Maturation of mCherry inside this construct was found by the authors to be dependent on the media and was determined after the addition of chloramphenicol (0.3g/L). Addition of chloramphenicol stops the synthesis of new mCherry molecules, thus the increase in the fluorescence of mCherry is just due to the maturation of the immature mCherry. Cells grown in LB media had the maturation time of 60min, while the ones grown in M9 media supplemented with 0.2% glucose had the maturation time of 85min. The half-life was found to be around 25h.

14.2 Observation of the cells inside the microfluidic device

Microfluidic chip was first casted in polydimethylsiloxane (PDMS). In order to create a microfluidic chip first select and mix PDMS base and the curing agent in ration 10:1 in a plastic dish using a pipet tip. Mix thoroughly. Once the mixture was thoroughly mixed, bubbles should appear. Pour the mixture on the epoxy copy of the microfluidic chip design and place it in a vacuum desiccator to degas the chip. Once all the bubbles are removed ($\sim 30 min$) remove the chip from the vacuum chamber and place it in the oven at 65℃. Baking should take place at least for 2 hours. For *E.coli* colonies the best results were obtained after an overnight bake.

Once the chip was baked it could be removed from the epoxy wafer. Cut the PDMS around the patterns and peel off the chip. Carefully punch the holes at the inlet and an outlets of the chip. Upon punching clean the PDMS patter using a regular tape to remove the dust. Take the cover glass, clean it with a gas duster and place it with the punched microfluidic chip inside a plasma cleaner. The tape cleaned PDMS pattern of the chip should be placed upwards throughout the procedure. Once placed inside the plasma cleaner, turn on the vacuum pump, set the power of the plasma cleaner to high and ignite the plasma. Once the violet plasma is spotted, wait for 1min10sec to turn off the plasma cleaner and remove the chip and the cover glass outside the plasma cleaner. Quickly but gently place the chip with the PDMS patter on the glass cover slide. Carefully and gently press the chip and leave it to bake in the laboratory oven at 65℃ for minimum for 2h or for overnight.

Once the baking is done, remove the chip from the oven, leave it on the room temperature and let it cool down (for about 5min) prior to pluronic treatment. The passivation of the surfaces inside the microfluidic chip with pluronic F127 is crucial as it prevents the bubbles from sticking on inside the channel and blocking the flow. For pluronic treatment use distilled water supplemented with 5g/L pluronic and insert it through the input of the microfluidic device using a syringe/pipette. Incubate the chip at room temperature for 30min at room temperature. Once incubation process is done, the chip is ready to be loaded with bacteria.

For loading the cells, prior to making the chip, pick a single colony from a plate of E.coli culture and grow in 5ml LB media overnight in a 37℃ shaking incubator. In the morning at the day of the experiments dilute the overnight culture 1:100 in the appropriate culture media and leave them to grow to mid exponential phase. Once the diluted culture reaches the mid exponential phase. Centrifuge the 5ml culture at high speed (7000rpm) for 5min and resuspend the pellet in 100μL of fresh media. Before loading the cell inside the chip with syringe, it is crucial to first pour a drop of liquid on the inlet where the cells are going to be injected as it prevents the bubbles to get inside the chip. Once the cells have been loaded, tape the chip into a centrifuge so that the side chambers are put in the opposite direction then the direction towards the center of the centrifuge. Centrifuge for 10min at 2500rpm to assist the cells to enter the side chambers. Once loading is done, flush the remaining cells in the side channel and connect the inlet and the outlet of the chip to the media and waste. To be sure that all the excess cells and potential bubbles are removed from the main channel, set the flow on maximum speed for about 5-10min and then set the flow to be constant at 5μL/min.

The cells were observed under the 10x magnification over long periods of time. Throughout the experiment the temperature of the microscopic chamber was maintained at 37℃. μManager was used for time-lapse acquisition [132]. Commands to the μManager, the real time control and actuation of the microfluidic valves and peristaltic pump was performed in MATLAB. For online PIV analysis, MATLAB openPIV version was used[135]. Offline PIV analysis was performed by FIJI [169]and ImageJ[170] plugin PIVanalyzer[133]. For one of the experiments a spatial drift was spotted. For the correction of the manual drift for that particular experiment a FIJI plugin was used[171].

14.3 RECIPE FOR M9 MEDIA

Composition for M9+0.4% glycerol media is shown at the table bellow. Instead of glycerol any other carbon source can be used. The detailed protocol for M9 media can be found at [172].

quantity	chemical	sterilization	storage
40ml	5xM9 minimal salts	autoclave to sterilize	4°C
6.8ml	10mg/ml thiamine hydrochloride	filter sterilize (0.22µM)	prepare fresh
2ml	40 % glycerol (or any other carbon source)	autoclave to sterilize	4°C
4ml	10% casamino acids	filter sterilize (0.22µM)	4°C
400µL	1M MgSO4	autoclave to sterilize	4°C
20µL	1M CaCl2	autoclave to sterilize	4°C
Fill to 200ml	Sterelized H2O	autoclave to sterilize	4°C

14.4 CONTROL LAWS AND WHY TIME DELAY REPRESENT A STABILITY PROBLEM

After monitoring the maximum detected speed inside the side channel this information is compared to the desired value. The difference between these two is then given to the controller which determines the appropriate control effort that needs to be taken so that the current value reaches the desired one. Closing the feedback changes the dynamical properties of the open loop system, thus before applying/designing a certain control, we need to take into the account the dynamics of the open loop system. Since the initial plan was to use IPTG to control the velocity the main designing efforts were made considering the IPTG response of the system. From the open loop dynamics of the IPTG switch experiment big time delay between the input and the output of the system was observed. System with huge time delays are notoriously difficult to control as they are prone to instability when closing the loop, but why is this and where does it come from?

The best way to illustrate the destructive effect of the time delay on the closed loop characteristics of the system is to look at the behavior in complex s-domain. The switch to this domain happens after applying Laplace transform. In here I would try to avoid as much as possible mathematical notations and derivation and will use them only when necessary. Laplace transform is a integral transform defined as:

$$\mathcal{L}[f(t)] = F(s) = \int_0^{\infty} f(t)e^{-st}dt$$

Where

-s is a complex variable with real and imaginary part $s = \sigma + j\omega$

- $f(t)$ is a function in time domain such as $f(t) = 0$ for $t \leq 0$

- $F(s)$ is a Laplace transform of $f(t)$

For instance if we look at the exponential signal in the form of:

$$f(t) = \begin{cases} 0 & when\ t < 0 \\ Ae^{-\alpha t} & when\ t \geq 0 \end{cases}$$

Its Laplace transform would look like

$$F(s) = \int_0^\infty Ae^{-\alpha t}e^{-st}dt$$

$$F(s) = \int_0^\infty Ae^{-(s+\alpha)t}dt$$

$$F(s) = \frac{1}{s+\alpha}$$

Plotting this signal on the s-domain graph, where x axis represents real axis while y axis imaginary ones gives

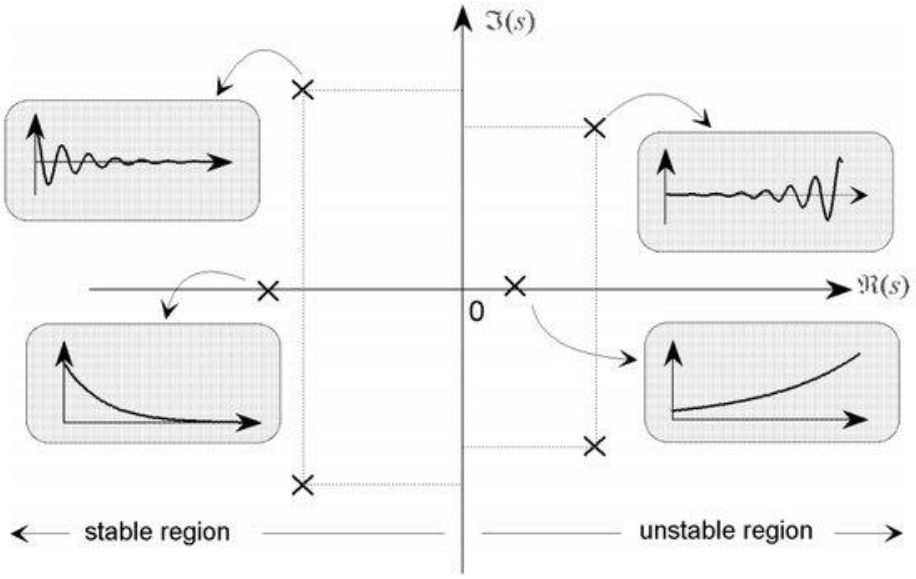

Figure 13.3. **Zeros od denominator in complex plain and behavior of the signals**. In here *x* axis is representing real numbers while *y* axis represents the imaginary axis. Positions of the zeros of the denominator determine the stability of the signal. Signals are stable if and only if the zeros are position in the left part of the complex plane (negative part of the *x* axis). When zeros are positioned on the imaginary axis itself signal is oscillatory. Figure taken from [173]

Position of the zeros of the denominator impact the stability. Negative side of the real axis gives stable signals, while the right, positive side yields unstable ones. If denominator zeros are positioned on the imaginary axis itself, signals are oscillatory.

The real beauty of Laplace transform comes when we look at the differential equations. For instance let us imagine a simple system described by a differential equation:

$$\frac{dy(t)}{dt} + Ay(t) = Bx(t)$$

Where $A, B = const > 0$

Laplace transform of that differential equation yields an algebraic equation.

$$sY(s) + AY(s) = BX(s)$$

Relationship between input and output is called a transfer function and it is describing how a system changes given the input.

$$G(s) = \frac{Y(s)}{X(s)} = \frac{B}{s + A}$$

a

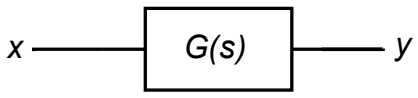

b

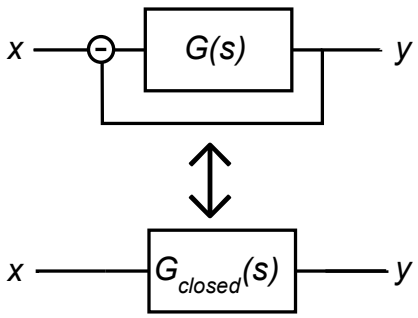

$$G_{CLOSED}(s) = \frac{G(s)}{1 + G(s)}$$

Figure 13.4. Closing the loop. a) Open loop system and transfer function which describes the behavior of the system b) Closing the loop with a simple negative feedback. Input to the system $G(s)$ is now the difference between the input and the output. Transfer function of such a system is given with $G_{CLOSED}(s)$

Closing the loop with a simple negative feedback changes the system dynamics in such way that:

$$G_{CLOSED}(s) = \frac{G(s)}{1 + G(s)}$$

What happens when we have a time delay in our system? Time delay T in s domain is defined as e^{-sT} and a system described by transfer function $G(s)$ that experiences the same time delay can be written as $G(s)e^{-sT}$. Time delay in s domain can be approximated by Pade approximation[174], which for smaller time delays can be written as

$$e^{-sT} \approx \frac{2 - sT}{2 + sT}$$

When we look at the closed loop system transfer function we get:

$$G_{closed}(s) = \frac{\frac{B}{s+A}\left(\frac{2-Ts}{2+Ts}\right)}{1 + \frac{B}{s+A}\left(\frac{2-Ts}{2+Ts}\right)}$$

By rearranging the previous expression:

$$G_{closed}(s) = \frac{B(2 - Ts)}{Ts^2 + s(AT - 2BT + 2) + 2B + 2A}$$

As we saw earlier a lot is told by looking at the zeros of the denominator. In the previous equation denominator is

$$Ts^2 + s(AT - 2BT + 2) + 2B + 2A$$

The solution of this equation gives us information about the system dynamics. For systems to be stable it needs to have real parts of this equation in the right plane of the s-domain. For it to be

so, for the case of second order system all coefficients should be the same sign, which translates to:

$$T < \frac{2}{2B - A}$$

Thus time delay needs to be less then $\frac{2}{2B-A}$ for system to be stable. We can see that for some values of the time delay this won't be true and the denominator will yield zeros in the positive part of the real part of the complex plane triggering instability. Having in mind that this is the simplest case where we just closed the loop with a simple proportional controller (K=-1), adding additional control components would just add on the complexity with no guarantees that we will be able to control the system. Even though the PI control was incorporated in the control platform it wasn't used on biological experiments for the reasons that would be explained later in the text. For biological experiments bang-bang control was used. In addition of not needing any extra parameters, it enabled the fastest response of the system, as it will apply immediately the maximal control effort. It worth mentioning that there exist a way to combat the time delay but this requires an accurate representation of the model and its uncertainties and again doesn't offer the guarantees of success.

14.5 SINGLE CELL DATA FROM SINGLE EVENTS OBTAINED FROM FLOW CYTOMETER COUPLED WITH A 60X MICROSCOPE

Ch01 BF – Channel 1, the brightfield channel

Ch04 mCherry – Channel 4, mCherry channel (RNA polymerase)

Ch06 – Channel 6, Side scatter signal

Ch07- Channel 7, Hoechst dye (DNA dye)

Ch09 – Channel 9, bright field channel.

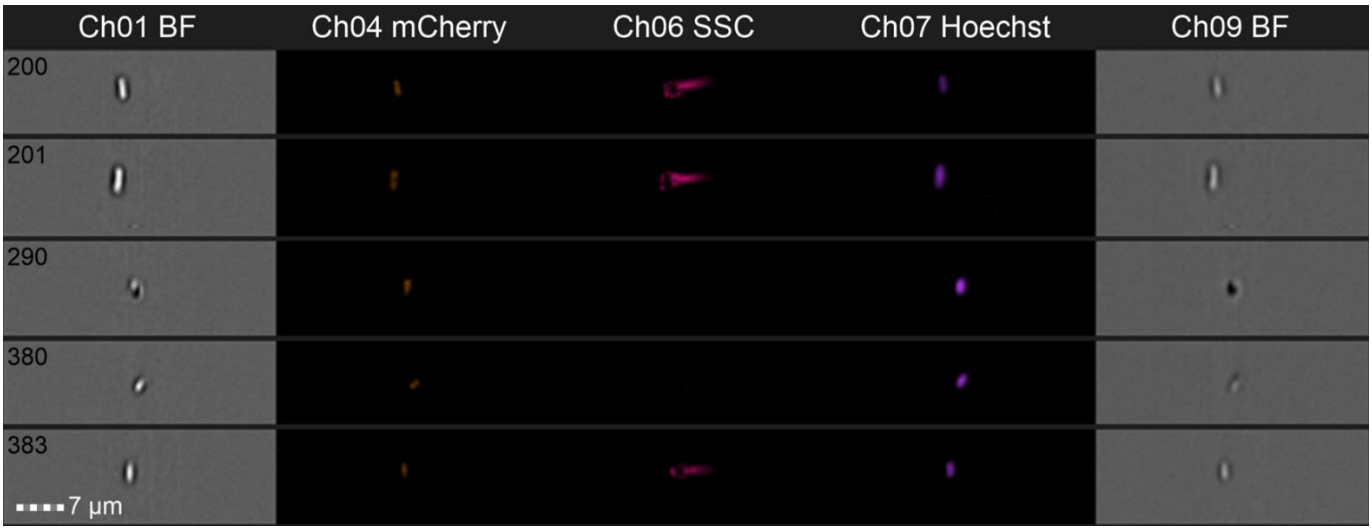
Ch01 BF
Ch04 mCherry
Ch06 SSC
Ch07 Hoechst
Ch09 BF
200
201
290
380
383
7 µm

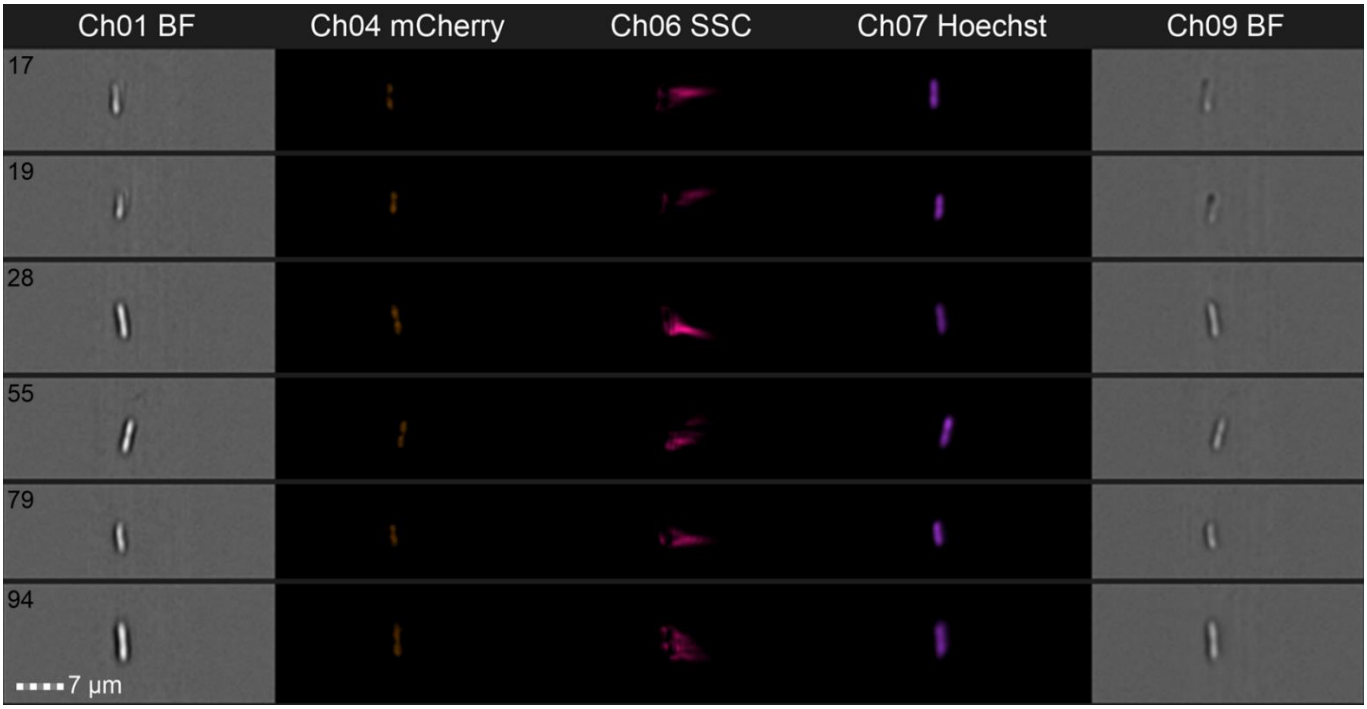
Ch01 BF
Ch04 mCherry
Ch06 SSC
Ch07 Hoechst
Ch09 BF
17
19
28
55
79
94
7 µm

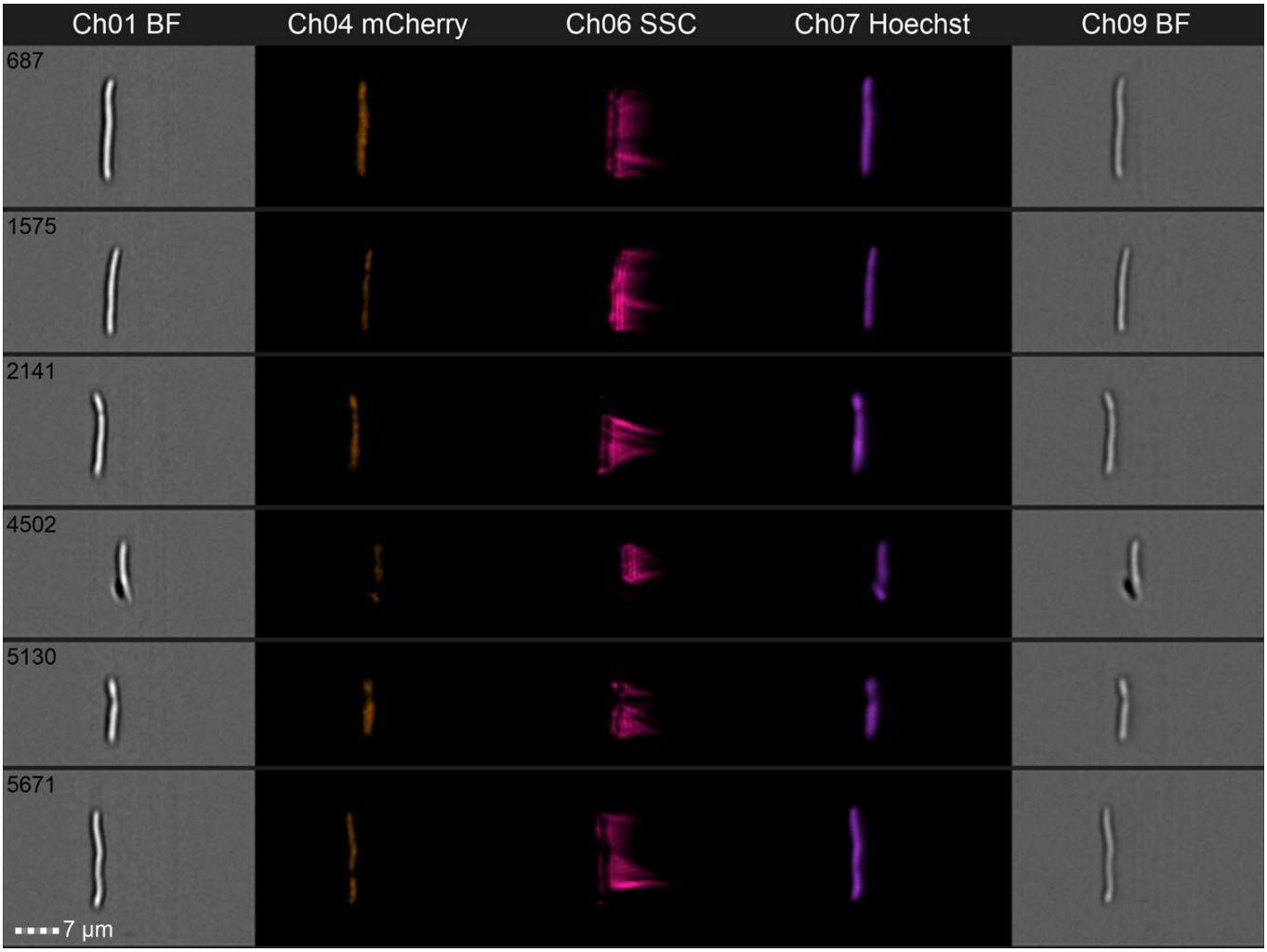
Ch01 BF
Ch04 mCherry
Ch06 SSC
Ch07 Hoechst
Ch09 BF
687
1575
2141
4502
5130
5671
7 µm

15 REFERENCES

[1] N. Wiener, *Cybernetics Or Control and Communication in the Animal and the Machine*. MIT Press, 1961.

[2] W. Self, "Rise of the robots: I feedback, therefore I am," *Prospect Magazine*, Sep. 14, 2016. https://www.prospectmagazine.co.uk/magazine/i-feedback-therefore-i-am-cybernetics-robots-technology (accessed Nov. 10, 2022).

[3] J. H. Koschwanez, K. R. Foster, and A. W. Murray, "Improved use of a public good selects for the evolution of undifferentiated multicellularity," *eLife*, vol. 2, p. e00367, Apr. 2013, doi: 10.7554/eLife.00367.

[4] M. A. Nowak, "Five rules for the evolution of cooperation," *Science*, vol. 314, no. 5805, pp. 1560–1563, Dec. 2006, doi: 10.1126/science.1133755.

[5] J. H. Koschwanez, K. R. Foster, and A. W. Murray, "Sucrose Utilization in Budding Yeast as a Model for the Origin of Undifferentiated Multicellularity," *PLoS Biol*, vol. 9, no. 8, p. e1001122, Aug. 2011, doi: 10.1371/journal.pbio.1001122.

[6] M. A. Brockhurst, A. Buckling, and A. Gardner, "Cooperation Peaks at Intermediate Disturbance," *Current Biology*, vol. 17, no. 9, pp. 761–765, May 2007, doi: 10.1016/j.cub.2007.02.057.

[7] H.-C. Flemming and S. Wuertz, "Bacteria and archaea on Earth and their abundance in biofilms," *Nat Rev Microbiol*, vol. 17, no. 4, pp. 247–260, Apr. 2019, doi: 10.1038/s41579-019-0158-9.

[8] M. Thattai and A. van Oudenaarden, "Stochastic Gene Expression in Fluctuating Environments," *Genetics*, vol. 167, no. 1, pp. 523–530, May 2004, doi: 10.1534/genetics.167.1.523.

[9] A. Dal Co, M. Ackermann, and S. van Vliet, "Metabolic activity affects the response of single cells to a nutrient switch in structured populations," *J. R. Soc. Interface.*, vol. 16, no. 156, p. 20190182, Jul. 2019, doi: 10.1098/rsif.2019.0182.

[10] A. D. Co, S. van Vliet, and M. Ackermann, "Emergent microscale gradients give rise to metabolic cross-feeding and antibiotic tolerance in clonal bacterial populations," p. 10.

[11] J. A. Cole, L. Kohler, J. Hedhli, and Z. Luthey-Schulten, "Spatially-resolved metabolic cooperativity within dense bacterial colonies," *BMC Systems Biology*, vol. 9, no. 1, p. 15, Mar. 2015, doi: 10.1186/s12918-015-0155-1.

[12] E. Wolfsberg, C. P. Long, and M. R. Antoniewicz, "Metabolism in dense microbial colonies: 13C metabolic flux analysis of E. coli grown on agar identifies two distinct cell populations with acetate cross-feeding," *Metabolic Engineering*, vol. 49, pp. 242–247, Sep. 2018, doi: 10.1016/j.ymben.2018.08.013.

[13] A. Dal Co, S. van Vliet, and M. Ackermann, "Emergent microscale gradients give rise to metabolic cross-feeding and antibiotic tolerance in clonal bacterial populations," *Philosophical Transactions of the Royal Society B: Biological Sciences*, vol. 374, no. 1786, p. 20190080, Nov. 2019, doi: 10.1098/rstb.2019.0080.

[14] J. Liu *et al.*, "Metabolic co-dependence gives rise to collective oscillations within biofilms," *Nature*, vol. 523, no. 7562, pp. 550–554, Jul. 2015, doi: 10.1038/nature14660.

[15] A. Prindle, J. Liu, M. Asally, S. Ly, J. Garcia-Ojalvo, and G. M. Süel, "Ion channels enable electrical communication in bacterial communities," *Nature*, vol. 527, no. 7576, pp. 59–63, Nov. 2015, doi: 10.1038/nature15709.

[16] Y.-C. Lin, W. C. Cornell, J. Jo, A. Price-Whelan, and L. E. P. Dietrich, "The Pseudomonas aeruginosa Complement of Lactate Dehydrogenases Enables Use of d- and l-Lactate and Metabolic Cross-Feeding," *mBio*, vol. 9, no. 5, pp. e00961-18, Sep. 2018, doi: 10.1128/mBio.00961-18.

[17] H.-K. Yum, I.-N. Park, B.-M. Shin, and S.-J. Choi, “Recurrent Pseudomonas aeruginosa Infection in Chronic Lung Diseases: Relapse or Reinfection?,” *Tuberc Respir Dis (Seoul)*, vol. 77, no. 4, pp. 172–177, Oct. 2014, doi: 10.4046/trd.2014.77.4.172.
[18] D. Worlitzsch, K. C. Meyer, and G. Döring, “Lactate Levels in Airways of Patients with Cystic Fibrosis and Idiopathic Pulmonary Fibrosis,” *Am J Respir Crit Care Med*, vol. 188, no. 1, pp. 111–111, Jul. 2013, doi: 10.1164/rccm.201211-2042LE.
[19] T. Bensel *et al.*, “Lactate in cystic fibrosis sputum,” *J Cyst Fibros*, vol. 10, no. 1, pp. 37–44, Jan. 2011, doi: 10.1016/j.jcf.2010.09.004.
[20] A. J. Moorcroft, M. E. Dodd, J. Morris, and A. K. Webb, “Symptoms, lactate and exercise limitation at peak cycle ergometry in adults with cystic fibrosis,” *European Respiratory Journal*, vol. 25, no. 6, pp. 1050–1056, Jun. 2005, doi: 10.1183/09031936.05.00011404.
[21] K. T. Schiessl *et al.*, “Phenazine production promotes antibiotic tolerance and metabolic heterogeneity in Pseudomonas aeruginosa biofilms,” *Nat Commun*, vol. 10, no. 1, p. 762, Dec. 2019, doi: 10.1038/s41467-019-08733-w.
[22] H. Sakhtah *et al.*, “The Pseudomonas aeruginosa efflux pump MexGHI-OpmD transports a natural phenazine that controls gene expression and biofilm development,” *Proceedings of the National Academy of Sciences*, vol. 113, no. 25, pp. E3538–E3547, Jun. 2016, doi: 10.1073/pnas.1600424113.
[23] D. Vordermark, T. Shibata, and J. M. Brown, “Green fluorescent protein is a suitable reporter of tumor hypoxia despite an oxygen requirement for chromophore formation,” *Neoplasia*, vol. 3, no. 6, pp. 527–534, 2001, doi: 10.1038/sj.neo.7900192.
[24] L. E. P. Dietrich, C. Okegbe, A. Price-Whelan, H. Sakhtah, R. C. Hunter, and D. K. Newman, “Bacterial Community Morphogenesis Is Intimately Linked to the Intracellular Redox State,” *J Bacteriol*, vol. 195, no. 7, pp. 1371–1380, Apr. 2013, doi: 10.1128/JB.02273-12.
[25] Z. S. Marinkovic *et al.*, “A microfluidic device for inferring metabolic landscapes in yeast monolayer colonies,” *eLife*, vol. 8, p. e47951, doi: 10.7554/eLife.47951.
[26] V. Sourjik, “Receptor clustering and signal processing in E. coli chemotaxis,” *Trends Microbiol*, vol. 12, no. 12, pp. 569–576, Dec. 2004, doi: 10.1016/j.tim.2004.10.003.
[27] J. M. Keegstra, F. Carrara, and R. Stocker, “The ecological roles of bacterial chemotaxis,” *Nat Rev Microbiol*, Mar. 2022, doi: 10.1038/s41579-022-00709-w.
[28] X. Zhang *et al.*, “Escape band in *Escherichia coli* chemotaxis in opposing attractant and nutrient gradients,” *Proc. Natl. Acad. Sci. U.S.A.*, vol. 116, no. 6, pp. 2253–2258, Feb. 2019, doi: 10.1073/pnas.1808200116.
[29] B. Ni, R. Colin, H. Link, R. G. Endres, and V. Sourjik, “Growth-rate dependent resource investment in bacterial motile behavior quantitatively follows potential benefit of chemotaxis,” *Proceedings of the National Academy of Sciences*, vol. 117, no. 1, pp. 595–601, Jan. 2020, doi: 10.1073/pnas.1910849117.
[30] J. Cremer, T. Honda, Y. Tang, J. Wong-Ng, M. Vergassola, and T. Hwa, “Chemotaxis as a navigation strategy to boost range expansion,” *Nature*, vol. 575, no. 7784, pp. 658–663, Nov. 2019, doi: 10.1038/s41586-019-1733-y.
[31] M. Deforet, C. Carmona-Fontaine, K. S. Korolev, and J. B. Xavier, “Evolution at the Edge of Expanding Populations,” *The American Naturalist*, vol. 194, no. 3, pp. 291–305, Sep. 2019, doi: 10.1086/704594.
[32] U. of C.-S. Diego, “Quantitative biology opens trail to ecological exploration, evolutionary prediction.” https://phys.org/news/2019-11-quantitative-biology-trail-ecological-exploration.html (accessed Nov. 10, 2022).

[33] M. Klausen, A. Aaes-Jørgensen, S. Molin, and T. Tolker-Nielsen, “Involvement of bacterial migration in the development of complex multicellular structures in Pseudomonas aeruginosa biofilms,” *Molecular Microbiology*, vol. 50, no. 1, pp. 61–68, 2003, doi: 10.1046/j.1365-2958.2003.03677.x.
[34] G. Keller, “Embryonic stem cell differentiation: emergence of a new era in biology and medicine,” *Genes Dev*, vol. 19, no. 10, pp. 1129–1155, May 2005, doi: 10.1101/gad.1303605.
[35] K. W. Rogers and A. F. Schier, “Morphogen gradients: from generation to interpretation,” *Annu Rev Cell Dev Biol*, vol. 27, pp. 377–407, 2011, doi: 10.1146/annurev-cellbio-092910-154148.
[36] M. Kerszberg and L. Wolpert, “Specifying Positional Information in the Embryo: Looking Beyond Morphogens,” *Cell*, vol. 130, no. 2, pp. 205–209, Jul. 2007, doi: 10.1016/j.cell.2007.06.038.
[37] B. Houchmandzadeh, E. Wieschaus, and S. Leibler, “Establishment of developmental precision and proportions in the early Drosophila embryo,” *Nature*, vol. 415, no. 6873, pp. 798–802, Feb. 2002, doi: 10.1038/415798a.
[38] C. W. Kwan, J. Gavin-Smyth, E. L. Ferguson, and U. Schmidt-Ott, “Functional evolution of a morphogenetic gradient,” *eLife*, vol. 5, p. e20894, Dec. 2016, doi: 10.7554/eLife.20894.
[39] M. Christofidou-Solomidou and T. J. Goodwin, *Oxidative Stress and Space Biology An Organ-Based Approach*. MDPI, 2018.
[40] P. Sonveaux *et al.*, “Targeting lactate-fueled respiration selectively kills hypoxic tumor cells in mice,” *J Clin Invest*, vol. 118, no. 12, pp. 3930–3942, Dec. 2008, doi: 10.1172/JCI36843.
[41] I. Marchiq and J. Pouysségur, “Hypoxia, cancer metabolism and the therapeutic benefit of targeting lactate/H+ symporters,” *J Mol Med (Berl)*, vol. 94, pp. 155–171, 2016, doi: 10.1007/s00109-015-1307-x.
[42] S. Walenta and W. F. Mueller-Klieser, “Lactate: mirror and motor of tumor malignancy,” *Semin Radiat Oncol*, vol. 14, no. 3, pp. 267–274, Jul. 2004, doi: 10.1016/j.semradonc.2004.04.004.
[43] D. Hanahan and R. A. Weinberg, “Hallmarks of cancer: the next generation,” *Cell*, vol. 144, no. 5, pp. 646–674, Mar. 2011, doi: 10.1016/j.cell.2011.02.013.
[44] F. Hirschhaeuser, U. G. A. Sattler, and W. Mueller-Klieser, “Lactate: a metabolic key player in cancer,” *Cancer Res*, vol. 71, no. 22, pp. 6921–6925, Nov. 2011, doi: 10.1158/0008-5472.CAN-11-1457.
[45] K. G. de la Cruz-López, L. J. Castro-Muñoz, D. O. Reyes-Hernández, A. García-Carrancá, and J. Manzo-Merino, “Lactate in the Regulation of Tumor Microenvironment and Therapeutic Approaches,” *Front Oncol*, vol. 9, p. 1143, Nov. 2019, doi: 10.3389/fonc.2019.01143.
[46] Y. Chen, R. Cairns, I. Papandreou, A. Koong, and N. C. Denko, “Oxygen Consumption Can Regulate the Growth of Tumors, a New Perspective on the Warburg Effect,” *PLoS One*, vol. 4, no. 9, p. e7033, Sep. 2009, doi: 10.1371/journal.pone.0007033.
[47] C. Dunnill *et al.*, “Reactive oxygen species (ROS) and wound healing: the functional role of ROS and emerging ROS-modulating technologies for augmentation of the healing process,” *Int Wound J*, vol. 14, no. 1, pp. 89–96, Dec. 2015, doi: 10.1111/iwj.12557.
[48] P. Niethammer, C. Grabher, A. T. Look, and T. J. Mitchison, “A tissue-scale gradient of hydrogen peroxide mediates rapid wound detection in zebrafish,” *Nature*, vol. 459, no. 7249, pp. 996–999, Jun. 2009, doi: 10.1038/nature08119.
[49] G. Velve-Casquillas, M. Le Berre, M. Piel, and P. T. Tran, “Microfluidic tools for cell biological research,” *Nano Today*, vol. 5, no. 1, pp. 28–47, Feb. 2010, doi: 10.1016/j.nantod.2009.12.001.
[50] S. Bakshi, E. Leoncini, C. Baker, S. Cañas, B. Okumus, and J. Paulsson, *Dynamic Regulation of Growth and Physiology of Microbes under Complex Changing Conditions*. 2020. doi: 10.1101/2020.03.27.006403.
[51] P. Wang *et al.*, “Robust growth of Escherichia coli,” *Curr Biol*, vol. 20, no. 12, pp. 1099–1103, Jun. 2010, doi: 10.1016/j.cub.2010.04.045.

[52] M. Kaiser *et al.*, “Monitoring single-cell gene regulation under dynamically controllable conditions with integrated microfluidics and software,” *Nat Commun*, vol. 9, no. 1, Art. no. 1, Jan. 2018, doi: 10.1038/s41467-017-02505-0.
[53] S. Jaramillo-Riveri, J. Broughton, A. McVey, T. Pilizota, M. Scott, and M. El Karoui, “Growth-dependent heterogeneity in the DNA damage response in Escherichia coli,” *Molecular Systems Biology*, vol. 18, no. 5, p. e10441, May 2022, doi: 10.15252/msb.202110441.
[54] N. M. V. Sampaio, C. M. Blassick, V. Andreani, J.-B. Lugagne, and M. J. Dunlop, “Dynamic gene expression and growth underlie cell-to-cell heterogeneity in Escherichia coli stress response,” *Proceedings of the National Academy of Sciences*, vol. 119, no. 14, p. e2115032119, Apr. 2022, doi: 10.1073/pnas.2115032119.
[55] L. Potvin-Trottier, S. Luro, and J. Paulsson, “Microfluidics and single-cell microscopy to study stochastic processes in bacteria,” *Curr Opin Microbiol*, vol. 43, pp. 186–192, Jun. 2018, doi: 10.1016/j.mib.2017.12.004.
[56] “The Green Mother Machine: a microfluidics device for cyanobacteria,” *Biomaker.org*. https://www.biomaker.org/projects/the-green-mother-machine-a-microfluidics-device-for-cyanobacteria (accessed Nov. 10, 2022).
[57] D. Volfson, S. Cookson, J. Hasty, and L. S. Tsimring, “Biomechanical ordering of dense cell populations,” *Proceedings of the National Academy of Sciences*, vol. 105, no. 40, pp. 15346–15351, Oct. 2008, doi: 10.1073/pnas.0706805105.
[58] M. Stevanovic, T. Boukéké-Lesplulier, L. Hupe, J. Hasty, P. Bittihn, and D. Schultz, “Nutrient gradients mediate creation of highly resistant layers in structured microbial populations during antibiotic exposures,” Microbiology, preprint, Feb. 2022. doi: 10.1101/2022.02.02.478895.
[59] A. K. Wessel *et al.*, “Oxygen Limitation within a Bacterial Aggregate,” *mBio*, vol. 5, no. 2, pp. e00992-14, May 2014, doi: 10.1128/mBio.00992-14.
[60] P. Bittihn, A. Didovyk, L. S. Tsimring, and J. Hasty, “Genetically engineered control of phenotypic structure in microbial colonies,” *Nat Microbiol*, vol. 5, no. 5, pp. 697–705, May 2020, doi: 10.1038/s41564-020-0686-0.
[61] P. Bittihn, A. Didovyk, L. S. Tsimring, and J. Hasty, “Genetically engineered control of phenotypic structure in microbial colonies,” *Nat Microbiol*, vol. 5, no. 5, pp. 697–705, May 2020, doi: 10.1038/s41564-020-0686-0.
[62] R. Hornung, A. Grünberger, C. Westerwalbesloh, D. Kohlheyer, G. Gompper, and J. Elgeti, “Quantitative modelling of nutrient-limited growth of bacterial colonies in microfluidic cultivation,” *J. R. Soc. Interface.*, vol. 15, no. 139, p. 20170713, Feb. 2018, doi: 10.1098/rsif.2017.0713.
[63] V. Venturi, “Control of rpoS transcription in Escherichia coli and Pseudomonas: why so different?,” *Molecular Microbiology*, vol. 49, no. 1, pp. 1–9, 2003, doi: 10.1046/j.1365-2958.2003.03547.x.
[64] K. Martínez-Gómez *et al.*, “New insights into Escherichia coli metabolism: carbon scavenging, acetate metabolism and carbon recycling responses during growth on glycerol,” *Microb Cell Fact*, vol. 11, no. 1, p. 46, Dec. 2012, doi: 10.1186/1475-2859-11-46.
[65] J. Izard *et al.*, “A synthetic growth switch based on controlled expression of RNA polymerase,” *Mol Syst Biol*, vol. 11, no. 11, p. 840, Nov. 2015, doi: 10.15252/msb.20156382.
[66] H. Bremer and P. P. Dennis, “Modulation of Chemical Composition and Other Parameters of the Cell at Different Exponential Growth Rates,” *EcoSal Plus*, vol. 3, no. 1, Sep. 2008, doi: 10.1128/ecosal.5.2.3.
[67] M. Patrick, P. P. Dennis, M. Ehrenberg, and H. Bremer, “Free RNA polymerase in Escherichia coli,” *Biochimie*, vol. 119, pp. 80–91, Dec. 2015, doi: 10.1016/j.biochi.2015.10.015.

[68] H. Bremer, P. Dennis, and M. Ehrenberg, “Free RNA polymerase and modeling global transcription in Escherichia coli,” *Biochimie*, vol. 85, no. 6, pp. 597–609, Jun. 2003, doi: 10.1016/s0300-9084(03)00105-6.
[69] M. Schaechter, O. Maaloe, and N. O. Kjeldgaard, “Dependency on medium and temperature of cell size and chemical composition during balanced grown of Salmonella typhimurium,” *J Gen Microbiol*, vol. 19, no. 3, pp. 592–606, Dec. 1958, doi: 10.1099/00221287-19-3-592.
[70] J. Izard *et al.*, “A synthetic growth switch based on controlled expression of RNA polymerase,” *Mol Syst Biol*, vol. 11, no. 11, p. 840, Nov. 2015, doi: 10.15252/msb.20156382.
[71] C. Sutherland and K. S. Murakami, “An Introduction to the Structure and Function of the catalytic core enzyme of Escherichia coli RNA polymerase,” *EcoSal Plus*, vol. 8, no. 1, p. 10.1128/ecosalplus.ESP-0004–2018, Aug. 2018, doi: 10.1128/ecosalplus.ESP-0004-2018.
[72] A. Ishihama, “Role of the RNA polymerase alpha subunit in transcription activation,” *Mol Microbiol*, vol. 6, no. 22, pp. 3283–3288, Nov. 1992, doi: 10.1111/j.1365-2958.1992.tb02196.x.
[73] N. Shepherd, P. Dennis, and H. Bremer, “Cytoplasmic RNA Polymerase in Escherichia coli,” *J Bacteriol*, vol. 183, no. 8, pp. 2527–2534, Apr. 2001, doi: 10.1128/JB.183.8.2527-2534.2001.
[74] J.-B. Lugagne, S. Sosa Carrillo, M. Kirch, A. Köhler, G. Batt, and P. Hersen, “Balancing a genetic toggle switch by real-time feedback control and periodic forcing,” *Nat Commun*, vol. 8, no. 1, Art. no. 1, Nov. 2017, doi: 10.1038/s41467-017-01498-0.
[75] S. Preibisch, S. Saalfeld, and P. Tomancak, “Globally optimal stitching of tiled 3D microscopic image acquisitions,” *Bioinformatics*, vol. 25, no. 11, pp. 1463–1465, Jun. 2009, doi: 10.1093/bioinformatics/btp184.
[76] A. Ainla, I. Gözen, O. Orwar, and A. Jesorka, “A Microfluidic Diluter Based on Pulse Width Flow Modulation,” *Anal. Chem.*, vol. 81, no. 13, pp. 5549–5556, Jul. 2009, doi: 10.1021/ac9010028.
[77] J. Westerweel, “Fundamentals of particle image velocimetry.” 1997.
[78] F. Si *et al.*, “Invariance of Initiation Mass and Predictability of Cell Size in Escherichia coli,” *Curr Biol*, vol. 27, no. 9, pp. 1278–1287, May 2017, doi: 10.1016/j.cub.2017.03.022.
[79] S. Vadia and P. A. Levin, “Growth rate and cell size: A re-examination of the growth law,” *Curr Opin Microbiol*, vol. 24, pp. 96–103, Apr. 2015, doi: 10.1016/j.mib.2015.01.011.
[80] Z. Yao, R. M. Davis, R. Kishony, D. Kahne, and N. Ruiz, “Regulation of cell size in response to nutrient availability by fatty acid biosynthesis in Escherichia coli,” *Proc Natl Acad Sci U S A*, vol. 109, no. 38, pp. E2561-2568, Sep. 2012, doi: 10.1073/pnas.1209742109.
[81] I. Golding, Y. Kozlovsky, I. Cohen, and E. Ben-Jacob, “Studies of bacterial branching growth using reaction–di usion models for colonial development,” *Physica A*, 1998.
[82] N. Luo, S. Wang, J. Lu, X. Ouyang, and L. You, “Collective colony growth is optimized by branching pattern formation in Pseudomonas aeruginosa,” *Molecular Systems Biology*, vol. 17, no. 4, p. e10089, Apr. 2021, doi: 10.15252/msb.202010089.
[83] A. V. Narla, J. Cremer, and T. Hwa, “A traveling-wave solution for bacterial chemotaxis with growth,” *Proc. Natl. Acad. Sci. U.S.A.*, vol. 118, no. 48, p. e2105138118, Nov. 2021, doi: 10.1073/pnas.2105138118.
[84] “Bartlett et al. - 1975 - Comparative Effect of Tetracycline and Doxycycline.pdf.” Accessed: Sep. 30, 2022. [Online]. Available: https://journals.asm.org/doi/pdf/10.1128/AAC.7.1.55
[85] I. Chopra and M. Roberts, “Tetracycline Antibiotics: Mode of Action, Applications, Molecular Biology, and Epidemiology of Bacterial Resistance,” *Microbiol Mol Biol Rev*, vol. 65, no. 2, pp. 232–260, Jun. 2001, doi: 10.1128/MMBR.65.2.232-260.2001.
[86] R. S. Patel and M. Parmar, “Doxycycline Hyclate,” in *StatPearls*, Treasure Island (FL): StatPearls Publishing, 2022. Accessed: Jul. 27, 2022. [Online]. Available: http://www.ncbi.nlm.nih.gov/books/NBK555888/

[87] Y. Yang *et al.*, “Changes in the Carbon Metabolism of Escherichia coli During the Evolution of Doxycycline Resistance,” *Frontiers in Microbiology*, vol. 10, 2019, Accessed: Sep. 30, 2022. [Online]. Available: https://www.frontiersin.org/articles/10.3389/fmicb.2019.02506
[88] K. J. Åström and R. M. Murray, *Feedback Systems: An Introduction for Scientists and Engineers*. Princeton University Press, 2010.
[89] P. V. Röder, B. Wu, Y. Liu, and W. Han, “Pancreatic regulation of glucose homeostasis,” *Exp Mol Med*, vol. 48, no. 3, p. e219, Mar. 2016, doi: 10.1038/emm.2016.6.
[90] “4. Regulation of Blood Glucose | ATrain Education.” https://www.atrainceu.com/content/4-regulation-blood-glucose (accessed Nov. 13, 2022).
[91] S. Hohmann, “Control of high osmolarity signalling in the yeast Saccharomyces cerevisiae,” *FEBS Letters*, vol. 583, no. 24, pp. 4025–4029, Dec. 2009, doi: 10.1016/j.febslet.2009.10.069.
[92] E. de Nadal and F. Posas, “The HOG pathway and the regulation of osmoadaptive responses in yeast,” *FEMS Yeast Res*, vol. 22, no. 1, p. foac013, Mar. 2022, doi: 10.1093/femsyr/foac013.
[93] D. Muzzey, C. A. Gómez-Uribe, J. T. Mettetal, and A. van Oudenaarden, “A systems-level analysis of perfect adaptation in yeast osmoregulation,” *Cell*, vol. 138, no. 1, pp. 160–171, Jul. 2009, doi: 10.1016/j.cell.2009.04.047.
[94] A. Miermont, J. Uhlendorf, M. McClean, and P. Hersen, “The Dynamical Systems Properties of the HOG Signaling Cascade,” *J Signal Transduct*, vol. 2011, p. 930940, 2011, doi: 10.1155/2011/930940.
[95] S. Hohmann, M. Krantz, and B. Nordlander, “Chapter Two - Yeast Osmoregulation,” in *Methods in Enzymology*, vol. 428, D. Häussinger and H. Sies, Eds. Academic Press, 2007, pp. 29–45. doi: 10.1016/S0076-6879(07)28002-4.
[96] O. Brandman and T. Meyer, “Feedback Loops Shape Cellular Signals in Space and Time,” *Science*, vol. 322, no. 5900, pp. 390–395, Oct. 2008, doi: 10.1126/science.1160617.
[97] M. Freeman, “Feedback control of intercellular signalling in development,” *Nature*, vol. 408, no. 6810, pp. 313–319, Nov. 2000, doi: 10.1038/35042500.
[98] N. T. Ingolia and A. W. Murray, “Positive feedback loops as a flexible biological module,” *Curr Biol*, vol. 17, no. 8, pp. 668–677, Apr. 2007, doi: 10.1016/j.cub.2007.03.016.
[99] E. Ozbudak, M. Thattai, H. Lim, B. Shraiman, and A. Oudenaarden, “Multistability in the lactose utilization network of Escherichia coli,” *Nature*, vol. 427, pp. 737–40, Mar. 2004, doi: 10.1038/nature02298.
[100] “Clocks and Ctesibius.” https://www.hellenicaworld.com/Greece/Technology/en/Clocks.html (accessed Dec. 19, 2022).
[101] MdeVicente, *English: Centrifugal governor*. Accessed: Dec. 19, 2022. [Online]. Available: https://commons.wikimedia.org/wiki/File:Centrifugal_governor.svg
[102] H. S. Black, “Stabilized Feedback Amplifiers*,” *Bell System Technical Journal*, vol. 13, no. 1, pp. 1–18, 1934, doi: 10.1002/j.1538-7305.1934.tb00652.x.
[103] A. Visioli, *Practical PID Control*. Springer Science & Business Media, 2006.
[104] K. J. Åström and T. Hägglund, *PID Controllers: Theory, Design, and Tuning*. Research Triangle Park, North Carolina: ISA - The Instrumentation, Systems and Automation Society, 1995.
[105] Turajlić, “Upravljanje procesima, Elektrotehnički fakultet Univerziteta u Beogradu,” 2011. https://www.ucg.ac.me/skladiste/blog_2146/objava_31944/fajlovi/uip_2010.pdf (accessed Jun. 06, 2022).
[106] J. A. Rossiter, *Model-Based Predictive Control: A Practical Approach*. CRC Press, 2003.
[107] M. Arnold, R. R. Negenborn, G. Andersson, and B. De Schutter, “Multi-Area Predictive Control for Combined Electricity and Natural Gas Systems,” *2009 European Control Conference, ECC 2009*, Mar. 2015.

[108] M. Khammash, M. Di Bernardo, and D. Di Bernardo, “Cybergenetics: Theory and Methods for Genetic Control System,” in *2019 IEEE 58th Conference on Decision and Control (CDC)*, Nice, France, Dec. 2019, pp. 916–926. doi: 10.1109/CDC40024.2019.9030209.
[109] J. Uhlendorf *et al.*, “Long-term model predictive control of gene expression at the population and single-cell levels,” *Proceedings of the National Academy of Sciences*, vol. 109, no. 35, pp. 14271–14276, Aug. 2012, doi: 10.1073/pnas.1206810109.
[110] L. Wang, B. L. Walker, S. Iannaccone, D. Bhatt, P. J. Kennedy, and W. T. Tse, “Bistable switches control memory and plasticity in cellular differentiation,” *Proceedings of the National Academy of Sciences*, vol. 106, no. 16, pp. 6638–6643, Apr. 2009, doi: 10.1073/pnas.0806137106.
[111] J. De Caluwé and G. Dupont, “The progression towards Alzheimer’s disease described as a bistable switch arising from the positive loop between amyloids and Ca(2+),” *J Theor Biol*, vol. 331, pp. 12–18, Aug. 2013, doi: 10.1016/j.jtbi.2013.04.015.
[112] G. Perrino *et al.*, “Automatic synchronisation of the cell cycle in budding yeast through closed-loop feedback control,” *Nat Commun*, vol. 12, no. 1, Art. no. 1, Apr. 2021, doi: 10.1038/s41467-021-22689-w.
[113] G. Perrino, C. Wilson, M. Santorelli, and D. di Bernardo, “Quantitative Characterization of α-Synuclein Aggregation in Living Cells through Automated Microfluidics Feedback Control,” *Cell Rep*, vol. 27, no. 3, pp. 916-927.e5, Apr. 2019, doi: 10.1016/j.celrep.2019.03.081.
[114] C. A. Ross and M. A. Poirier, “Protein aggregation and neurodegenerative disease,” *Nat Med*, vol. 10 Suppl, pp. S10-17, Jul. 2004, doi: 10.1038/nm1066.
[115] T. Scheibel and J. Buchner, “Protein Aggregation as a Cause for Disease,” in *Molecular Chaperones in Health and Disease*, K. Starke and M. Gaestel, Eds. Berlin, Heidelberg: Springer, 2006, pp. 199–219. doi: 10.1007/3-540-29717-0_9.
[116] A. Aguzzi and T. O’Connor, “Protein aggregation diseases: pathogenicity and therapeutic perspectives,” *Nat Rev Drug Discov*, vol. 9, no. 3, Art. no. 3, Mar. 2010, doi: 10.1038/nrd3050.
[117] J. T. Pedersen and N. H. H. Heegaard, “Analysis of Protein Aggregation in Neurodegenerative Disease,” *Anal. Chem.*, vol. 85, no. 9, pp. 4215–4227, May 2013, doi: 10.1021/ac400023c.
[118] C. Fracassi, L. Postiglione, G. Fiore, and D. di Bernardo, “Automatic Control of Gene Expression in Mammalian Cells,” *ACS Synthetic Biology*, vol. 5, no. 4, pp. 296–302, Sep. 2015, doi: 10.1021/acssynbio.5b00141.
[119] G. Kretzmer and K. Schügerl, “Response of mammalian cells to shear stress,” *Appl Microbiol Biotechnol*, vol. 34, no. 5, pp. 613–616, Feb. 1991, doi: 10.1007/BF00167909.
[120] T. Tanzeglock, M. Soos, G. Stephanopoulos, and M. Morbidelli, “Induction of Mammalian Cell Death by Simple Shear and Extensional Flows,” *Biotechnology and bioengineering*, vol. 104, pp. 360–70, Oct. 2009, doi: 10.1002/bit.22405.
[121] J. Xu and N. Zhang, “On the way to commercializing plant cell culture platform for biopharmaceuticals: present status and prospect,” *Pharm Bioprocess*, vol. 2, no. 6, pp. 499–518, Dec. 2014, doi: 10.4155/pbp.14.32.
[122] “Derivation of embryonic stem-cell lines from human blastocysts - PubMed.” https://pubmed.ncbi.nlm.nih.gov/14999088/ (accessed Jun. 16, 2022).
[123] J. Fan *et al.*, “Glutamine-driven oxidative phosphorylation is a major ATP source in transformed mammalian cells in both normoxia and hypoxia,” *Mol Syst Biol*, vol. 9, p. 712, Dec. 2013, doi: 10.1038/msb.2013.65.
[124] Y. Genzel, I. Behrendt, S. König, H. Sann, and U. Reichl, “Metabolism of MDCK cells during cell growth and influenza virus production in large-scale microcarrier culture,” *Vaccine*, vol. 22, no. 17–18, pp. 2202–2208, Jun. 2004, doi: 10.1016/j.vaccine.2003.11.041.
[125] O. H. Iversen, U. Iversen, J. L. Ziegler, and A. Z. Bluming, “Cell kinetics in Burkitt lymphoma,” *Eur J Cancer*, vol. 10, no. 3, pp. 155–163, Mar. 1974, doi: 10.1016/0014-2964(74)90148-0.

[126] R. B. Phillips, J. Kondev, and J. Theriot, *Physical Biology of the Cell*. Garland Science, 2009.
[127] "File:Signal transduction pathways.svg - Wikimedia Commons." https://commons.wikimedia.org/wiki/File:Signal_transduction_pathways.svg (accessed Dec. 19, 2022).
[128] A. C. Gorodetsky Juana Alejandra Cerna Sanchez, Toyohiko Yamauchi, Vanessa Taupin, Justin Couvrette &. Alon A., *English: (Left) A schematic of a human cell before transfection, which contains organelles as its only subcellular structures. The cell directly transmits (purple arrows) most of the incident visible light (black arrow) with relatively minimal scattering (green arrows). (Middle) A schematic of a human cell after the expression of reflectin and the formation of photonic architectures, i.e. a disordered arrangement of high refractive index, reflectin-based structures (orange circles), within its interior. The cell diffusely transmits and/or diffusely reflects, i.e. scatters (green arrows), some of the incident visible light (black arrow). (Right) A schematic of a human cell after exposure to a chemical stimulus that influences reflectin assembly, which demonstrates a plausible modification of the geometries and/or arrangements of its photonic architectures (orange circles). The cell now diffusely transmits and/or diffusely reflects, i.e. scatters (green arrows), a different amount of the incident visible light (black arrow).[1]*. 2020. Accessed: Dec. 19, 2022. [Online]. Available: https://commons.wikimedia.org/wiki/File:Engineered_human_cells_with_tunable_optical_properties.svg
[129] G. Weller, *English: Diagram showing the common stages of the cell cycle. The mitotic phase usually takes up about 10% of the time. M = mitosis, C = cytokinesis, G1 = gap phase 1, S = synthesis phase, G2 = gap phase 2.* 2013. Accessed: Dec. 19, 2022. [Online]. Available: https://commons.wikimedia.org/wiki/File:The_Cell_Cycle.svg
[130] Gustavb, *English: Exploded view of a personal computer:* 2006. Accessed: Dec. 19, 2022. [Online]. Available: https://commons.wikimedia.org/wiki/File:Personal_computer,_exploded_4.svg
[131] D. C. for L. Science, *English: 50ml tube 日本語: 50ml チューブ*. 20AD. Accessed: Dec. 19, 2022. [Online]. Available: https://commons.wikimedia.org/wiki/File:202004_50ml_tube.svg
[132] A. Edelstein, N. Amodaj, K. Hoover, R. Vale, and N. Stuurman, "Computer Control of Microscopes Using μManager," *Current Protocols in Molecular Biology*, vol. 92, no. 1, p. 14.20.1-14.20.17, 2010, doi: 10.1002/0471142727.mb1420s92.
[133] "fiji/PIV_analyser." Fiji, Dec. 01, 2021. Accessed: Oct. 30, 2022. [Online]. Available: https://github.com/fiji/PIV_analyser
[134] "Miji," *ImageJ Wiki*. https://imagej.github.io/plugins/miji (accessed Dec. 18, 2022).
[135] H. Ben-Gida, R. Gurka, and A. Liberzon, "OpenPIV-MATLAB — An open-source software for particle image velocimetry; test case: Birds' aerodynamics," *SoftwareX*, vol. 12, Jul. 2020, doi: 10.1016/j.softx.2020.100585.
[136] O. Pust, "PIV: Direct Cross-Correlation compared with FFT-based Cross-Correlation," p. 12.
[137] "lecture3eight.pdf." Accessed: Dec. 18, 2022. [Online]. Available: https://www.control.lth.se/fileadmin/control/Education/DoctorateProgram/Optimal_Control/2018/lecture3eight.pdf
[138] "ex4.pdf." Accessed: Dec. 18, 2022. [Online]. Available: https://www.math.kth.se/optsyst/grundutbildning/5B1872/Ex/ex4.pdf
[139] O. Hájek, "Discontinuous differential equations, I," *Journal of Differential Equations*, vol. 32, no. 2, pp. 149–170, May 1979, doi: 10.1016/0022-0396(79)90056-1.
[140] M. Bardi and M. Falcone, "Discrete approximation of the minimal time function for systems with regular optimal trajectories," 2008, pp. 103–112. doi: 10.1007/BFb0120033.

[141] J. Nguyen, V. Fernandez, S. Pontrelli, U. Sauer, M. Ackermann, and R. Stocker, “A distinct growth physiology enhances bacterial growth under rapid nutrient fluctuations,” *Nat Commun*, vol. 12, no. 1, Art. no. 1, Jun. 2021, doi: 10.1038/s41467-021-23439-8.
[142] A. G. Marr, “Growth rate of Escherichia coli.,” *Microbiol Rev*, vol. 55, no. 2, pp. 316–333, Jun. 1991.
[143] E. Vasilakou, M. C. M. van Loosdrecht, and S. A. Wahl, “Escherichia coli metabolism under short-term repetitive substrate dynamics: adaptation and trade-offs,” *Microbial Cell Factories*, vol. 19, no. 1, p. 116, May 2020, doi: 10.1186/s12934-020-01379-0.
[144] H. Taymaz-Nikerel, W. M. van Gulik, and J. J. Heijnen, “Escherichia coli responds with a rapid and large change in growth rate upon a shift from glucose-limited to glucose-excess conditions,” *Metab Eng*, vol. 13, no. 3, pp. 307–318, May 2011, doi: 10.1016/j.ymben.2011.03.003.
[145] V. R. Segovia, T. Hägglund, and K. J. Åström, “Noise filtering in PI and PID Control,” in *2013 American Control Conference*, Jun. 2013, pp. 1763–1770. doi: 10.1109/ACC.2013.6580091.
[146] A. Bar-Even *et al.*, “Noise in protein expression scales with natural protein abundance,” *Nat Genet*, vol. 38, no. 6, pp. 636–643, Jun. 2006, doi: 10.1038/ng1807.
[147] P. S. Swain, M. B. Elowitz, and E. D. Siggia, “Intrinsic and extrinsic contributions to stochasticity in gene expression,” *Proc. Natl. Acad. Sci. U.S.A.*, vol. 99, no. 20, pp. 12795–12800, Oct. 2002, doi: 10.1073/pnas.162041399.
[148] A. Eldar and M. B. Elowitz, “Functional roles for noise in genetic circuits,” *Nature*, vol. 467, no. 7312, Art. no. 7312, Sep. 2010, doi: 10.1038/nature09326.
[149] B. Munsky, G. Neuert, and A. van Oudenaarden, “Using gene expression noise to understand gene regulation,” *Science*, vol. 336, no. 6078, pp. 183–187, Apr. 2012, doi: 10.1126/science.1216379.
[150] L. Wolf, O. K. Silander, and E. van Nimwegen, “Expression noise facilitates the evolution of gene regulation,” *eLife*, vol. 4, p. e05856, Jun. 2015, doi: 10.7554/eLife.05856.
[151] A. Hilfinger and J. Paulsson, “Separating intrinsic from extrinsic fluctuations in dynamic biological systems,” *Proceedings of the National Academy of Sciences*, vol. 108, no. 29, pp. 12167–12172, Jul. 2011, doi: 10.1073/pnas.1018832108.
[152] M. B. Elowitz, A. J. Levine, E. D. Siggia, and P. S. Swain, “Stochastic gene expression in a single cell,” *Science*, vol. 297, no. 5584, pp. 1183–1186, Aug. 2002, doi: 10.1126/science.1070919.
[153] M. B. Elowitz, A. J. Levine, E. D. Siggia, and P. S. Swain, “Stochastic Gene Expression in a Single Cell,” *Science*, vol. 297, no. 5584, pp. 1183–1186, Aug. 2002, doi: 10.1126/science.1070919.
[154] S. Yang *et al.*, “Contribution of RNA polymerase concentration variation to protein expression noise,” *Nat Commun*, vol. 5, p. 4761, Sep. 2014, doi: 10.1038/ncomms5761.
[155] “Quantifying E. coli proteome and transcriptome with single-molecule sensitivity in single cells - PMC.” https://www.ncbi.nlm.nih.gov/pmc/articles/PMC2922915/ (accessed Oct. 14, 2022).
[156] A.-M. Ladouceur *et al.*, “Clusters of bacterial RNA polymerase are biomolecular condensates that assemble through liquid–liquid phase separation,” *Proceedings of the National Academy of Sciences*, vol. 117, no. 31, pp. 18540–18549, Aug. 2020, doi: 10.1073/pnas.2005019117.
[157] J. E. Cabrera and D. J. Jin, “The distribution of RNA polymerase in Escherichia coli is dynamic and sensitive to environmental cues,” *Mol Microbiol*, vol. 50, no. 5, pp. 1493–1505, Dec. 2003, doi: 10.1046/j.1365-2958.2003.03805.x.
[158] D. J. Jin, C. Cagliero, C. M. Martin, J. Izard, and Y. N. Zhou, “The dynamic nature and territory of transcriptional machinery in the bacterial chromosome,” *Front Microbiol*, vol. 6, p. 497, 2015, doi: 10.3389/fmicb.2015.00497.
[159] D. J. Jin, C. Cagliero, and Y. N. Zhou, “Role of RNA Polymerase in the Organization of the Bacterial Nucleoid,” *Chem Rev*, vol. 113, no. 11, p. 10.1021/cr4001429, Nov. 2013, doi: 10.1021/cr4001429.
[160] A. Urchueguía, L. Galbusera, D. Chauvin, G. Bellement, T. Julou, and E. van Nimwegen, “Genome-wide gene expression noise in Escherichia coli is condition-dependent and determined by

propagation of noise through the regulatory network," *PLOS Biology*, vol. 19, no. 12, p. e3001491, Dec. 2021, doi: 10.1371/journal.pbio.3001491.
[161] "Connecting growth with gene expression: of noise and numbers - ScienceDirect." https://www.sciencedirect.com/science/article/pii/S1369527415000636 (accessed Oct. 14, 2022).
[162] F. Bertaux, S. Marguerat, and V. Shahrezaei, "Division rate, cell size and proteome allocation: impact on gene expression noise and implications for the dynamics of genetic circuits," *Royal Society Open Science*, vol. 5, no. 3, p. 172234, doi: 10.1098/rsos.172234.
[163] "Multiscale spatial organization of RNA polymerase in Escherichia coli - PubMed." https://pubmed.ncbi.nlm.nih.gov/23823236/ (accessed Oct. 14, 2022).
[164] "Overflow metabolism in Escherichia coli results from efficient proteome allocation - PubMed." https://pubmed.ncbi.nlm.nih.gov/26632588/ (accessed Oct. 14, 2022).
[165] "ilastik: interactive machine learning for (bio)image analysis | Nature Methods." https://www.nature.com/articles/s41592-019-0582-9 (accessed Dec. 19, 2022).
[166] "Microbiology and flow cytometry." http://www.cyto.purdue.edu/archive/flowcyt/research/micrflow/robert/robert.htm (accessed Oct. 16, 2022).
[167] C. Hult *et al.*, "Enrichment of dynamic chromosomal crosslinks drive phase separation of the nucleolus," *Nucleic Acids Res*, vol. 45, no. 19, pp. 11159–11173, Nov. 2017, doi: 10.1093/nar/gkx741.
[168] P. S. Maddox, N. Portier, A. Desai, and K. Oegema, "Molecular analysis of mitotic chromosome condensation using a quantitative time-resolved fluorescence microscopy assay," *Proceedings of the National Academy of Sciences*, vol. 103, no. 41, pp. 15097–15102, Oct. 2006, doi: 10.1073/pnas.0606993103.
[169] J. Schindelin *et al.*, "Fiji: an open-source platform for biological-image analysis," *Nat Methods*, vol. 9, no. 7, Art. no. 7, Jul. 2012, doi: 10.1038/nmeth.2019.
[170] C. A. Schneider, W. S. Rasband, and K. W. Eliceiri, "NIH Image to ImageJ: 25 years of image analysis," *Nat Methods*, vol. 9, no. 7, Art. no. 7, Jul. 2012, doi: 10.1038/nmeth.2089.
[171] "Manual Drift Correction Plugin." Scientific Computing Facility @ MPI-CBG, Jul. 12, 2017. Accessed: Oct. 30, 2022. [Online]. Available: https://github.com/mpicbg-scicomp/Manual_drift_correction
[172] "T--Northwestern--M9SupplementedMedia.pdf." Accessed: Dec. 06, 2022. [Online]. Available: https://static.igem.org/mediawiki/2017/7/73/T--Northwestern--M9SupplementedMedia.pdf
[173] B. Albing, "Poles & Zeroes: I Understand, Mostly," *Planet Analog*, Jan. 28, 2013. https://www.planetanalog.com/poles-zeroes-i-understand-mostly/ (accessed Dec. 19, 2022).
[174] E. Frazzoli, "Recitation 11: Time delays".